CRANFIELD INSTITUTE OF TECHNOLOGY

COLLEGE OF AERONAUTICS

CRANFIELD IMPACT CENTRE

Ph.D. THESIS

ACADEMIC YEAR 1988

EFFORD CLIVE CHIRWA

Theoretical Analysis and Pressure Distribution of Thin-walled Metal Inverbuckle Energy Absorbing Tubes

Supervisor: Dr. M. M. Sadhegi

May 1988

SYNOPSIS

This dissertation presents an investigation in the energy absorbing capacity of thin-walled metal inverbucktubes loaded in axial compression. It also presents the inversion-buckling(curling-buckling) behaviour achieved in both, quasi-static and dynamic loading conditions.

In addition, for the first time, the experimental results of the pressure or normal stress distribution between the inside surface of the inverbucktube and die fillet radius interface are stipulated. These were very successful, using the pressure transducer method.

Furthermore, a mathematical model has been developed, based on theory of plasticity and making use of energy method. This predicts the amount of energy absorbed in the assumed seperate collapse processes. Results yielded from the theory, showed good agreement with the experimental results which had geometry factor within feasibility boundaries of inverbuckling collapse ($6.5 \leq \bar{D}/2t_o \leq 22.5$).

The successful prediction of energy absorbed, inverbuckling load and pressure distribution, not only proves the validity of the model, but also confirms the quality of the modelling approach proposed in this dissertation. Using this mathematical model, inverbucktubes could be designed, developed and applied.

ACKNOWLEDGEMENTS

I wish to express my thanks to M.M.Sadeghi, whose help, valuable technical guidance and encouragement contributed a great deal to the project and whose pleasant personality made the stay at the institute very enjoyable. I would also like to use this opportunity to thank G.H. Tidbury for his technical advice and help.

The support and advice by all of my friends and colleagues, especially to R.N.Jones for help in the component testing, is gratefully acknowledged.

Especially to my wife Elena for her love and sons, Dennis and Daniel for their love and affection, I should like again to express my heartfelt thanks.

CONTENTS

CONTENETS(Cont.)

CONTENTS(Cont.)

CONTENTS(Cont.)

FIGURES

FIGURES(Cont.)

FIGURES(Cont.)

FIGURES(Cont.)

FIGURES(Cont.)

FIGURES(Cont.)

TABLES

NOTATION

D_i	Internal inverbucktube diameter
$\bar{D}$	Mean inverbucktube diameter
t_a	Average thickness
A	Strength coefficient
n	Strain hardening exponent
L	Inverbucktube length
α	Die fillet angle
r	Die fillet radius
l_1	Tapered length
l_2	Constant middle length
$\bar{R}, \bar{R}'$	Original mean radius, expanded mean radius
ϕ	Middle length ratio factor ($\phi = l_2/2\bar{R}$)
K	Geometry ratio factor($K = \bar{R}/t_a$)
t_1	Middle part constant thickness
t_2	Tapered part end tip thickness
δ, δ_d	Static, dynamic shortening distance
M_b	Trolley mass
V_o	Impact velocity
V_R	Rebound velocity
V	Quasi-static velocity
E_{KI}	Kinetic energy input($\frac{1}{2}M_b Vo^2$)
E_{KA}	Kinetic energy absorbed($\frac{1}{2}M_b(Vo^2 - Vr^2)$)

NOTATION(Cont.)

$\bar{P}_D$	Mean dynamic load(E_{KA}/δ_D)
P_{in}	Inverting load
P_{BUCK}	Buckling load
$\bar{P}$	Mean static load
η_{IT}	Inverbuckling tightness
N	Normal stress or pressure
W_D	Work done due to deformation
W_T	Work involved with the compressive load
W_F	Work done due to friction force
W_B	Work done due to bending in the fillet radius
W_E	Work done due to expansion in the fillet radius
W_{BL}	Work done in the formation of circumferential plastic hinges in the buckling region
W_{BBL}	Work done in bending of circuferential plastic hinges
W_{EBL}	Work done in expansion between circumferential plastic hinges
V_1	Inverbucktube tapered part volume
$\bar{\sigma}$	Effective stress
$\bar{\varepsilon}$	Effective strain
ε_θ	Circumferential strain
ε_1	Longitudinal strain
ε_t	Thickness strain
$\varepsilon_1, \varepsilon_2, \varepsilon_3$	Principal strains

NOTATION(Cont.)

θ	Tapering inverbucktube angle
θ_1	Angle of collapse during axisymmetric buckling
μ	Friction coefficient
M_p	Plastic bending moment($M_p = 2/\sqrt{3}\sigma_y t_z^2/4$)
σ_y	Yield stress
σ_a	Average flow stress
σ_x	Longitudinal stress
σ_θ	Hoop or circumferential stress
R_i	Internal inverbucktube radius
t_x, t_z	Thickness at distance x, thickness at distance z
R_o'	Expanded external inverbucktube radius
R_i'	Expanded internal inverbucktube radius
Z, Z_1, Z'	Distance travelled by inverbucktube over the die
m	Strain hardening plastic deformation factor
τ	Shear stress
s	Surface area of the die fillet
σ_{nom}	Nominal stress
P	Tensile load
A_o	Initial cross-section area
σ_u	Ultimate stress
A_f	Final cross-section area

NOTATION(Cont.)

l_1	Extended gauge length
l_0	Initial gauge length
ε	True strain
e	Engineering strain
σ	True stress
ψ	Inclined angle
L_m	Final length of the collapsed inverbucktube
δ_1, δ_2	Extended distance, collapse distance due to bending
δ_3, δ_4	Collapse distance due to buckling, collapse distance passing through the die fillet radius

CHAPTER I

INTRODUCTION AND LITERATURE SURVEY

1.1 INTRODUCTION

Concern about safety in load bearing structures is an important factor which needs a lot of attention. This is why the last two decades has seen a colossal amount of work in the development of mechanical devices which dissipate energy through plastic deformation in controlled manner and at a predetermined rate. The study of these systems was prompted by the demand for favourable devices which bring a moving mass to a controlled stop.

This same period, a considerable amount of research has been carried out on methods of absorbing the impact energy using thin-walled tube structures. A number of these studies have assessed the energy absorption using the following criteria: (i) Collapse behaviour, which defines goemetrical changes of the tube structure; (ii) mass-specific energy absorption (this gives the collapse energy absorbed by the tube in relation to the mass); (iii) length-specific energy absorption (this quantifies the collapse energy absorbed by the structure in relation to the collapse distance) and (iv) force-deformation characteristic, which is important mainly in the development of the tube structure, and in some cases predicts the real condition of dynamic situation as long as the velocities involved are not high enough to alter the quasi-static collapse behaviour significantly.

To add to the list of these machanical devices, an Inversion-Buckling thin-walled metal tube was designed and

developed. This was called *"INVERSION-BUCKLING TUBE"* or in short "INVERBUCKTUBE". Throughout this dissertation, inverbucktube will be used to signify the scrolling or curling and buckling collapse of the tube. However, the original design was developed by C.I.C. (Cranfield Impact Centre, at Cranfield Institute of Technology)(17)* for use in nuclear reactor support structure. This was developed basically from testing. What this dissertation has got in store though, is the thorough study through which inverbuckling tubes could be designed, developed and applied in real situations.

The inverbucktube system is a cylindrical thin-walled tube with constant middle thickness and tapered at both ends. For it to absorb energy through plastic deformation, dies with fillet radii are employed at both ends to trigger the collapse mechanism when continuous compressive load is applied. Compared with a materially similar tube of equal mass, an inverbucktube utilises material more efficiently by allowing severe deformation as well as a range of deformation processes - expansion, bending, buckling as the main ones.

Energy is not only absorbed through plastic deformation alone. Between the inverbucktube/die interface, work is done due to friction stress. Its quantity is governed by both inverbuckling tube and die geometry, and the friction coefficient encountered. In the present work a lot of effort was devoted towards this and determined the friction stress through experimental and theoretical results of normal stress.

(* Numbers in brackets designate references at the end of the dissertation)

1.2 REVIEW OF ENERGY ABSORBERS IN GENERAL

The collapse behaviour and energy absorption of thin-walled tubes with circular and square cross-sections subjected to axial loadings were pioneered by Pugsley and Macaulay in their revolutionary paper(1)* and later in (2 and 4)*. Here, the authors for the first time, presented the physical understanding of the non-axisymmetric or diamond collapsing mode of cylindrical shells. This type of mode was achieved in tubes of D/2t ≥ 50.

However, other thin-walled circular metal tubes when subjected to the type of loading as in (1)*, are liable to develop one or two forms of collapse behaviour, depending on the ratio of the tube diameter to its wall thickness. When the ratio of D/2t is less than about 50, tubes develop a collapse behaviour which appear as an accordion around the tube circumference. This collapse behaviour became to be known as *"concertina"* or axisymmetric and was pioneered by Alexander(3)*.

The first half of sixties saw a lot of work in this field, especially in the United States of America where methods for providing soft landings to space vehicles on lunar or planetary surfaces were being investigated. Published papers are numerous, but (5-10)* give a wide range of systems employed. Some of these devices are depicted in figs.1.1-1.6. While, an elaborate survey of energy absorbers are epitomized by Esgar(60)*.

The second half of sixties saw a transfer of technology from space vehicles to motor vehicles. During this period, mechanical devices for dissipating kinetic energy in steering columns were being researched throughout by motor manufacturers. General Motors(11)* as the innovating company called it *"Energy Absorbing Steering Column"*, see

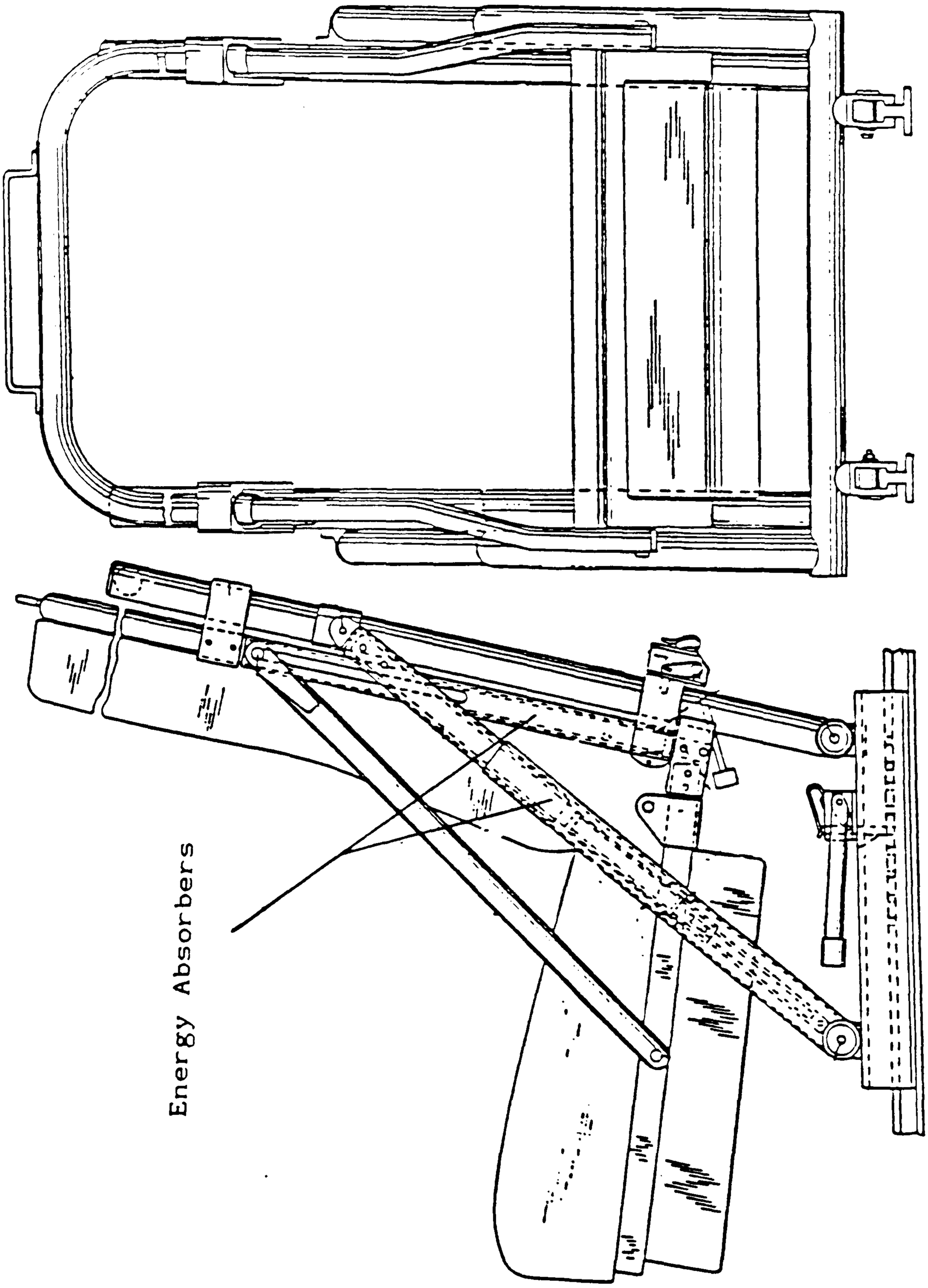

Fig. 1.1 Assembled drawing of crew seat (5)

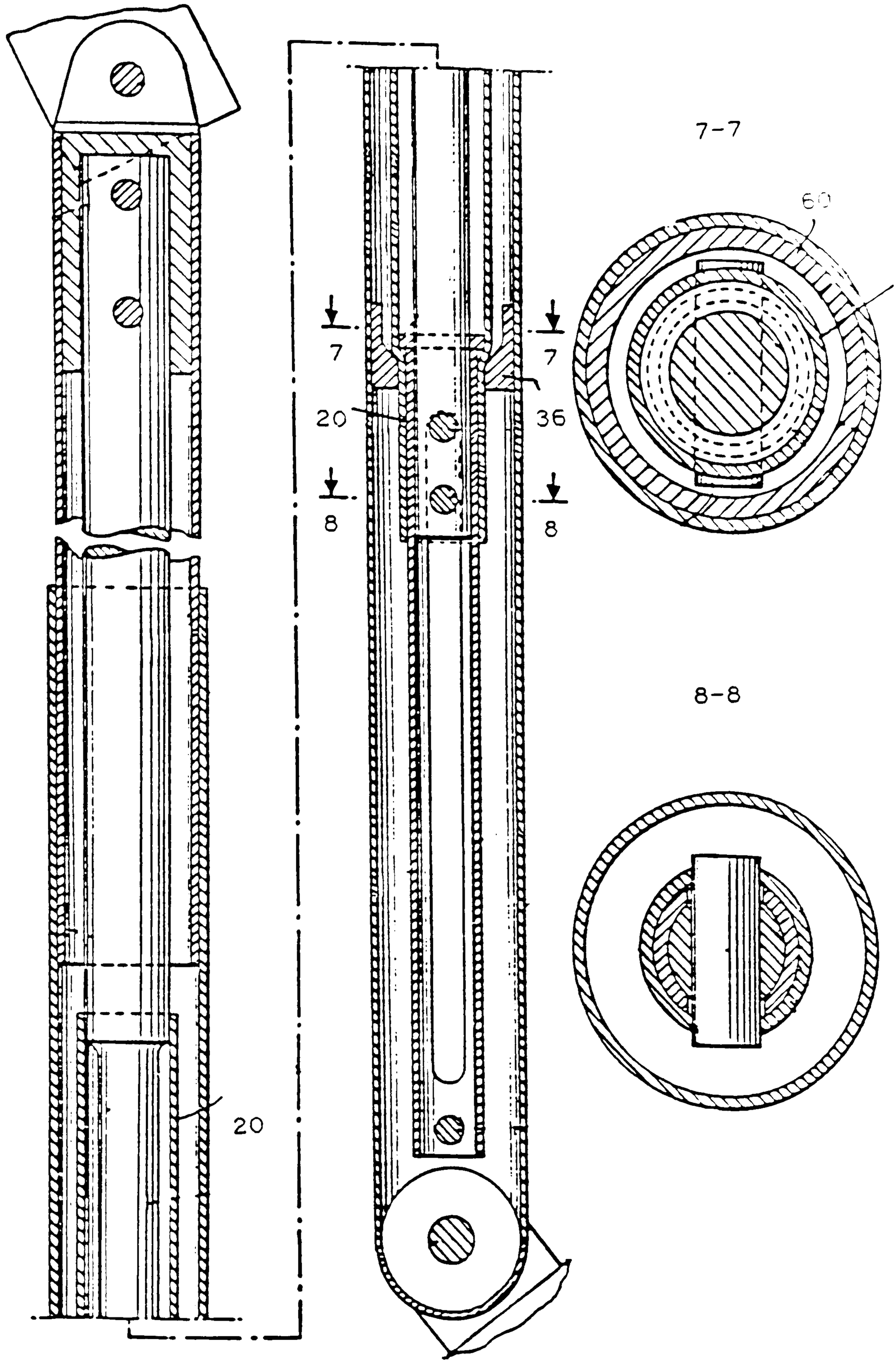

Fig. 1.2 Energy absorbing elements (5)*

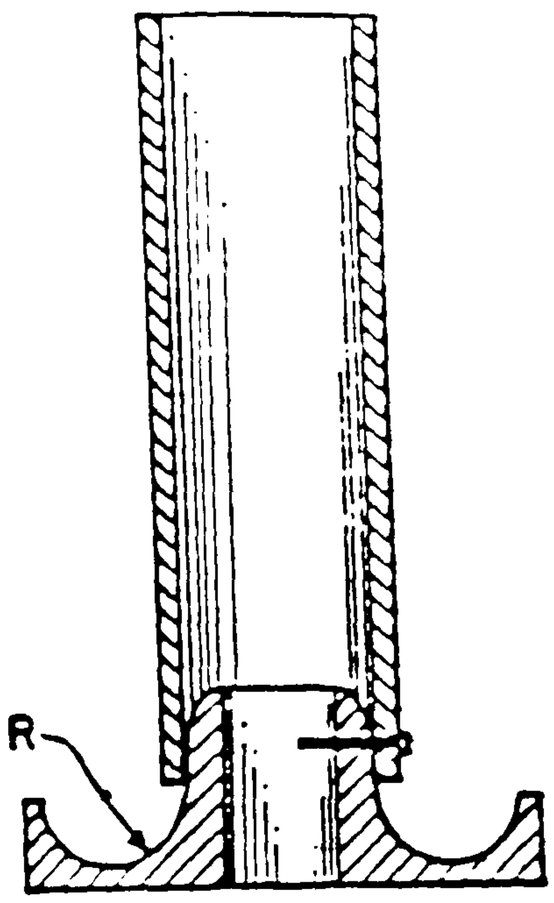

a)

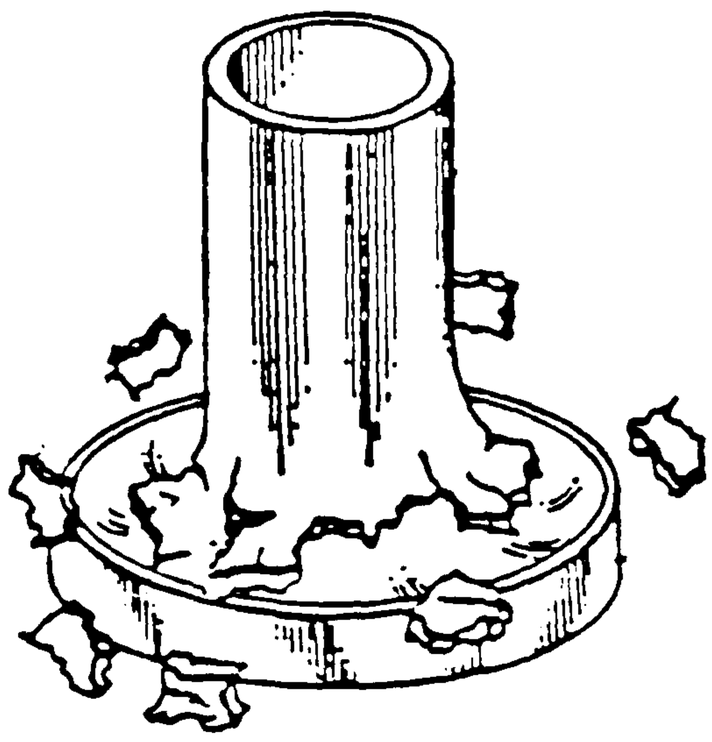

b)

Fig. 1.3 Detailed energy absorber(6)

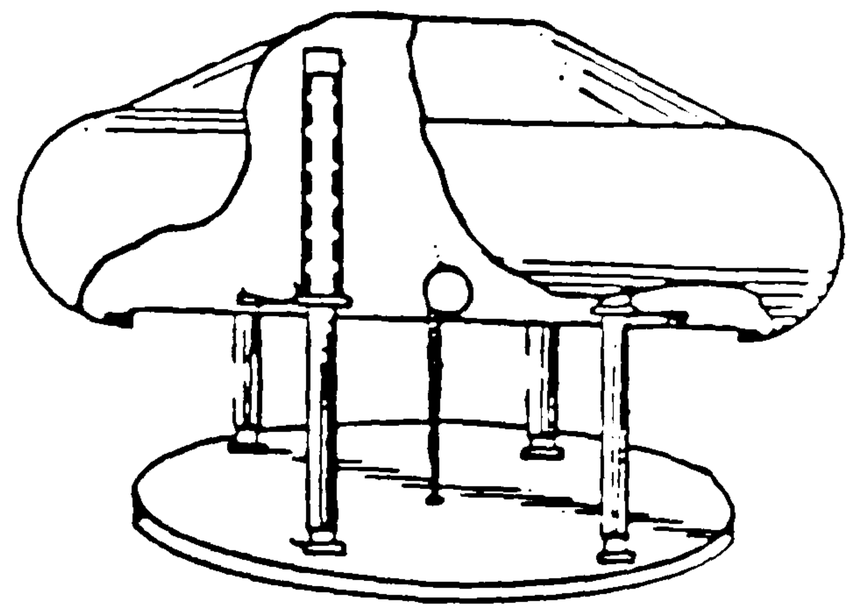

a)

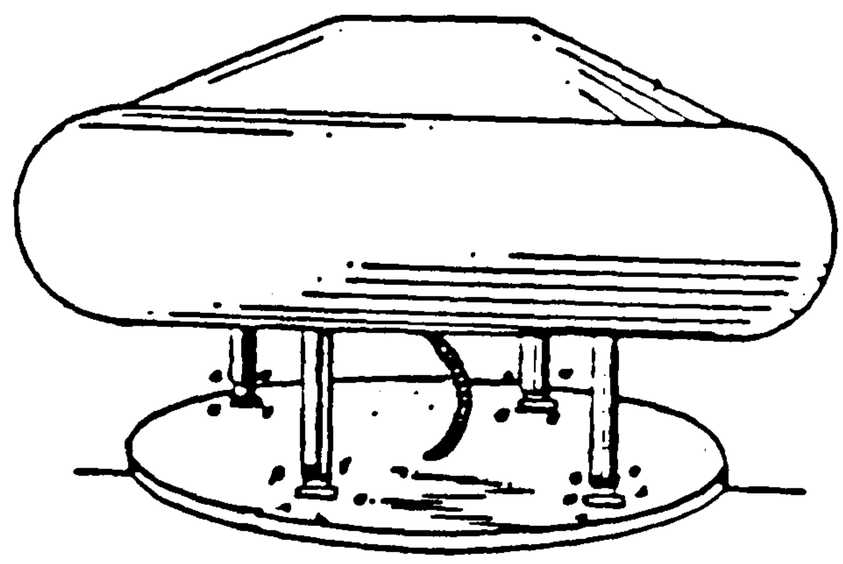

b)

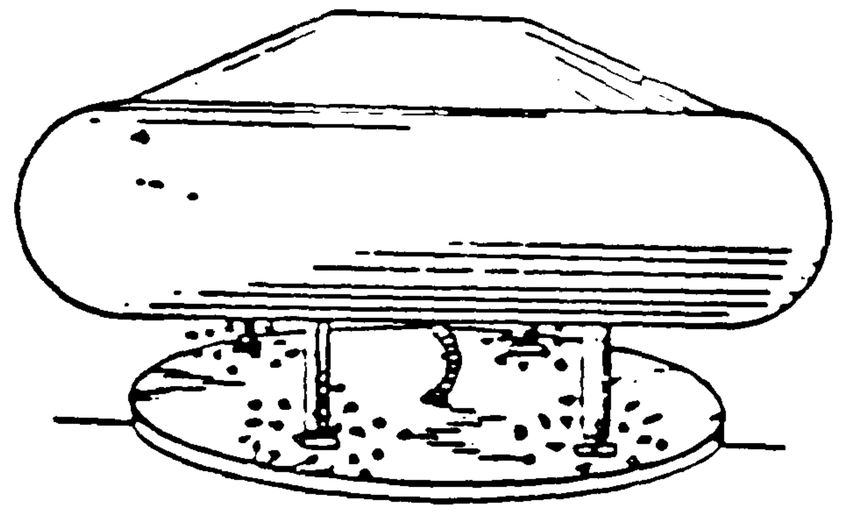

c)

Fig. 1.4 Energy absorbers emp on an aerial vehicle

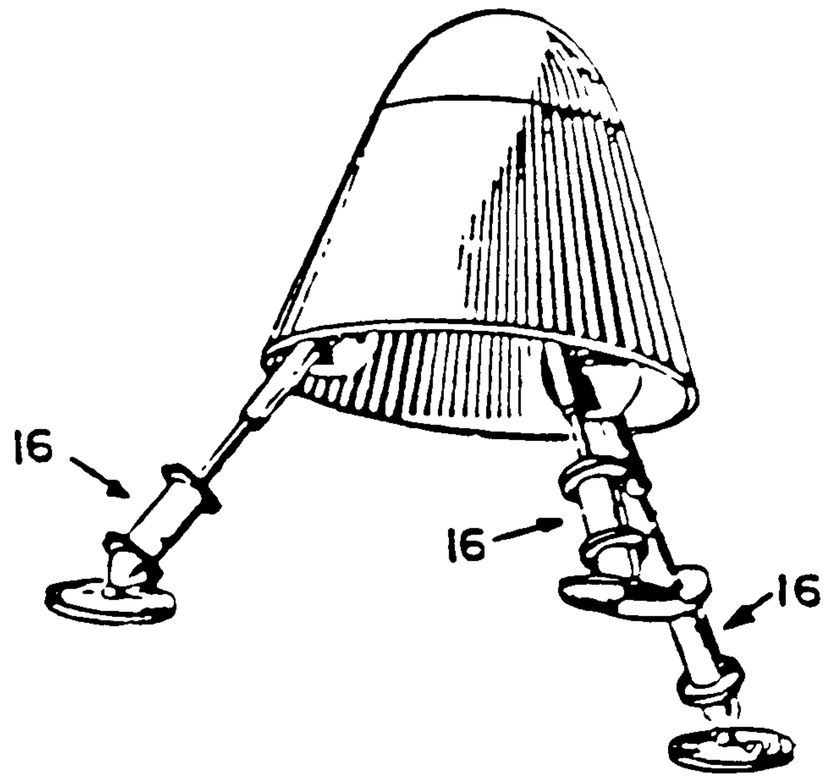

Fig. 1.5 Assembled drawing of space vehicle (8)*

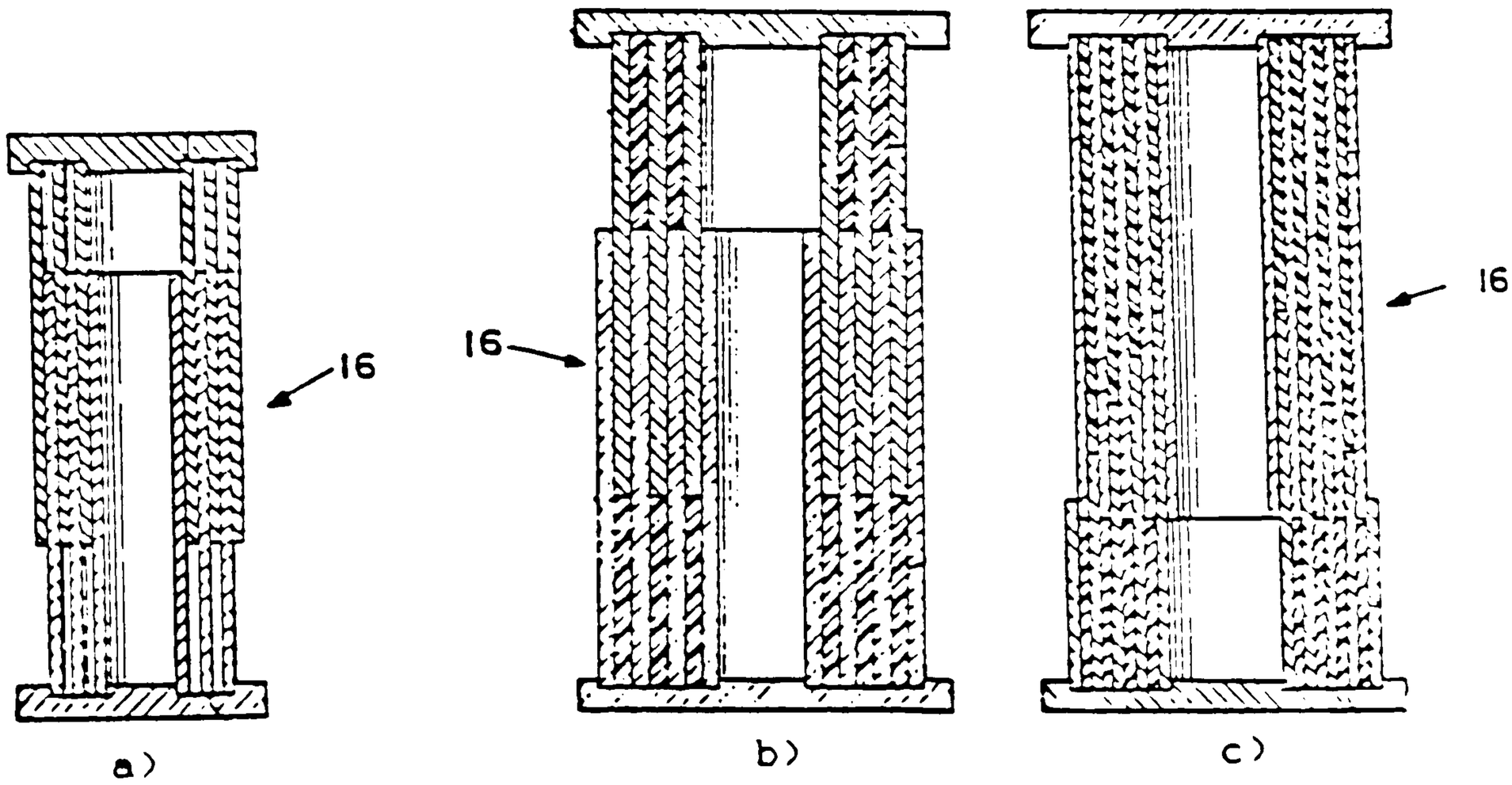

Fig. 1.6 Energy absorbing elements (8)*

figs.1.7-1.12. Other alternative mechanical devices researched and used during this period in steering columns are presented in (12,54)*.

At the beginning of seventies, the study in the collapse behaviour and quantification of energy absorbed by thin-walled tubes became high on the list in many research institutions. A comprehensive list of published literature on impact energy dissipation is given in Johnson and Reid's paper(49)* on metallic energy-dissipating systems subjected relatively to low velocities.

In addition, the use of metallic devices discussed above, various other energy absorbing systems with rectalinear cross-sections (18-21)* have been proposed for dissipating kinetic energy. Under axial loading, these tubes tend to produce more complex collapse behaviour than those with cylindrical cross-sections. Their greatest disadvantage though has been to the amount of energy they could absorb. It was shown in (22)* that these types of tubes dissipate about a third less energy than circular tubes for an equal volume of material.

In general, metallic devices which dissipate energy through plastic deformation, came in all configurations. It will be impossible to numerate them all, but additional literature to those given above could be found in (46-48)* and (50-59)*.

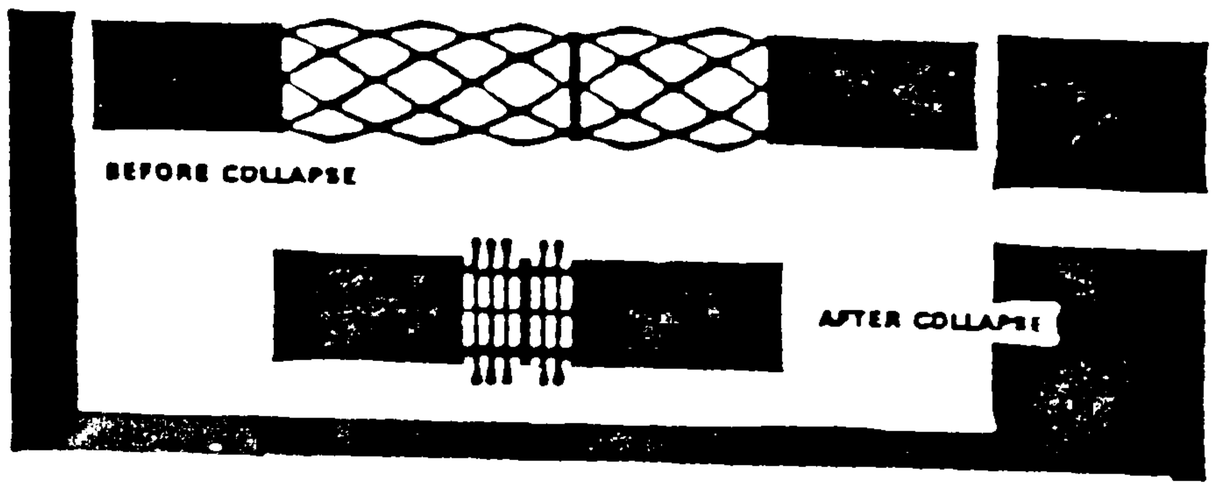

Fig. 1.7 Mesh type jacket energy absorber (11)*

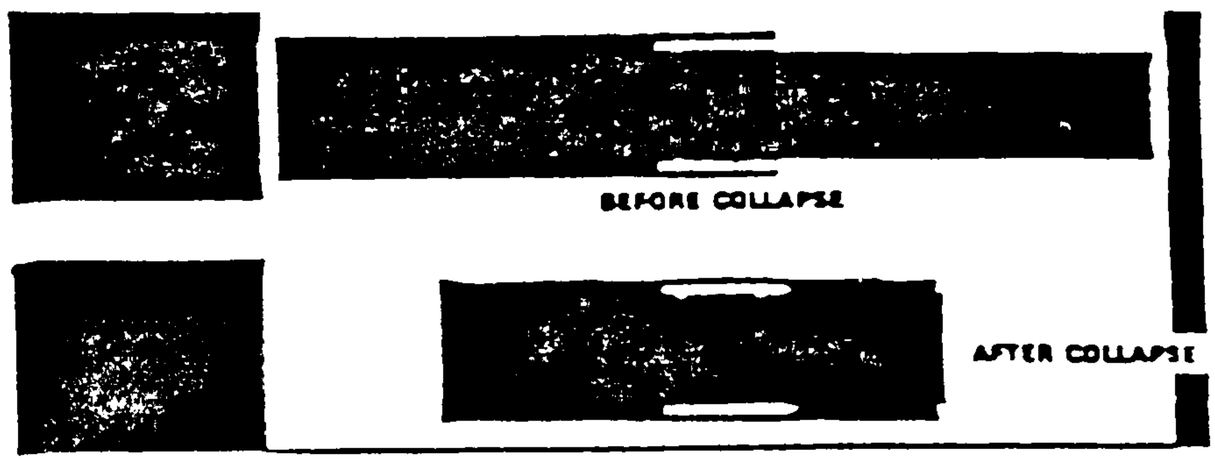

Fig. 1.8 Ball type jacket energy absorber (11)*

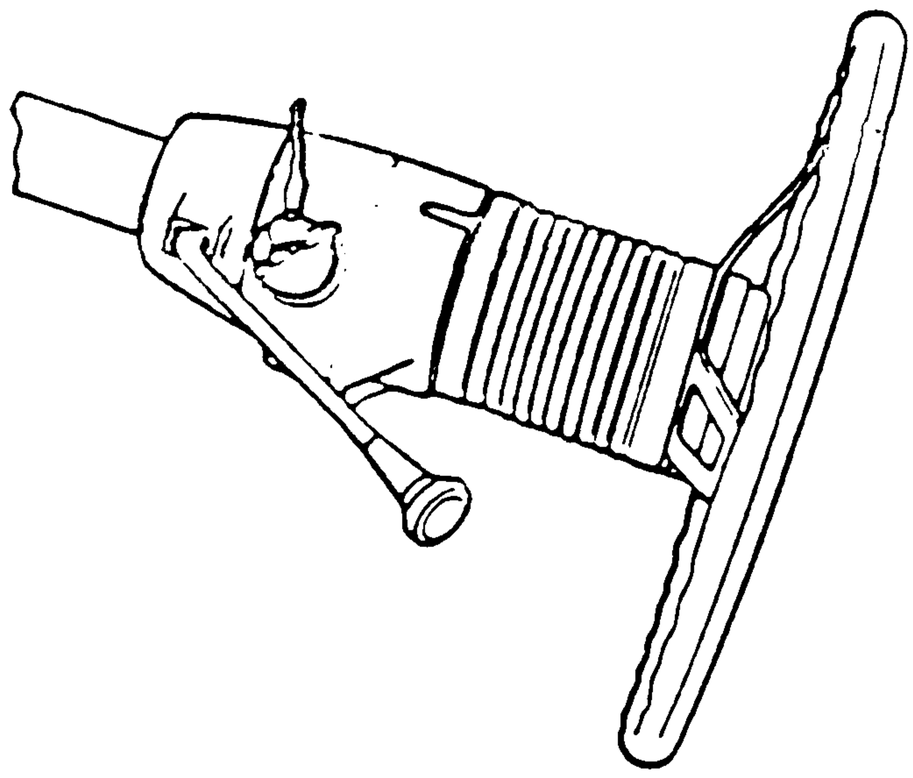

Fig. 1.9 Thin-wall convoluted cylinder located between steering wheel armature and steering column (54)'

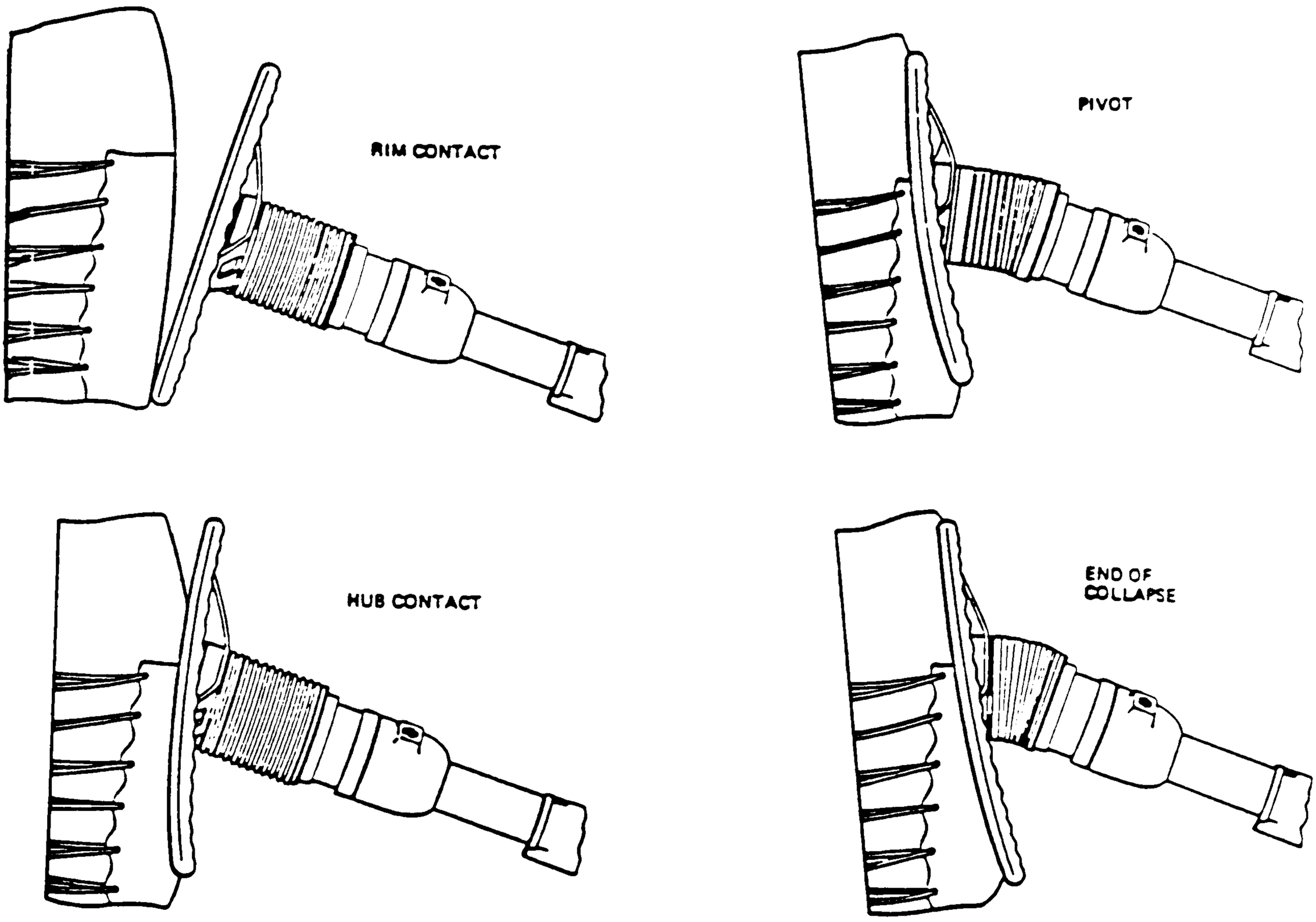

Fig. 1.10 Collapse sequence taken from test film represents typical impact of a tapered profile canister (54)'

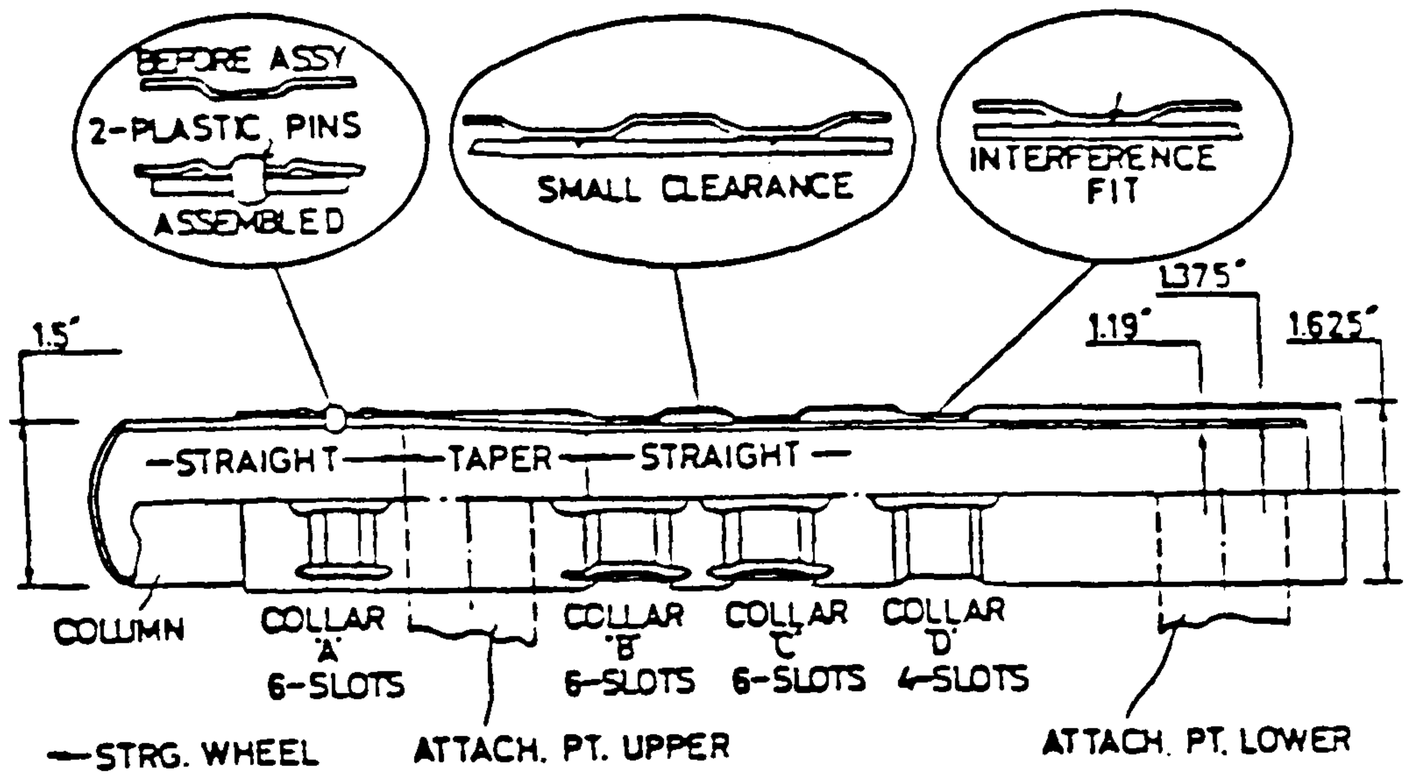

Fig. 1.11 Assembly of outer jacket and column (12)*

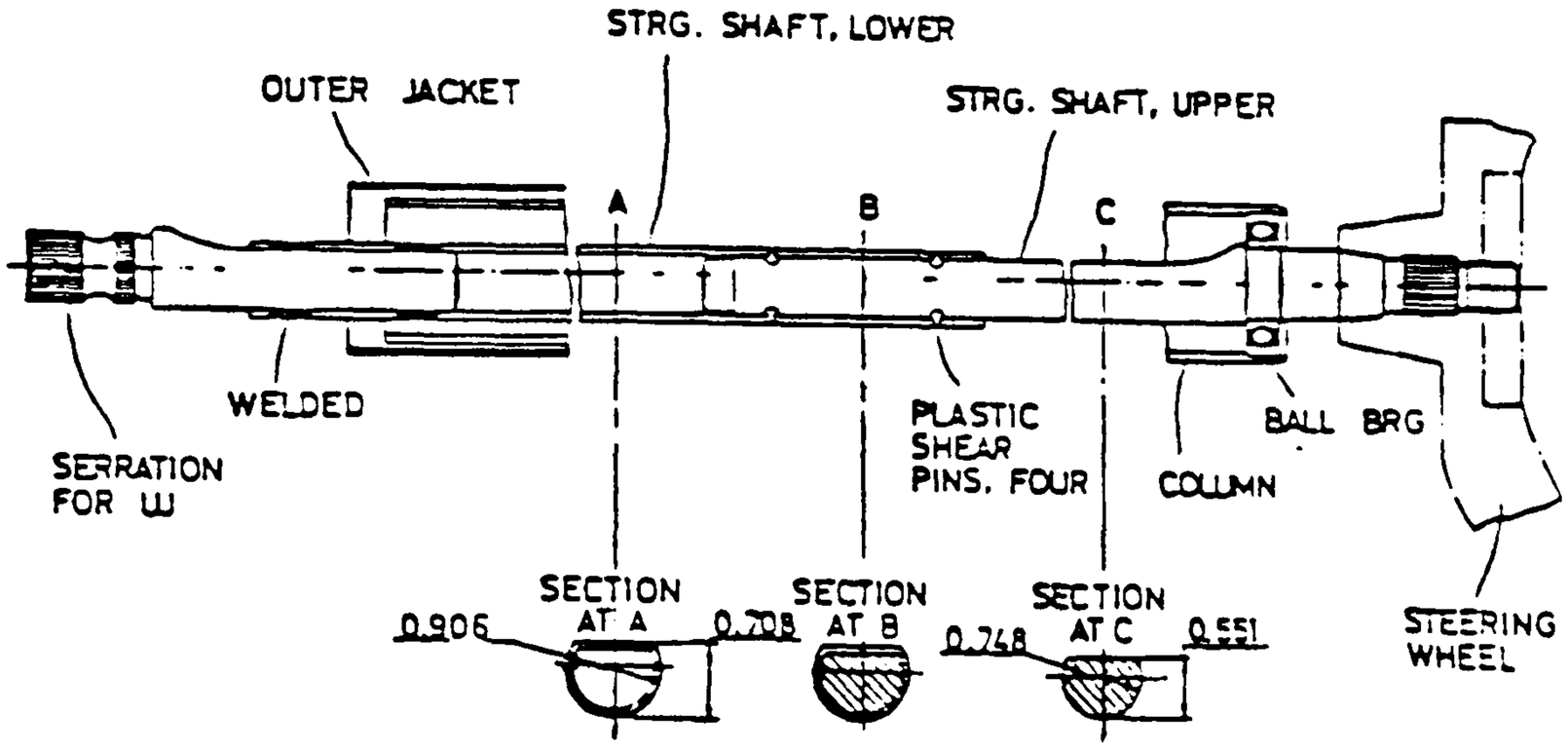

Fig. 1.12 Two parts of steering shaft assembly (12)*

1.2.1 COMPOSITE ENERGY ABSORBERS

In the seventies, advanced material fabrication reflected a significant increase in emphasis on composite materials as genuine substitutes for steel structures. This was because of their high strength, stiffness and low density. A lot of work has been carried out in this sphere and some significant work could be seen in (29-33)*.

A recent review into axial crush behaviour of composite tubes was presented by Thornton(34,35)*. His studies indicated that most of the composite tubes under axial loading absorbed kinetic energy through disintegration, either completely into small fragments or else into larger pieces which tended to retain some cohesion with the base structure. According to Thornton, the most interesting composite material was the Kevlar (trade-name of DuPont Inc., for aramid fibres). The tube made from this material showed some tensile ductility and under compression, the crush behaviour was axisymmetric buckling (for 45°/45°). On the other hand once the aramid fibres had been orientated into 0°/90°, the Kevlar tubes collapsed largely by fracture or disintegration.

In his resume', Thornton pointed out some of the drawbacks of using composite tubes. These disadvantages were of interest and he classified them as follows: (i) Unlike metal tubes, for which specific energy depends upon geometry, specific energy for composite tubes was essentially constant with respect to change in tube dimensions in the stable crush regime and (ii) when a composite tube was mounted on a die (like in invertube), collapse was found to be unstable, whereas crack propagation and fibre seperation occured well ahead of the specimen/die interface. In this case the crush load and consequently the specific energy were very low. It must be

pointed out however, that despite the disadvantages presented here, composite energy absorbers in some cases (depending on design and area of application) have shown better characteristics than their metallic counterparts.

1.3 REVIEW OF INVERTUBE ENERGY ABSORBERS

The invertube referred to as *"rolling tube"* is a method of absorbing energy by turning a tube on itself over a die radius until part of it is inside-out or outside-in. Tubes which have such collapse behaviour were invented by Kroell(13)* of General Motors about 1959. It was only in 1966 interest in invertubes arose from consideration of energy absorbing devices suitable for use in the landing structure of space vehicles(14)*.

This same year, Guist and Marble(61)* carried out a so-called thourough theoretical study on the collapse and deformation of invertubes. They presented an analysis which incorporated the effects of both circumferential bending and stretching of tube material. Two emperical equations pertaining to the inversion load and to the specific energy absorption were obtained. In addition they gave an account on the experimental results which indicated that the process (inversion) was feasible only for certain very ductile materials and only for a certain range of tube diameter to thickness ratios. However, the theory underestimated the observed load in the range of 20% to 30%; and within 10% to 20% when the experimental value of the parameter 'c' (curvature parameter) was used in the prediction. The discrepancies were attributed to the neglect of strain-hardening effect. The configurations used in the inversion processes are shown in fig.1.13. From the illustrations it can be clearly seen that the tip of the tubes in both inside-out and outside-in inversions were prebuckled, slotted into attachments and

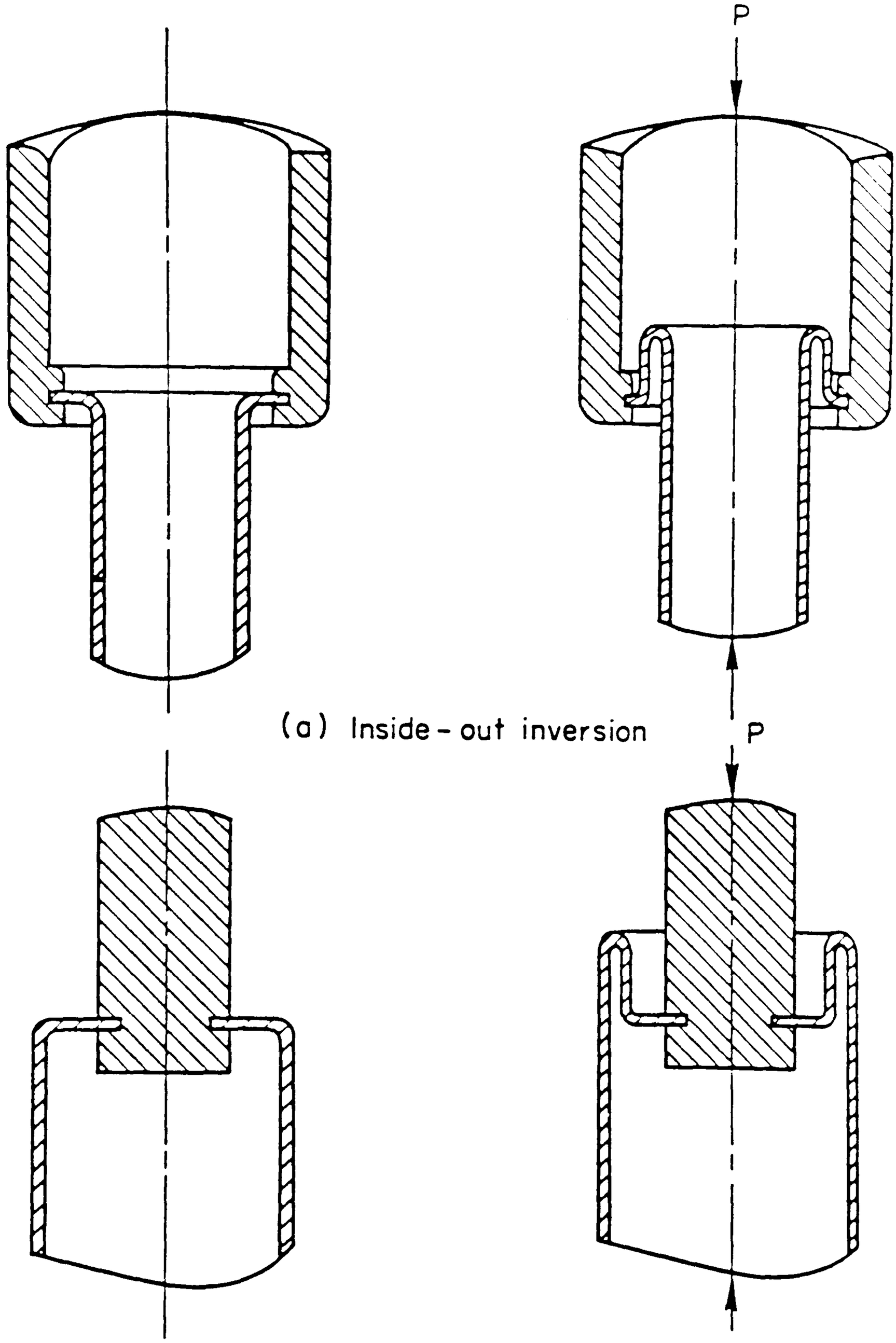

(a) Inside - out inversion

(b) Outside - in inversion

Fig. 1.13 Inversion of aluminium tube (61)

welded. It is well known that this type of adherence initiates problems like embrittlement. Finally in the conclusion, the authors summed up the validity of their analytical prediction and wisely enough added a note of caution.

Brabin(16)* while working at MIRA (Motor Industry Research Association) recommended to employ invertubes in motor vehicles. In his paper he went to the extent of describing the invertube, and its place among other energy absorbing devices. Therein, giving a calculated account of their forming sequence. Two years later Searle, together with Brabin(15)* presented a newly developed invertube which had no attachments (fig.1.14), but had to use an inverting die (inside-out) for accomplishing its collapse behaviour. By doing so, straight away they eliminated the problem of embrittlement faced by Guist and Marble(61)*. Figure 1.14 shows type 'A' and type 'B' which are virtually the designs of Guist and Marble(61)*. Type 'A' has been described above and type 'B' in this case suffers from the disadvantage that a bolt attachment to the tube has to be made, with consequent problems of local stresses. Type 'C' although looks impressive, is difficult to make and expensive especially in small quantities. The theory however, was exactly the same as that of Guist and Marble. By doing so the theory was completely spoiled. The reason being, when an inverting die is used there's a third component induced in the total work done equation and this is the energy dissipated due to friction between the tube and die interface. Neglecting friction caused the expression of true inverting load to be underrated. To compensate for this error, they employed an assumption of stress being constant at a very high value of 90% of the ultimate tensile strength. Nevertheless the predicted inverting load showed some discrepancy. In addition Searle and Brabin(15)* studied material ductility and the

effect it had over proper inversion. The results were very good and showed how tubes made from moderate ductility split open after the strain became too high for them to handle. Apart from this, for the first time, experimental results of tapered tubes and dynamic behaviour of square circular tubes were presented.

C.I.C (Cranfield Impact Centre)(17)* designed type 'E' which can be seen in fig.1.15, for use in neuclear reactor's support system. More about this type will be presented in depth later as it is the theme of this dissertation.

Al-Hassani et al (62)* observing the same objectives, produced a magnificent paper which introduced outside-in inversion using an internal inverting die. Their experiments included quasi-static and dynamic tests. In the tests they employed various materials for the tube and established the effect of material properties. They also studied the effect of tube variation thickness, which showed that the inside-out (externally) inverted tubes suffered no significant change in thickness, while the inverted portion of outside-in (internally) inverted tubes had 1½ times the original thickness. This attributed to more energy absorbed by internal inversion. The most interesting part of their work was the study on the effect of die radius and die angle upon inversion. The load-deflection curves for 2.38mm, 3.97mm, 6.35mm and 9.53mm die radii are depicted in fig.1.16. It can be seen that as the radius is decreased from the critical value of 3.97mm the initial peak load is amplified to more than twice for the 2.38mm radius die and consequently early buckling is followed. Increasing the radius has the opposite effect. The initial peak diminishes until the 9.53mm radius die is used when no initial peak is noticed due to the tube fracture. With view of inverting load, the 6.35mm die

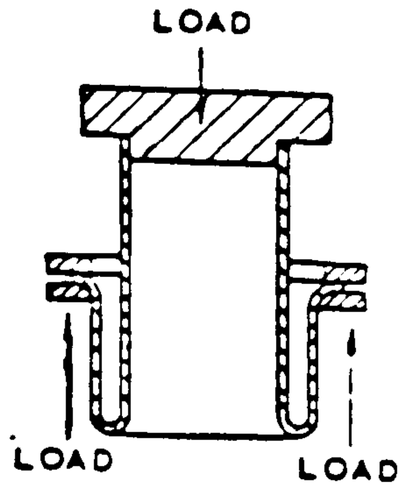

Type 'A'

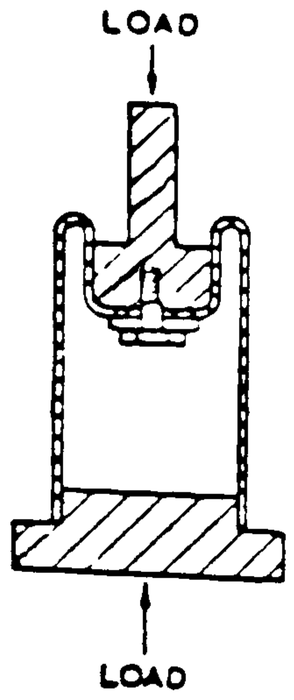

Type 'B'

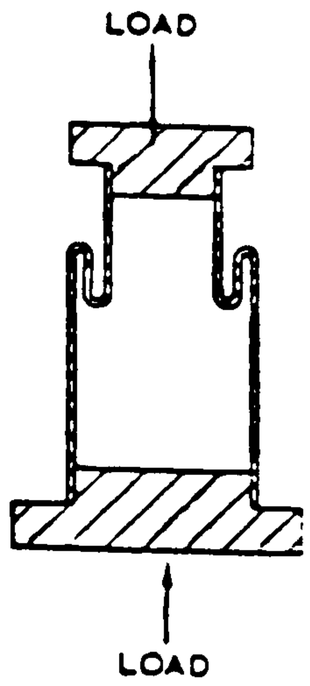

Type 'C'

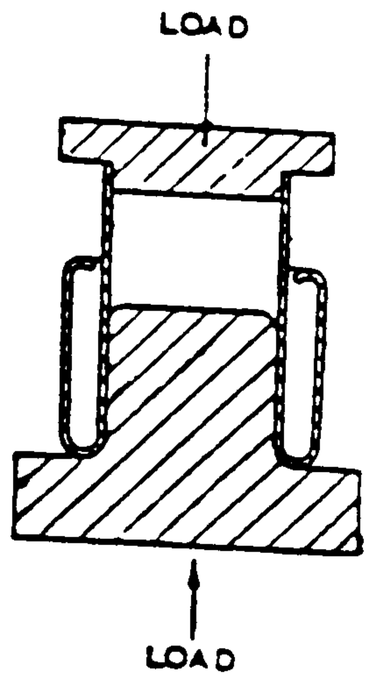

Type 'D'

Fig. 1.14 Types of inversion (15)*

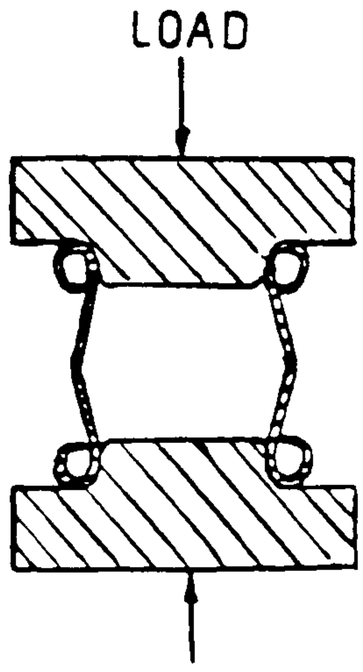

Type 'E'

Fig. 1.15 C.I.C. inverbucktube (17)*

radius produced the best curve with a maximum relatively steady load to collapse distance. By using 75°, 90°, 105° and 120° (fig.1.17) angle dies, little effect in the change of steady-state inverting load is noticed.

The theory however, followed the same footsteps as that of Guist and Marble(61)*, although here the assumptions were becoming more realistic. As mentioned before Guist and Marble(61)* assumed that the material was rigid plastic, but in reality materials normally used for inversion are strain-hardening. This is exactly what Al-Hassani et al assumed and utilised an empirical effective stress-strain relationship which closely fitted the stress-strain curve obtained from the tensile test.

However, there was one component missing from the total energy absorbed equation, i.e. work done due to friction. They lubricated the surfaces and assumed there was no friction. In invertubes, this process just minimises the amount of energy dissipated to overcome friction (64)*. The experience acquired, showed that this component (friction energy) increases the total energy by a great portion of about 25% on the inside-out inversion and could go up to about 45% on the outside-in inversion depending on the tube and die geometry. In short, it is thought they knew all about the friction but did not know how to approach the problem as it is very complicated and as will be seen later in this work.

Two years later Al-Hassani(63)* extended his work(62)* with an additional part which tried to describe the limit in which proper inversion was forseeable. Friction was also mentioned but not tackled. He noted that due to the neglect of friction in particular his inversion load expression underestimated the actual value.

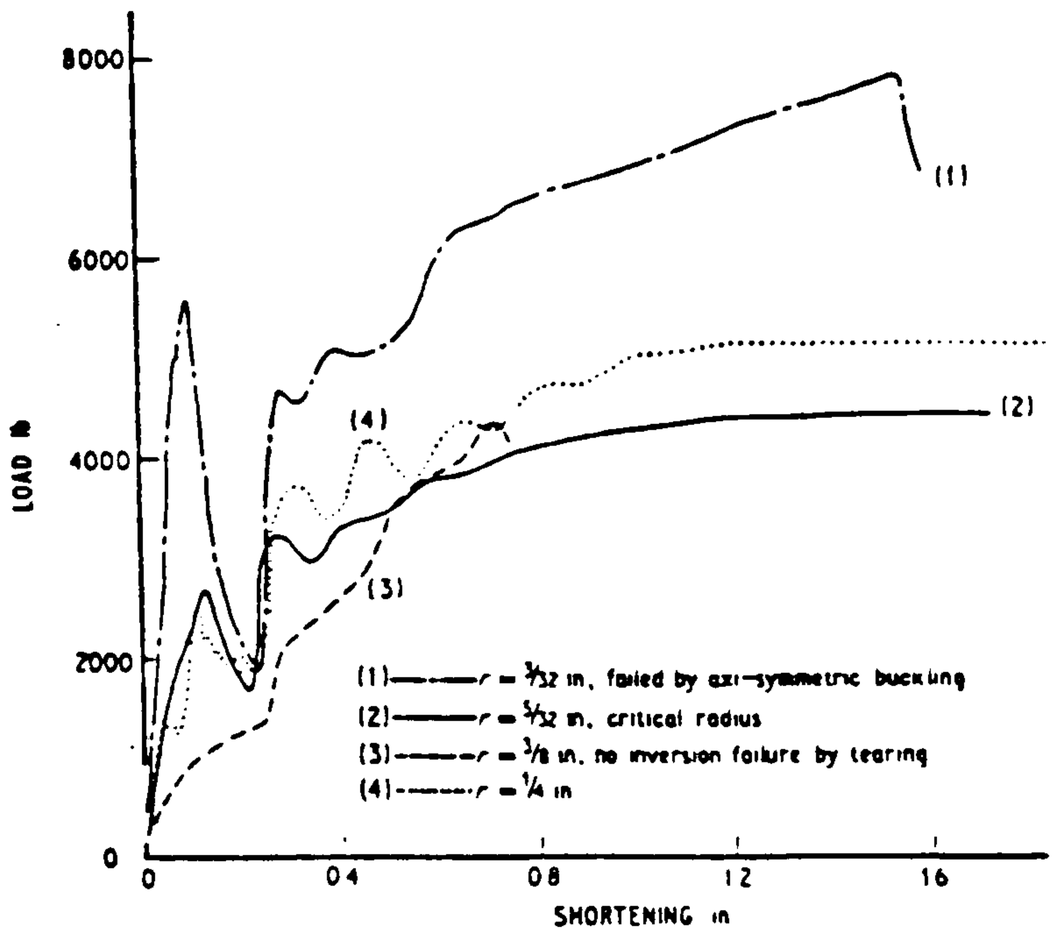

Fig. 1.16 Load-shortening curves for external inversion of 2 in outside diameter, 3.5 in long, 0.064 in thick h-h aluminium tubes at various die radii (62)*

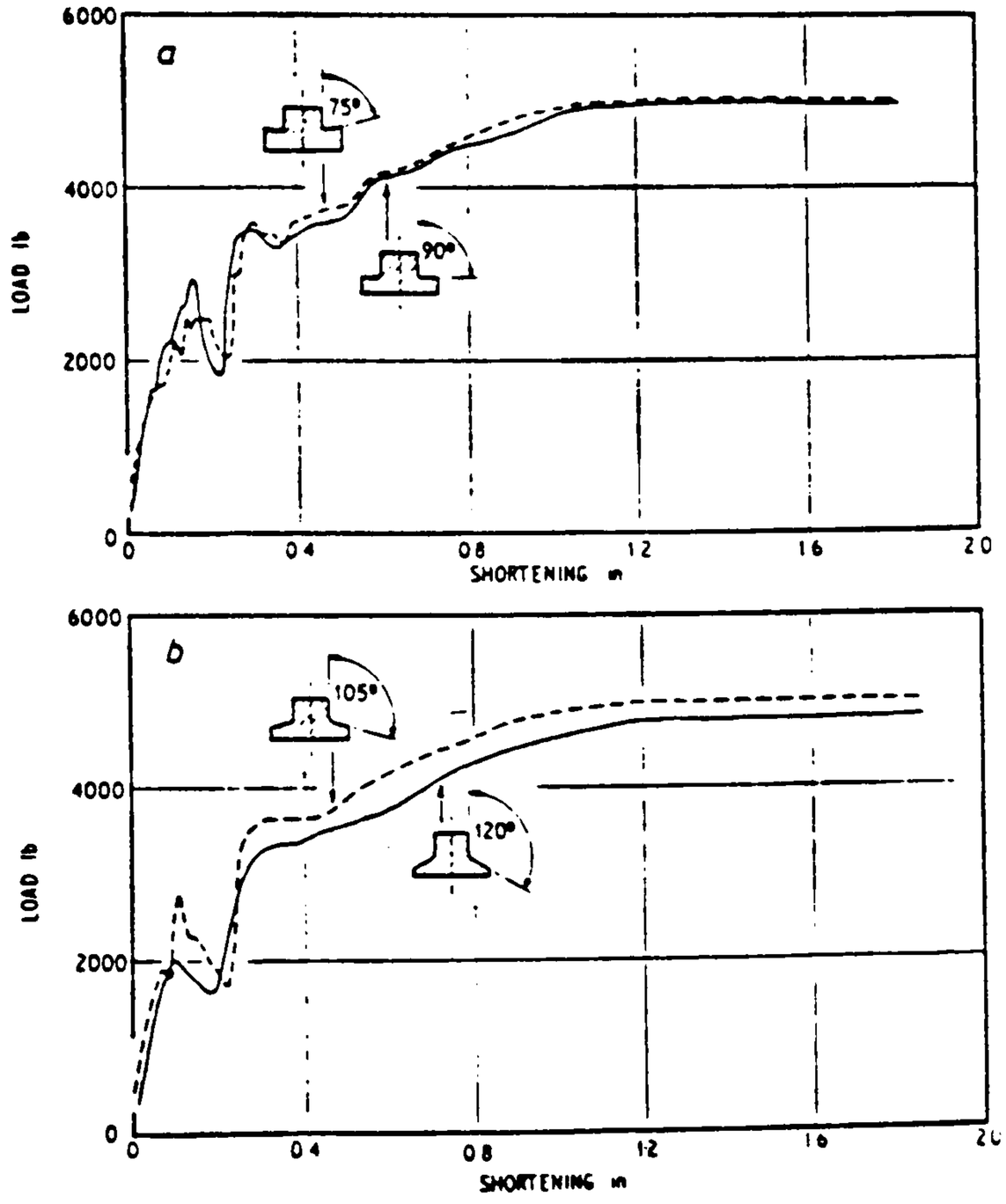

Fig. 1.17 Load-shortening curves for external inversion of 2 in outside diameter, 3.5 in long, 0.064 in thick, h-h aluminium tubes at various die; constant die radius 5/32 in (62)*

Al-Qureshi and DeMorais(64)* studied the inversion of copper and brass tubes. They proposed the same theory as previously stated, but this time the friction component in the total work done was incorporated. In addition, instead of using the full Ludwik's expression for the emperical effective stress-strain relationship, they opted for the expression which had yield stress equal to zero. This sounded to be reasonable. Furthermore, they studied the hardness distribution of the inverted part of the tube material. Results showed that there was a considerably greater increase in hardness in the outside-in inversion than in the inside-out inversion and a significant increase in hardness was noticed towards the central section of the radiused region than in the entrance and exit regions. In addition, a microstructure analysis was carried out. Here, severe deformation pertaining on the decrease in sizes of grains were observed.

The only problem noticed, was to understand how they determined the energy dissipated due to friction forces. Going through the paper, the total contact area between the die and the inside bore of the tube was exagerated, thus overestimating the work done, which in return pushed up the total energy consumption. Nevertheless, the method used for friction energy forces was right in principle and introduced us to new avenue.

Abramowicz and Sawczuk(65)* studied the case of outside-in plastic inversion and proposed a theoretical model where the yield criteria and inverting load could be determined. Using the model, they presented results which had a discrepancy of up to 20% with the experimental values.

Kinkead(66)* carried out two theoretical approaches in the mechanics of inside-out and outside-in inversions, and extended the theory presented previously by introducing two additional sub-structural mechanical processes. These were namely, the energy absorbed in flexure in the direction normal to the meridional plane while each element of the tube was straightened from initial curvature and the reversed bending of the element until it attained finally the curvature. In his theories, he put an emphasy on using the engineering strain units rather than the natural strain units which were normally was used by his predecessors. It was thought that this was just a duplication of work, because the differences according to his results of engineering and natural strain units were very small. Furthermore, the incorporation of two other processes in the theory pushed up the predicted load away from the experimental value in the wrong direction. Their work is not disputed, infact it is thought that, it is correct to add these two processes, but how to theoretically formulate them is another matter.

Stronge et al (67)* studied scrolling and fracture of square tubes which dissipated energy by fracture, friction and plastic deformation. They carried out a series of tests on which they based their limit analysis.

On the other hand, Reddy and Reid(20)* proposed similar type of dissipating energy as Stronge et al(67)* but using circular tubes.

1.4 REVIEW OF AXISYMMETRIC BUCKLING ENERGY ABSORBERS

Earlier on in this chapter, Alexander's(3)* work in which he developed an approximate theory of thin-walled circular tubes with a concertina mode of deformation was introduced, see fig.1.18. Twelve years later Johnson(69)*

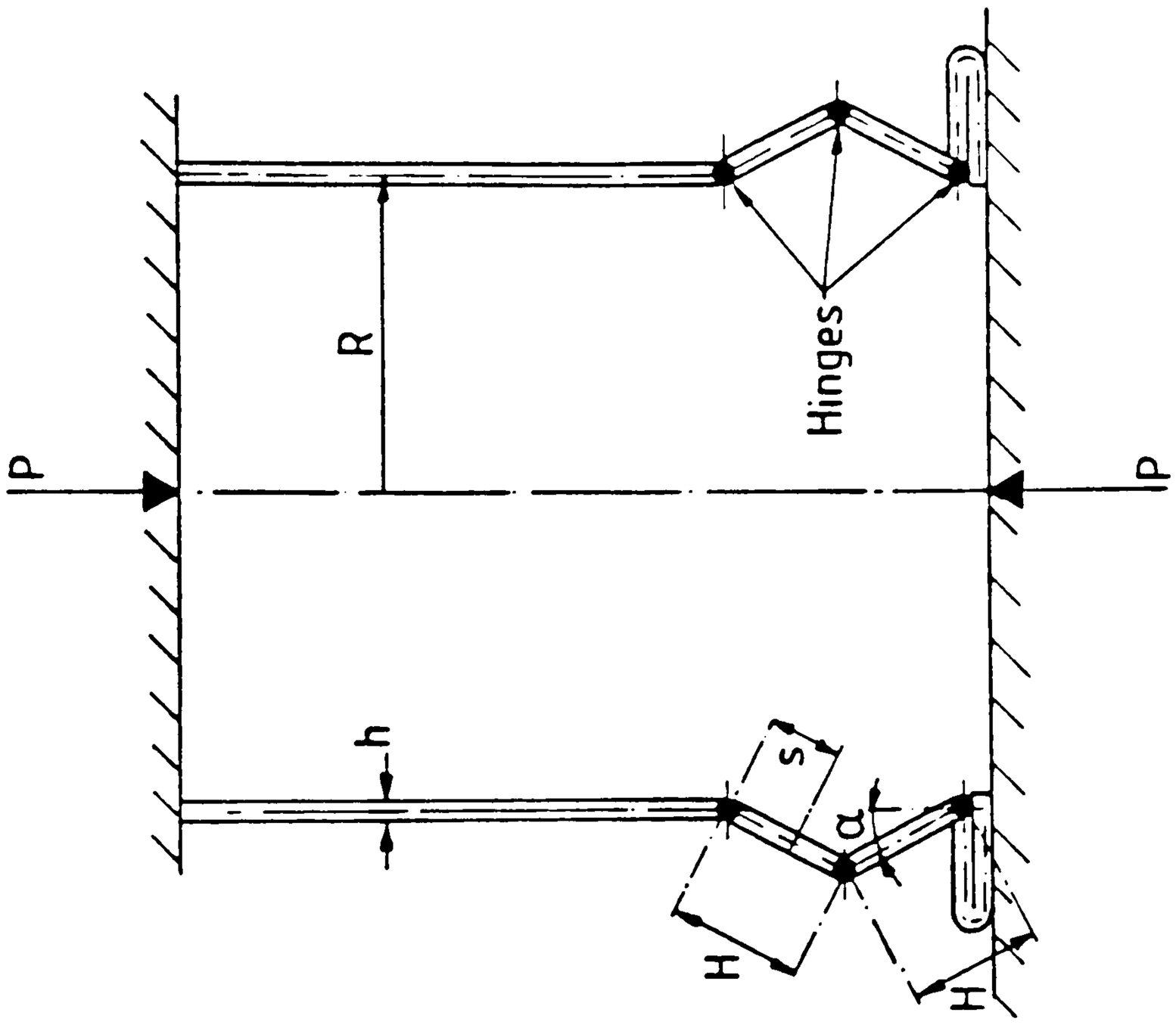

Fig.1.18 Ideallised axisymmetric collapse mode for an axially compressed cylindrical shell (3)

produced an alternative derivation of this analysis, with the assumption that the material was rigid-perfectly plastic and circumferential plastic hinges were stationary.

A modified version of Alexander's and Johnson's theoretical analysis was developed by Abramowicz and Jones(36)*. They used similar assumptions for the energy dissipated in the three stationary circumferential plastic hinges during the collapse of one lobe. The difference came into the assumption used to determine the energy dissipated due to circumferential forces. The latter took into account the variation with the distance between two hinges. However, the two theories ((3)* and (36)*) did not have a significant difference. When figures were put into the equations, the variance found was about 5.7% for D/2t=9.5 and got even smaller with an increase in D/2t. Two years later the theory in (36)* was again modified to that found in (70)*. This was based on Wierzbicki's and Bhat's theory(71)*.

1.4.1 SUMMARY OF THE REVIEW OF ENERGY ABSORBERS

All these studies have presented tube crushing in relation to energy dissipation. Infact few of the past experiments and analyses have considered largely the quasi-static deformation of these structural elements.

As stated earlier on, quasi-static analyses are very useful in providing insight into structural element responses under impulsive loading. This behaviour could be feasible only when structural velocities are not sufficiently high for inertia and strain-rate effects to significantly affect the mode of deformation.

On the whole, there has been much less work devoted to the dynamic response and deformation of invertubes. This is because, the inclusion of inertia and strain-rate effects into problems dealing with large non-linear displacements often makes a purely analytical approach without simplifications untenable. In general most researchers have adopted the philosophy that quasi-static results are applicable to dynamic situations for the reasons given above. In cases where this holds, designs of impact absorption devices have been successfully implemented based on quasi-static analyses, though an emperical approach to account for dynamic effects has occasionally been incorporated.

The theory of invertubes which was introduced by Guist and Marble(61)* through to Kinkead(66)* presented a good physical understanding of inversion type of collapse behaviour.

Up to date, nobody has introduced the theory for tapered inverting tubes, although some experiments were conducted by some of the predecessors. This dissertation will introduce this for the first time and will combine two modes of collapse behaviour, namely inversion(curling) and axisymmetric buckling.

1.5 REVIEW OF THE CONTACT STRESSES DETERMINATION

For many years it has been a prime requirement in metal rolling to obtain a measure of the way in which pressure varies across two surfaces in contact. A number of attempts have been made, especially in cold metal rolling.

On the other hand, despite vast amount of work done in invertubes, so far nobody has tried to determine the

pressure distribution between the inverting tube and the die. This dissertation will do so for the first time.

To have an idea of the way the tests will be conducted, a survey of published material concerning pressure distribution in roll gaps and the methods used was made.

1.5.1 METHODS OF MEASURING NORMAL CONTACT STRESSES USING PRESSURE TRANSDUCERS

It is very difficult to pick out the first experimenter in this field. To our knowledge in the western world, Siebel in colaboration with Lueg(23)* in 1933, was able to make the first practicable demonstration of the method which was the only satisfactory approach to the problem at the time. The two used a fairly large *"pressure pins"* of 2x2mm, to obtain results of pressure variations in the roll gap during cold rolling of copper, aluminium and iron specimens.

The pressure pin as shown in fig.1.19 was mounted in the roll, made flush with the roll at the outer end and pressed upon a piezoelectric crystal at the inner end. This method produced results, although due to the large ratio of pin width to the length of the arc of contact, all recorded outputs needed substantial alterations using empirical correction factors.

In the eastern world, the work of Frolov and Golubev(24)* at the Siberian Institute of Metals in 1937, made a significant impact on the use of pressure pins, fig.1.20. Although the technique employed followed that of Lueg(23)*, it was asserted that the method used a practical realisation of an original idea by Rodzevich-Belevich in 1913. Their sensing *"pressure pin"* had a

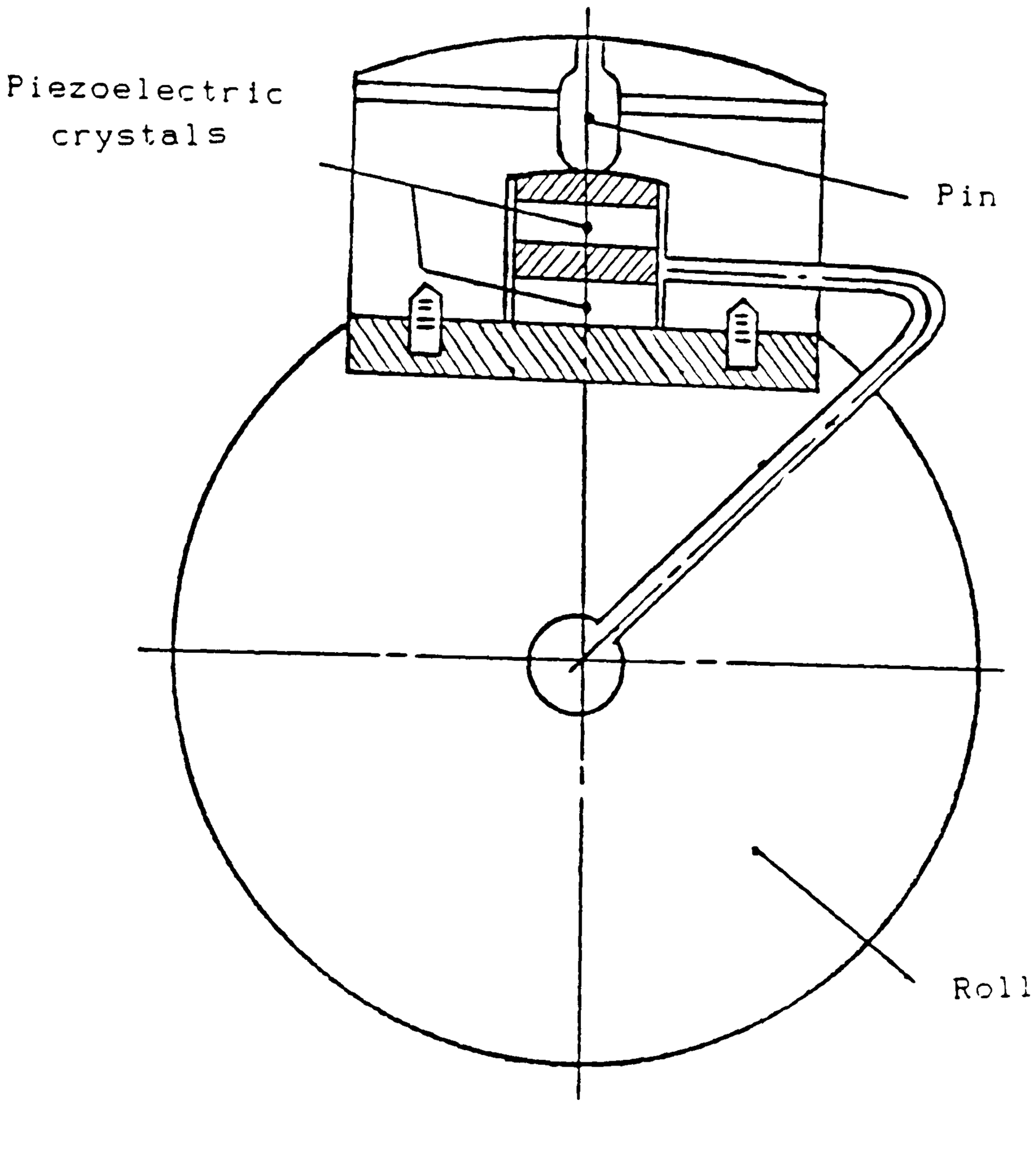

Fig. 1.19 Piezoelectric pin loadcell (23)'

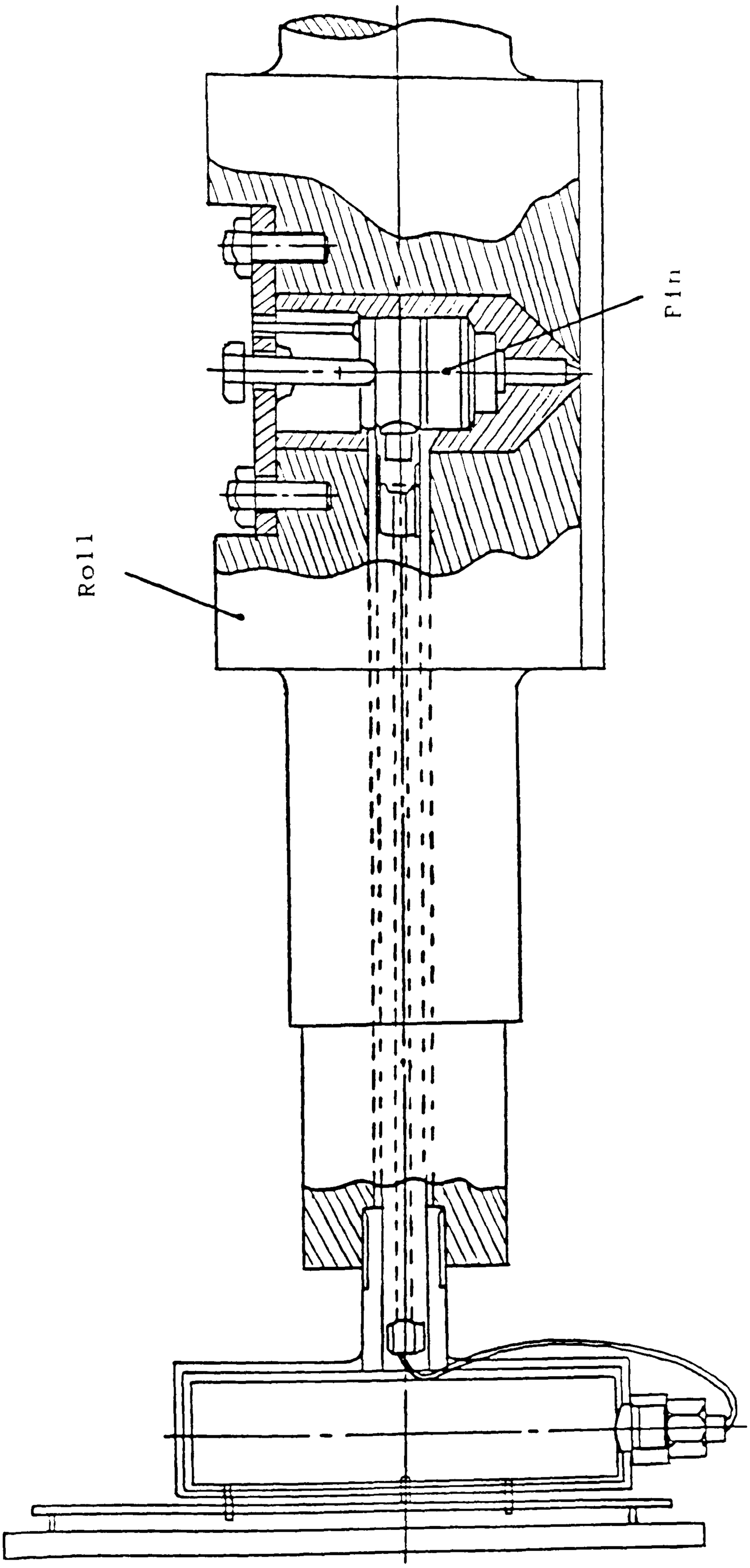

Fig.1.20 Sensing pin with hydraulic system actuating recording chart (24)

diameter of approximately 1.5mm and actuated a plunger on to an hydraulic system which presented the final results by movement of a pen on a chart. In addition, this was used for determining the contact stresses during rolling of steel at temperatures up to 1000°C. Their results showed good agreement with the work in Lueg(23)* and the application to hot rolling showed a real progress in the technique.

In 1948, Mac Gregor and Palme(26,27)*, having in mind the same objective, used a cantilever weighbar shown in fig.1.21, to measure the distribution of contact stresses during cold rolling of mild steel, aluminium and copper square bars. The mode of action was that the pin deflected a cantilever carrying SR-4 electric resistance strain guages. This work produced the first ever comprehensive report on the mechanics of metal rolling and gave an introductory account of what is expected of pressure measuring devices.

Orowan et al (37)* took a rather different avenue to the solution of the problem of the conversion of pressure pin movement into a load signal. Their instrumentation was similar to that in Lueg(23)*, although they superseded the piezoelectric crystal by a photoelastic dynamometer. Results obtained are depicted in fig.1.22. Furthermore, this work reviewed for the first time the problem of recession or protrusion of the pressure pin with respect to the working surface. The results showed a protrusion of less than about 4% of the pin diameter, which brought about error in the maximum recorded stresses of less than 3%. In the overall view, this technique proved to have advantages over Siebel and Lueg's work.

To ackowledge this, Bergen and Scott(38)* in 1951, applied it to the calendaring process in which a mass of "plastic"

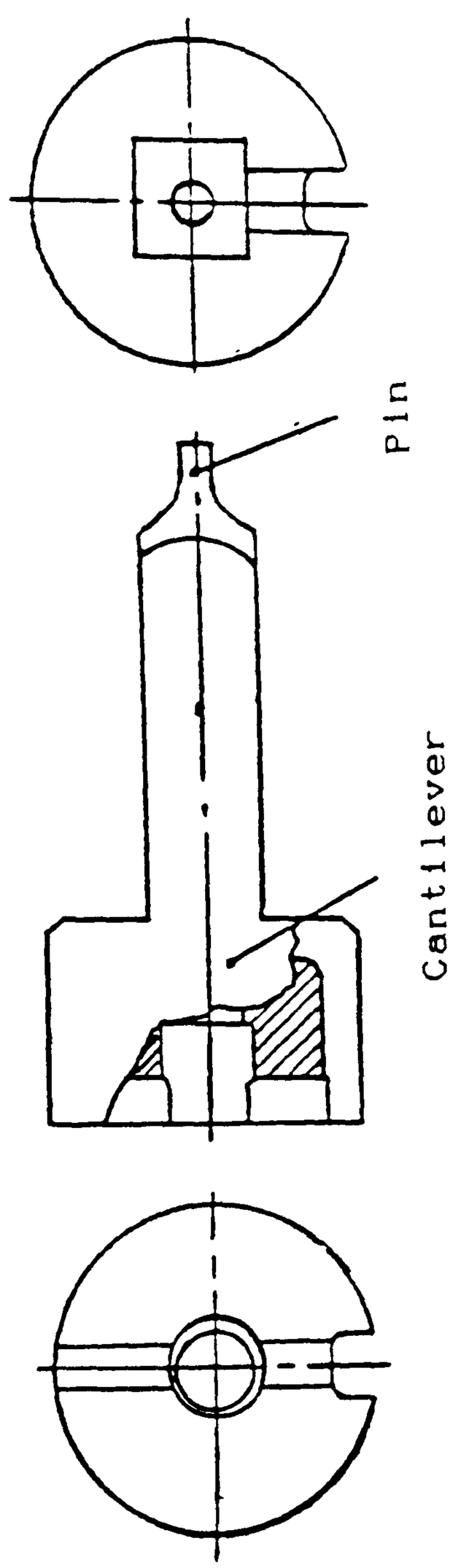

Fig. 1.21 Cantilever weighbar and pressure pin (26)'

material of indefinite shape was rolled between large rolls. That same year, Astakhov(39)* working with the flat rolling of steel, copper and brass strip specimens, presented oscillograph records from a pressure pin and pointed out the apparent length of the arc of contact.

To improve on the work in Orowan et al(37)*, Smith et al (25)* showed that the greatest difficulty in Lueg(23)* was that the finite width of the pressure pin being square. They therefore presented an analysis for the correction of the pressure pin width and were able to make a formal correction for the effect mentioned by Astakhov(39)*, in modifying the beginning and the end of a normal pressure distribution.

In 1957, Van Rooyen and Backofen(40)* published their first paper which set out the approach to the problem of measuring the coefficient of friction in cold rolling by the use of two pressure pins in a roll (One radial and the other oblique to the roll surface), fig.1.23. The radial pressure pin measured the normal stresses and the oblique measured tangential stresses. In their conclusions they stated that measurements using an oblique pin technique were distinctly less successful than those for the measurement of radial pressure only and they were unable to assess the probable accuracy of the values for the coefficients of friction.

On this same issue, in 1958, Chekmerev and Klimenko(41)* published results of similar work to that of Van Rooyen and Backofen(40)*. In this, three pressure pins were set in one roll instead of two, so that there was no need for the reversal of the direction of rolling in order to obtain a full picture of the variations in the arc of contact and of tangential stresses. From this brief paper,

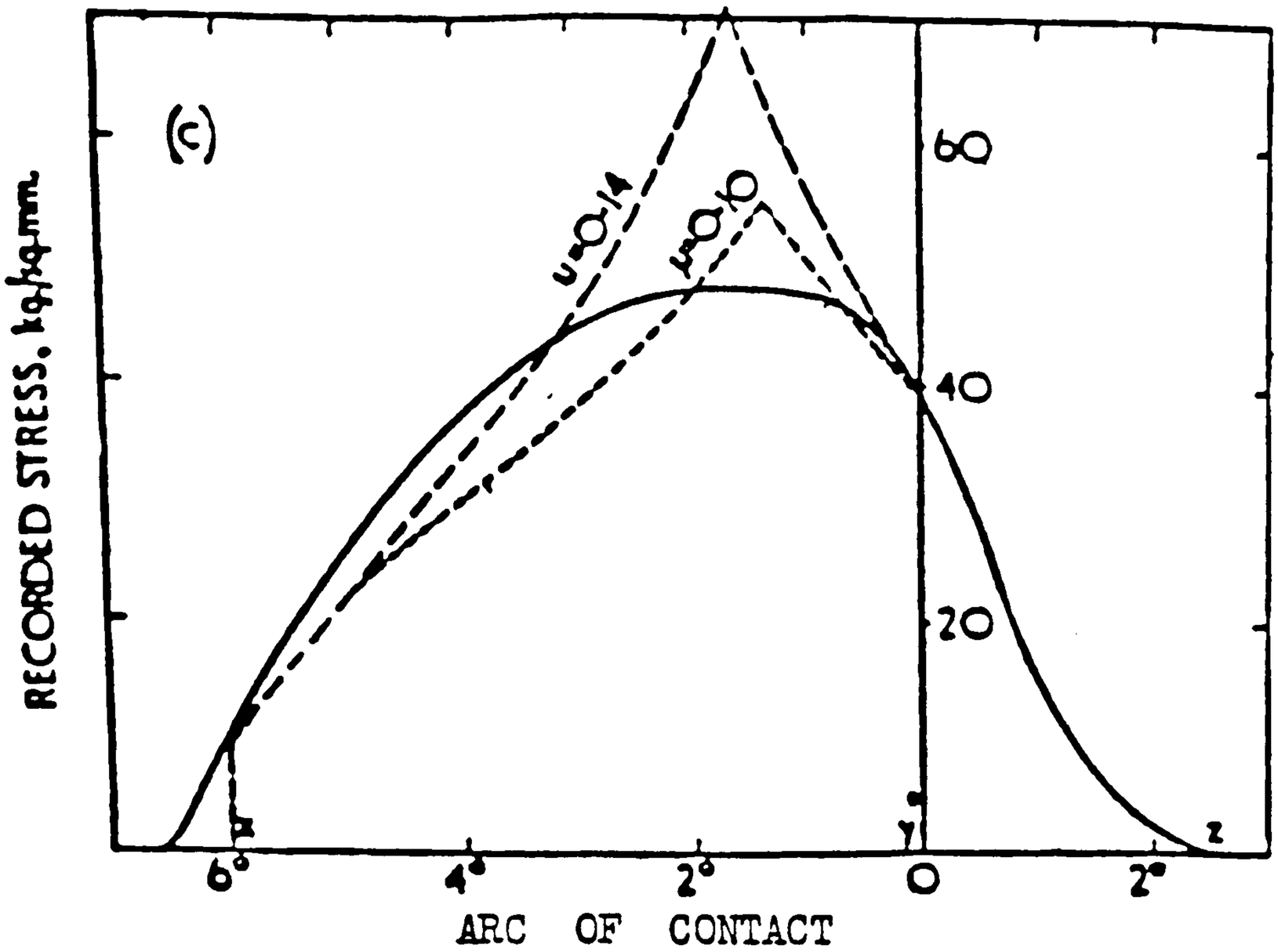

Fig. 1.22 Pressure distribution curves during cold rolling (37)*

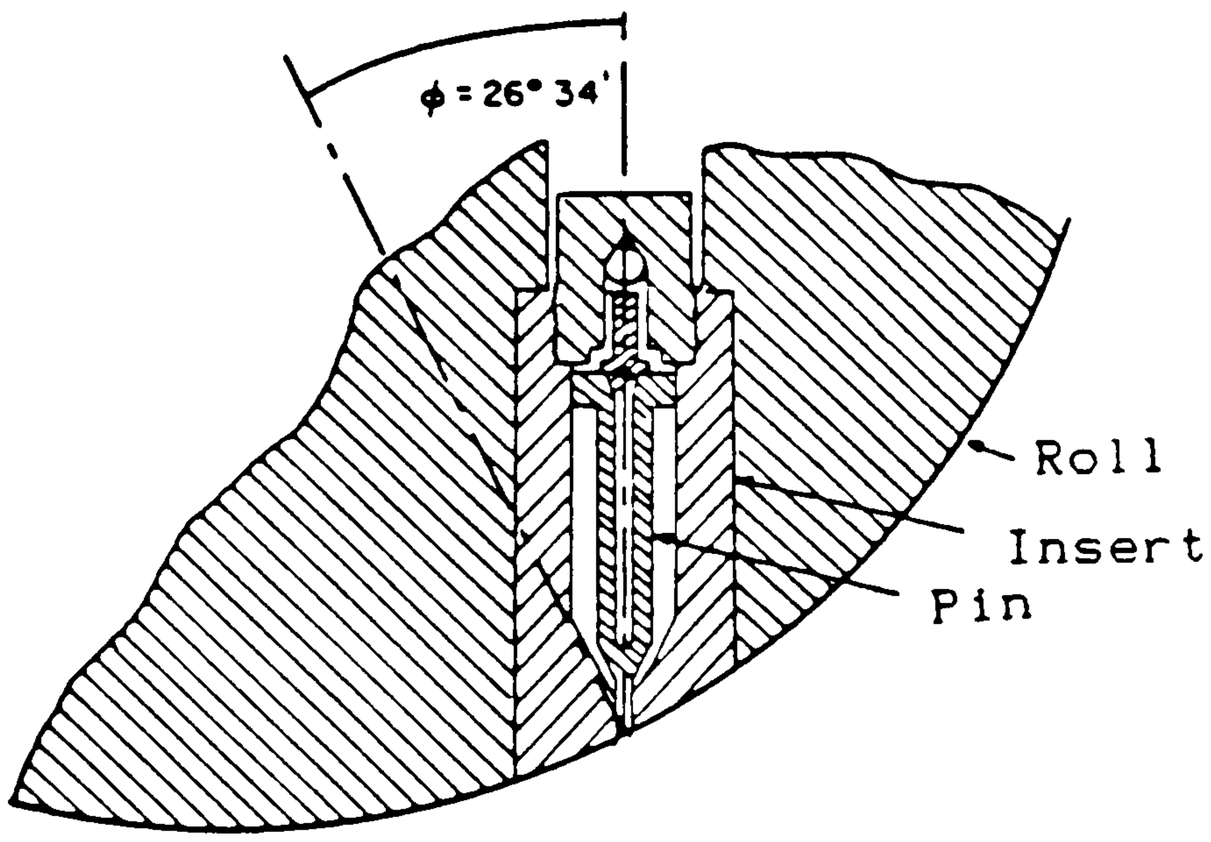

Fig. 1.23 Oblique mounted pressure pin (40)*

it was hard to say if their tangential stress measurements were a success.

The book by Korolev(42)* contained a paper on this same issue. But the sensing element in this case was a short column of carbon disc, and the effect utilised was the change in resistance of the carbon under load. On the other hand Matveev and Lavrov(43)* were concerned with tube rolling in a mandrel, the *"fillability"* of the roll groove and the effect upon the front and back forces.

El-Behery et al (44)* with the objective of applying the Van Rooyen and Backofen angled pin technique to measure the pressure and friction coefficient, developed and used a pressure pin which was identical to the Frish and Thomsen(45)* design. The results were claimed to be satisfactory, although the authors did not give an account of how they solved the problem faced by (45)*.

In 1967 Gokyn et al (72)* working at University of Tokyo on pressure distribution in wire drawing, claimed to have used pressure pins successfully. Their results was found encouraging, because if pressure pins could be used practically and effectively under such conditions, then the scope was assumed to have almost unlimited applications.

Al-Saheli et al(68)* presented a paper which described the design of transducers used by McGregor and Palme(26,27)* and measured the pressure distribution in the roll gap during cold metal rolling. In the matter of interest, a comprehensive list of published literature on the employment of pressure pins in the determination of normal stresses is given in Cole's(28)* paper on the review of the application of pin loadcell pressure measurement techniques to metal deformation processes.

1.5.2 SUMMARY OF THE REVIEW OF CONTACT STRESS DETERMINATION

It is clear from the foregoing that pin loadcells embedded in the body of metal working tools, such as rolls and dies, can be used to measure accurately the pressure distribution over the surface of the workpiece. Provided that considerable care is taken in the design. The pressure pin should be made with high precision and that it should be lapped to fit the outer housing to give minute clearance yet frictionless movement.

To make sure that the results being obtained are accurate, the pressure pin is calibrated internally in the tool before the operation. Furthermore, provided that the deflections of the pressure pin are high relative to the body of the tool, the loads reproduced by the instrument represent the stresses obtained in the workpiece.

CHAPTER II

QUASI-STATIC AND DYNAMIC TESTS OF INVERBUCKTUBE CONCEPT

2.1 MATERIAL SELECTION AND TENSILE TEST

The design of energy dissipating structures to meet legislations of crashworthiness, require a knowledge of material properties under tensile and impact conditions.

Before analysing the above, the first and foremost task was to identify materials which were relevant to this work. The short list from the numerous varieties were composites, steels and aluminium alloys.

Composite materials, are good energy absorbers as has been shown in the last few years by the data base accumulated. These materials possess numerous advantages(see Chapter I), from which one can be highlighted as the most important for the design. This was lack of plasticity which makes it unsuitable for invertubes, i.e. the ability to flow round the designed die without disintegration.

Due to this disadvantage, a choice of alternative material was inevitable. Therefore, there remained the task of either choosing steel or aluminium alloy. To select one of these for the thin-walled inverbucktubes, a few vital criteria were analysed. The characteristics which required consideration in this case were: (i) Mechanical properties; (ii) formability and consequent possible methods of inverbucktube manufacturing and (iii) costs attributable to the material per specific energy absorption.

Key points why steel was favoured to aluminium alloy included the following: (i) Strength per unit weight(22)*; (ii) energy absorption, which is nearly twice as much for equal material thickness; (iii) satisfaction of formability requirements, i.e. the need to have adequate ductility and strength, and (iv) exhibition of high energy absorption to minimal cost.

C.I.C.(Cranfield Impact Centre) used low-carbon high tensile steel in the original design. Therefore, it was thought to be appropriate to do the same, because its advantages corresponded to the requirements. The steel proposed was SKF280, which has the chemical analysis depicted in table 2.1.

The material was purchased in the form of 81.4*63.2mm round hollow tubes of length 3.0m, which were cut to near size of 150mm in length for larger tubes and 100mm for smaller tubes. Sample specimens were then cut from the tubes, prepared for tensile test using the British Standard 18: Part 4: 1971 procedures and tested to give results shown in table 2.2. In reality, what was done was to counter check the validity of mechanical properties issued by the manufacturers at the time of delivery. Test results shown in table 2.2 for *"as received"* tubes potray a very high value of strength and inadequate ductility.

In order to have a balance of these two properties, the tubes were normalized, thus eliminating the residual stresses induced during hot rolling. After normalization, new test specimens were prepared and tested to give the second set of results in table 2.2. Here, a reduction in strength and an increase in ductility is seen. This suited the purpose.

All tensile tests were conducted on a Denison testing

TABLE 2.1 CHEMICAL ANALYSIS (SKF280)

	Element %										
	C	Si	Mn	Ni	Cr	Mo	S	P	V	B	Cu
MIN	0.16	0.25	1.40				-	-	0.07		-
MAX	0.20	0.45	1.60				0.035	0.035	0.10		0.40

TABLE 2.2 MECHANICAL PROPERTIES (SKF280)

	Property			
	Yield point (σ_y) N/mm2	tensile strength (σ_T) N/mm2	elongation (δ) %	hardness V.H.
as recieved	470	650	20	134
normalised 900-920°C	430	600	28	116

machine installed at the Department of Materials, in the School of Industrial Sciences at Cranfield Institute of Technology. These were conducted at room temperature(10°C to 25°C) and at crosshead speed of $3.33*10^{-5}$ m/s. Measurements of extentions corresponding to the varying magnitudes of axial forces were determined by means of an extensiometer which was then directly connected to the X-Y plotter. The load-extension diagram obtained is shown in fig.2.1. Once the load-extention curve was achieved, it was easy to derive the stress-strain characteristic(see Appendix A) in fig.2.2. These two figures(2.1 and 2.2) clearly show that the material being used here is work-hardening. Thus, it was appropriate to represent the true stress-strain curve using a mathematical relationship which closely fits the characteristic. Many emperical mathematical relationships exist which claim to represent this, but it was found that the relationship in eq.2.1 closely fitted the experimental stress-strain curve.

$$\bar{\sigma} = A\bar{\varepsilon}^{n} \qquad 2.1$$

Values of A and n were found from the log true stress/ log true strain curve in fig.2.3. From this diagram A=812.8 N/mm^2 and n=0.249 were determined. Furthermore, hardness tests on *"as received"* and *"normalized"* specimens were conducted. Results are also presented in table 2.2. In addition the yield stress for the curve in fig.2.2 was obtained by assuming a bi-linear form(for the elastic and strain-hardening portions), and defining the yield stress as the intersection of the two linear portions. Here, it was seen that the departure from linear elastic behaviour began at a value of stress approximately 2% to 4% lower than the yield stress defined in table 2.2. Following this, there was a gradual transition to the relatively linear strain-hardening portion of the curve, which made

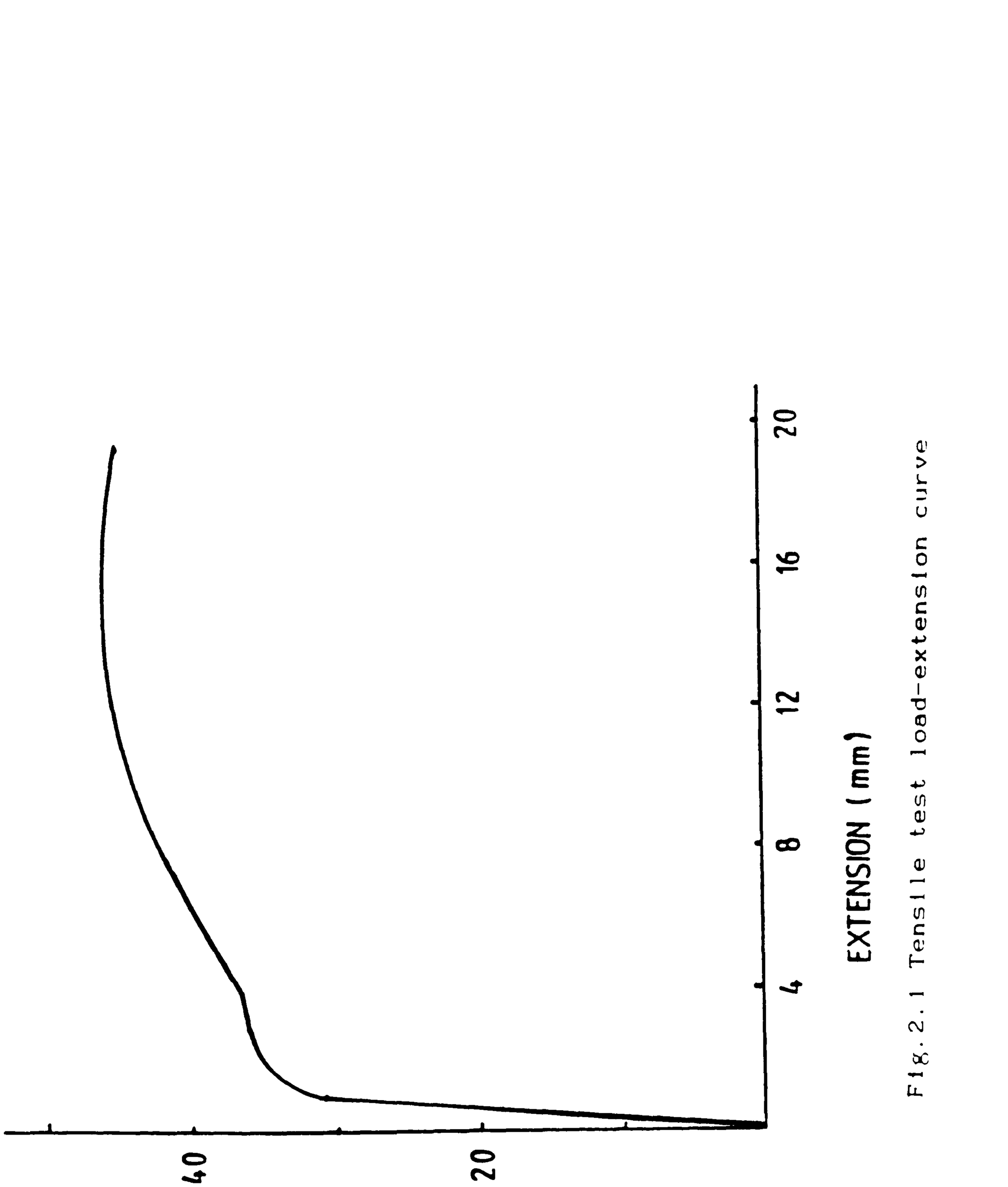

Fig.2.1 Tensile test load-extension curve

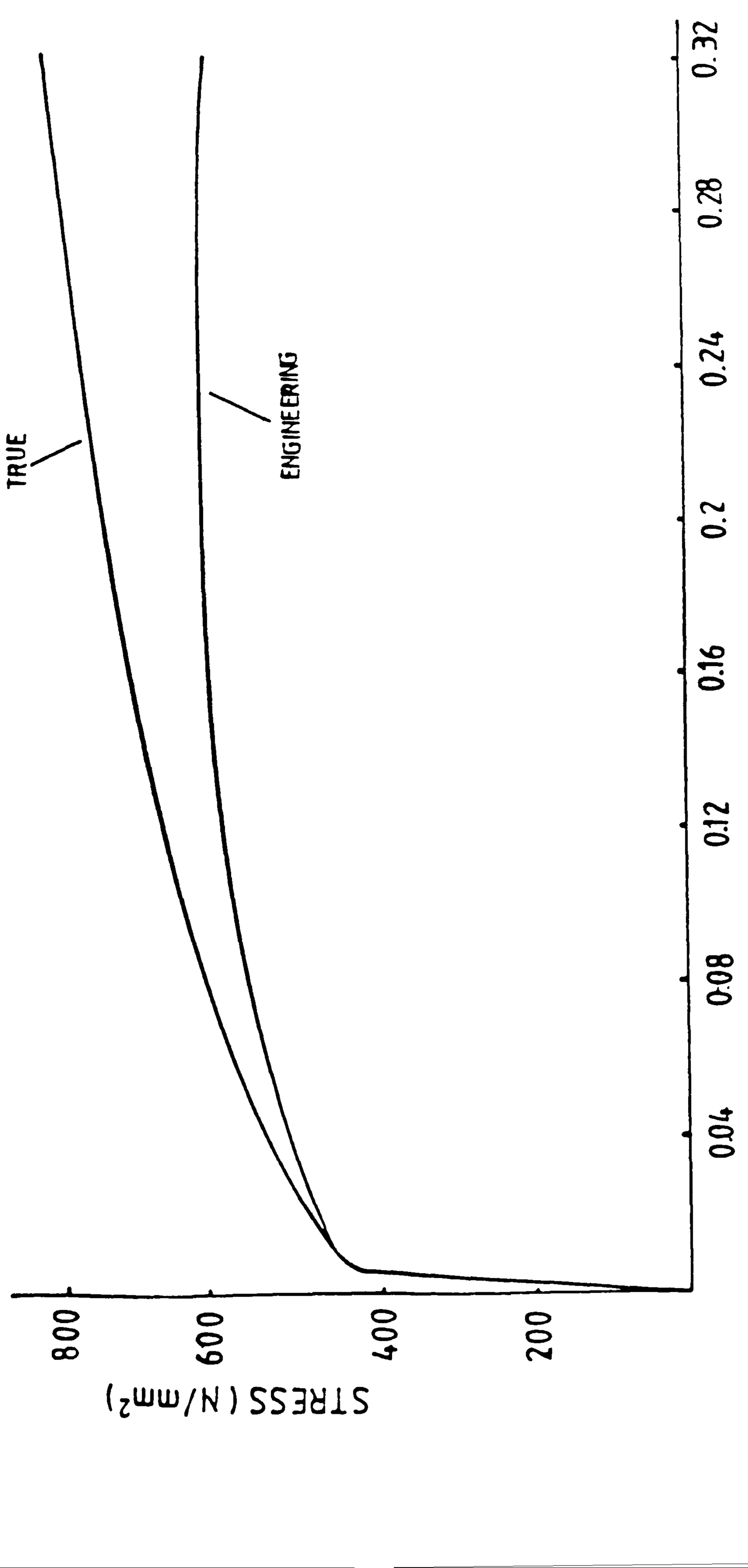

Fig.2.2 Stress-strain relationship

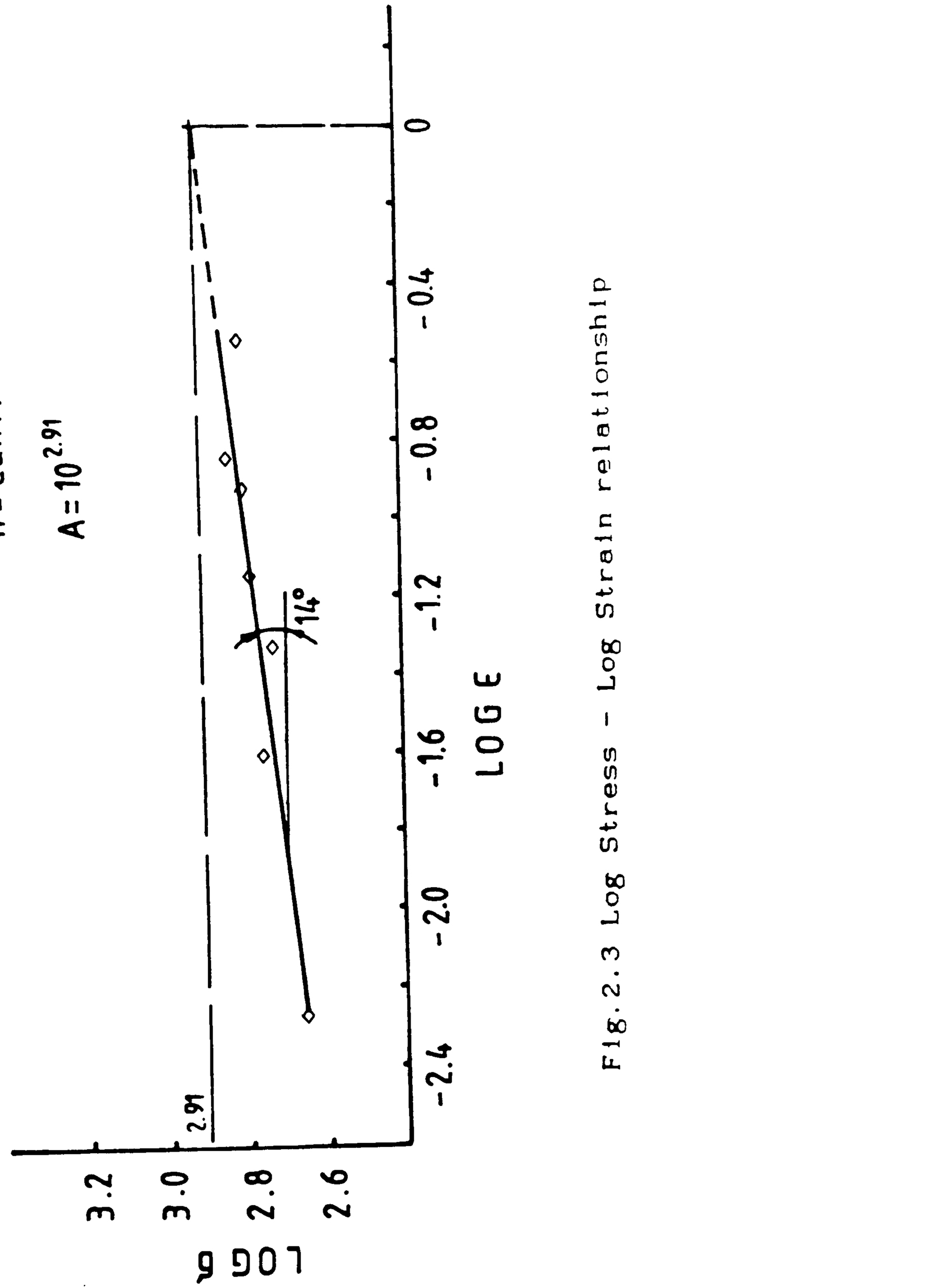

Fig. 2.3 Log Stress - Log Strain relationship

the choice of a yield point; hence, the above definition of the yield stress was used.

2.2 APPARATUS

2.2.1 QUASI-STATIC TEST EQUIPMENTS AND INSTRUMENTATIONS

The quasi-static experimental tests reported herein were conducted on a Servo-hydraulic Universal Machine type 'F' (figs.2.4a & 2.4b), installed in the College of Aeronautics at Cranfield Institute of Technology. This machine comprises of a two column loading frame mounted on a totally enclosed base cabinet which houses a fatigue actuator. The rig has a variable maximum static load of ±600KN and a variable crosshead quasi-static test speed of up to $5.83*10^{-4}$m/s.

Specimens were tested in a single working space between the actuator piston rod which projects through the base cabinet and the fatigue rated low profile load cell fitted to the underside of the crosshead. Electrically operated screws are incorporated to position the crosshead over the entire column length. Once the position of the crosshead had been chosen, manual clamping mechanisms are then employed to lock it in position. To this particular machine an adjustable trip rod assembly was fitted, to enable the crosshead to be repeatedly returned to the same position once moved.

The Universal machine type 'F' operated in conjuction with a R.D.P. System 2000 Control Console and 'M' Range Hydraulic Power Pack. Through the Console Control went all load cell signals and displacement potentiometer signals which when plotted on an X-Y plotter, gave a load-shortening history for all experiments. See the data acquisition flow chart shown in fig.2.5.

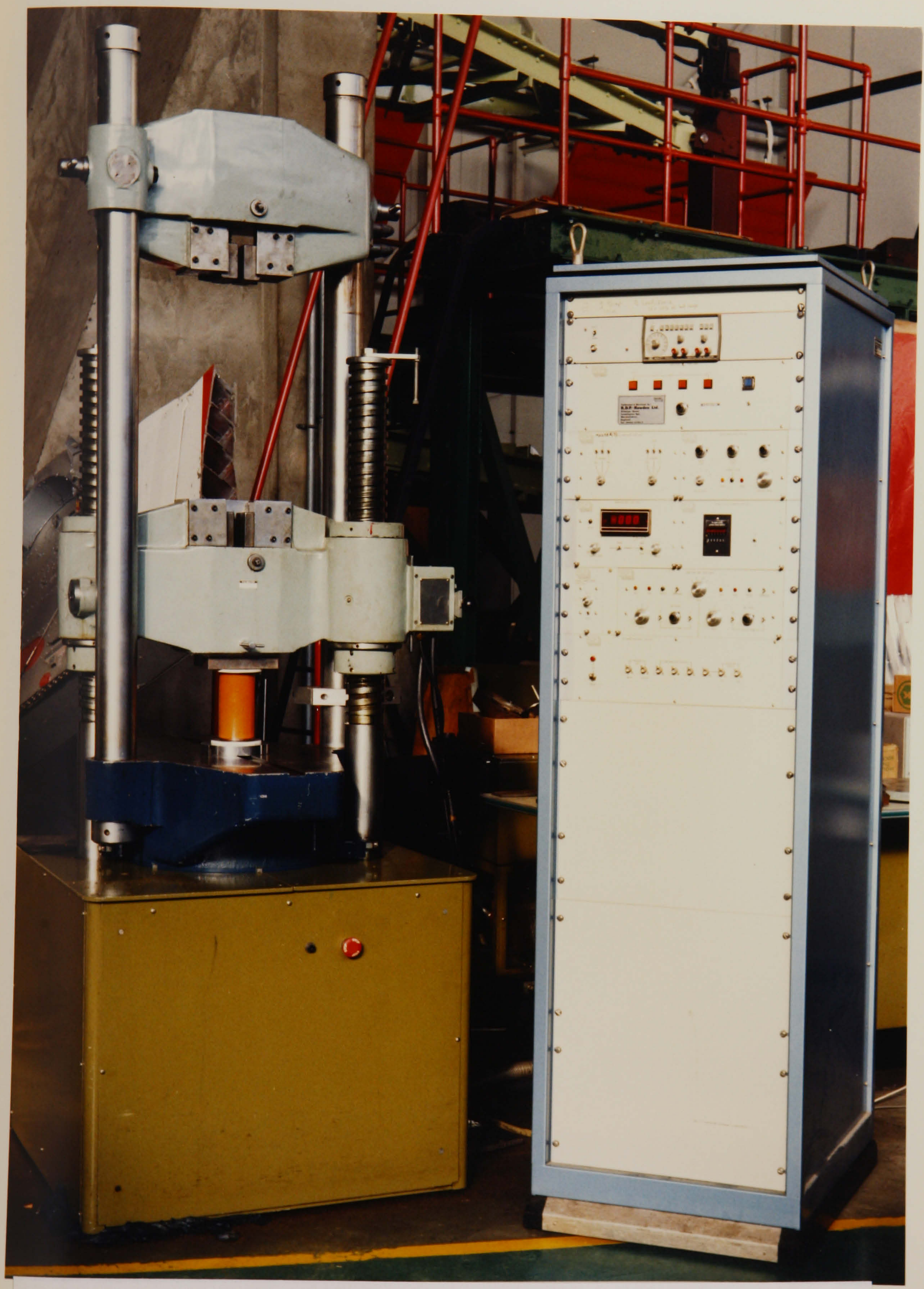

Fig.2.4a Quasi-static experimental test arrangement

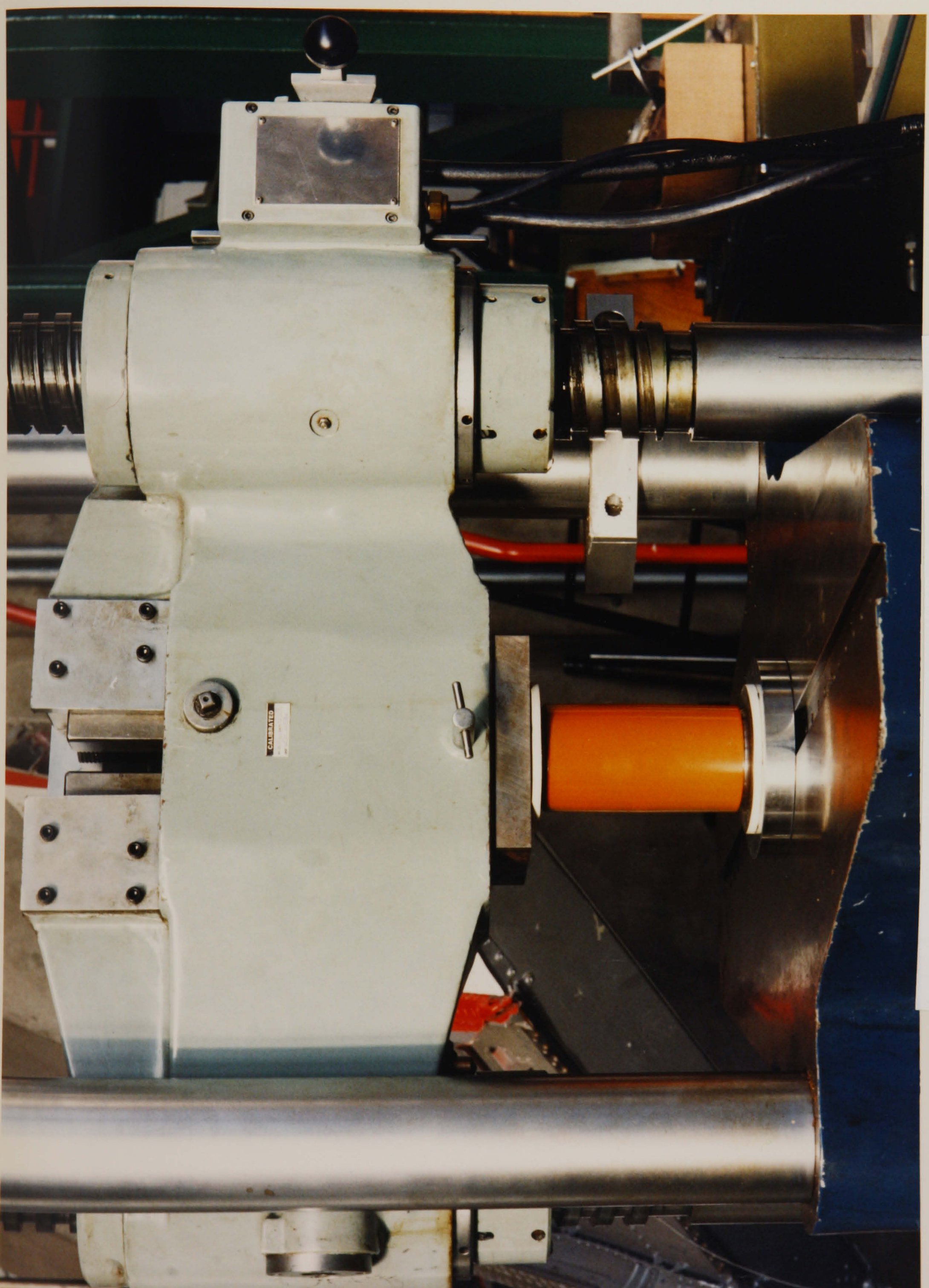

Fig.2.4b Application of axial load

STATIC TEST

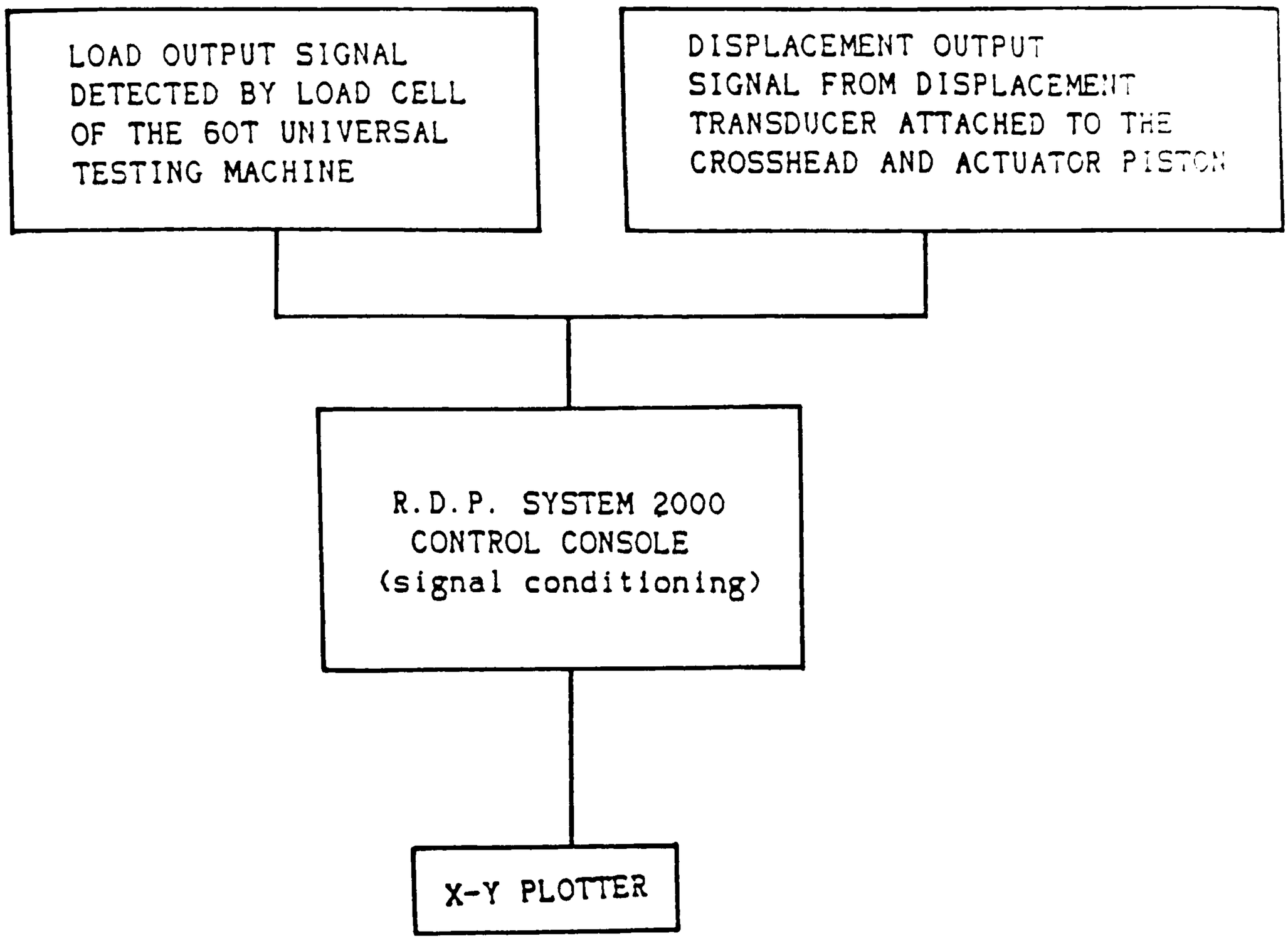

Fig.2.5 Data Aquisition Technique

2.2.2 DYNAMIC TEST EQUIPMENTS AND INSTRUMENTATIONS

All inverbucktubes were dynamically deformed by the impact of a trolley. This is a type of *"toboggan"*(fig.2.6) with a flat front face and aircushioned by air bellow springs. The rig as a whole, is owned by C.I.C Ltd., and installed in the College of Aeronautics impact laboratory at Cranfield Institute of Technology.

The impact mass on this particular rig varies from 700kg(effective mass of trolley) up to 11000kg, which could be placed behind the vertical impact block. The velocity of the trolley varies up to 8m/s depending on the height positioned.

For the purposes of analysing the impact characteristics and also the mechanism during the stroke, it was decided that the following parameters would need to be measured, using the following methods:

(i) Acceleration; Two peizoresistive accelerometers were mounted onto the rear surface of the impact block to measure its deceleration. These accelerometers had a frequency response of 1HZ to 36KHZ and were capable of measuring accelerations of up to ±1000g. Two were used so that a comparison between the signals could be made to check the relative consistency and accuracy of the results.

(ii) Velocity; Impact velocity measurements were made by using an optical sensor. This comprises of a light source positioned approximately 2000mm away from two photoelectric cells.

To measure, log, store and analyse the data from the above instruments the folowing equipments were used:

Fig.2.6 Trolley ramp dynamic rig

(i) Trigger operated timmer; to measure time between the breaking of light to two photoelectric cells, thus allowing the impact velocity to be calculated. This is determined by dividing the constant distance between the two photoelectric cells to the time measured by the timer between the breaking of light to the first and second photoelectric cells.

(ii) Filters and 'Fylde' transducer amplifiers; to modify the transients of an output waveform and amplify those signals too small for measurement.

(iii) 'Nicolet Explorer I' oscilloscope; for preparation, checking, calibration of the accelerometers before testing and immidiate display of the recorded acceleration-time history after testing.

(iv) Waveform Logger dL1200; to store the very short pulses of impact in preparation for interfacing with the analysis/store computer.

(v) High speed 16-Bit computer 'Hewlett Parckard 9121'; to store waveforms/signals on disc and allow analysis of data.

See data acquisition flow chart(fig.2.7), which is given herein to summarise the processes.

2.3 QUALITY ASSURANCE LIST

Both quasi-static and dynamic loads must be applied unidirectionally. Therefore, both test rigs and necessary attachments must be assessed carefully prior testing, to maintain the direction of load.

DYNAMIC TEST

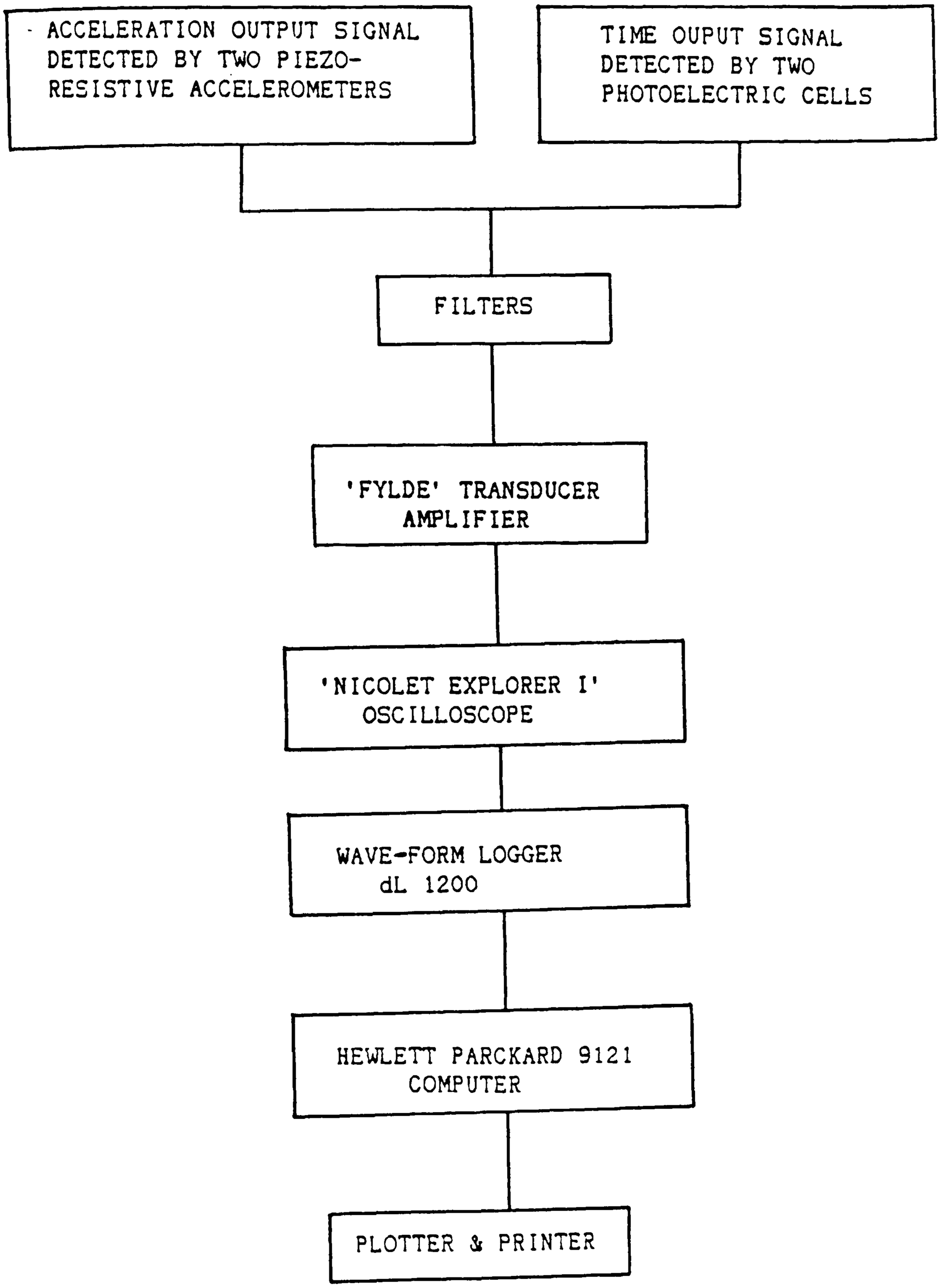

Fig.2.7 Data Aquisition Technique

The following requirements must be checked throughout testing:

(i) At load lower than 40KN no plastic deformation must be registered.

(ii) Initial plastic deformation must occur at a quasi-static load between 45KN and 350KN depending on the geometry factor, $\bar{D}/2t_{\bar{A}}$.

(iii) Initial collapse must occur at a dynamic load not exceeding 80KN depending on the geometry factor, $\bar{D}/2t_{\bar{A}}$.

(iv) The stroke of inverbucktube to do work must be in the range of 65% to 80% of the total inverbucktube length.

(v) Axisymmetric buckling must occur ONLY after the inversion(curling) has been attained.

(vi) Repeatability is very important. Therefore, inverbucktubes with exactly the same geometric parameters must indicate coherency.

(vii) In case of final design, the collapse mechanisms of quasi-static and dynamic must be similar.

(viii) The energy absorbing capacity of the dynamically tested inverbucktubes unlikely to be anything higher than 20% of the work done by quasi-static testing.

(ix) Perfect inverbuckling collapse mode must always be between proper inversion and axisymmetric buckling collapse modes.

(x) Inverbuckling must be the mode of collapse. Therefore, any other collapse is a mode of failure.

2.4 INVERBUCKTUBE AND DIE DESIGN

Inverbucktubes and corresponding dies were virtually designed from emperical method, based on the results obtained from the parametric study with a combination of theories produced here and in (3,36,62,64,66)*.

From the best random designs, results which showed perfect inverbuckling mode of collapse were chosen. The relation of dimensions were studied thouroughly and then transformed into mathematical concepts.

It was found that the total length(min.) of the inverbucktube was a function of all parameters encountered in the geometry and equalled

$$L = L(\alpha, r, \bar{D}, t_A) \qquad 2.2$$

By closely looking at eq.2.2, it can be said that, it is very important to get the relations of these parameters correctly, or else, modes of failure could be obtained. Subsequently, eq.2.2 can be written as

$$L(\alpha, r, \bar{D}, t_A) = 2l_1 + l_2 \qquad 2.3$$

If taking, say l_2, as a given data and knowing the complete rotation angle of the inverbucktube during inversion process, the minimum path or minimum curvature of the inverting part and consequently the minimum length of the tapered part can be predicted as

$$l_1 = \alpha r + t_A \qquad 2.4$$

where $\alpha = 310°$

This is the length which *"curls"* round the die and does work due to plastic deformation of the material.

Experimental results and experience gathered indicated the ratio of l_2 and $2\bar{R}$ to equal a constant value 'ϕ'. This lay between $0.132 \leq l_2/2\bar{R} \leq 0.151$. The best though, equalled the optimum average constant value of 0.145. All inverbucktubes designed using ϕ=0.145 showed excellent inverbuckling collapse modes with high specific energy and good repeatability. Once the value 'ϕ' starts decreasing, energy dissipation becomes less due early axisymmetric buckling. As it increases to the other extreme less energy dissipation is experienced, this time due to higher geometry factor.

If it is assumed that the optimum ratio is say

$$\bar{R}/t_A = K \qquad 2.5$$

knowing 'ϕ', $\bar{R}$ could be determined, which in turn can be substituted in eq.2.5 to get

$$t_A = l_2/2K\phi \qquad 2.6$$

From the experimental results, it was found that the thickness ratio was between $1.38 \leq t_1/t_2 \leq 1.43$, while the best results pointed to the ratio being $t_1/t_2 = 1.4$.

Substituting eq.2.6 into that developed for die radius in references(62,64,66)*, bearing in mind that $R_i=\bar{R}-0.5t_1$, the die fillet radius could be determined as

$$r = (l_2/4\phi)\sqrt{((1-1/K)/K)} \qquad 2.7$$

By writing a program giving l_2, ϕ and K, all geometrical parameters of both the inverbucktube and corresponding die could be determined, provided the geometry factor $\bar{D}/2t_o$ and required load is known.

To facilitate any design, a graphical method in Appendix B was developed and is easy to use and clear.

2.5 QUASI-STATIC EXPERIMENTAL TEST

Once again it must be emphasized that, it is initially very important to test any energy absorber quasi-statically before dynamic testing begins. This allows the approximate ranges of loads and the energy absorption to be quantified. Furthermore, it indicates the collapse mechanism which becomes important in the development of theory. In addition, not only is quasi-static testing cheaper option in the long term, but unexpected problems which might occur in dynamic testing could be made easier to identify.

2.5.1 QUASI-STATIC TEST METHOD

Figure 2.4a illustrates the experimental arrangement used. An inverbucktube with corresponding dies at both ends was placed on the base of the actuator piston through a solid protecting plate and raised at a very slow speed of

$1.66*10^{-5}$m/s until the top, through a second solid protecting plate was just touching the underside of the crosshead(fig.2.4b). After this, the inverbucktube assembly, the X-Y plotter and all related instruments were checked once more to see if they were on *"standby"*. Once convinced that everything was alright and functioning a uniaxial compressive force was then applied at a rate between $4.12*10^{-5}$m/s and $5.20*10^{-5}$m/s approximately. The variation in speed was brought about due to the difficulty in maintaining a constant rate, as the actuator piston was operated manually. Immediately when the complete collapse mechanism of the inverbucktube was observed, the actuator control knob on the control console was halted and then turned into the opposite direction for force removal.

Two load-shortening curves obtained from test 48 and test 49 are shown in fig.2.8 and fig.2.9 respectively. But test results of some of the 150 tests carried out are summarised in table 2.3.

2.5.2 QUASI-STATIC EXPERIMENTAL RESULTS

2.5.2.1 Inverbucktube collapse mode

To facilitate the initial discussion of the results, it is first suggested that the success of the inverbuckling process be assessed. However, a favourable outcome of the test depends on many factors. Before analysing the influence of these factors, an attempt is made to describe the attained process with reference to the tests carried out.

A typical load-shortening curve for inverbucktube having internal diameter 71.17mm, 3.99mm constant wall thickness in the middle part, 2.85mm wall thickness at both tip ends of the inverbucktube with tapering angle of 1.62° and

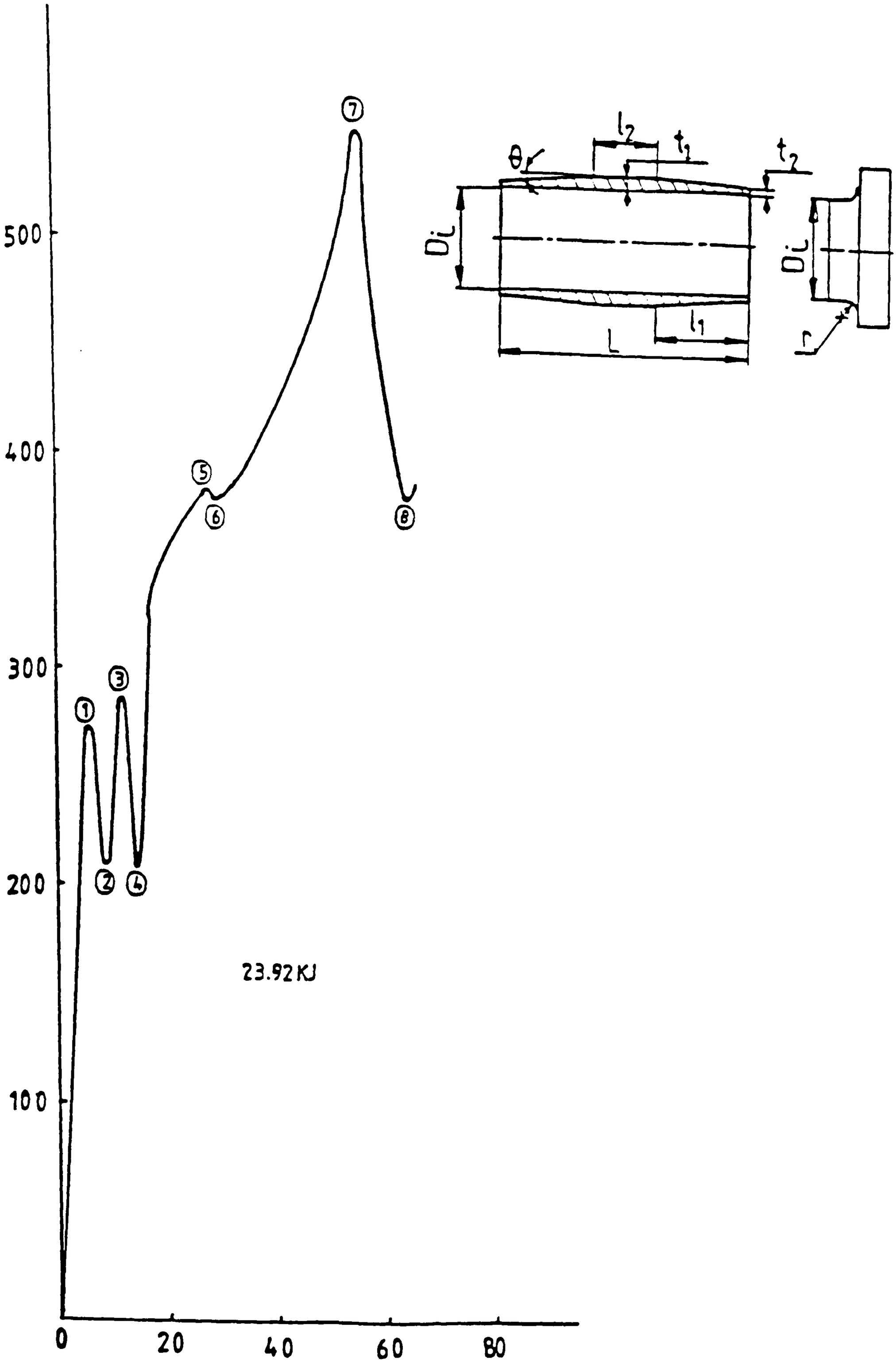

Fig. 2.8 Quasi-static load vs. shortening
(Test No. 49, Table 2.3)

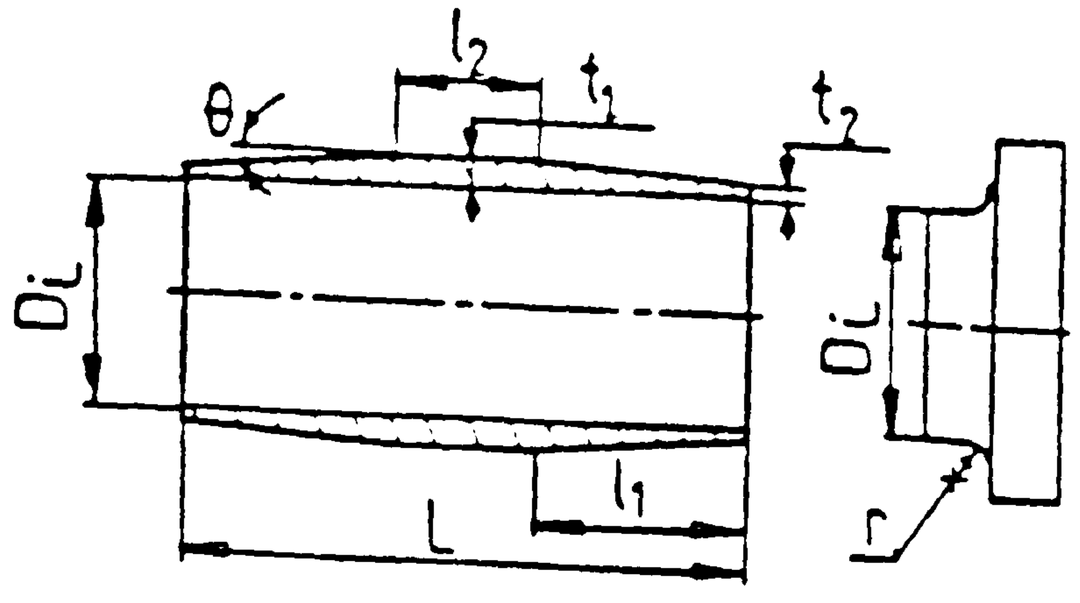

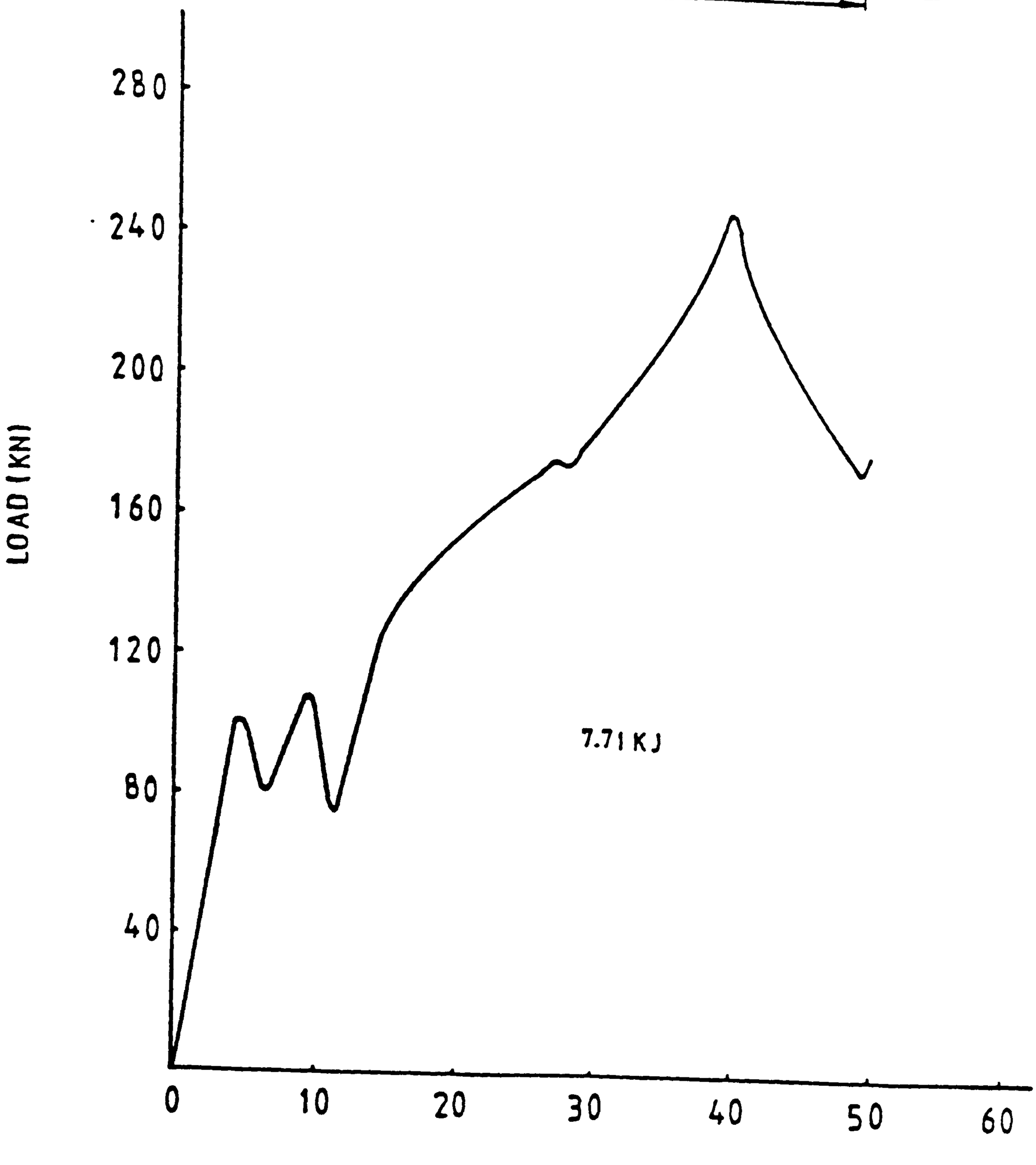

Fig.2.9 Quasi-static load vs. shortening
(Test No.48, Table 2.3)

TABLE 2.3 Quasi-static compression experimental data

TEST No.	D_t (mm)	t_o (mm)	r (mm)	L (mm)	θ (°)	V (ms^{-1}) $*10^{-6}$	δ (mm)	P_{in} (KN)	P_{buck} (KN)	$\bar{P}$ (KN)	W_T (KJ)	Remarks
1	72.14	2.67	5.8	143.0	1.27	4.45	97.5	137.5	349.5	243.5	20.43	IP
2	72.14	2.95	5.8	120.0	0.69	4.62	87.3	112.5	257.5	185.0	16.66	EAB
3	72.14	3.75	5.8	143.0	0.60	4.55	98.0	268.8	526.5	397.6	24.95	IP
34	72.14	3.57	5.8	144.0	0.78	5.16	84.0	275.0	520.0	397.5	34.00	IP
35	72.14	3.81	5.8	143.0	0.49	5.12	75.0	301.0	552.5	426.9	17.50	EAB
36	72.14	5.80	5.8	143.0	0.57	5.90	80.0	307.5	532.5	420.0	35.55	IP
45	52.46	2.45	4.3	76.0	1.74	4.56	58.5	108.0	204.0	156.0	6.52	IP
46	50.00	4.00	5.2	98.0	0.00	4.72	22.0	330.5	420.0	375.2	4.84	EAB
47	50.00	3.50	5.2	98.0	1.25	4.24	35.0	225.0	375.0	300.0	5.89	EAB
48	52.26	2.48	4.2	60.7	1.80	4.25	49.9	104.0	250.0	177.0	7.70	IP
49	71.17	3.42	5.8	81.0	1.62	4.55	65.1	281.0	550.0	415.4	23.90	IP
62	50.00	2.00	5.2	98.0	1.15	4.56	64.2	85.5	360.0	222.8	11.40	IP
63	50.00	3.50	5.2	98.0	0.58	4.62	65.0	79.5	405.0	242.3	13.70	IP
64	50.00	2.00	4.4	98.0	2.60	4.22	78.5	45.5	210.0	127.8	7.80	IP
65	50.00	2.25	4.4	98.0	1.95	4.72	83.0	86.8	228.0	157.4	10.10	IP
80	50.00	2.50	4.4	98.0	1.35	4.12	87.0	105.0	282.0	193.5	13.60	IP
81	50.00	2.00	3.6	98.0	1.30	4.32	80.0	32.0	108.0	70.0	4.90	EAB
82	50.00	1.75	3.6	98.0	0.65	4.22	83.0	55.0	135.0	95.0	7.70	IP
83	50.00	2.0	3.6	98.0	0.00	4.55	81.0	90.0	0.0	136.0	8.40	PI

IP - Inverbuckled Perfectly; EAB - Early Axisymmetric Buckling; PI - Proper Inversion only

total length of 81.0mm is shown in fig.2.8. The dies employed were of fillet radii of 5.82mm.

Looking closely at fig.2.8, it is possible to describe the various stages of deformation encountered during the inverbuckling process. It can be easily seen that the load initially rises steeply until it reaches maximum point '1'. The steep rise in load illustrates the elastic deformation of the tapered end part of the inverbucktube. At this stage(point '1'), it appears that the material of one end covering the die fillet radius partially flared outward and developed into a shape similar to a frustrum of a cone. Subsequently, a rapid fall in load to point '2' is observed due to plastic deformation of this one end, followed by full confirmity to the die at the same end. Immediately when the load reaches point '2' the inverbucktube seems to strengthen again due to compressive stresses being carried into parts with thicker cross-sections. During this same period the weaker end(second end) reached its maximum load, point '3', developed into frustrum of a cone as the previous end and accompanied by full confirmity to the second die. Then rapid fall in load to point '4' was observed. It can be clearly seen that point '4' is a little lower than point '2'. It is thought that this was brought about due to the second end trying to come in equilibrium with the first plastically collapsed end. In reality, if the material properties were spread exactly the same throughout the inverbucktube length, the two ends would have formed the shape of a frustrum of a cone at the same time. But in pratice, this is impossible as it was found from all tests carried out.

When the radii are fully formed on the tapered ends, the load rises very steeply to point '5' as the inverting parts are pushed round the dies at the same rate. From

point '5' to point '6' a shallow trough in the load-shortening curve is noted as the inverbucktube tapered end tips complete an angular movement of about 180° and come in contact with the main body, then bend slightly and hence lose strength before becoming locked. At this paraticular stage the inversion process of the tapered part is terminated just after tip bending and locking is made with the main body. Once the tip ends lock themselves to the main body, inverting load rises quickly making the middle part of the inverbucktube form a bellow like shape, which increases in its mean diameter until it reaches point '7'. At this stage, the inverting load becomes greater than the buckling load and a concertina collapse mode is observed in the middle part of the inverbucktube. After the collapse the load decreases to consecutive deformation until point '8' is reached when it strengthens due to the surfaces coming together after a complete circumferential hinge rotation of 90°. Thereafter the experiment is halted and the specimen removed from the test area.

2.5.2.2 Influencing factors to proper inverbuckling

The experimental results presented herein were concerned with inverbuckling as the mode of collapse. Therefore any other type of collapse such as tearing, early buckling(before curling is completed), complete inside-out inversion, etc. are modes of failure due to the inverbucktube not being designed and manufactured within the geometry factor limitations or improper operations.

In general, the modes of failure are dependent upon the inverbucktube/die geometry and mechanical properties, not forgetting other problems such as internal surface finish of the inverbucktube, tolerances and speed of operation.

2.5.2.2.1 *Effect of geometry limitations of the inverbucktube and corresponding die*

As stated earlier on in 2.4, inverbucktube and corresponding die geometry are interelated in their nature. The degree of perfect inverbuckling varies with its mean diameter and thickness. To be elaborate, this is dependent on the inverbucktube geometry factor, $\bar{D}/2t_A$.

Figure 5.1 depicts the relationship between all the geometrical parameters and the geometry factor. Here it can be seen that a very low $\bar{D}/2t_A \leq 6.5$ ratio, results in axisymmetric and rarely in a combination of axisymmetric and non-axisymmetric early buckling. This is thought to be brought about by the flowing material resisting smooth *"curling"* round the die fillet radius due to very high values of t_A. Consequently, this generated very high inverting loads which exceed the buckling loads, hence these failure modes(fig.2.10 E&F). In addition from the observations of fig.2.10 E&F, it was noted that early buckling into the axisymmetric mode consisted only of stretching in the hoop direction. Whereas the non-axisymmetric mode involved bending in the hoop direction. The hoop bending forces increased at a faster rate with increasing t_A. In fact the ratio of t_A with the die fillet was nearly 1:1. According to the investigations, this contributed to a great extent in early buckling.

Al-Qureshi and De Morais(64)* also observed this phenomenon in their work and suggested that $t_A \leq 0.6r$ should be used. Before referring to their work, it was conclusive enough from the results obtained that the average thickness limit was $t_A \leq 0.6r$.

With $6.5 \leq \bar{D}/2t_A \leq 22.5$, perfect inverbuckling collapse mode

is achieved. This type of collapse always lies between axisymmetric buckling and inside-out inversion. To attain this, the tube generally should be tapered at one or both ends. This is important, because it is the characteristic which triggers inverbuckling collapse in conjunction with thicker thicknesses than in inversion. Physically what happens during this process is the compression stresses are carried in sections which are always thicker than the section being deformed plastically(when inverting), until it reaches constant thickness when the inverting load becomes higher than the axisymmetric buckling load, hence the inverbuckling collapse mode. Figures 2.10c and 2.11, show one-ended and complete inverbuckling collapse modes respectively.

A high $\bar{D}/2t_{\mathcal{A}} \geqslant 22.5$ ratio results in inversion collapse mode. It is possible to elaborate on this, but there has been a lot of work done in this area by(15, 61-66)* which give a clear picture. Therefore, it is not a priority to talk about it in this work. For the matter of interest and for the determination of inverbuckling collapse mode boundaries, quite a number of tests were carried out. Two of these are shown in fig.2.10a and b.

2.5.2.2.2 *Effect of mechanical properties*

As this work was mostly based on machined normalized SKF280, variations in hardness and geometric parameters were found between batches which came from heat treatment and machining respectively. The hardness deviation from batch to batch was in the order of about 9.5%. The yield stress was in the same order too as it is directly proportional to hardness. But when analysing the yield stress, hardness and inverbucktube dimensions of one batch, discrepancies were found to be fairly small and consistent.

Fig.2.10 Possible modes of deformation depending on $\overline{D}/2t_A$

Fig.2.11 Inverbucktubes before and after collapse

It is known that the inverbuckling load is directly proportional to the yield stress of the material, thus any percentage error in the yield stress will cause an equal percentage error in the load. This applies to dimensions as well. Therefore, to maintain coherency in mechanical properties of the inverbucktube, a large number of cut tubes near to size were sent for heat treatment and consequently for machining. The variations noticed afterwards were very low, practically non-existent.

Furthermore, irregularities in mechanical properties of inverbucktube contribute to collapse mode variations, resulting in failure modes. Therefore, it is very important to have consistency in mechanical properties of every single inverbucktube.

2.5.2.2.3 *Effect of lubrication*

It is now well known that between the inverbucktube and die interface there is a friction force development which influences the work done and the collapse mode. To understand the effect of lubrication, hence determine how much work has been done by friction, a number of experiments were carried out using graphite based grease.

Results showed slight differences in the inverting load when compared to a non-lubricated sample. From here, it was decided to do all experiments without any lubrication whatsoever. What was done instead, was to have a good surface finish on both the internal area of the inverbucktube and the die fillet radius. After test with the employment of this method, it was noticed that there was slight ironing and a little bit of sticking which was not that alarming. The main reason why tests were carried

out without any lubrication whatsoever, was to get a feel of the real situation when inverbucktubes are applied as energy absorbers in the real world.

Quantification of frictional force experimentally is inevitable in these circumstances, but it was very difficult to monitor it in that small curvature. The method used was the same as that employed in the pressure distribution (see chapter III), but in this case the pin transducer was at an angle to the fillet radius surface. Anyway, the results obtained showed a large scatter and were not acceptable.

2.5.2.2.4 *Effect of loading speed variation*

In 2.5.1 it was shown how difficult it was to maintain the constant speed due to manual operation. this effect was not really a bother as it could have been in dynamic cases, due to low rates of strain which were too small to induce any strength increments.

2.5.2.2.5 *Effect of thickness variation*

To observe by how much the thickness varied before and after testing, pairs of inverbucktubes of exactly the same geometrical parameters were sectioned. One of the pair was cut along the longitudinal length before the test, while the other after the test. Thickness at various positions were measured using a micrometer and documented. Regions of measurements were divided into two, namely positions along the inverting section and along the buckling section. To achieve the objectives, some lines at 5mm interval were drawn at positions of measurement which became reference points when it came to measure the collapsed sectioned inverbucktubes. This showed clearly that the inverting region suffered no significant change

in thickness at all. But it could be said that the deviation started to be noticed when the tapered thickness was going towards constant thickness sections. The variation though was very small, of about 0.67% to 1.5% depending on geometry factor.

Small variations were also observed in the three circumferential buckling hinges. These were in the order of up to 1.25% depending on geometry factor.

2.5.3 INVERBUCKLING LOAD AND ENERGY ABSORPTION EFFECIENCY

Inverbuckling load is a composition of both loads due to inversion and concertina buckling. Table 2.3 gives experimental inverbuckling load results for some of the tests carried out.

To summarise these results a relationship between a non-dimensional inverbuckling load and the geometry factor is presented in fig.5.2. With effectively increasing the avarage thickness, the mean inverbuckling load increases in a manner broadly shown in fig.5.2.

Energy absorption effeciency also behaved in the same manner following the mean inverbuckling load. Within the limit of proper inverbuckling, the energy seems to be absorbed efficiently. But greater efficiencies according to fig.5.2 are achieved when $\bar{D}/2t_o$ nears 6.5. The reason is that the thicknesses in this region are favourably high, therefore increasing the axial stress which in turn approaches the compressive yield stress of the inverbucktube. It must be mentioned that in terms of energy absorbed per mass, inverbucktubes are more efficient than inversion tubes of the same mass.

2.6 DYNAMIC EXPERIMENTAL TEST

2.6.1 DYNAMIC TEST METHOD

The inverbucktube was mounted to the rigid back plate as shown in fig.2.12. Basically, the assembly of an inverbuctube with corresponding dies at both ends was bolted to the plate at a point just above the centre of gravity of the trolley. To avoid dropping and ensure that the centre line coincided with inverbucktube centre line, the die close to the trolley was sellotaped. This also stopped any instantaneous side forces which might get induced due to the impact not been unidirectional.

The trolley was accelerated by gravity from a high inclined height and moved freely on its air bellow cushions to impact the inverbucktube assembly at a predetermined velocity. Accelerometers were attached to the rear end of the trolley impact block. Their signals were processed and output as deceleration vs. time history by the computer. On the side of the trolley was a thin plate of about 10mm wide facing downwards. This measured the interval time taken between successive breaking of light to two photocells positioned at a fixed distance from each other.

High speed photography was also employed to give an independent obsevation of the development of deformation. Photography was done at a rate of 1000 frames per second, which in other words is 1ms per frame. To improve the clarity of photography, various finishes were tried, and it was found that spraying inverbucktubes with white paint was advantageous.

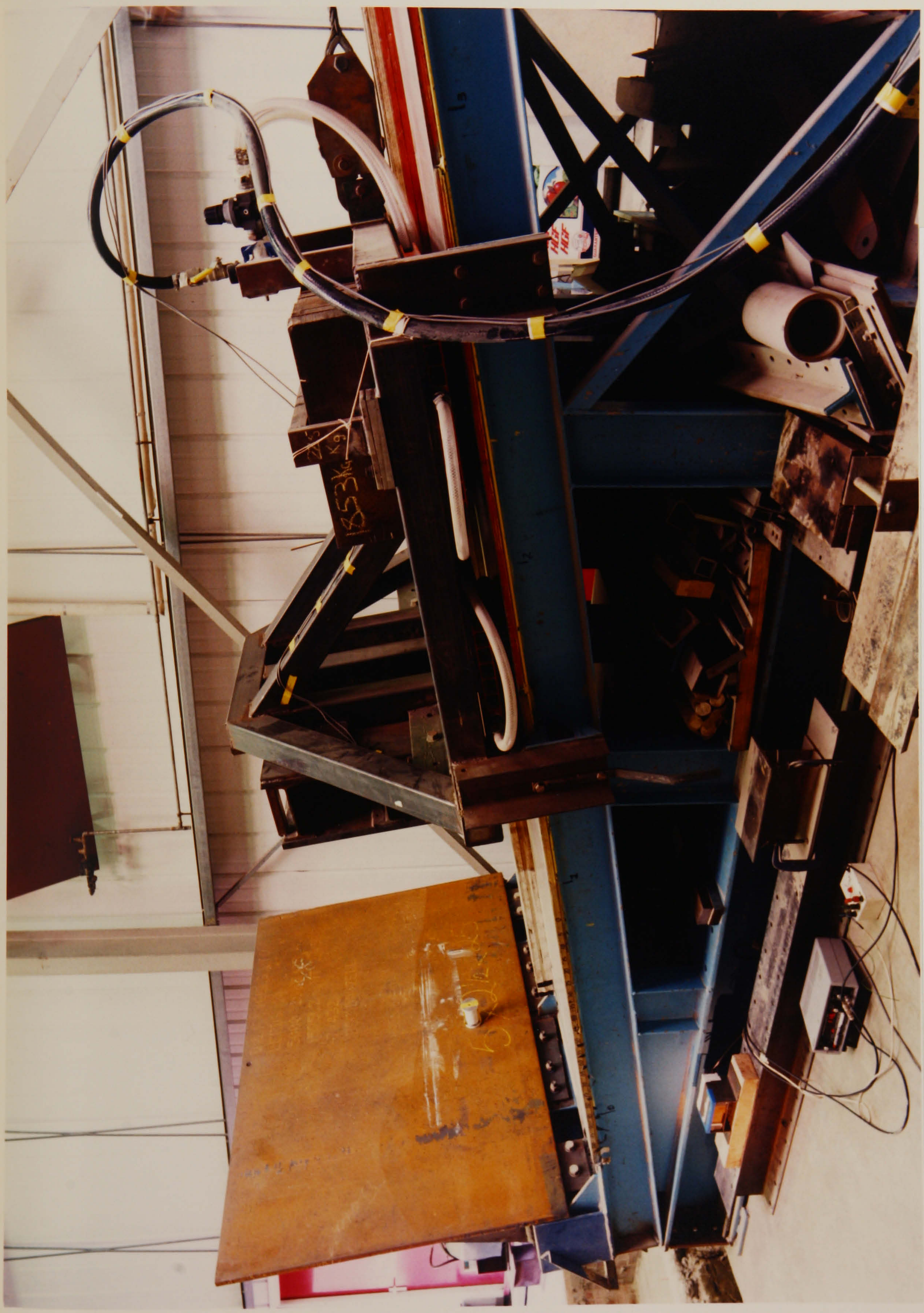

Fig.2.12 Inverbucktube attachment in the dynamic test rig

2.6.2 DYNAMIC EXPERIMENTAL RESULTS

The dynamic collapse behaviour of inverbucktubes appeared to be similar, if not identical to that of the quasi-static collapse modes. Therefore, the explanation of the inverbuckling processes could be as well referred to 2.5.2.1 of the static results.

Under dynamic axial loading, the inverbucktubes were deformed completely by the trolley placed at calculated heights as anticipated, with impact velocities varying depending on the geometry factor. High speed motion pictures, fig.2.13 and fig.2.14, show the sequence of collapse which is clear and follows the pattern observed during quasi-static tests.

Table 2.4 represents a summary of inverbuckling data from impact tests. Every test No. represents average values of 3 identical tets conducted. While typical characteristics are shown in figs.2.15 to 2.20 and give deceleration, velocity, shortening distance and dynamic force/time histories. As said earlier on, the only characteristic obtained from the test was deceleration vs. time history. The remainder (velocity and shortening distance) traces were achieved by integrating the deceleration vs. time history. To obtain the impact force characteristic, a constant was first of all determined, which was a product of the total mass of the trolley times the acceleration due to gravity. Once calculated, it was multiplied by the deceleration vs. time trace.

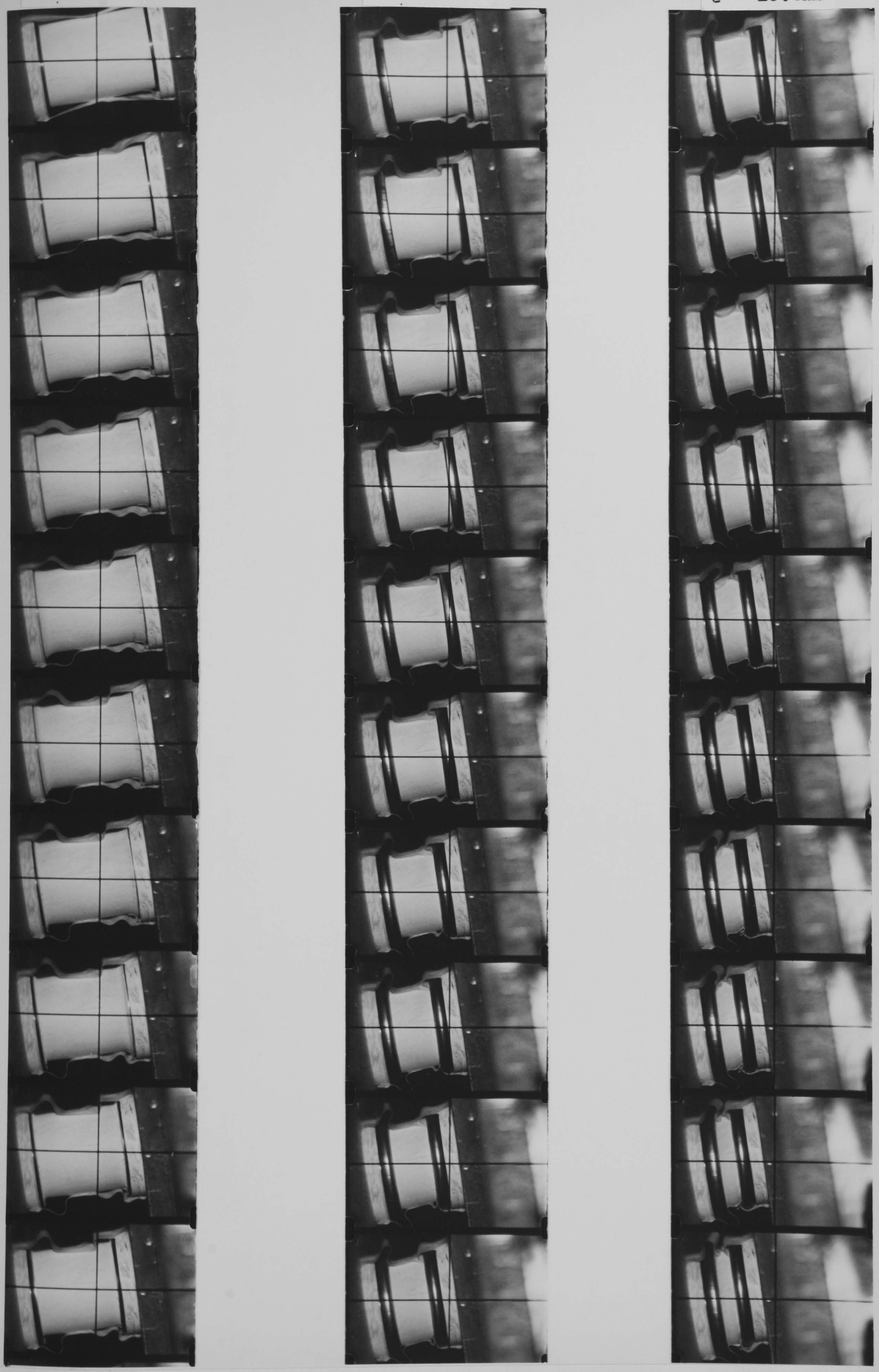

Fig.2.13 High speed photographs of dynamically inverbuckled tube. Test No.EFFT9100

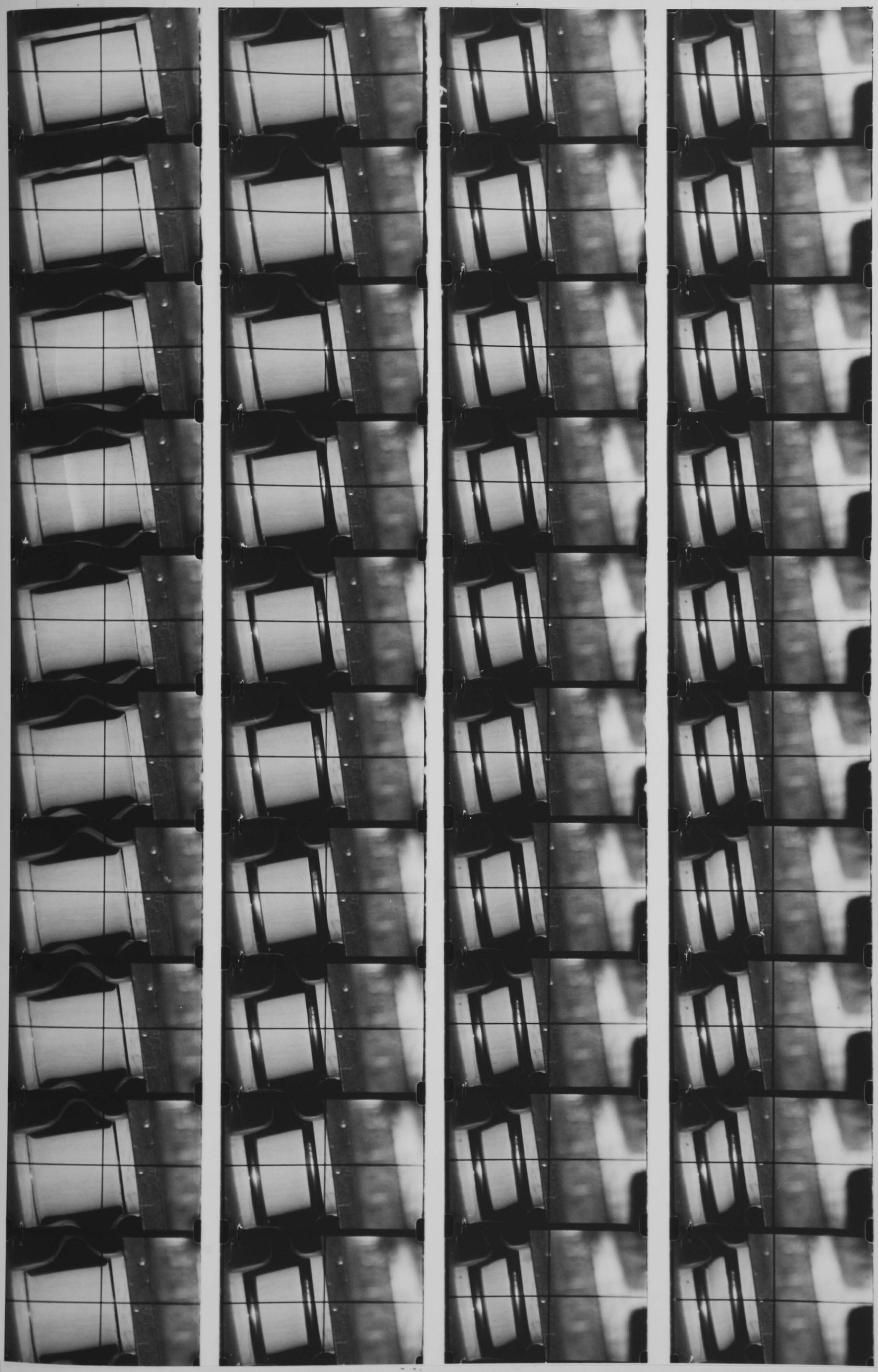

Fig.2.14 High speed photographs of dynamically inverbuckled tube. Test No.EFFT101

2.6.2.1 The effect of impact velocity on mean dynamic load

Impact velocity affects the mean dynamic inverbuckling load as seen from fig.2.21. This shows a linear variation of the increase in dynamic load with impact velocities.

To understand clearly, test No.64 from table 2.3 and test No.EFFT6100 from table 2.4 have been chosen for explanation. An identical inverbucktube was used in both these tests. The only difference was that they were deformed at different speeds, static and dynamic respectively. The mean static load was about 127.8KN. This compares with dynamic value of about 158.21KN. It can be seen that the dynamic value is about 19.22% higher. This effect is brought about by increase in strength of the material due to high rates of strain.

However, high strain rate is not the only parameter which tends to increase the mean dynamic load. The geometry factor in some extent has a tendency of increasing this load. It is known from the test that the geometry factor for this particular inverbucktube is low, then the effect is not significant. So it must be regarded that almost all increases in strength under dynamic loading has been due to high strain rates.

2.6.2.2 Effect of rebound velocity on mean dynamic load

Rebound velocity is very important in determining how much real energy has been absorbed by the inverbucktube. As it can be seen from figs.2.15 to 2.20, the trolley did not stop dead after impact, but it bounced back somewhat, releasing energy equal to $\frac{1}{2}M_{\oplus}V_{R}^{2}$; where V_R is the rebound velocity and $M_{\oplus}$ is the total mass of the trolley. This rebound must have been caused by energy stored in the inverbucktube or in the trolley, or in both. From table

2.4, it can be seen that the greater the rebound velocity the less kinetic energy absorbed by the inverbucktube. Therefore, the effects of rebound velocity are vital and not to be neglected.

2.6.2.3 Inverbuckling tightness

Inverbuckling tightness is a parametric measure in percentage of a ratio between shortening length (final length of the collapsed inverbucktube) to original length. This is formulated as

$$\eta_T = \frac{L_s}{L} * 100\% \qquad 2.8$$

From purely visual observation it was clear that the quasi-static inverbuckling was less tight than dynamic. This could be explained as follows; when quasi-static tests were conducted, there were means of stopping the experiment immediately after complete collapse mode was achieved. In dynamic tests, this was not the case, because energy to be absorbed by the inverbucktube was predicted prior to testing and used as input data to determine the height at which to position the trolley. The results showed that the tightness in this case was higher. The other thing noticed was that the predicted energy was somewhat overestimated, hence higher tightness than expected.

To be sure that this was the case, the effect of impact speed on inverbuckling tightness was studied. This showed no effect on tightness as seen in fig.2.22.

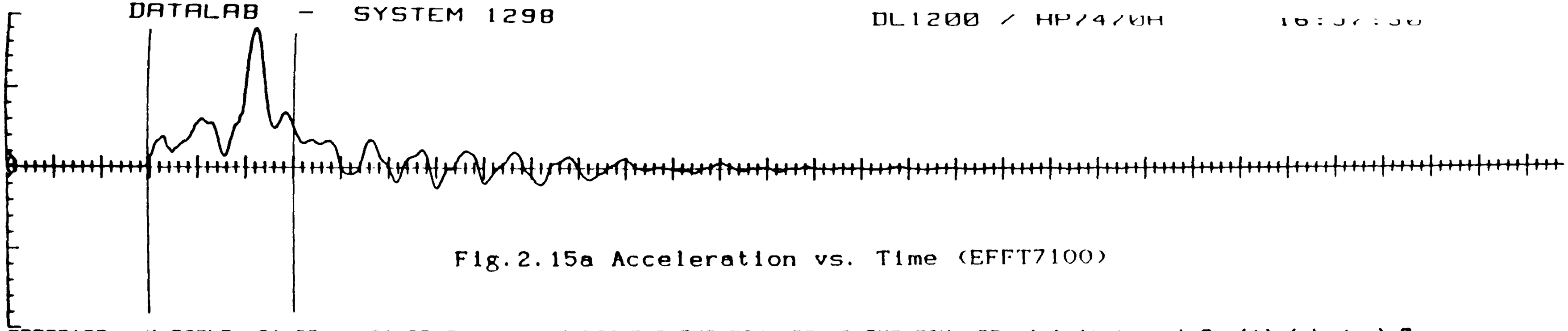

Fig.2.15a Acceleration vs. Time (EFFT7100)

EFFT7100. Y SCALE -31.25 to 31.25 G . X SCALE=2.5MS/DIV :SA. 2.5MS/DIV :SB. (*)-(trigger)-0. (+)-(chg/ov)-0

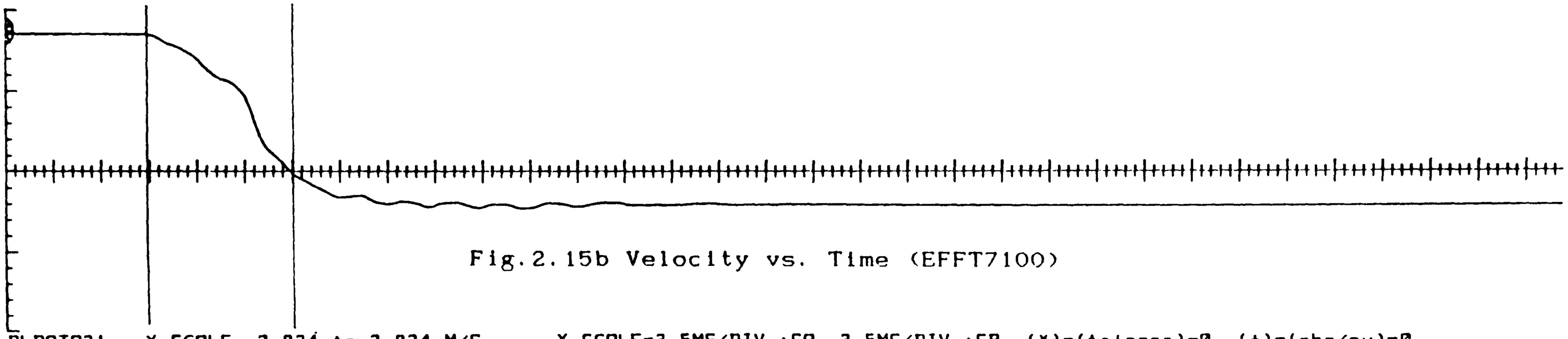

Fig.2.15b Velocity vs. Time (EFFT7100)

DLDATA21. Y SCALE -3.924 to 3.924 M/S . X SCALE=2.5MS/DIV :SA. 2.5MS/DIV :SB. (*)-(trigger)-0. (+)-(chg/ov)-0

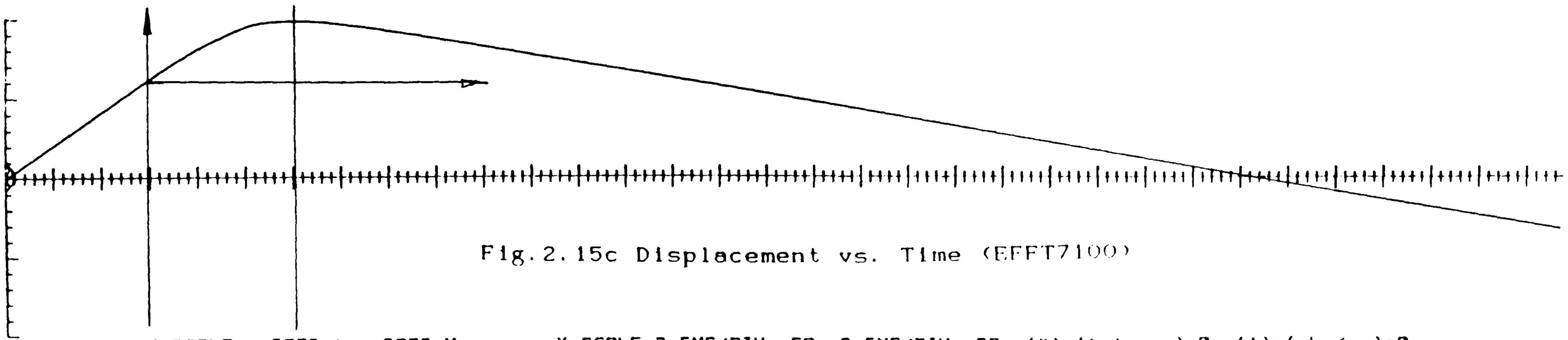

Fig.2.15c Displacement vs. Time (EFFT7100)

DLDATA31. Y SCALE -.2009 to .2009 M . X SCALE=2.5MS/DIV :SA. 2.5MS/DIV :SB. (*)-(trigger)-0. (+)-(chg/ov)-0

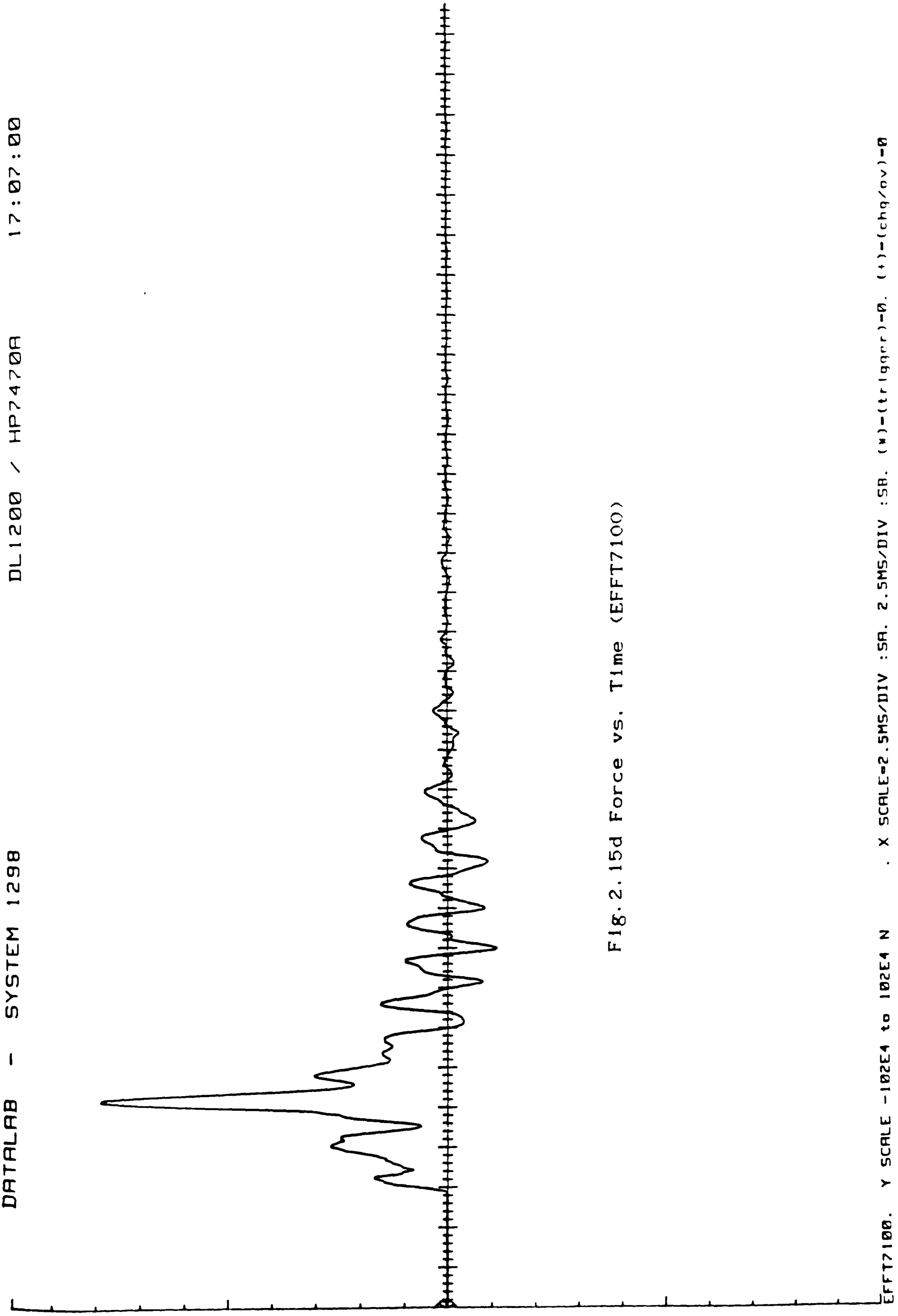

Fig. 2.15d Force vs. Time (EFFT7100)

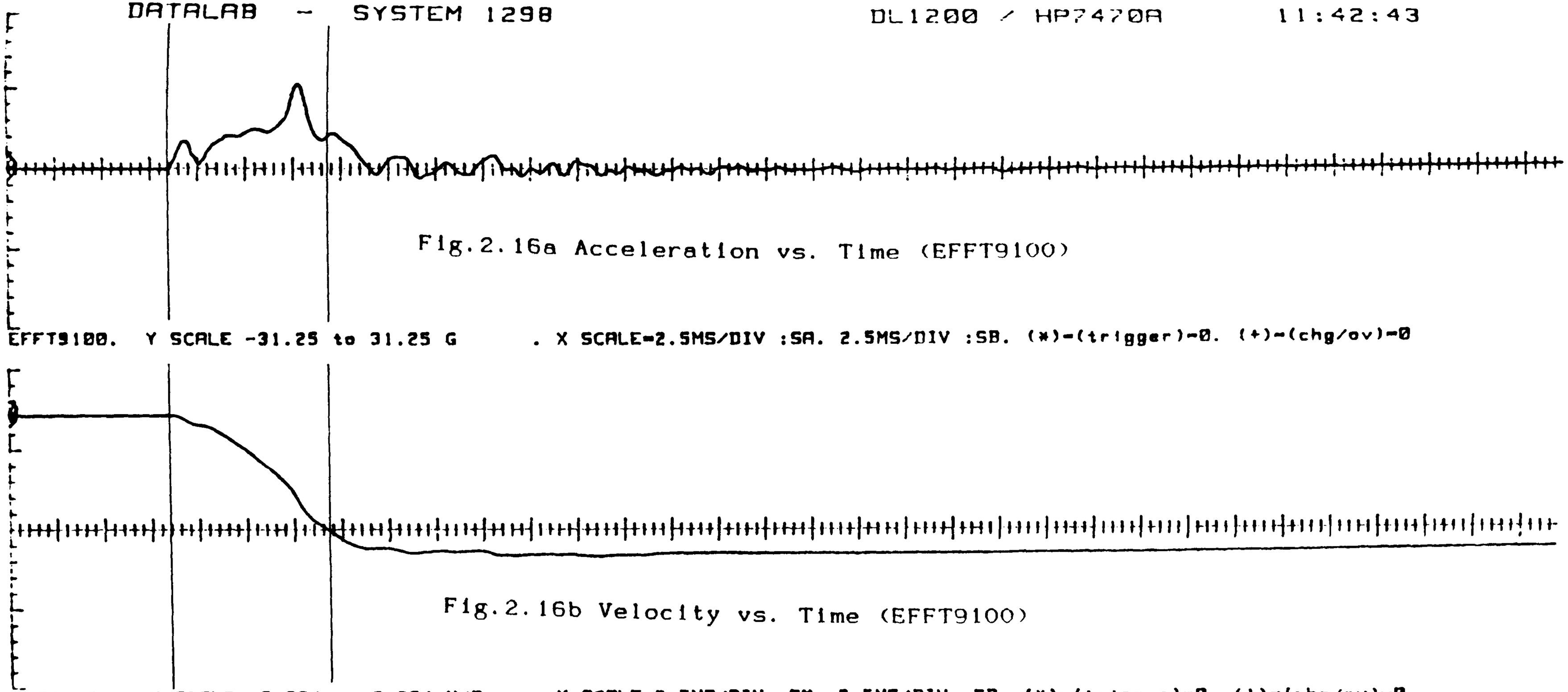

Fig.2.16a Acceleration vs. Time (EFFT9100)

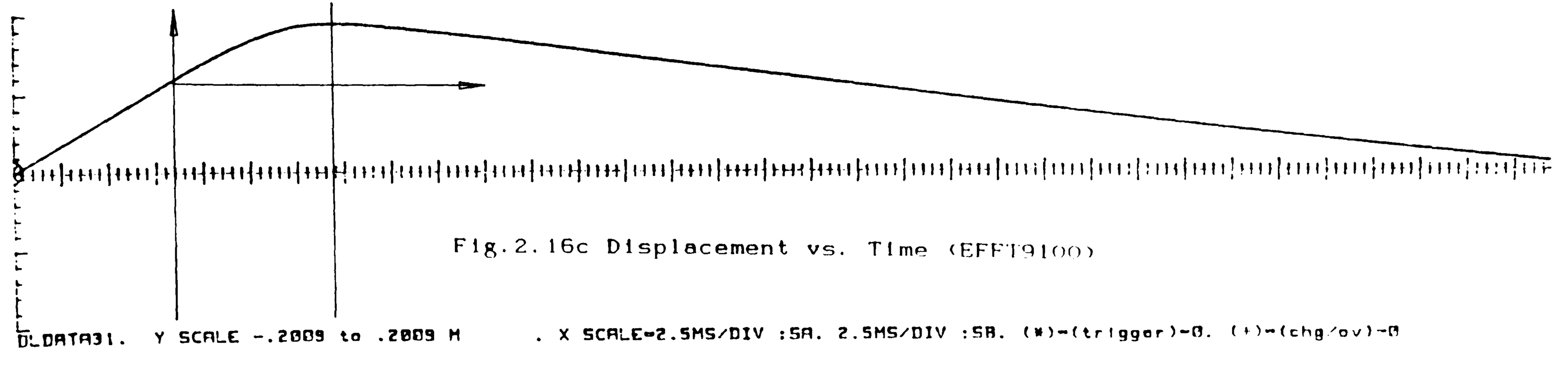

Fig.2.16b Velocity vs. Time (EFFT9100)

Fig.2.16c Displacement vs. Time (EFFT9100)

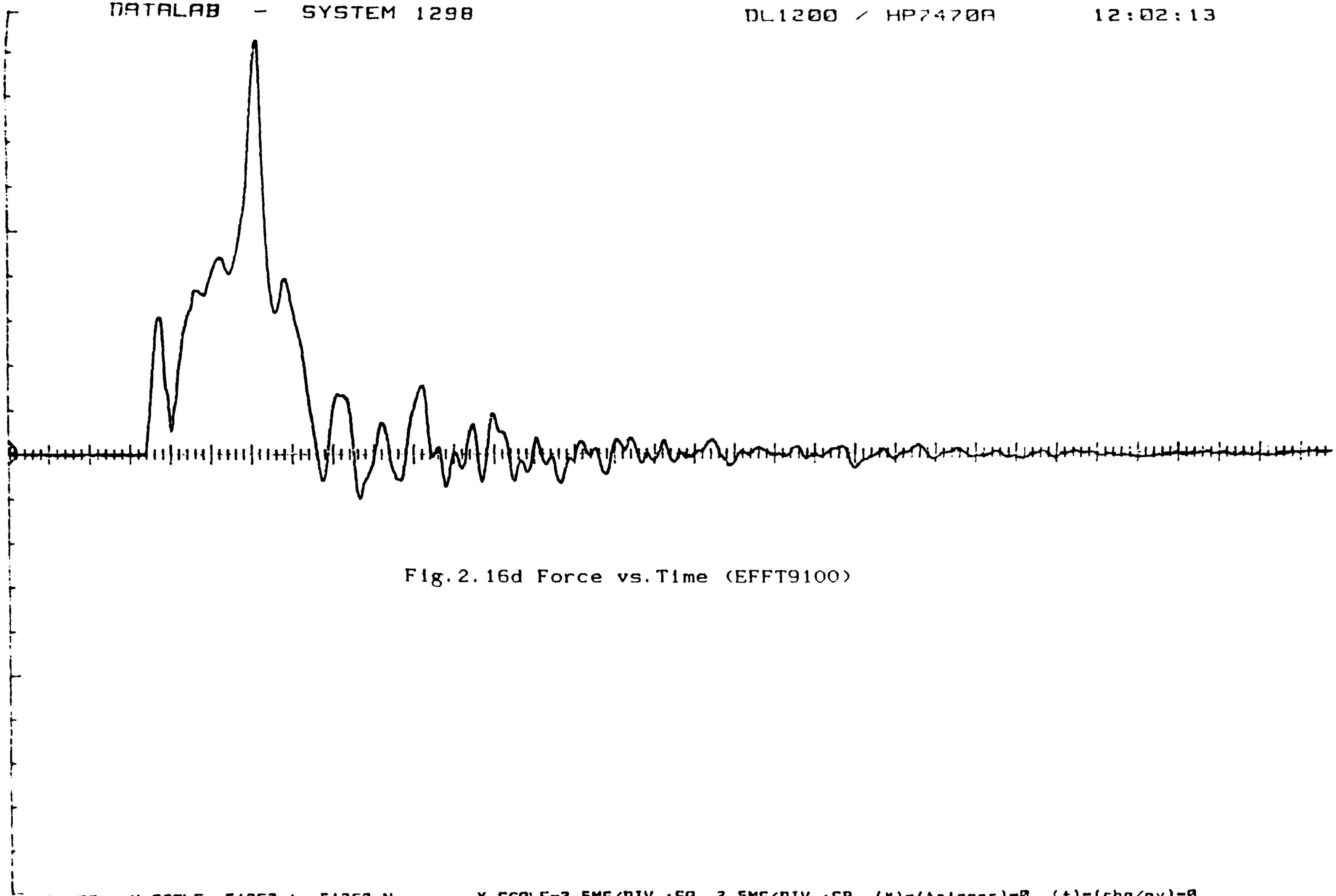

Fig. 2.16d Force vs. Time (EFFT9100)

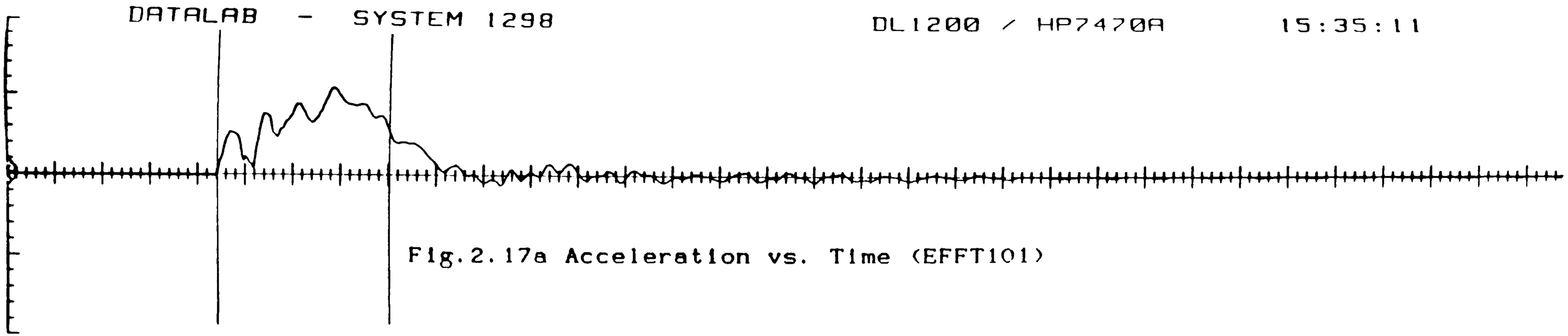

Fig.2.17a Acceleration vs. Time (EFFT101)

EFFT101 . Y SCALE -15.62 to 15.62 G . X SCALE=2.5MS/DIV :SA. 2.5MS/DIV :SB. (*)-(trigger)-0. (+)-(chg/ov)-0

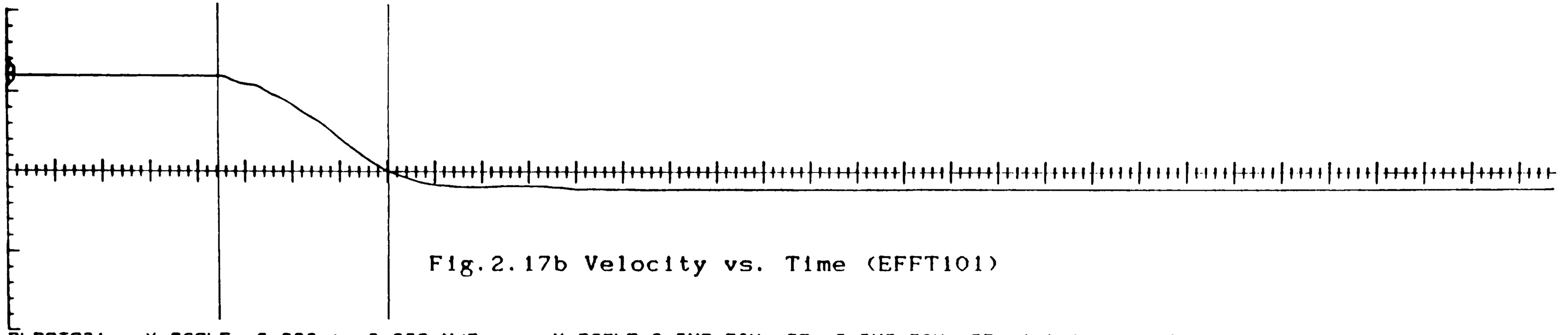

Fig.2.17b Velocity vs. Time (EFFT101)

DLDATA21. Y SCALE -3.923 to 3.923 M/S . X SCALE=2.5MS/DIV :SA. 2.5MS/DIV :SB. (*)-(trigger)-0. (+)-(chg/ov)-0

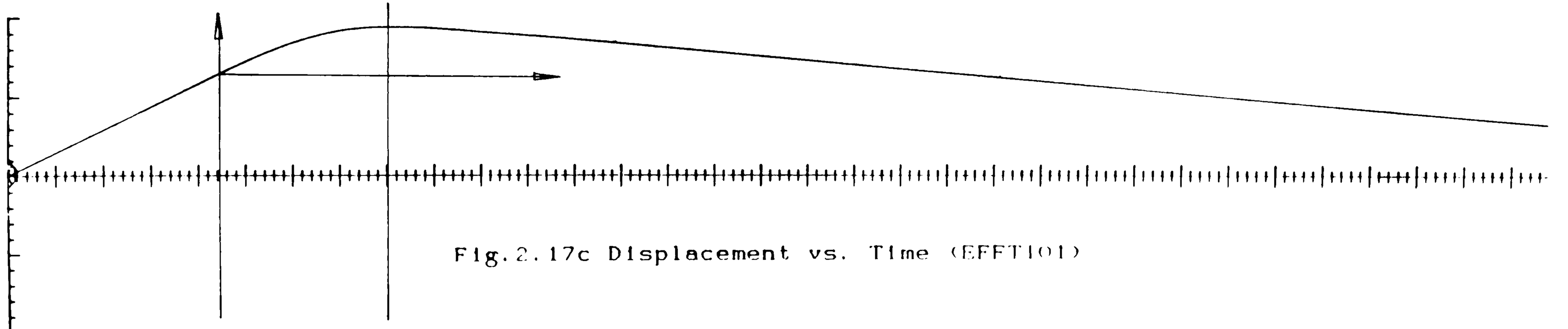

Fig.2.17c Displacement vs. Time (EFFT101)

DLDATA31. Y SCALE -.2009 to .2009 M . X SCALE=2.5MS/DIV :SA. 2.5MS/DIV :SB. (*)-(trigger)-0. (+)-(chg/ov)-0

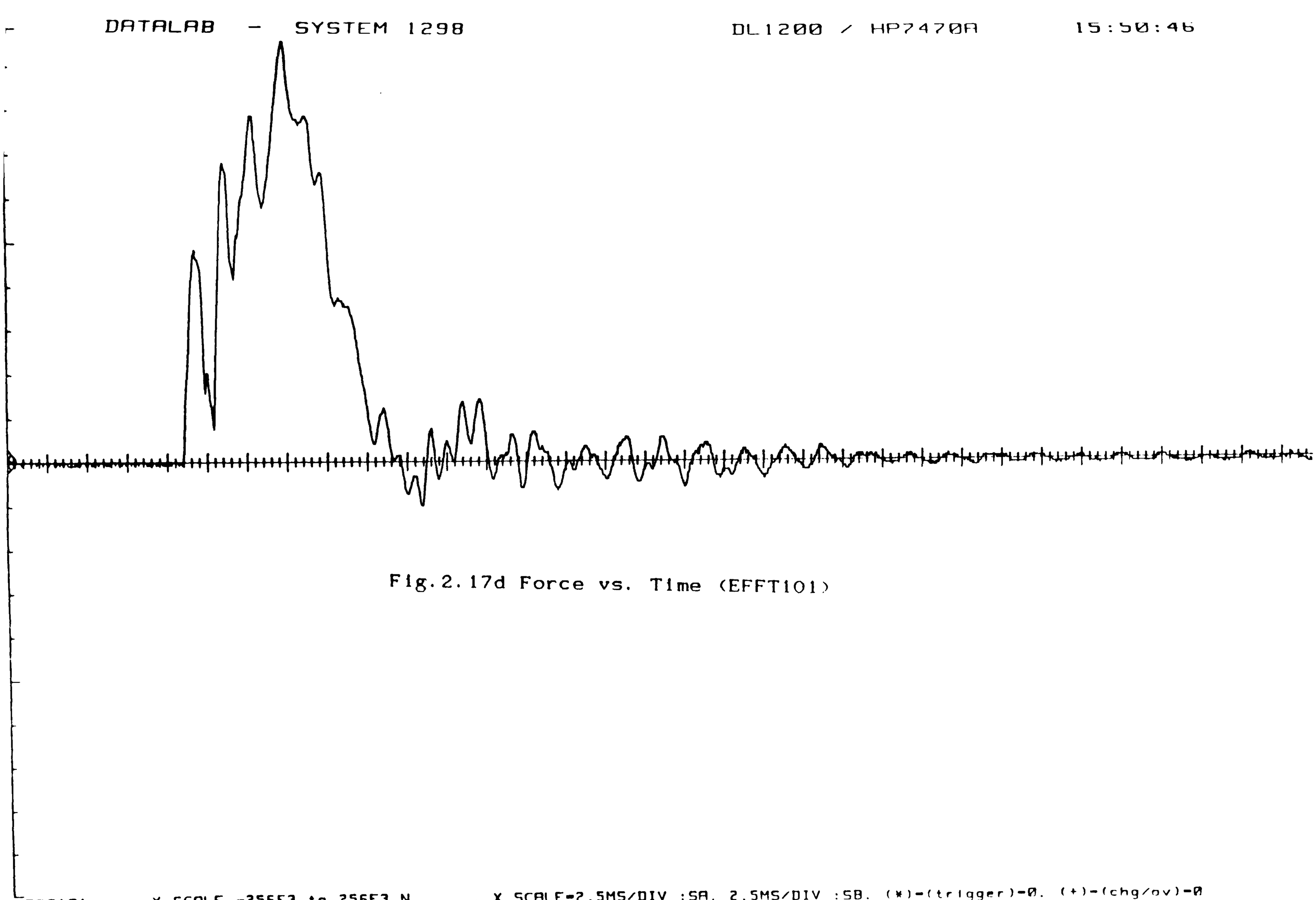

Fig. 2.17d Force vs. Time (EFFT101)

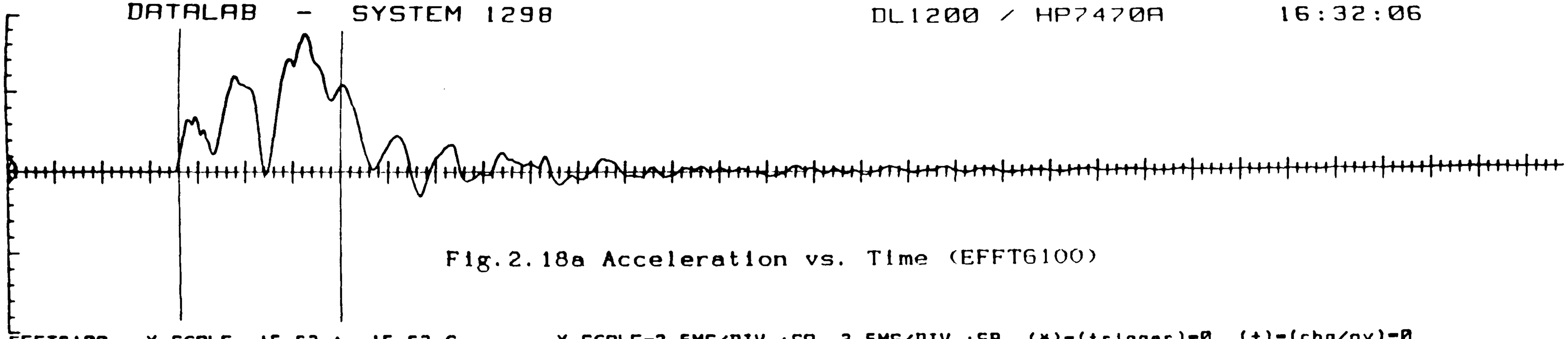

Fig.2.18a Acceleration vs. Time (EFFT6100)

EFFT6100. Y SCALE -15.62 to 15.62 G . X SCALE=2.5MS/DIV :SA. 2.5MS/DIV :SB. (*)=(trigger)=0. (+)=(chg/ov)=0

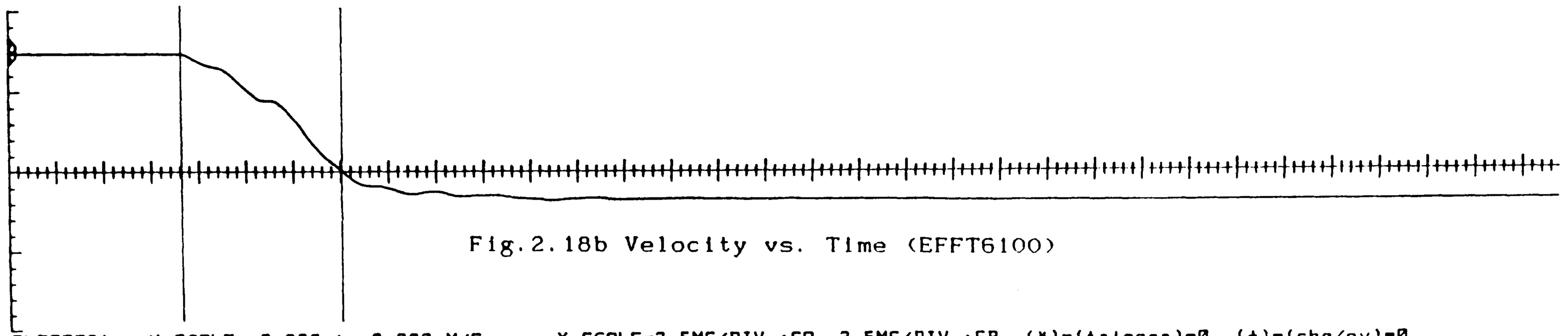

Fig.2.18b Velocity vs. Time (EFFT6100)

DLDATA21. Y SCALE -3.923 to 3.923 M/S . X SCALE=2.5MS/DIV :SA. 2.5MS/DIV :SB. (*)=(trigger)=0. (+)=(chg/ov)=0

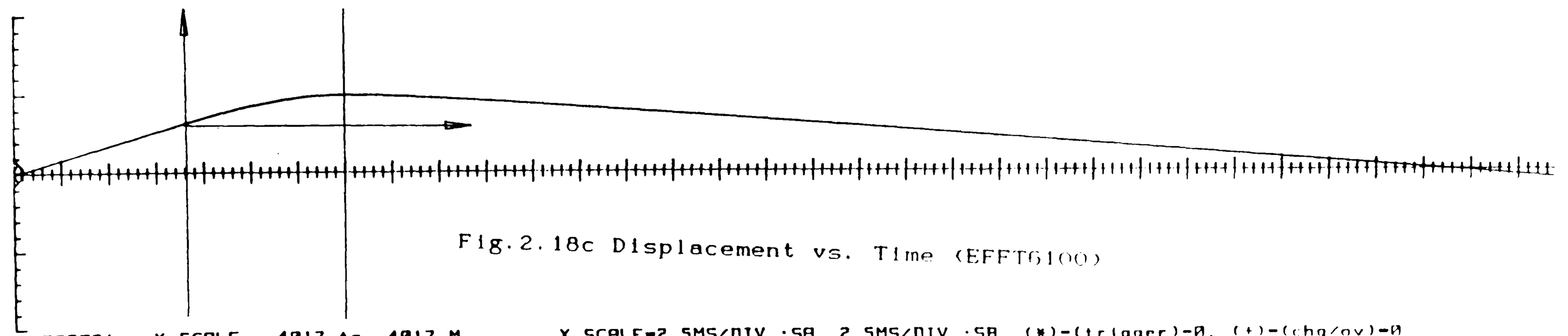

Fig.2.18c Displacement vs. Time (EFFT6100)

DLDATA31. Y SCALE -.4017 to .4017 M . X SCALE=2.5MS/DIV :SA. 2.5MS/DIV :SB. (*)=(trigger)=0. (+)=(chg/ov)=0

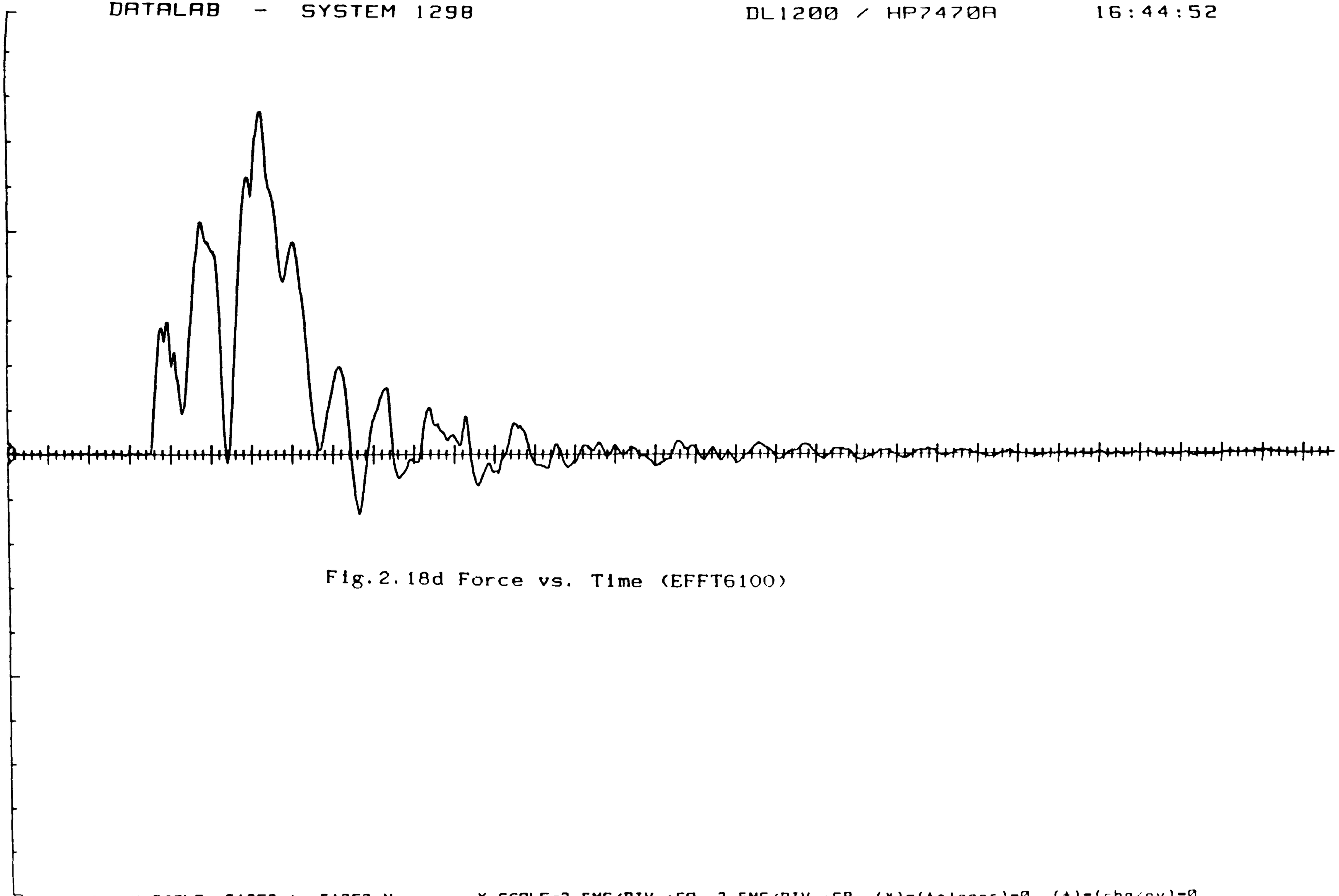

Fig. 2.18d Force vs. Time (EFFT6100)

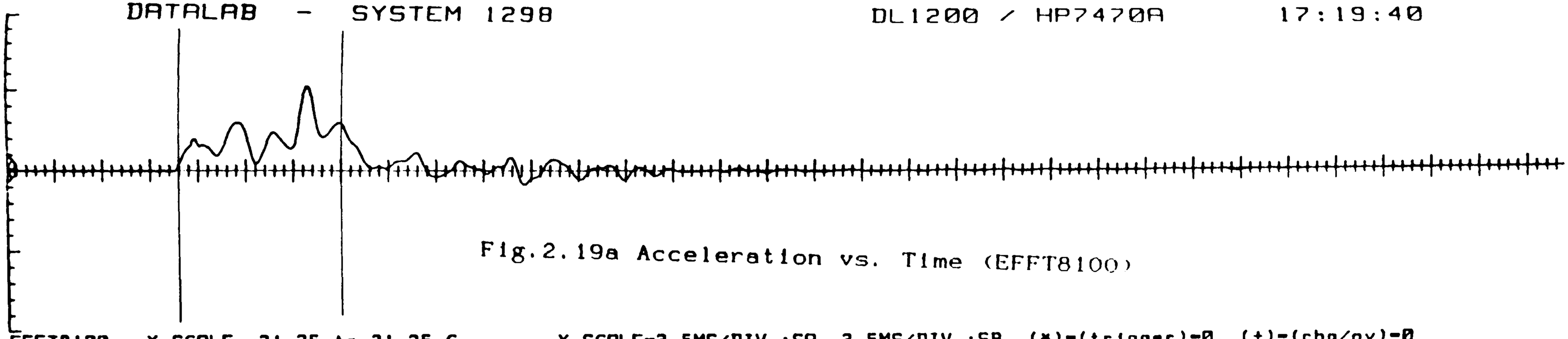

Fig.2.19a Acceleration vs. Time (EFFT8100)

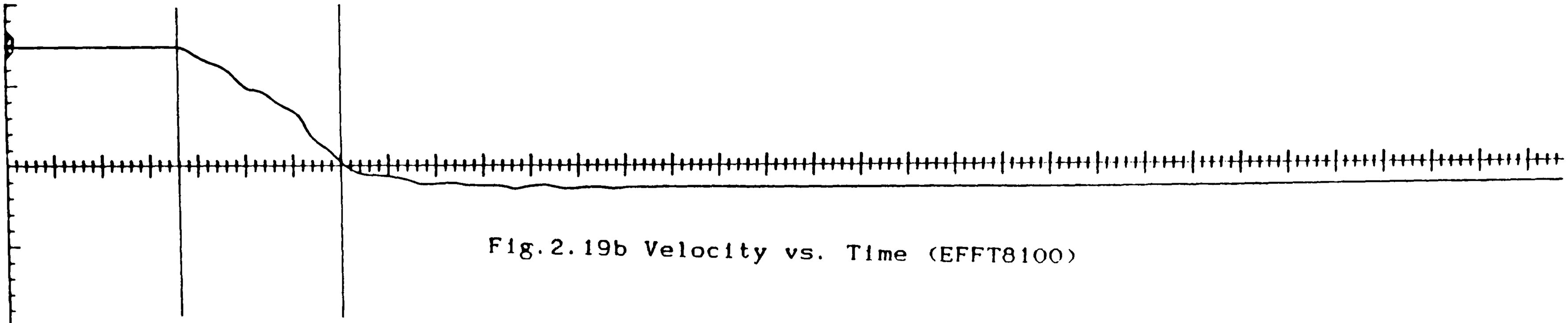

Fig.2.19b Velocity vs. Time (EFFT8100)

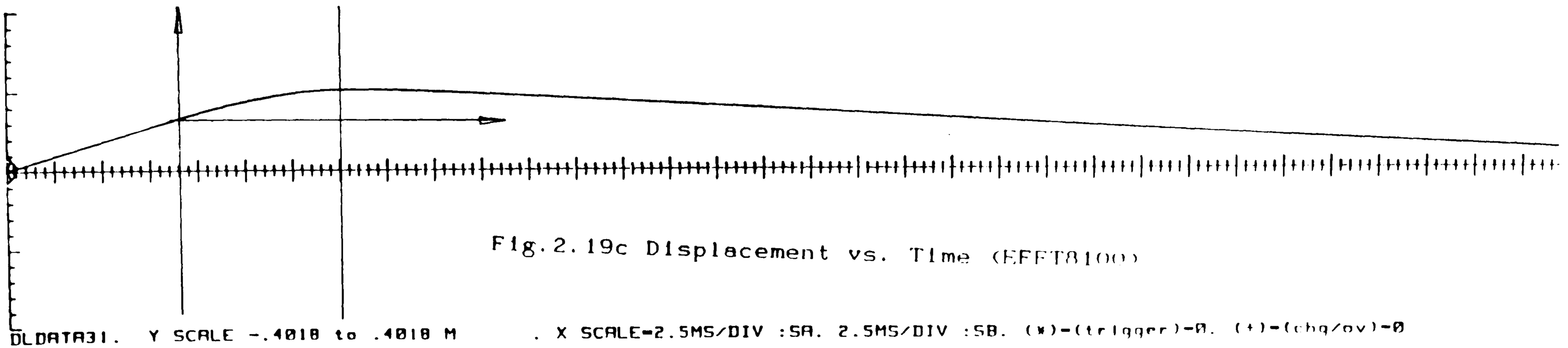

Fig.2.19c Displacement vs. Time (EFFT8100)

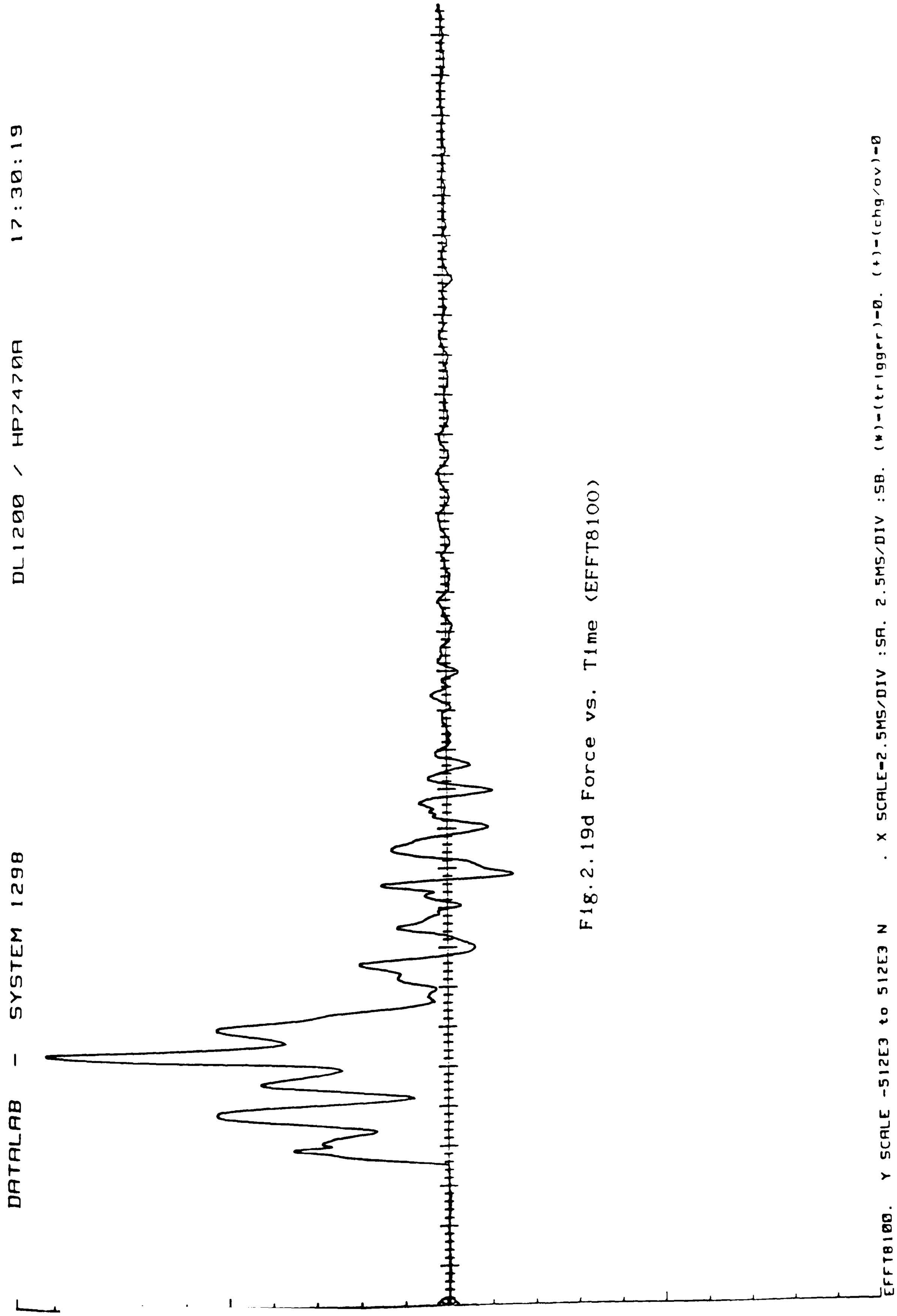

Fig.2.19d Force vs. Time (EFFT8100)

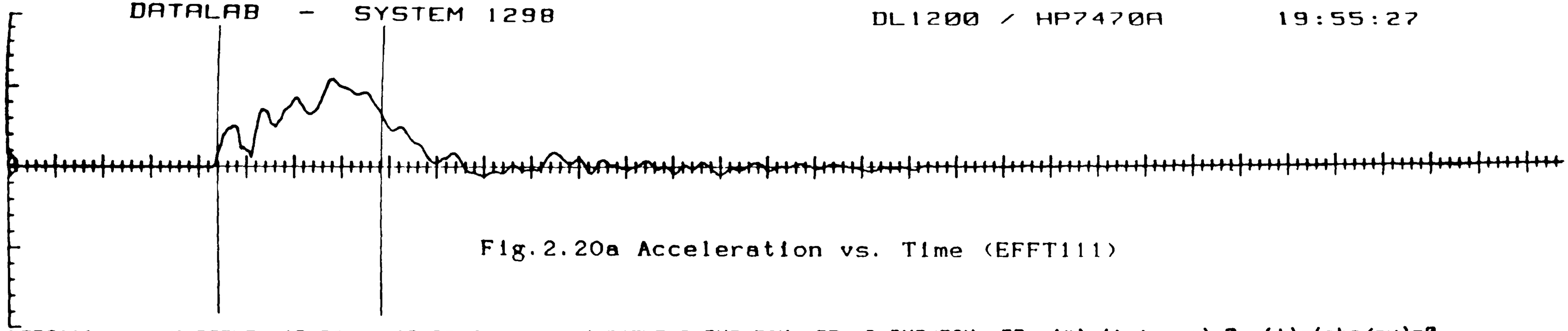

Fig.2.20a Acceleration vs. Time (EFFT111)

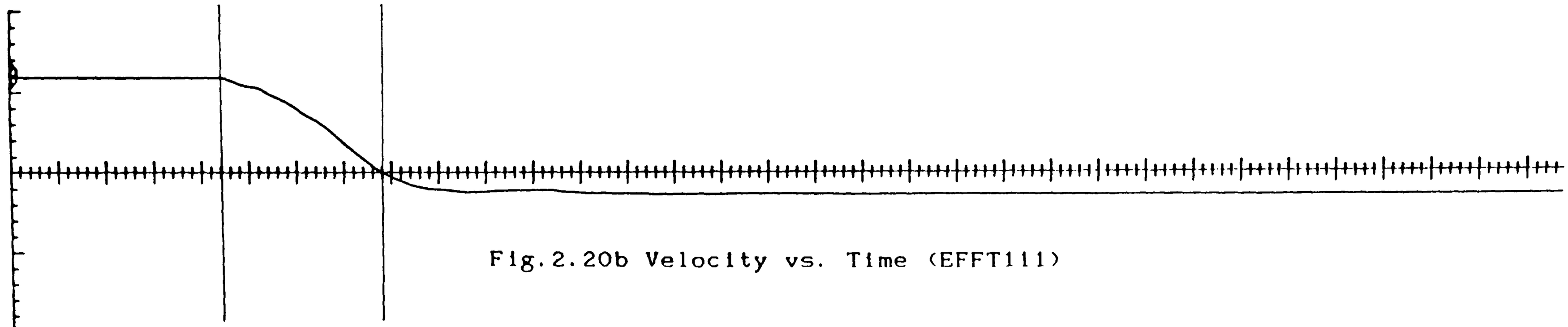

Fig.2.20b Velocity vs. Time (EFFT111)

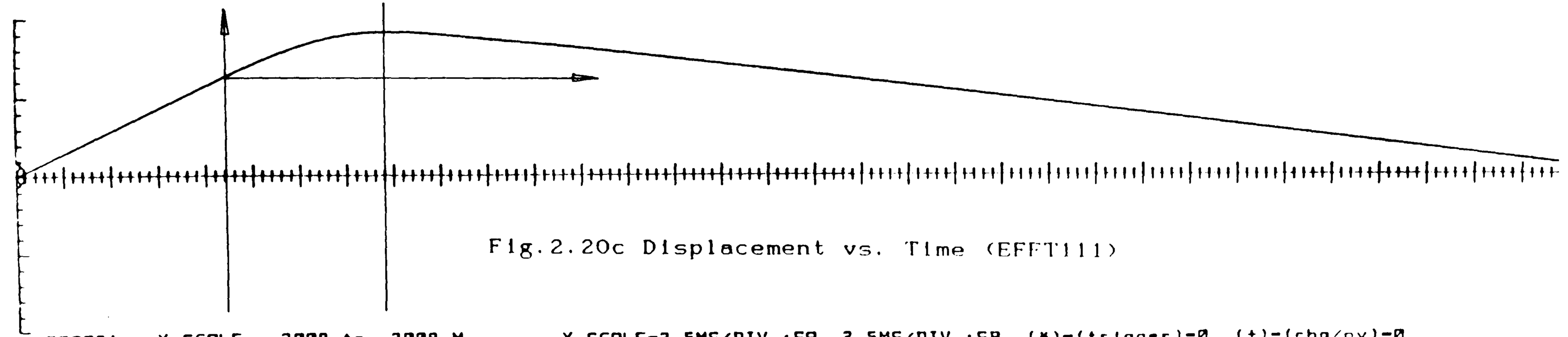

Fig.2.20c Displacement vs. Time (EFFT111)

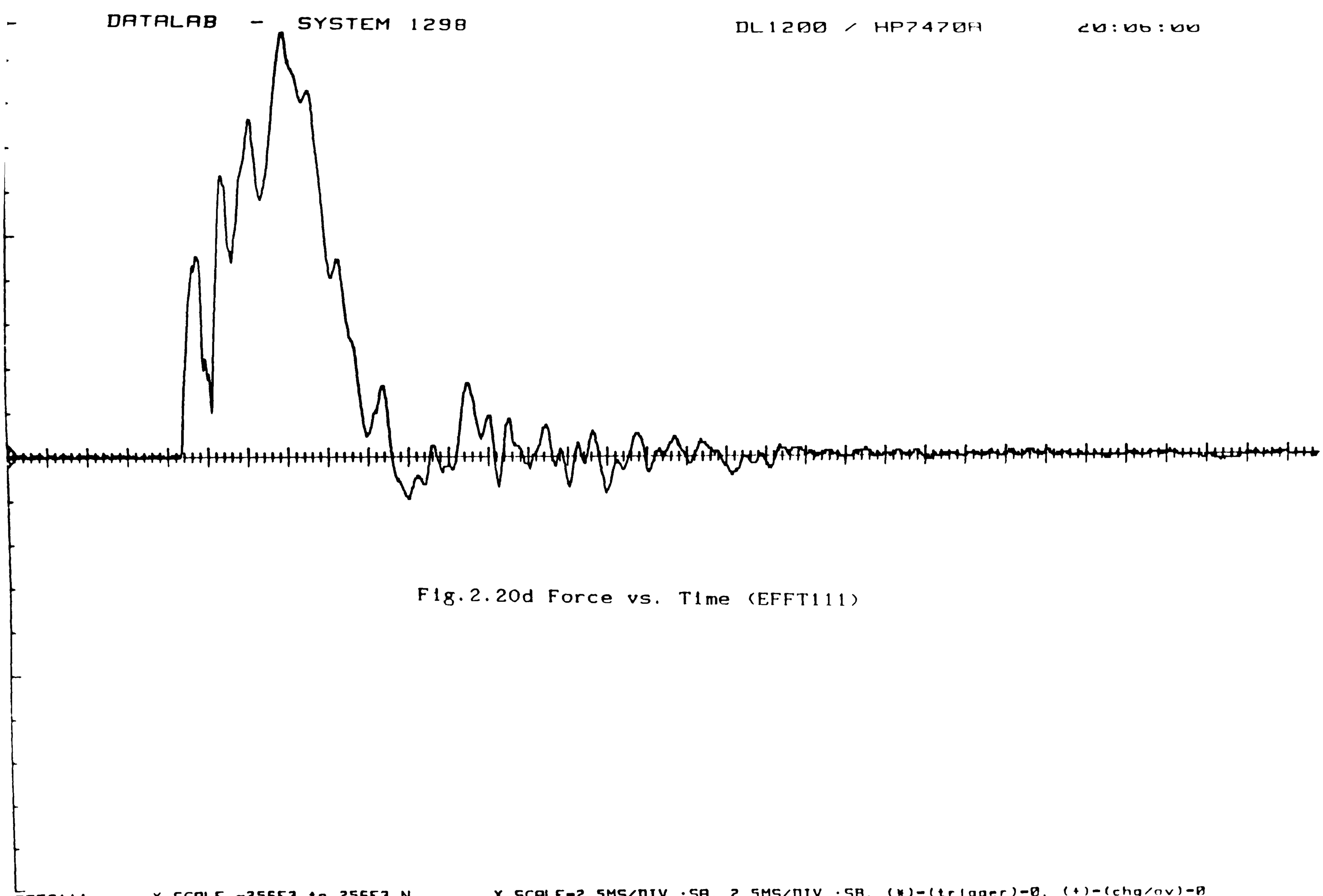

Fig.2.20d Force vs. Time (EFFT111)

TABLE 2.4 Inverbuckling impact test data

INVERBUCKTUBE												
TEST No.	Material (normal.)	D_i (mm)	t_o (mm)	L (mm)	δ_d (mm)	r (mm)	M_B (Kg)	V_c (ms^{-1})	V_R (ms^{-1})	E_{KI} (KJ)	E_{KA} (KJ)	P_D (KN)
EFFT7100	SKF280	50.00	2.65	98.0	70.35	4.36	2900	3.35	0.78	16.27	15.39	218.77
EFFT9100	SKF280	50.00	2.57	98.0	69.31	4.36	2900	2.81	0.69	11.45	10.76	155.23
EFFT101	SKF280	50.00	2.55	98.0	60.27	4.36	2900	2.34	0.39	7.94	7.72	128.07
EFFT6100	SKF280	50.00	2.00	98.0	72.31	4.36	2900	2.89	0.68	12.11	11.44	158.21
EFFT8100	SKF280	50.00	2.65	98.0	70.70	4.36	2900	2.91	0.52	12.28	11.89	168.13
EFFT1110	SKF280	50.00	2.50	98.0	56.25	4.36	2900	2.31	0.39	7.74	7.52	133.63

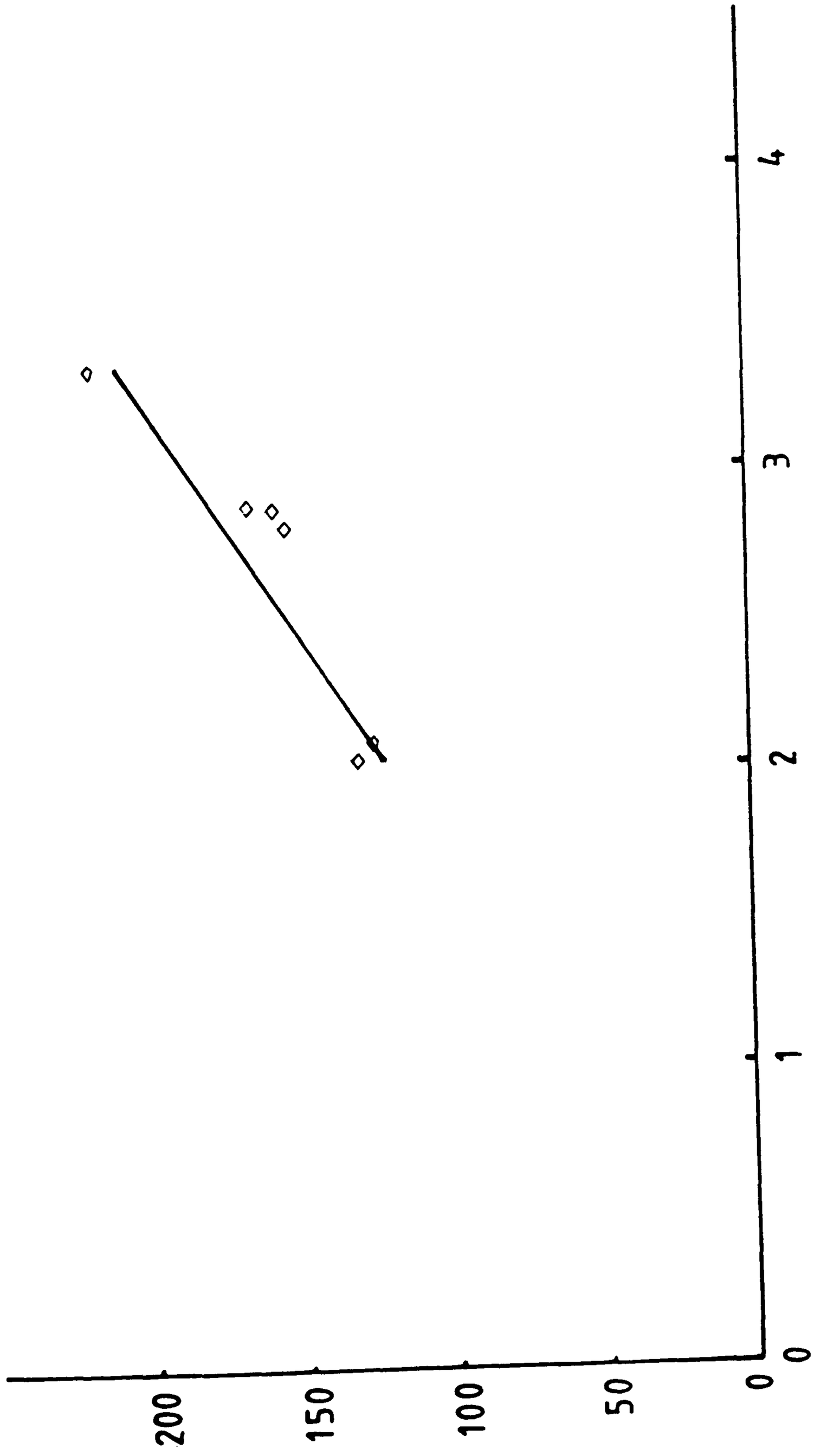

Fig.2.21 Mean dynamic load - Impact velocity relationship

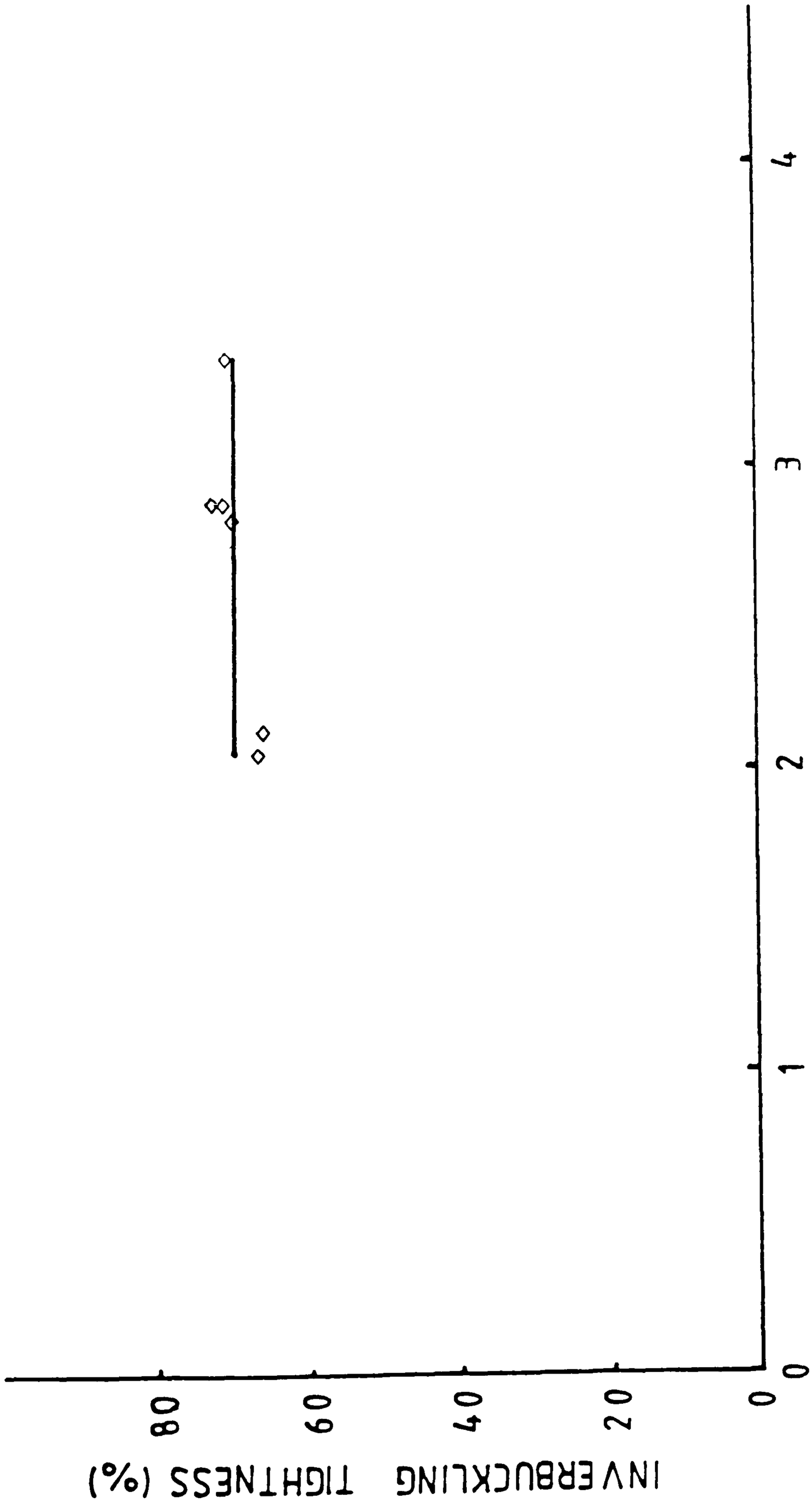

Fig.2.22 Inverbuckling tightness - Impact velocity relationship

CHAPTER III

PRESSURE DISTRIBUTION

3.1 GENERAL VIEW

For many years, inversion of thin-walled square cylindrical tubes have been carried out by a number of researchers such as (13-17 and 61-67)* without looking into the normal contact stresses(pressure distribution) between the inverting tubes and their corresponding dies. This investigation, will be devoted to the experimentally determined normal stresses encountered during this collapse behaviour.

The technique incorporated *"pressure transducers"* which were mounted in the dies normal to the fillet radii surfaces as shown in fig.3.1. Results from these tests gave a new insight into the study of tubes going round the dies.

Friction force, which is one of the measurements this investigation wanted to acquire from the experiments, proved to be very difficult to measure. Therefore, no experimental results are presented herein.

3.2 TEST EQUIPMENT

3.2.1 DIE PREPARATION

The dies designed for the quasi-static and dynamic tests were employed in the contact stresses determination. A total of five holes were dilled into each die at 0°, 24°, 45°, 67° and 90° in a scatter form around the fillet

radius for the purpose of accomodation as shown in the schematic diagram, fig.3.2.

The accuracy in drilling these holes was very vital in the work. It was therefore important to make sure that when the pressure transducers were mounted, the pressure pins did not overlap each other, but were just very close. The other vital point was to make sure the pressure pins covered the whole fillet radius continuously for correct measurement interpretations.

3.2.2 PRESSURE TRANSDUCER AND INSTRUMATATION

A lot of work has been carrried out in the measurements of contact stresses in the rolling gap during metal forming using pressure transducers. This was seen in the literature survey. But none of the works defined the design parameters of its components, apart from making emphases on the pin dimensions. Therefore, it was a big task designing and developing the pressure transducer shown in fig.3.3 for this particular purpose.

Looking closely at fig.3.3a from left to right, the following can be seen; (i) the steel ball which ensures axial loading; (ii) the transducer cup which virtually houses the steel ball; (iii) the pressure pin; (iv) the compression pillar with the pressure pin mounted on it; (v) the inner and (vi) outer housings. The assembled pressure transducer is also shown in fig.3.3b, while the pocedure of assembly is schematically given in fig.3.4.

To assemble a pressure transducer into the die the following sequence of events were obeyed:

(i) First and foremost, the semi-conducter strain guages were adhered carefully on the compression pillar in

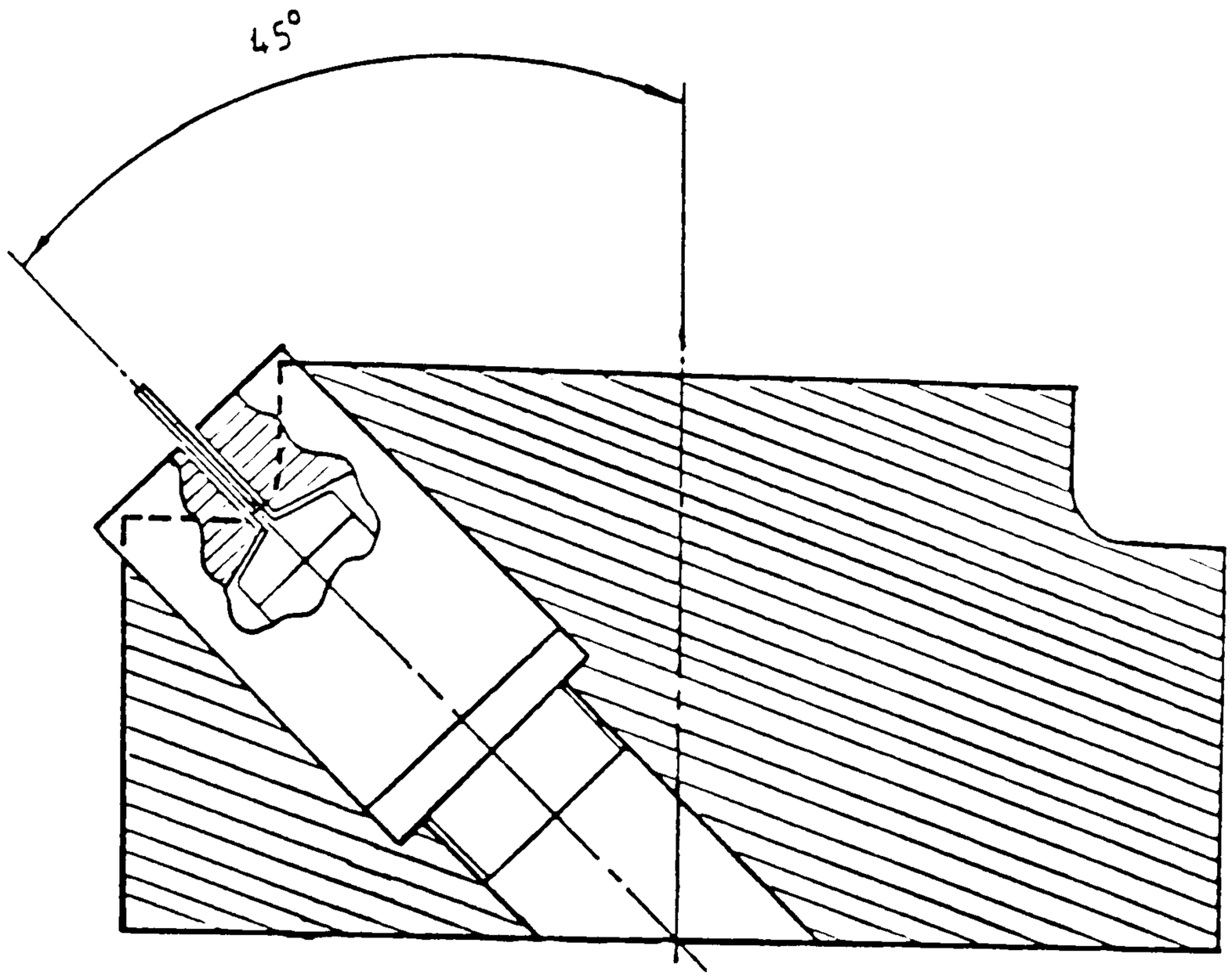

Fig.3.1 Die/pressure transducer assembling arrangement

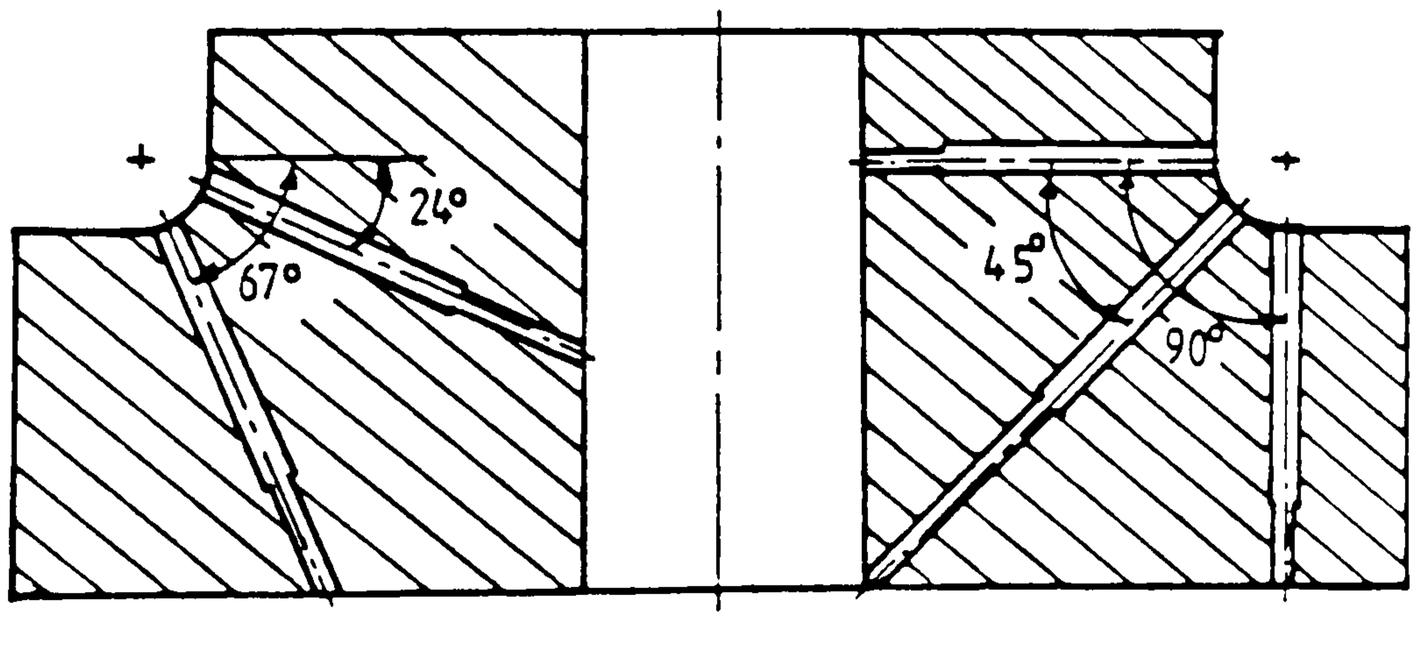

Fig.3.2 Schematic positioning of pressure transducers in one die

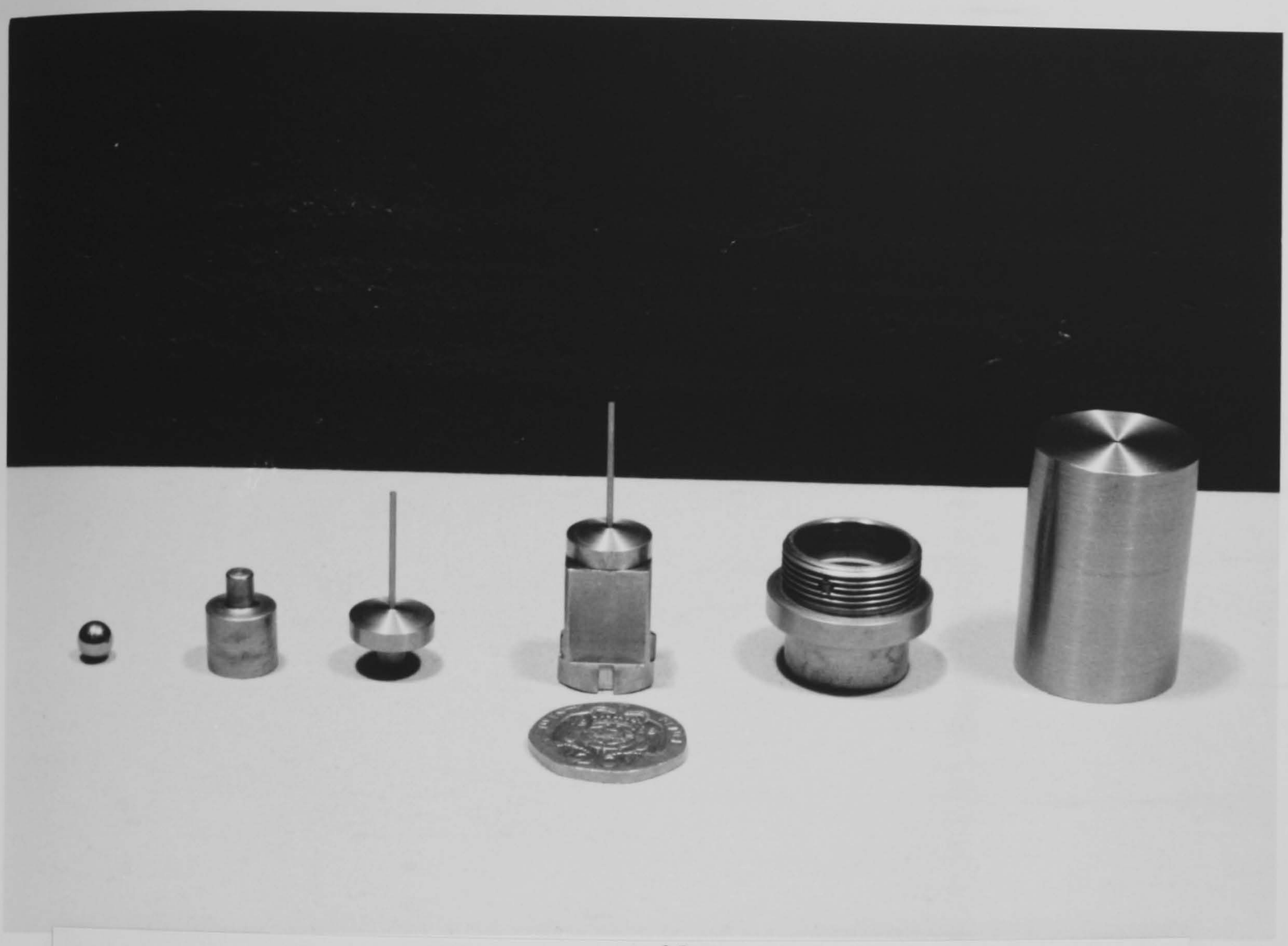

Fig.3.3a Typical pressure transducer components

Fig.3.3b Assembled pressure transducer

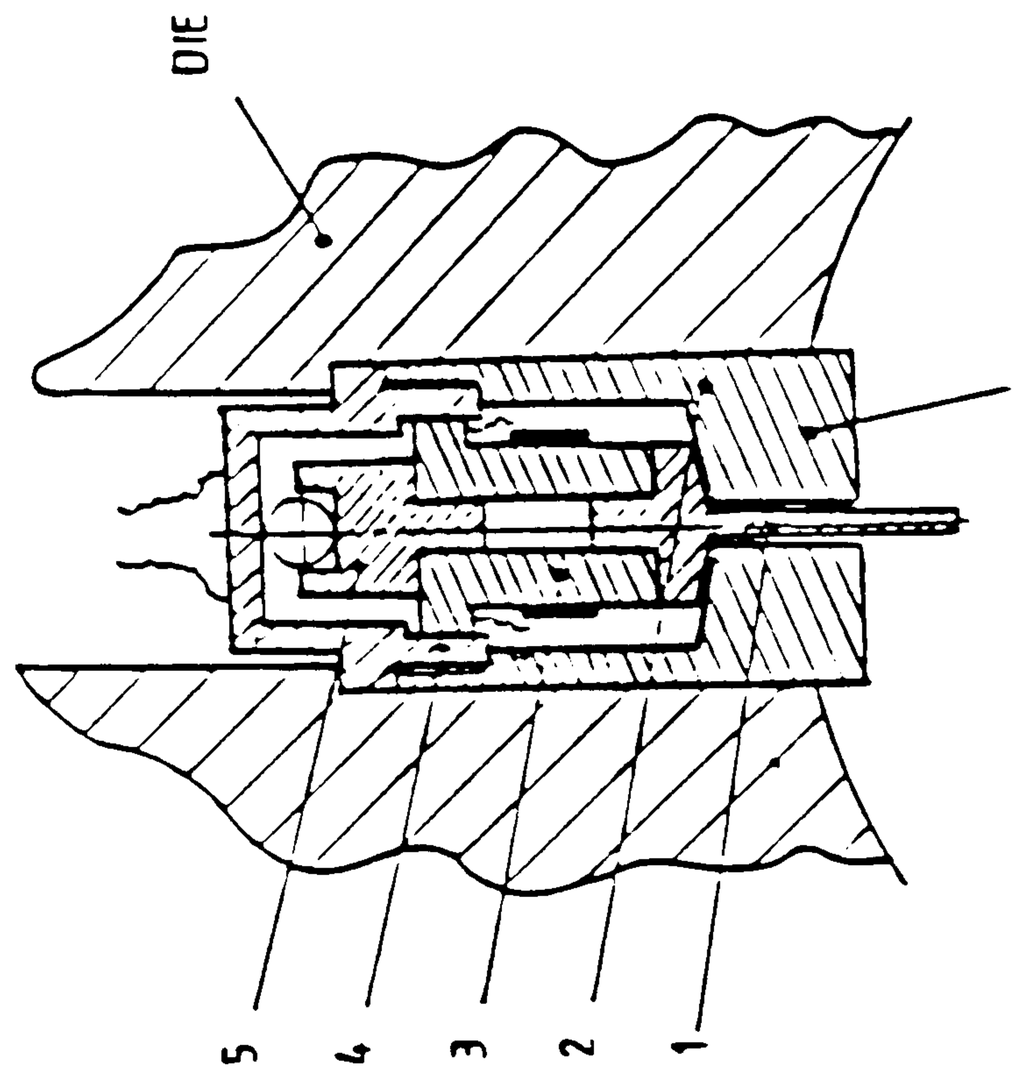

Fig. 3.4b Sectional view of pressure transducer mounted in the die

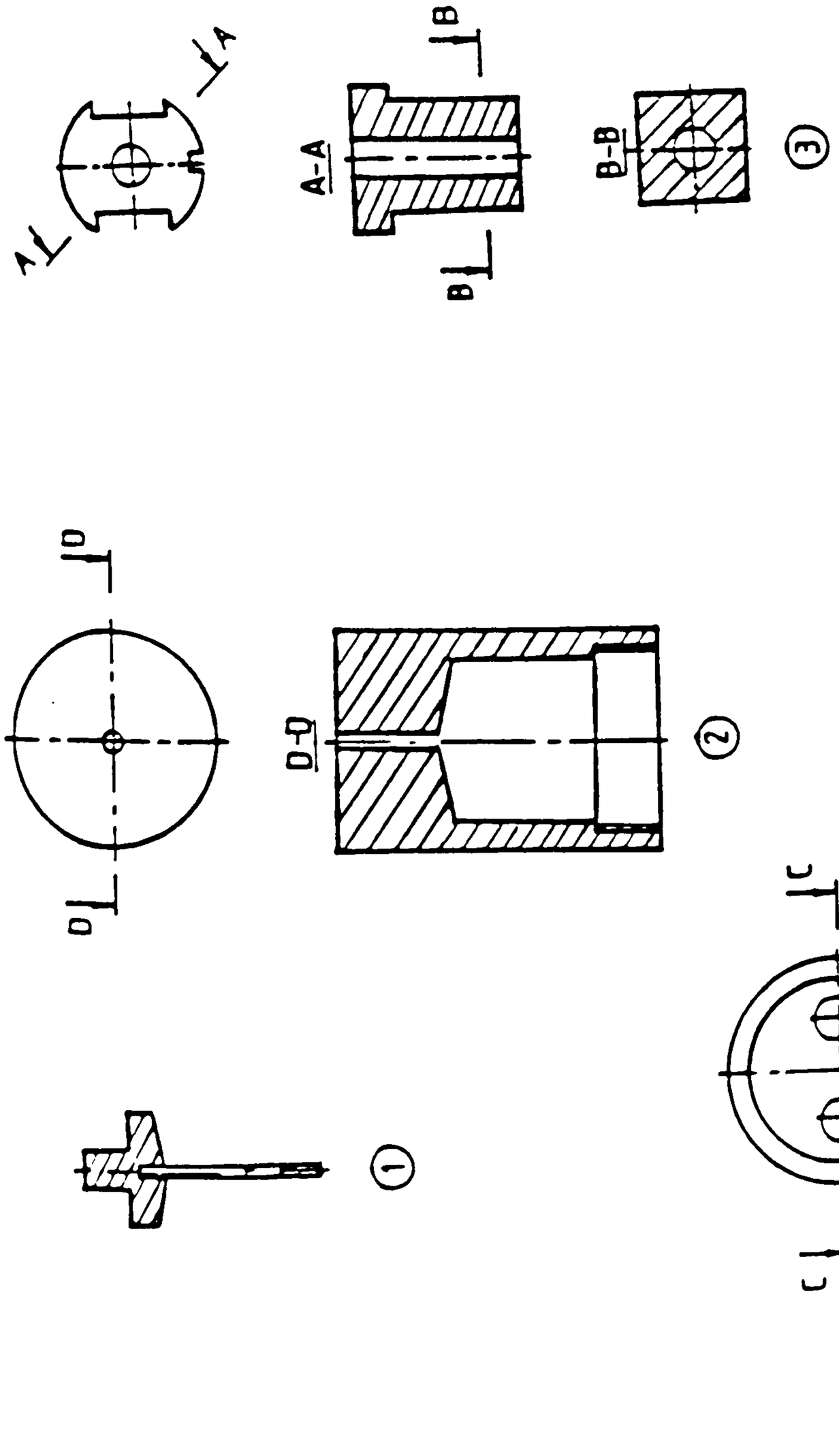

Fig. 3.4a Sectioned diagrams of pressure transducer components

compression(SGC) and in tension(SGT). The guages were self-temperature compensating KSN type with an output of about 20 times that of ordinary wire guages and therefore required small amplification to have readable data.

(ii) When the adhered strain guages were dry, wire leads were soldered to their terminal indices and thereafter the transducer cup was pressed(interference fit) into the back end of the compression pillar. The steel ball was then placed into the cup and the wire leads pushed through exit holes provided in the inner housing.

(iii) After the inner housing had been placed at the back, the pressure pin was then carefully pressed(interference fit) into the front end of the compression pillar. It must be noted that, to have successful experiments, the ratio between the cross-section of the compression pillar to that of the pressure pin must be in the order of at least 10:1. Above that the compression pillar tends to become very stiff and way below that it becomes too flexible. It must also be stated that during pressing of the pressure pin into the compression pillar, no load must be exerted on the pin itself, or else this will cause unecessary deformation and hence bring about friction forces between the pressure pin and the outer housing passage.

(iv) Then the pressure pin was lapped into the passage of the outer housing. The fit between the pin and the housing must be of high-precision, so that no room around it is left and on the other hand very low friction is experienced.

(v) After the complete pressure transducer has been assembled, then it is pressed into the die (interference fit) until it locks against a shoulder provided.

(vi) When all the five transducers were in place, the die was then taken for grinding to make the pressure pins flush in the fillet radius.

Before tests were conducted a die with three mounted pressure transducers was prepared for calibration. It was placed in a jig specially designed for this purpose. Once fixed, the calibration of the pressure transducers were carried out with the method shown diagrammatically in fig.3.5. Basically to get the calibration factor, a series of increasing and decreasing normal loads were applied. The loads were transmitted to the pressure pins through a pellet of soft aluminium which ensured no damage.

The average calibration graph obtained is shown in fig.3.6 of which the calibration factor is equal to 13.714KN/Volt. It must be stated that the difference in voltage output of the three tested pressure transducers gave very small discrepancies of about 2.68%, which was considered to be negligable.

3.3 TEST METHOD

The test method employed was exactly the same as that of quasi-static experimental tests. Thus, the Universal Avery machine was used for uniaxial compression test of the inverbucktube, figs.3.7 and 3.8. Before tests, all wire leads from the five pressure transducers were connected to the carrier amplifier in the sequence shown in fig.3.9 for signal amplification of up to ten times. From here, the voltage outputs were sent to the data Logger 2200B where the signals were digitised and printed on paper.

Thereafter, the die with half inverbucktube was placed on the piston actuator through a protecting plate, raised at a very slow speed of $1.65*10^{-5}$ m/s until the top of the

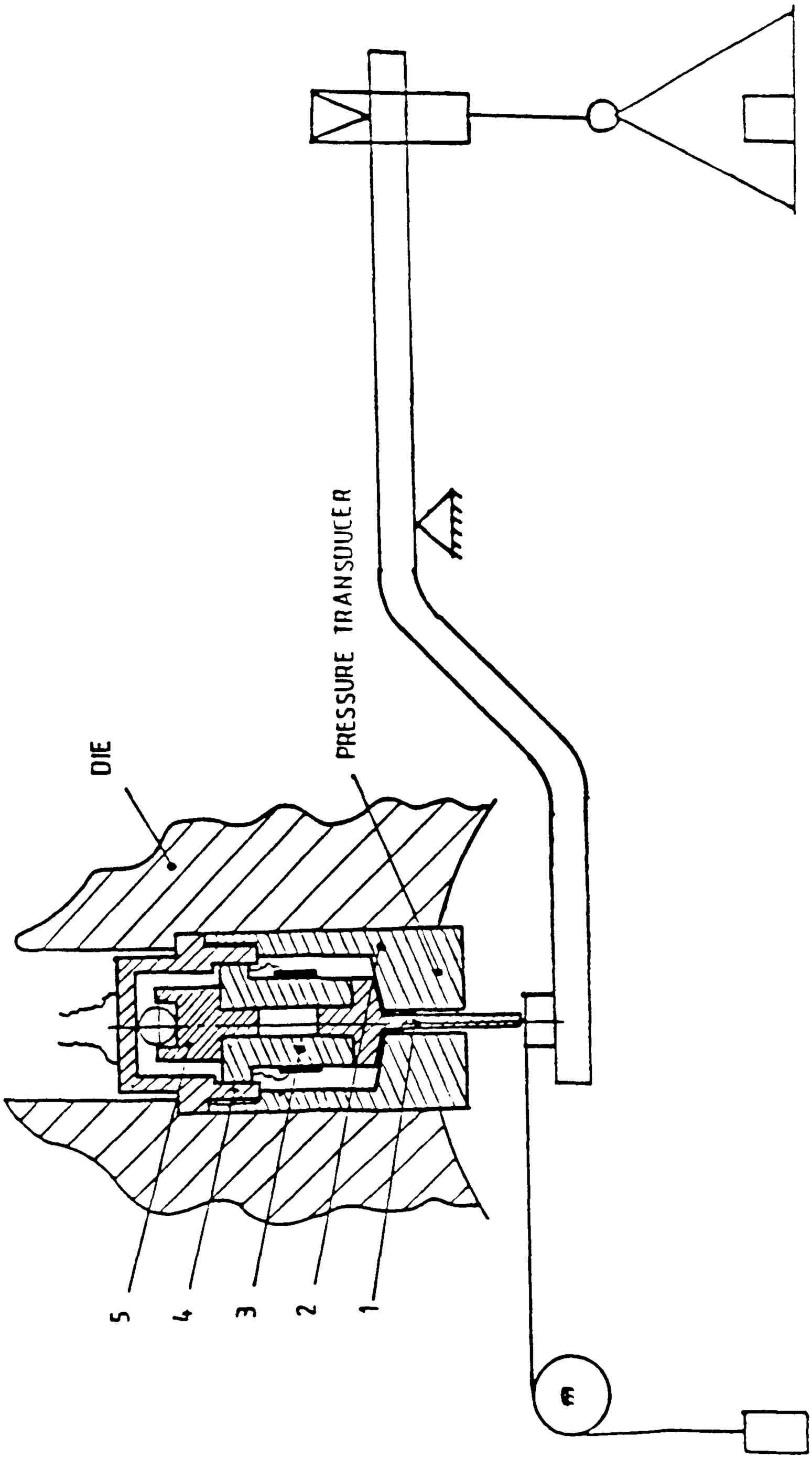

Fig.3.5 Apparatus for calibrating the pressure transducer

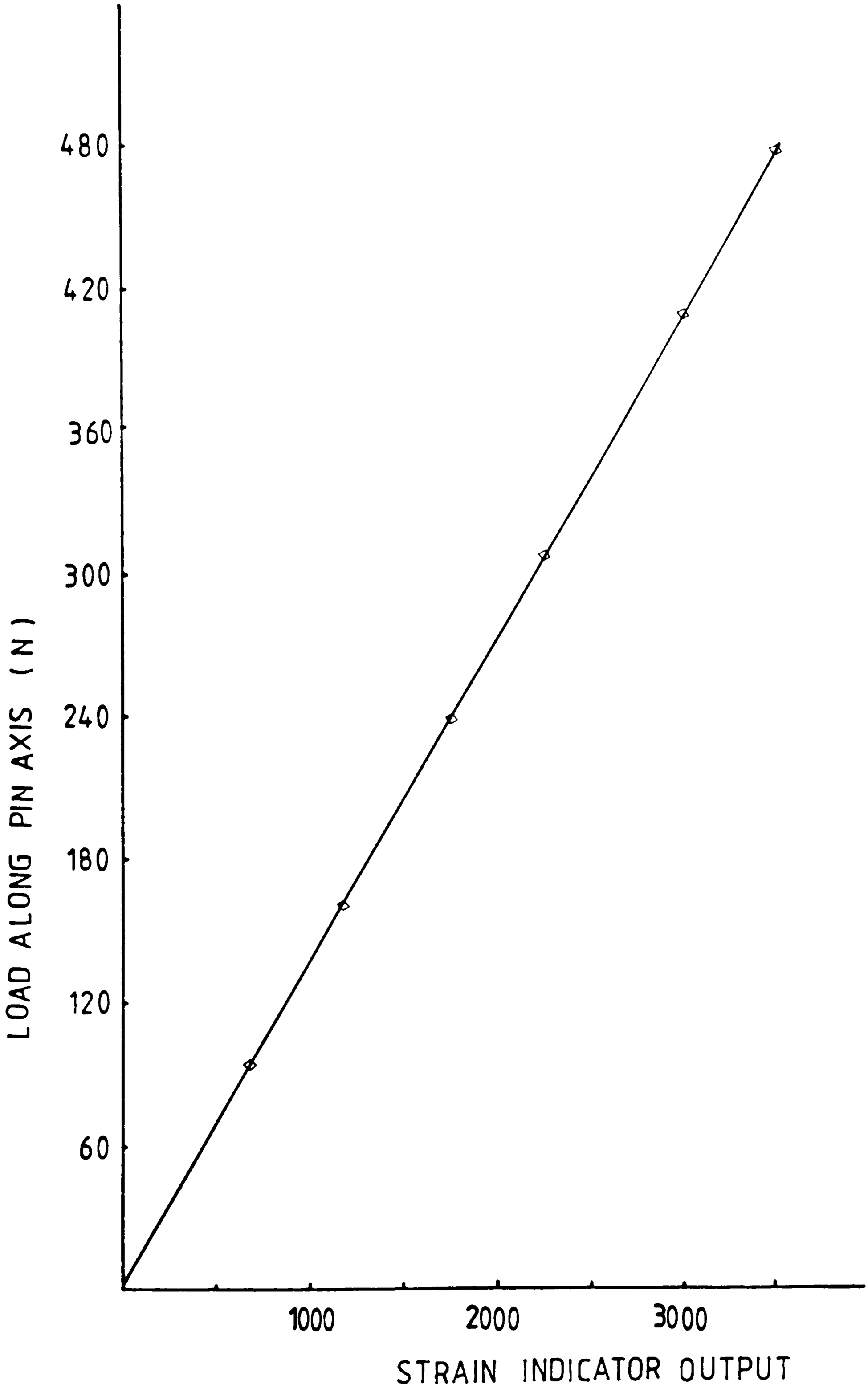

Fig.3.6 Calibration graph for pressure transducer

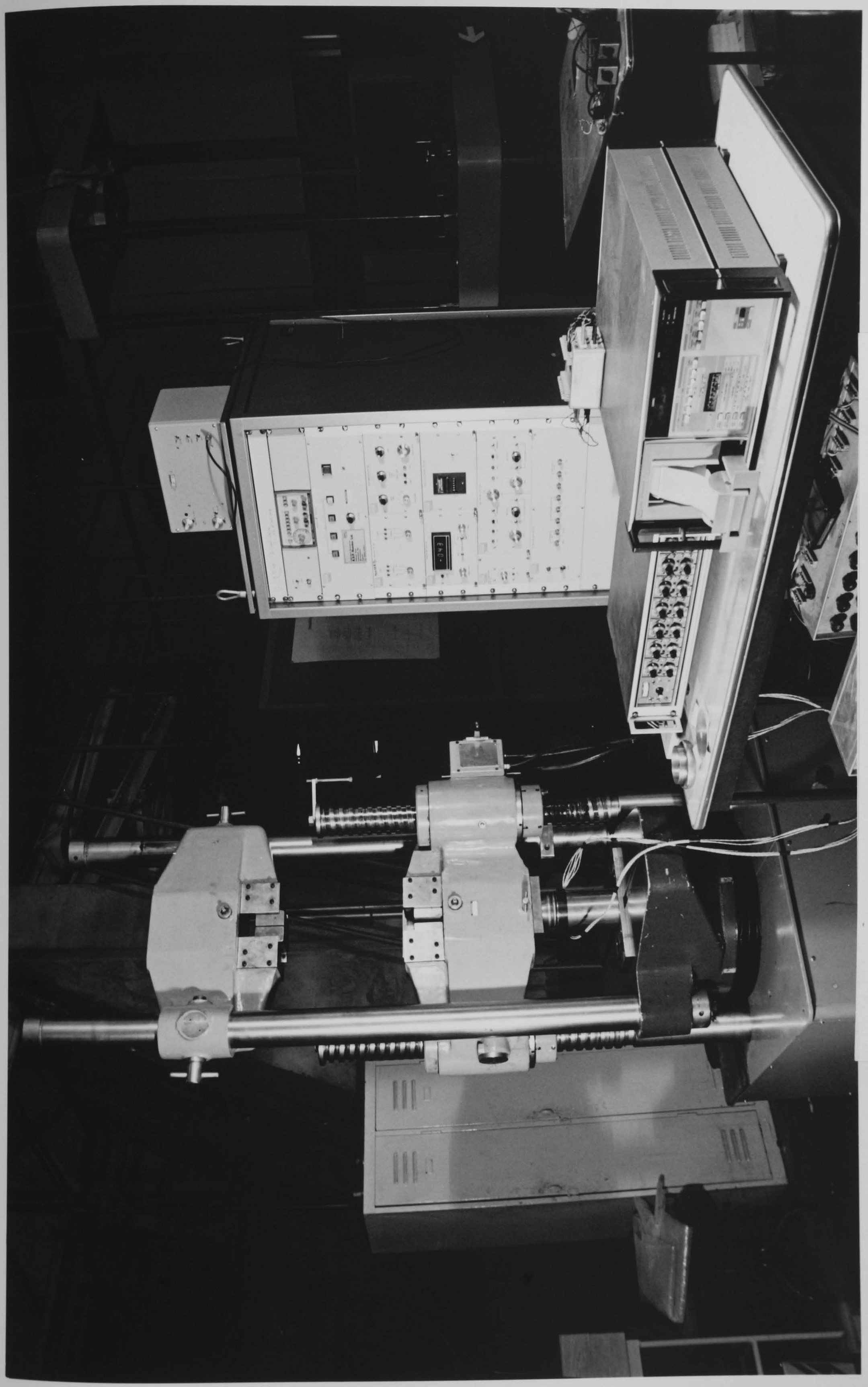

Fig.3.7 Normal pressure measuring arrangement

Fig.3.8 Close up of deforming inverbuckling tube during normal pressure measurement

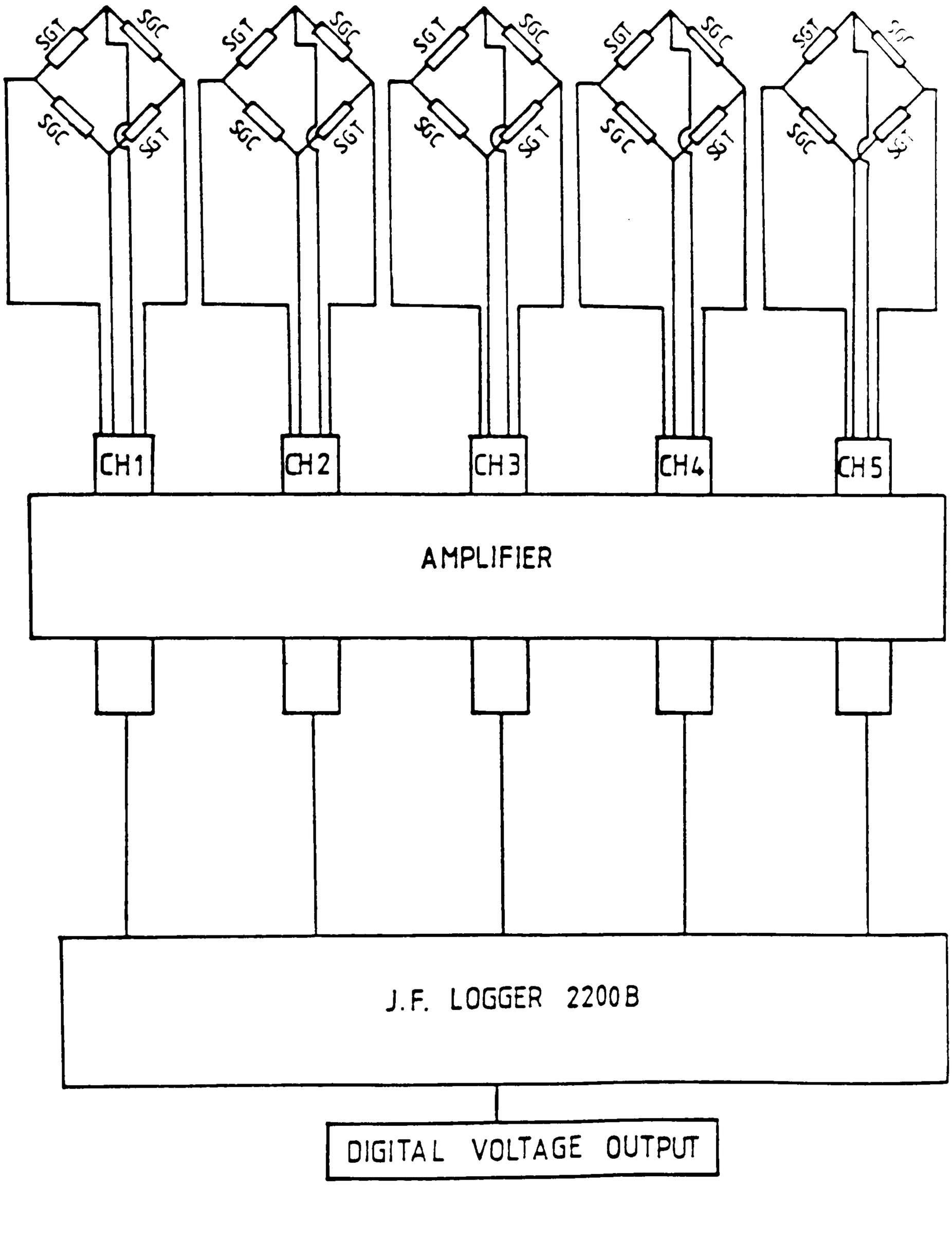

Fig.3.9 Schematic diagram of instrumentations used in the measurement of normal pressure

half inverbucktube was just touching the lower surface of the crosshead through a second protecting plate. Then all related instruments were checked once more to see if they were on *"standby"*. Once convinced, the test then was carried out at the approximate speed of that used in the quasi-static tests.

3.4 PRESSURE DISTRIBUTION TEST RESULTS

A total of 24 tests were conducted and pressure distribution curves recorded. A number of these recorded curves were virtually identical as they were purposely experimented under the same conditions to check repeatability. Results are presented in table 3.1 and each test represents the average of three tets conducted.

However, typical pressure distribution curve for the inverbucktube of internal diameter, D_i=72mm and $\bar{D}/2t_o$=13.85 is shown in fig.3.10.

Closely looking at fig.3.10, stages of deformation and pressure distribution can be described. It can be easily seen that as the load increases the pressure rises from point '1' until it reaches point '2'. It was very difficult at first to know exactly what was happening in this region until more identical tests were carried out for careful observation. It was determined that, as the tapered part was being pushed from 0° to 24° round the die fillet radius, the inverbucktube appeared to being elastically deformed until it reached 24° when it developed into the shape similar to a frustrum of a cone and started inverting(curling).

From point '2' where inversion began, the pressure seemed to increase as the inverbucktube's cross-sectional area increased until point '3' when the pressure started

decreasing. The reason of decrease according to our observation and understanding was that, the inverbucktube after 65° started *"separating"* from the die fillet radius, thus applying less normal stresses with subsequent inversion(curling).

From table 3.1, it can be seen that as the geometry factor increases, the normal pressure distribution peak reduces. The position of peak pressure with reference to the radius angle seemed to depend mainly on the ratio between t_1 and t_2. This ratio in turn characterized the form of inversion or curling.

It was also observed that, as the inverbucktube thickness increased, i.e. the reduction in taper angle, the stage from point '1' to '2' became steeper, showing the increase in stiffness. As the inverbucktube went to constant thickness the kink which can be seen at point '2' virtually disappeared, producing a nearly straight smooth curve right from point '1'. On the other hand, simultaneously pushing the maximum pressure upwards.

The effect of loading speed on the pressure distribution was assessed. The great majority of tests were carried out at speeds between $4.55*10^{-5}$ m/s and $4.65*10^{-5}$ m/s. For comparison purposes, some tests on identical half inverbucktubes were carried out at speeds higher than those stated above. The results were as expected and showed no detectable change.

To assess the effect of lubrication on the pressure distribution, three tests were carried out on again identical inverbucktubes. Graphite based grease was applied and the results showed a generally slight reduction in pressure values from those recorded under dry

lubrication conditions. Some of the results are in table 3.1 (tests 5 and 6).

All tests were very successful, infact beyond expectation, although more tests could have been carried out. For example, it would have been possible to find the behaviour of pressure distribution to geometry factor and die radii. However, the former was determined theoretically and this is shown in fig.5.4. The main problem which hindered the progress in doing more tests was the expense towards pressure transducers. The reason being - high-precision of manufacturing required. The other reason was, to get very good results, the pressure transducers had to be used only once and sometimes twice. If used more than that, they gave errors in the readings.

TABLE 3.1 Normal pressure experimental data

TEST No.	$\bar{D}/2t_e$	r (mm)	lubrication	V (ms^{-1}) *10-5	α (°)	N_{max} (N/mm^2)
1	11.08	5.8	dry	4.62	65	980.0
2	12.00	5.8	dry	4.58	52	920.0
3	10.07	5.8	dry	4.60	63	1106.9
4	11.52	5.8	dry	4.59	60	965.0
5	10.29	5.8	dry	4.62	59	1020.0
6	10.29	5.8	G.G.	4.61	62	875.0

G.G. - Graphite based grease

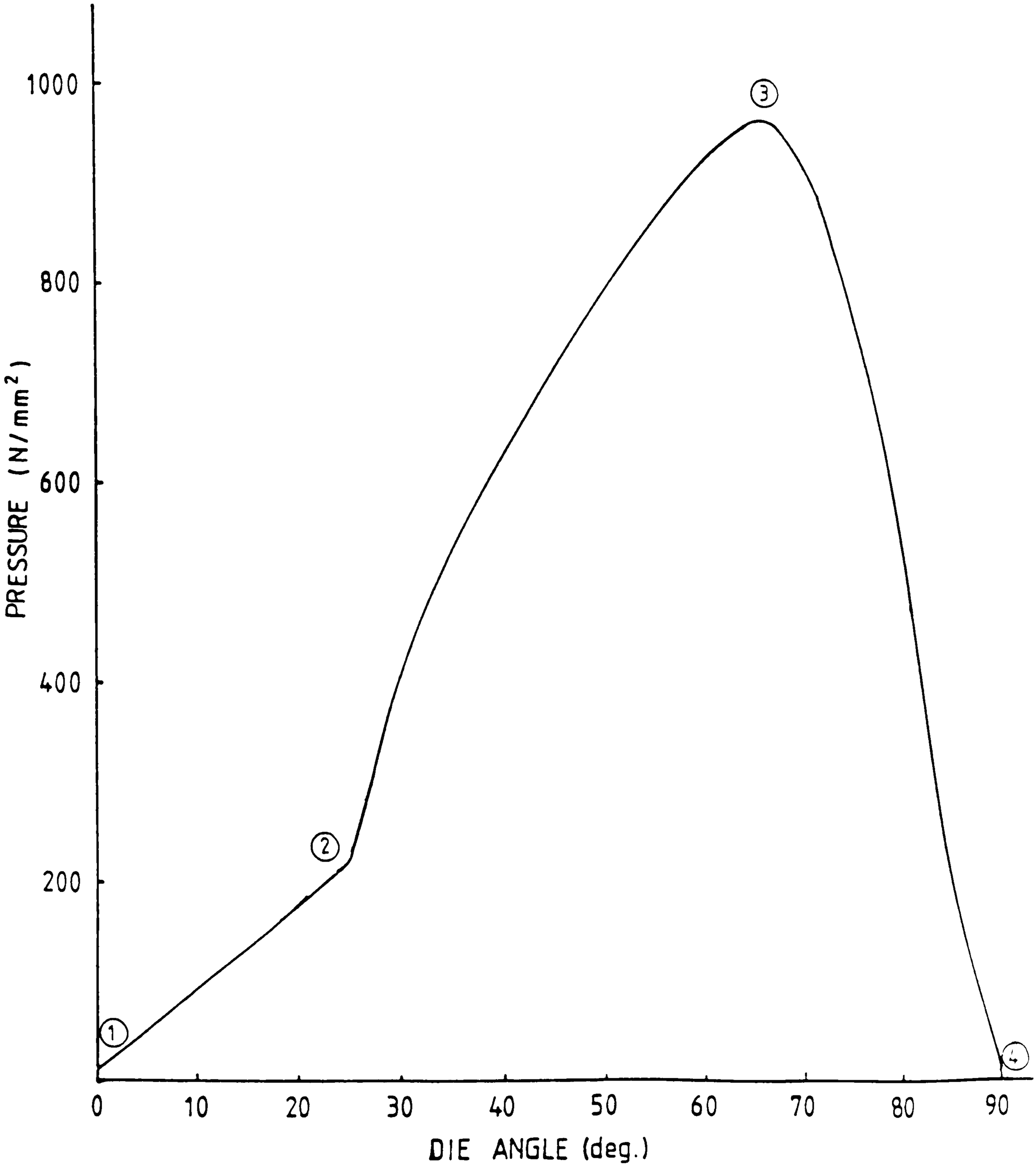

Fig. 3.10 Experimental normal pressure distribution curve ($\bar{D}/2t_o$ = 13.85)

CHAPTER IV

THEORETICAL CONSIDERATION OF INVERBUCKTUBE

4.1 INTRODUCTION

The analytical model involved here, is an inverbucktube shown in fig.4.1. A combination of two distinctive collapse modes can be easily seen. These are namely, (i) inversion(curling) of the tapered parts and (ii) axisymmetric buckling(concertina) of the constant thickness middle part.

Consider a thin-walled tube tapered at both ends and constant thickness in the middle part, whose constraints in longitudinal direction is limited by the corresponding dies, fig.4.1a. If subjected to an increasing axial compressive load, the tube will *"curl"* over the die fillet radii. As a result, simultaneous bending, stretching and finally bending again takes place to form the inverted tapered parts. Once inversion or curling is complete on both sides, the compressive loads keep on increasing as the lips of the outer tube lock themselves to the main body until bulging of the middle part is observed. As a result, there is again simultaneous bending in the three circumferential hinges and expansion between these hinges.

In general, plastic-strain energy approach, similar to that adopted by references(3, 36, 61-64, 66)* will be employed in the analysis. This is based on the velocity conditions and also to satisfy incompressibility and continuity of plastically deforming solids. Therefore, the energies involved in compressing an inverbucktube are: (i) Work done due to deformation, (W_D); (ii) Energy loss due to friction between inverbucktube and die interface,

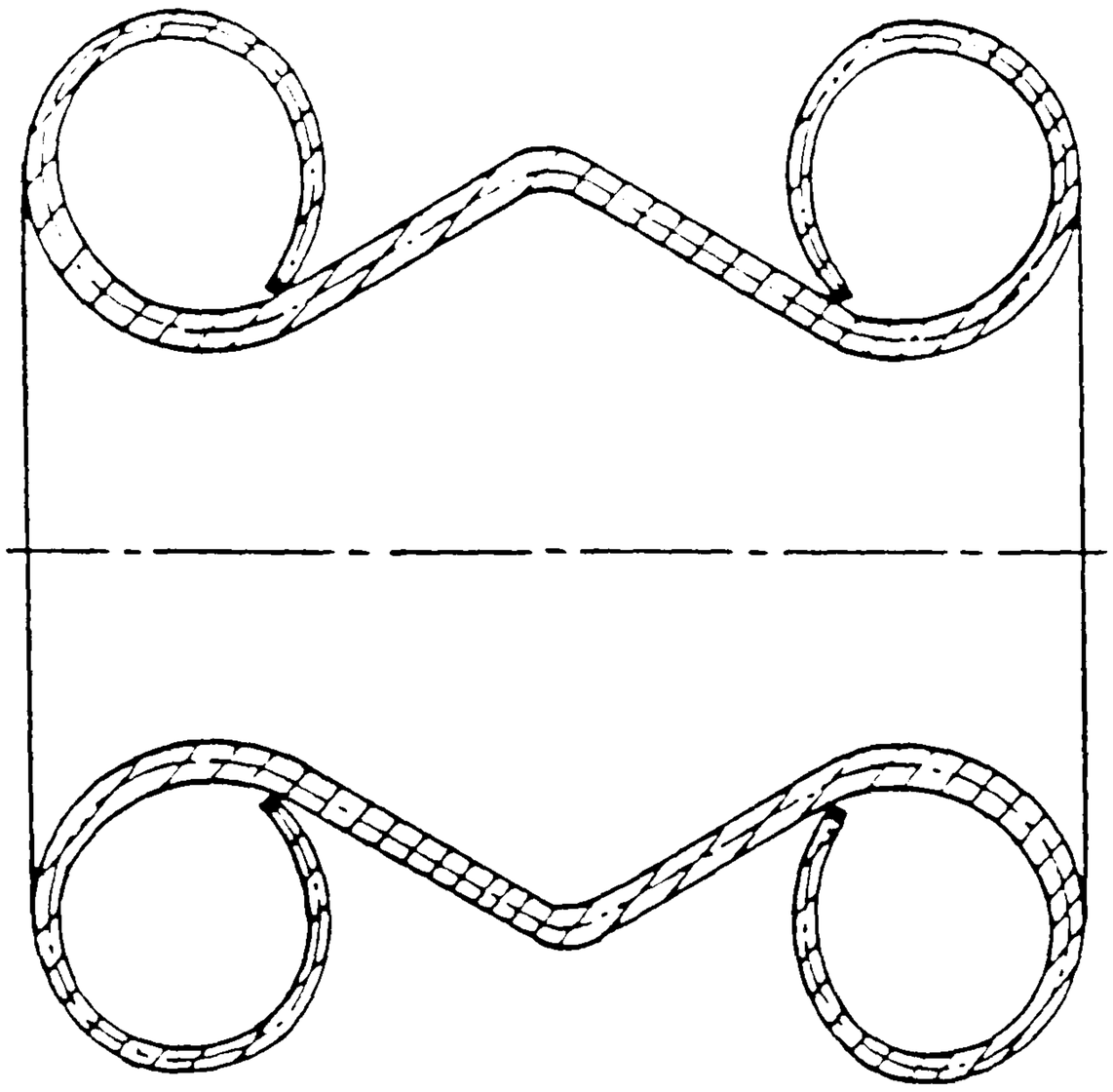

Fig. 4.1b Idealized inverbucktube after collapse

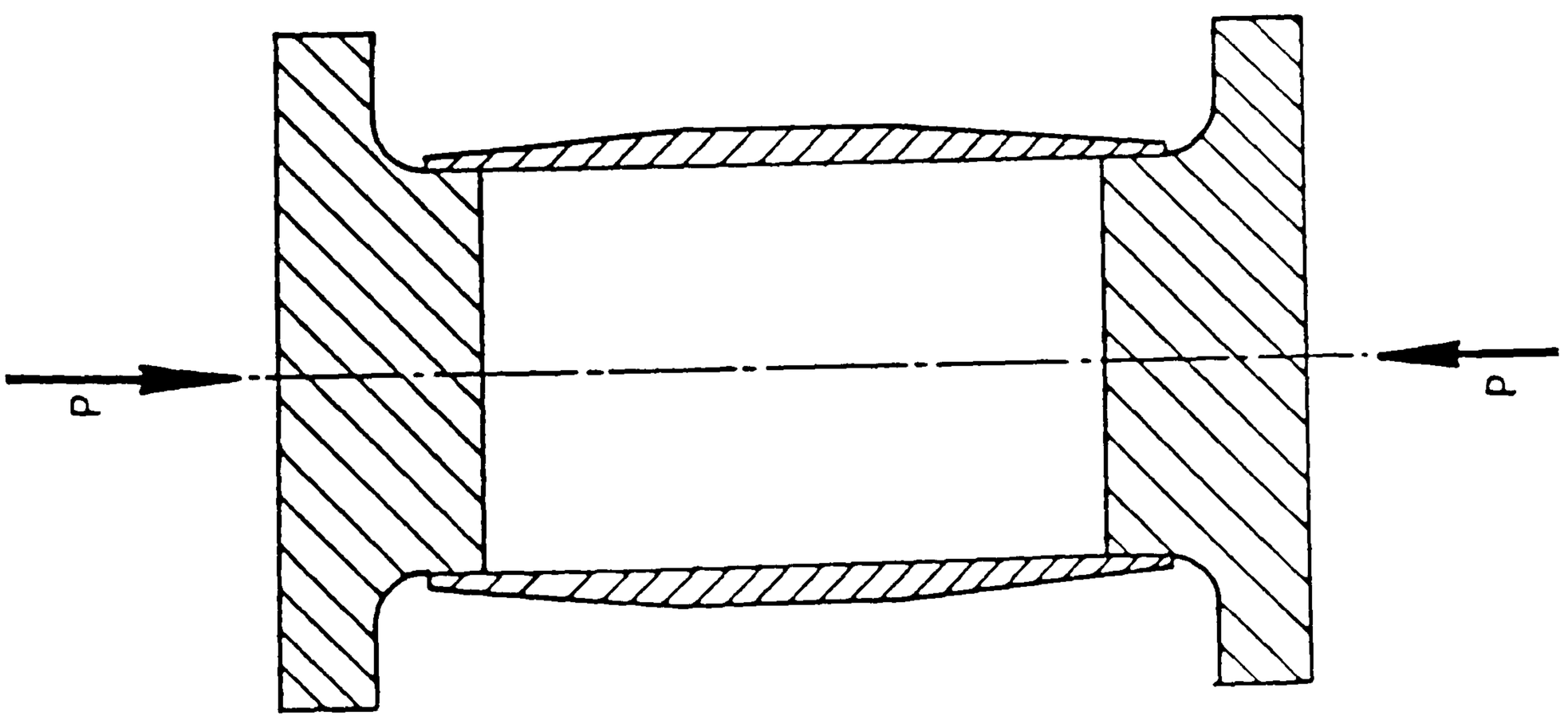

Fig. 4.1a Idealized inverbucktube before collapse

(W_F) and (iii) work involved with the external compressive load, ($W_T = \bar{P} * \delta$).

The interrelation of these plastic process variables are determined by setting the energy balance to zero as in eq.4.1

$$\sum W_i = 0$$

or

$$W_D + W_F - W_T = 0 \qquad 4.1$$

The work done due to deformation is therefore divided into three defferent plastic processes, namely: (i) Work done by bending at A (fig.4.4), (W_B); (ii) work done by expansion of the material between A and B, (W_E) and (iii) work done by axisymmetric buckling, (W_{BL}).

The expression for deformation then becomes

$$W_D = W_B + W_E + W_{BL} \qquad 4.2$$

where, $$W_{BL} = W_{BBL} + W_{EBL} \qquad 4.3$$

Substituting eq.4.3 and 4.2 into eq.4.1, the energy balance equation becomes

$$W_B + W_E + W_{BBL} + W_{EBL} + W_F - W_T = 0 \qquad 4.4$$

or

$$W_T = W_B + W_E + W_{BBL} + W_{EBL} + W_F \qquad 4.5$$

Before analysing eq.4.5 into details, it is better to introduce the following assumptions to the analysis:

(i) Material of the inverbucktube is work hardening and the effect of biaxial stresses on the yield stresses are neglected.

(ii) Work done by the compressive load is entirely dissipated as internal plastic work and heat in substructural processes.

(iii) Change in wall thickness at any point of the inverbucktube is very small(from experiments, 0.67% to 1.5% depending on $\bar{D}/2t_o$). Consequently, the wall thickness is assumed to remain constant throughout its length, i.e., plane strain condition.

(iv) Friction is considered to be constant along the whole fillet radius interface and defined by Coulomb law, which implies a constant coefficient of friction.

(v) Dies are considered to be very stiff, therefore rigid bodies.

(vi) Sticking is ignored between the inverbucktube internal surface and the die fillet radius.

(vii) Bauchinger effects are not considerable.

(viii) Strain distribution across sections vary linearly.

(ix) Axisymmetric buckling occurs ONLY when inversion or curling is complete.

(x) Circumferential hinges in buckling are considered as stationary.

4.2 WORK DONE DUE TO EXPANSION IN THE TAPERED PART DURING INVERSION

From all the above mentioned processes, this takes care of the plastic energy in rotation of each element of the tapered part length which goes through points A and B, fig.4.4.

The energy consumed due to material expansion between A and B is expressed in strain energy theory as

$$W_E = V \left[\int \bar{\sigma} \, d\bar{\varepsilon} \right] \qquad 4.6$$

$$\text{where, } \bar{\sigma} = A \, \bar{\varepsilon}^n \qquad 4.7$$

Physically speaking, eq.4.6 is the plastic work increment dissipated in the body during expansion between A and B, and corresponds to materials which obey the Mises yield criterion and Levy-Mises flow rule.

4.2.1 VOLUME OF INVERBUCKTUBE

The volume of the tapered part material could be easily determined from fig. 4.2 as

$$V_1 = \frac{2\pi l_1}{3} \left[l_1^2 \tan\theta + 3 l_1 \tan\theta (R_i + t_2) + 3 t_2 (2R_i + t_2) \right] \qquad 4.8$$

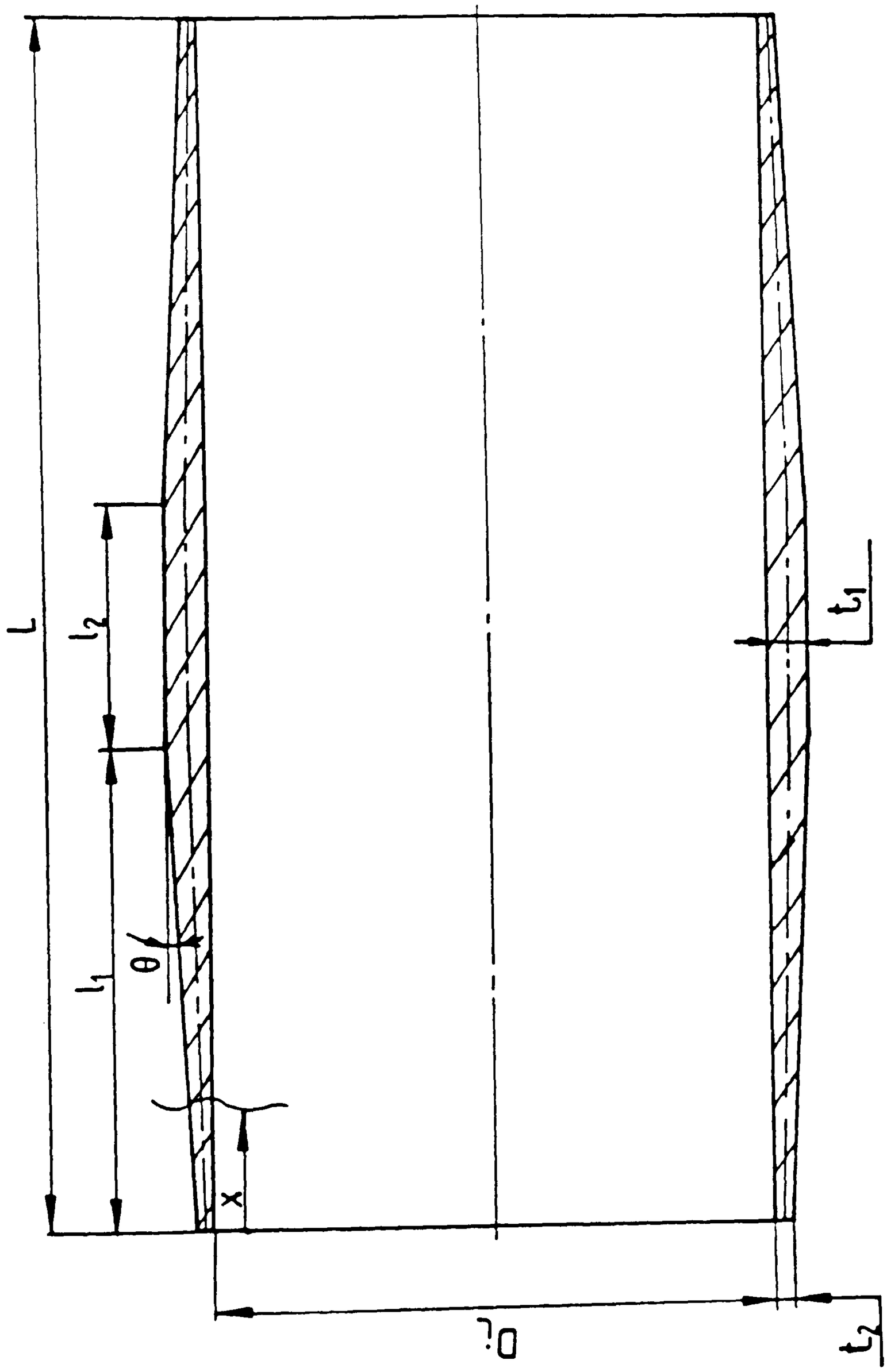

Fig.4.2 Detailed inverbucktube

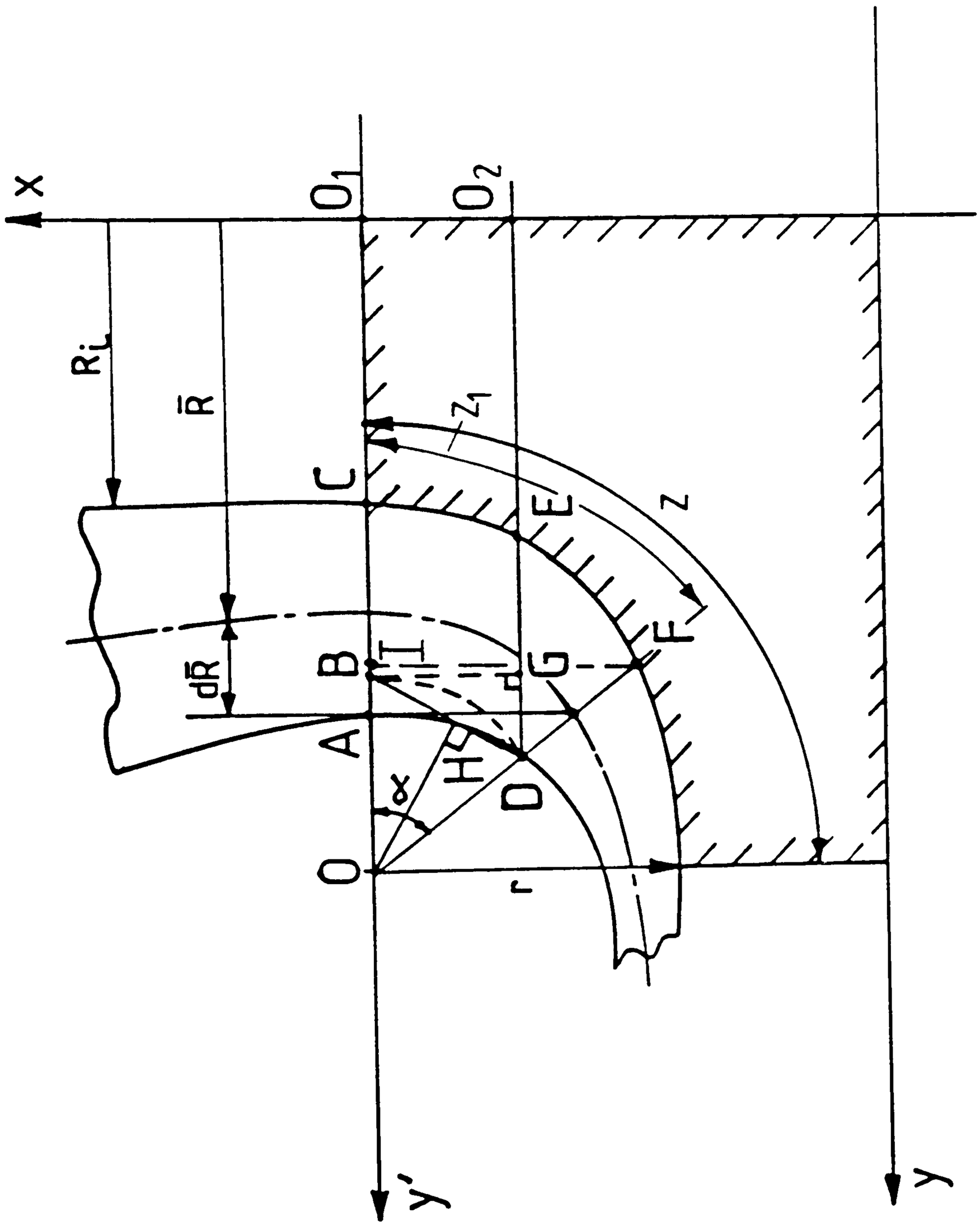

Fig.4.3 Geometry analysis diagram

4.2.2 STRAIN

Under the action of axisymmetric forces that are acting at the surfaces, the three principal strains are circumferential, ε_θ; longitudinal ε_l and thickness, ε_t.

From incompressibility condition, the sum of principal strains equal to zero, thus

$$\varepsilon_\theta + \varepsilon_l + \varepsilon_t = 0 \qquad 4.9$$

It is known from the experiments that thickness strains were negligible, therefore it can be confidently assumed that $\varepsilon_t = 0$.

Then equation 4.9 becomes

$$\varepsilon_l = -\varepsilon_\theta \qquad 4.10$$

The circumferential or hoop expansion strain is

$$\varepsilon_\theta = \ln \frac{\bar{R}'}{\bar{R}} \qquad 4.11$$

Looking at fig.4.2, the original mean inverbucktube radius $\bar{R}$ of the tapered part can be presented as a function of 'X'.

when, $x = 0$, $\bar{R} = R_i + t_x/2$

$$x = x_1,\ \bar{R} = R_i + \frac{t_\alpha + x_1 \tan\theta}{2}$$

Therefore, the general equation for the mean radius before plastic deformation, becomes

$$\bar{R}(x) = R_i + \frac{t_\alpha + x\tan\theta}{2} \qquad 4.12$$

If compressive load is applied to the inverbucktube, the tapered ends will move *"round"* the die fillet radii. Looking closely at one end as shown in fig.4.3, this will move a distance z_1. If a line is drawn from the die fillet radius centre O, it will cut the tapered part at D and F. By drawing from point F, a perpendicular to point I which lies on reference axis Y', the increased inverbucktube internal radius $R'_i(\alpha)$ can be determined as follows

$$IO = OF\cos\alpha$$

$$\text{and} \quad IO = r - IC = r - \Delta r$$

$$\text{where,} \quad \Delta r = r(1 - \cos\alpha)$$

from geometry,

$$R'_i(\alpha) = R_i + \Delta r$$

or

$$R'_i(\alpha) = R_i + r(1-\cos\alpha) \qquad 4.13$$

where, α is from 0 to 310°.

By drawing an arc of radius OD to cut the reference axis at B, the increased outer radius R'_o can be found as follows;

Draw a perpendicular from point B to cut DO_2 at G, then

$$a)\ DO_2 = R'_o(x,\alpha) = GO_2 + DG$$

where $$b)\ GO_2 = BO_1 = R'_o(x,\alpha=0) \qquad 4.14$$

$$c)\ DG = BD \sin\frac{\alpha}{2}$$

and $$d)\ BD = 2OB \sin\frac{\alpha}{2}$$

substitute eq.4.14d into eq. 4.14c

$$DG = 2OB \sin^2\frac{\alpha}{2} \qquad 4.15$$

where $$OB = R_1 + r - R'_o(x,\alpha=0) \qquad 4.16$$

substituting eq.4.16 into eq.4.15, then into eq.4.14b and finally in eq.4.14a, becomes

$$R'_o(x,\alpha) = R'_o(x,\alpha=0) + 2\left[(R_1 + r) - R'_o(x,\alpha=0)\right] \sin^2\frac{\alpha}{2} \qquad 4.17$$

where $$\sin^2\frac{\alpha}{2} = \frac{1-\cos\alpha}{2}$$

Then eq.4.17 becomes

$$R'_o(x,\alpha) = R_i + r - [(R_i + r) - R'_o(x,\alpha=0)] \cos\alpha \qquad 4.18$$

where $R'_o(x,\alpha=0) = qx + y_1$

and $q = \tan\theta$; $x = z - \alpha r$; $y_1 = R_i + t_2$

Substituting these values in eq.4.18 and taking $z=\pi r$, the external increased radius at any distance travelled can be found as

$$R'_o(z,\alpha) = (R_i + r) - [\, r - r\tan\theta\ (\pi - \alpha) - t_2] \cos\alpha \qquad 4.19$$

The mean increased radius therefore becomes

$$\bar{R}' = \frac{R'_i + R'_o}{2}$$

or

$$2\bar{R}' = 2(R_i+r) - r\cos\alpha - \{\, r[1-(\pi-\alpha)\tan\theta] - t_x\} \cos\alpha \qquad 4.20$$

where, $t_x = t_2(z)$

$\bar{R}$ and $\bar{R}'$ are known. Therefore, they can be substituted into eq.4.11, bearing in mind that $x=2r(\pi-\alpha)$ when an element of the half tapered part length has rotated through π radians.

Therefore, the circumferential strain becomes,

$$\varepsilon_\theta = \ln \frac{\bar{R}'}{\bar{R}} = \ln\left[\frac{2R_i + r(2-\cos\alpha) - \{r[1-(\pi-\alpha)\tan\theta] - t_x\}\cos\alpha}{2R_i + t_x + r(\pi-\alpha)\tan\theta} \right] \qquad 4.21$$

The effective strain is expressed in terms of principal strains ε_1, ε_2 and ε_3 as

$$\bar{\varepsilon} = \left[\frac{2}{9} \{(\varepsilon_1-\varepsilon_2)^2 + (\varepsilon_2-\varepsilon_3)^2 + (\varepsilon_3-\varepsilon_1)^2\} \right]^{1/2} \qquad 4.22$$

Substituting ε_1, ε_2, ε_3 by ε_θ, ε_t and ε_1 respectively into eq.4.22 and simplify as $\varepsilon_t=0$, the effective strain in terms of circumferential strain becomes

$$\bar{\varepsilon} = \frac{2}{\sqrt{3}} \varepsilon_\theta$$

or

$$\bar{\varepsilon} = \frac{2}{\sqrt{3}} \ln\left[\frac{2R_i + r(2-\cos\alpha) - \{r[1-(\pi-\alpha)\tan\theta] - t_x\}\cos\alpha}{2R_i + t_x + r(\pi-\alpha)\tan\theta} \right] \qquad 4.23$$

If let say $\varepsilon_\theta = \Omega_1$, then eq.4.23 becomes

$$\bar{\varepsilon} = \frac{2}{\sqrt{3}} \Omega_1 \qquad 4.24$$

Then eq.4.24 can be substituted into eq.4.6 taking into account eq.4.7. Thus, the plastic work done in circumferential expansion at both ends is

$$We = 2\, V \int A\, \bar{\varepsilon}^n\, d\bar{\varepsilon}$$

or

$$\frac{We}{\delta_1} = \frac{2\pi\bar{D}t_z A}{n+1}\left[\frac{2}{\sqrt{3}} - \Omega_1\right]^{n+1} / \text{ unit length} \qquad 4.25$$

This is the work done due to expansion per unit length of the tapered parts of inverbucktube.

4.3 WORK DONE DUE TO BENDING IN THE TAPERED PART DURING INVERSION

Work done in deforming the inverbucktube during invesion can be identified by looking closely at fig.4.4, as the plastic process due to bending at 'A'. Where point 'A' signifies the mark where the tapered part of the inverbucktube starts entering the die fillet radius. From experiments, it was observed that at this particular point, the tapered part took a new internal radius, $R'_i = R_i(\alpha)$, and a shape similar to a frustrum of a cone was noticed developing. While 'B' signifies the point where lips of the inverbucktube bend inside towards the main body.

Bearing in mind eq.4.22, and taking into account incompressibility condition, the following is obtained

$$\bar{\varepsilon} = \frac{2}{\sqrt{3}} - \varepsilon_B \qquad 4.26$$

The amount of work done in bending the inverbucktube tapered element at point 'A' is

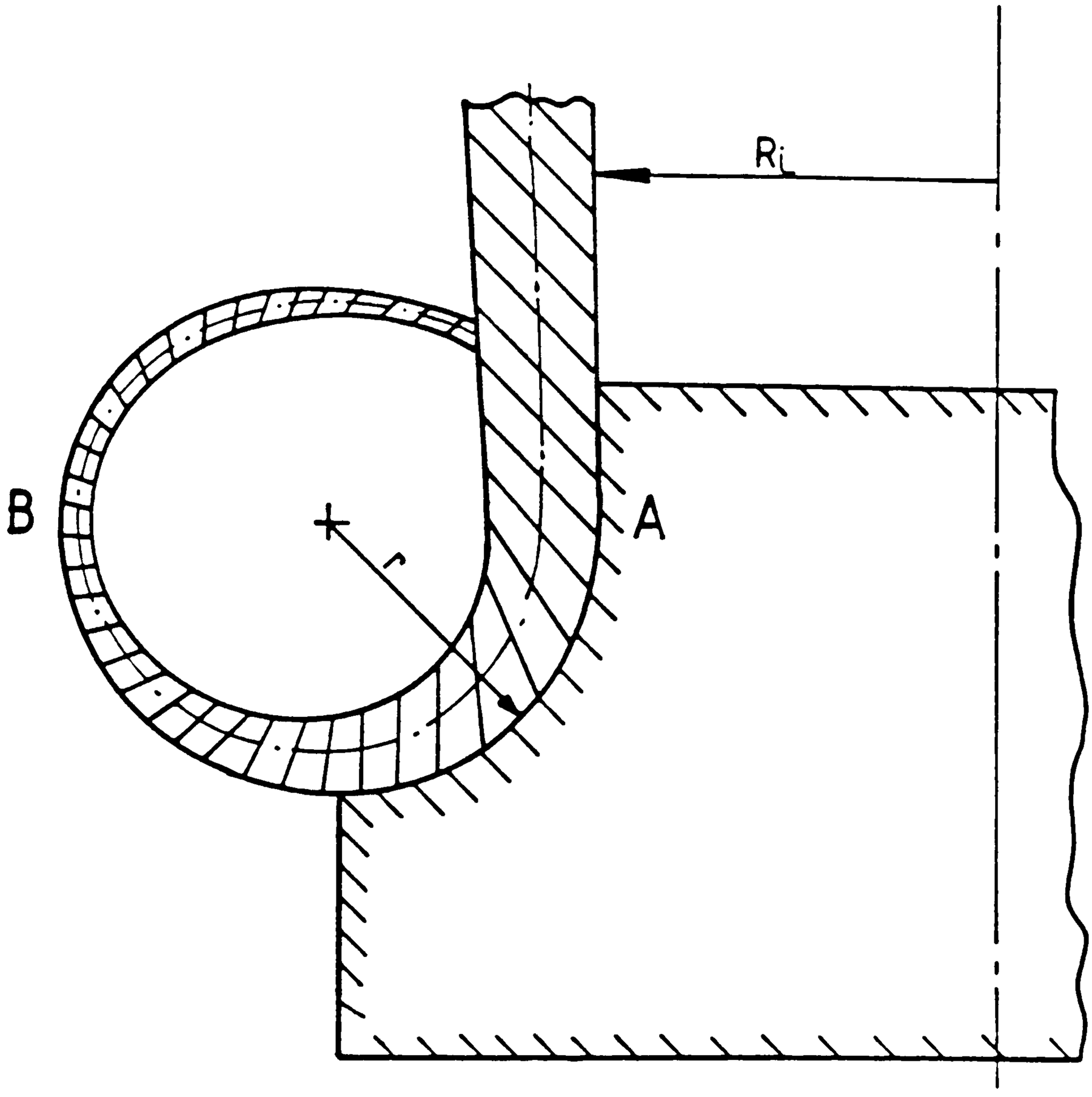

Fig. 4.4 Configuration of the inverted part of inverbucktube

$$W_B = V \left[\int \bar{\sigma}\, d\bar{\varepsilon} \right] \qquad 4.27$$

If it is assumed that the neutral axis remains at the centroid of the section and strain distribution across a section varies linearly, then the average bending strain to bend a straight element with a constant thickness is approximately

$$\varepsilon_B \approx \frac{1}{2} \ln\left[\frac{2r+t}{2r} \right] \qquad 4.28$$

It is known that t≠const. Therefore, with the assumption of no volume change, the value of thickness t_x of inverbucktube element which passes point 'A' can be found. From the geometry in fig.4.3, this can be as

$$DF = t_x = t_2 + r(\pi-\alpha)\tan\theta \qquad 4.29$$

Substitute eq.4.29 into 4.28

$$\varepsilon_B = \frac{1}{2} \ln\left[\frac{2r+t_2+r(\pi-\alpha)\tan\theta}{2r} \right] \qquad 4.30$$

If it is assumed that bending is only at 'A'. Therefore it follows that

$$2\varepsilon_B = \ln\left[\frac{2r+t_2+r(\pi-\alpha)\tan\theta}{2r} \right] \qquad 4.31$$

Substituting eq.4.30 into eq.4.26, the effective strain is written as

$$\bar{\varepsilon} = \frac{2}{\sqrt{3}} \ln\left[\frac{2r+t_2+r(\pi-\alpha)\tan\theta}{2r} \right] \qquad 4.32$$

The plastic work done due to bending at 'A' and taking into account eq.4.7 is

$$W_B = 2V\int A\bar{\varepsilon}^n d\bar{\varepsilon}$$

or

$$W_B = \frac{2\pi\bar{D}t_z A}{n+1} \left\{ \frac{2}{\sqrt{3}} \ln\left[\frac{2r+t_2+r(\pi-\alpha)\tan\theta}{2r} \right] \right\}^{n+1} \qquad 4.33$$

If let say $\varepsilon_B = \Omega_2$, then eq.4.33 becomes

$$\frac{W_B}{\delta_2} = \frac{2\pi\bar{D}t_z A}{n+1} \left[\frac{2}{\sqrt{3}} \Omega_2 \right]^{n+1} / \text{ unit length} \qquad 4.34$$

4.4 WORK DONE DUE TO AXISYMMETRIC BUCKLING OF THE CONSTANT THICKNESS PART OF INVERBUCKTUBE

Figure 4.5 shows the idealized axisymmetric buckling collapse mode of the inverbucktube. During experiments, the following were revealed which will act as the basis of assumptions during this analysis:

(i) Inversion terminated just after the lips came in contact with the main inverbucktube body;

(ii) at this moment, the inverbucktube became like a square cylindrical tube placed between two rigid surfaces.

(iii) Angle θ_1 increased from 0 to approximately the maximum of $\pi/2$. Immediately when θ_1 approached $\pi/2$, the two straight-sided convolutions came in contact to each other and after which complete collapse of the inverbucktube was perceived.

The analysis of the work done in deforming the constant thickness part of the inverbucktube into a single hinge system will follow the theory developed by Alexander(3)* and Abramovicz and Jones(36)*. Here though, the theory will be modified to incorporate the work-hardening effect.

The work done therefore is the sum of;

(a) Energy absorbed in the formation of three circumferential plastic hinges, (W_{EBL});

(b) and energy absorbed in expansion under substantially circumferential stress in metal between the hinges, (W_{EBL}).

If it is assumed that axisymmetric buckling will occur ONLY when (i) and (ii) are obeyed, then the work done can be determined.

Threfore, the total work done in collapsing one convolution, i.e. for θ_1 increasing from 0 to $\pi/2$ is

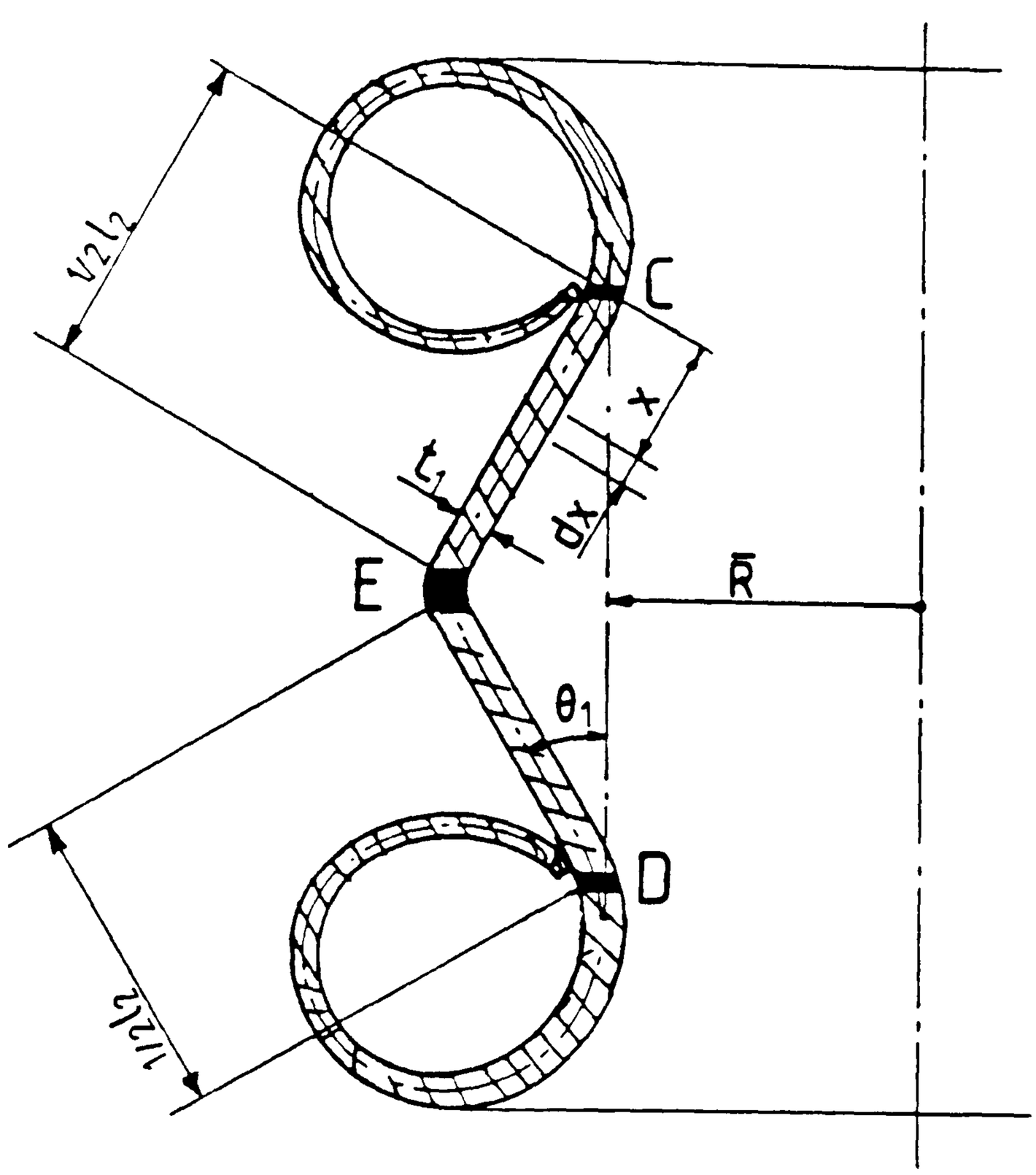

Fig. 4.5 Idealized inverbuckling collapse mode for analysis

$$W_{BL} = W_{BBL} + W_{EBL} \qquad 4.35$$

From Alexander(3)*, the energy absorbed in three stationary circumferential plastic hinges was given as

$$W_{BBL} = 4M_p\pi(\pi\bar{R} + \frac{1}{2}l_2) \qquad 4.36$$

Where, the plastic bending moment per unit circumferential length of the hinge using von Mises yield criterion was

$$M_p = \frac{2}{\sqrt{3}}\sigma_y\frac{t^2}{4}$$

In this present analysis the work-hardening effect has been incorporated by introducing an average stress flow, which will be the average stress much higher than the yield stress, but below the ultimate stress. Therefore, in this case instead of using σ_y in the plastic bending moment, σ_A will be used. From experimental point of view it was found that a better value of σ_A to correlate with experimental results was

$$\sigma_A = \sigma_y e^n \qquad 4.37$$

The energy absorbed in expansion between plastic hinges is therefore

$$W_{EBL} = \pi\sigma_A t_1\frac{l_2^2}{2}\left[1 + \frac{l_2}{6\bar{R}}\right] \qquad 4.38$$

Substituting eq.4.36, eq.4.37 and eq.4.38 into eq.4.35, the total work done in collapsing one convolution can be determined as

$$\frac{W_{BL}}{\delta_3} = \frac{\pi\sigma_y e^n t_1}{2\sqrt{3}l_2}\left[4t_1\left(\pi\bar{R} - \frac{l_2}{2}\right) + \sqrt{3}l_2^2\left(1 + \frac{l_2}{6\bar{R}}\right)\right] / \text{ unit length} \qquad 4.39$$

4.5 WORK DONE DUE TO FRICTION STRESS BETWEEN INVERBUCKTUBE AND DIE INTERFACE

The influence of friction has a more pronounced effect on the prediction of work done due to forces in the interface. For friction energy dissipation to be found, it will be wise to take an element of the inverbucktube in the radius fillet curvature and analyse all the stresses exerted on as shown in fig.4.6 and fig.4.7.

4.5.1 PRESSURE OR NORMAL STRESS

Looking closely at fig.4.6, all the forces exerted on the element could be resolved. If all forces in this figure are resolved parallel to the surface of the die fillet radius, the equation obtained is

$$2\pi\bar{R}(\sigma_r+d\sigma_r)t_z\cos\alpha - 2\pi(\bar{R}+d\bar{R})\sigma_r t_z\cos(\alpha+d\alpha) -$$

$$-2\pi\left(\bar{R} - \frac{t_z}{2}\right)\mu N dZ\cos\left(\alpha + \frac{d\alpha}{2}\right) = 0 \qquad 4.40$$

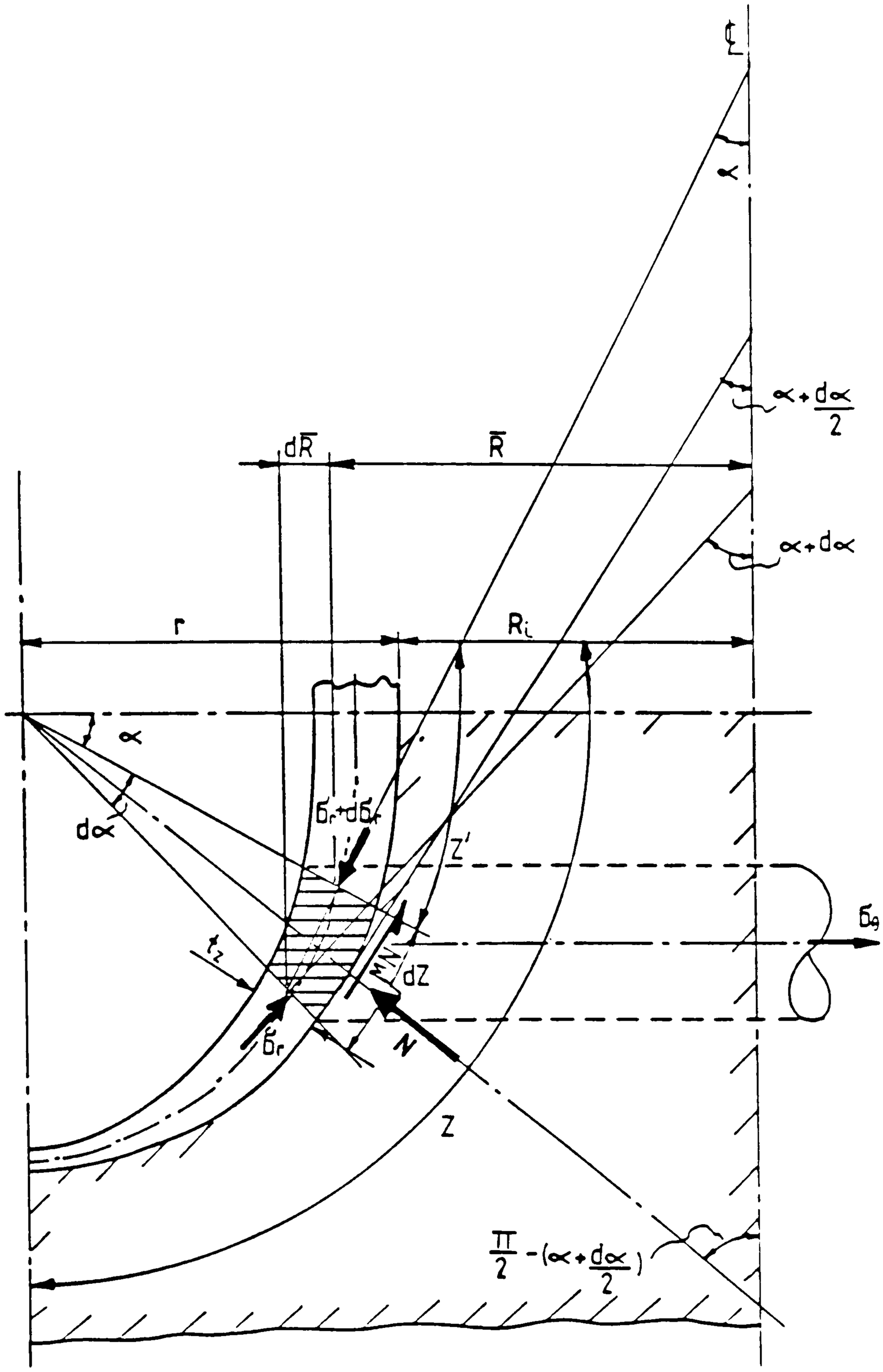

Fig. 4.6 Stresses acting on an element of the inverbucktube in 2-D

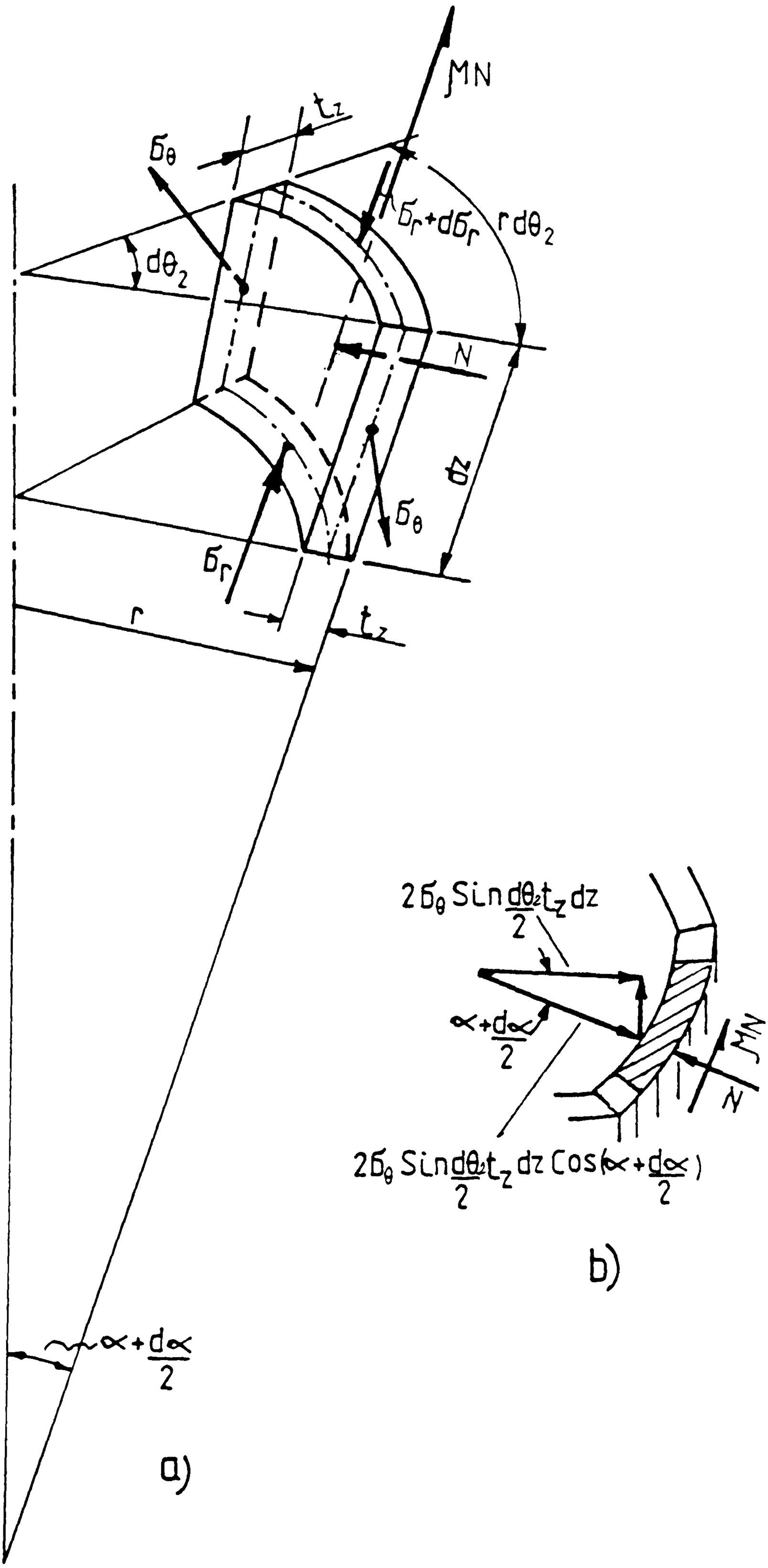

Fig. 4.7 a) Stresses acting on an element of the inverbucktube in 3-D; b) component of the radial force due to hoop stress exerted on the element in a direction normal to the die fillet radius

Assuming that $\bar{R}-t_x/2 \approx \bar{R}$, true for thin shells, and eliminating all second order small quantities, eq.4.40 becomes eq.4.41. If the geometry in fig.4.6 is taken into account and say; $dZ = rd\alpha$ and $d\bar{R}/d\alpha = r\sin\alpha$; and thus $dZ = d\bar{R}/\sin\alpha$, $d\alpha = d\bar{R}/r\sin\alpha$, then it can be written as

$$\sigma_r = \frac{N\bar{R}(1 + \mu\cot\alpha)}{t_x\cos\alpha[\,1-\Omega_3(1 + \bar{R}/r\cos\alpha)\,]} \qquad 4.41$$

where,
$$\Omega_3 = \ln\left[\frac{2R_i + r(2-\cos\alpha)-\{r[\,1-(\pi/2-\alpha)\tan\theta\,]-t_x\}\cos\alpha}{2R_i + t_x + r(\pi/2-\alpha)\tan\theta}\right] \qquad 4.42$$

Looking closely at fig.4.7, all forces exerting on the element could be resolved perpendicular to the surface of the die fillet radius, and the equation obtained is

$$2\pi R_i N r d\theta_2 dZ - 2\pi R_i 2\sigma_\theta \sin\frac{d\theta_2}{2}\, t_x dZ\cos(\alpha + \frac{d\alpha}{2}) = 0 \qquad 4.43$$

Assuming $\sin d\theta_2/2 \approx d\theta_2/2$, then eq.4.43 becomes

$$\sigma_\theta = \frac{Nr}{t_x\cos(\alpha + d\alpha/2)} \qquad 4.44$$

Using $\cos(\alpha+d\alpha/2) = \cos\alpha\,\cos d\alpha/2 - \sin\alpha\,\sin d\alpha/2$

and assuming that $d\alpha/2$ is very small and goes to zero, then eq.4.44 becomes

$$\sigma_\theta = \frac{Nr}{t_z \cos\alpha} \qquad 4.45$$

The stresses and strains in the inverbucktube material during inversion process can be determined by the application of the plasticity theories. From the von Mises yield criterion, the yield stress $\bar{\sigma}$, which is the effective stress expressed in principal stresses as

$$\bar{\sigma} = \{\tfrac{1}{2}[(\sigma_r-\sigma_\theta)^2 + (\sigma_\theta-\sigma_t)^2 + (\sigma_t-\sigma_r)^2]\}^{1/2} \qquad 4.46$$

The strain-hardening characteristic of the material may be expressed by relating the effective stress $\bar{\sigma}$ to the effective strain $\bar{\varepsilon}$ which can be found in eq.4.22.

Considering the earlier assumption of volume constancy condition, $\varepsilon_1+\varepsilon_\theta = 0$, the effective strain in eq.4.22 may be rewritten as

$$\bar{\varepsilon} = \{2/9(6\varepsilon_\theta^2)\}^{1/2} = \{4/3\varepsilon_\theta^2\}^{1/2} \qquad 4.47$$

The Levy-Lode stress-strain relationship is

$$\frac{\varepsilon_r-\varepsilon_\theta}{\sigma_r-\sigma_\theta} = \frac{\varepsilon_\theta-\varepsilon_t}{\sigma_\theta-\sigma_t} = \frac{\varepsilon_t-\varepsilon_r}{\sigma_t-\sigma_r} \qquad 4.48$$

From eqs.4.47 and 4.48 and 4.46, it follows that

$$\frac{\varepsilon_r-\varepsilon_\theta}{\sigma_r-\sigma_\theta} = \frac{\varepsilon_\theta-\varepsilon_t}{\sigma_\theta-\sigma_t} = \frac{\varepsilon_t-\varepsilon_r}{\sigma_t-\sigma_r} = \frac{3}{2}\frac{\bar{\varepsilon}}{\bar{\sigma}}$$

Hence,

$$\sigma_r-\sigma_\theta = \frac{2}{3}\frac{\bar{\sigma}}{\bar{\varepsilon}}(\varepsilon_\theta-\varepsilon_r) = \frac{2}{3}\frac{\bar{\sigma}}{\bar{\varepsilon}}(2\varepsilon_\theta+\varepsilon_t) \qquad 4.49$$

From experimental results $\varepsilon_t=0$, then eq.4.49 becomes

$$\sigma_r-\sigma_\theta = \frac{4}{3}\frac{\bar{\sigma}}{\bar{\varepsilon}}\varepsilon_\theta \qquad 4.50$$

It must be emphasized that only the plastic component of the total strain should be used in above equations, as the elastic component in the inverbuckling processes is negligible in comparison, hence the plastic strain will be assumed to equal the total strain.

Substituting eq.4.41 and eq.4.45 into eq.4.52 becomes

$$\frac{N\bar{R}(1+\mu\cot\alpha)}{(1-\Omega_3)t_z\cos\alpha} - \frac{Nr}{t_z\cos\alpha} = \frac{4}{3}\frac{\bar{\sigma}}{\bar{\varepsilon}}\varepsilon_\theta \qquad 4.51$$

Substituting the empirical effective stress-strain into eq.4.51 becomes

$$N = \frac{\frac{4}{3}\frac{A\bar{\varepsilon}^n}{\bar{\varepsilon}}\varepsilon_\theta(1-\Omega_3)t_z\cos\alpha}{\bar{R}(1+\mu\cot\alpha)-r(1-\Omega_3)} \qquad 4.52$$

From algebra, $\bar{\varepsilon}^n/\bar{\varepsilon} = \bar{\varepsilon}^{n-1}$

and, $\varepsilon_\theta^{n-1}\varepsilon_\theta = \varepsilon_\theta^n$

Therefore, the pressure or normal stress at any angle α in the fillet radius is

$$N = \frac{-\left[\frac{4}{3}-\frac{2}{\sqrt{3}}\right]^{n-1} A\bar{\varepsilon}_e^{\,n}(1-\Omega_3)t_x\cos\alpha}{\bar{R}(1+\mu\cot\alpha) - r(1-\Omega_3)} \qquad 4.53$$

4.5.2 WORK DONE DUE TO FRICTION

After determining the normal pressure distribution, it will be wise to look closely at fig.4.6 and say the friction work will be

$$W_F = \int_s \tau ds dz \qquad 4.54$$

which is the same as

$$W_F = \int s\tau d\bar{\varepsilon} dz \qquad 4.55$$

Equation 4.24 says that the incremental effective strain is $d\bar{\varepsilon}=2/\sqrt{3}d\varepsilon_\theta$ and the shear stress $\tau=\tau(\sigma_r, d\sigma_r, t_{zz}, \alpha)=\mu N$. Assuming that the coefficient of friction along the surface,s, is costant. Then these relationships could be substituted into eq.4.55 to give

$$W_F = \frac{2}{\sqrt{3}}\int s\mu N d\varepsilon_\theta dz \qquad 4.56$$

Bringing in the N terms and integrating, bearing in mind that $s = \pi r(2R_i+r)$, the friction work is then

$$\frac{W_F}{\delta_4} = \frac{\left[\frac{4}{3}\left[\frac{2}{\sqrt{3}}\right]^n \mu\pi r(2R_i+r)A(1-\Omega_3)t_x\cos\alpha\right]}{\bar{R}(n+1)\left[(1+\mu\cot\alpha)-r(1-\Omega_3)\right]}[\Omega_4]^{n+1}/\text{ unit length} \qquad 4.57$$

where,

$$\Omega_4 = \ln\left[1 + \frac{r}{Ri}\right]$$

If say $m = 4/3(2/\sqrt{3})^n$ and call it strain hardening plastic deformation factor, then for the normalized SKF280, m = 1.382. This factor will change with material depending on the exponent, n.

Therefore, the work done due to friction becomes finally as

$$\frac{W_F}{\delta_4} = \frac{Am\mu\pi r(2R_i+r)(1-\Omega_3)t_x\cos\alpha}{\bar{R}(n+1)\left[(1+\mu\cot\alpha)-r(1-\Omega_3)\right]}[\Omega_4]^{n+1}/\text{ unit length} \qquad 4.58$$

Thus, the total work done or the applied energy per unit length of the inverbucktube is expressed as

$$\frac{W_T}{\delta} = \frac{2\pi\bar{D}t_x}{n+1}\left[\left(\frac{2}{\sqrt{3}}-\Omega_1\right)^{n+1} + \left(\frac{2}{\sqrt{3}}-\Omega_2\right)^{n+1}\right] +$$

$$+ \frac{Am\mu\pi r(2R_i+r)(1-\Omega_3)t_x\cos\alpha}{\bar{R}(n+1)\left[(1+\cot\alpha)-r(1-\Omega_3)\right]}[\Omega_4]^{n+1} +$$

$$+ \frac{\pi\sigma_y e^n t_1}{2\sqrt{3}l_2}\left[4t_1(\pi\bar{R} - \frac{l_2}{2}) + \sqrt{3}l_2^2(1 + \frac{l_2}{6\bar{R}})\right] / \text{ unit length} \qquad 4.59$$

Assuming that the process occurs in such a manner that the curvature or the path taken makes the inverbuckling load to be mean, then consequently, the mean inverbuckling load can be simply expressed as

$$\bar{P} = W_T/\delta \qquad 4.60$$

CHAPTER V

THEORETICAL RESULTS, CONCLUSION AND FUTURE WORK

5.1 THEORETICAL RESULTS

The theoretical analysis presented here, has been developed to predict the energy absorption and mean inverbuckling load of inverbucktubes. Based on the equations developed in the analysis, a computer program was developed. Using the program, the necessary data, mostly parametric, was read into the computer and results were obtained. These are given in fig.5.1 and fig.5.2.

Figure 5.1 shows the relationship between the geometrical parameters and geometry factor. For the purpose of designing the inverbucktube, these characteristics were computed for each case and are clearly shown in appendix B.

Figure 5.2 gives the comparison between theoretical and experimental results. These are therefore, made between specific energy and dimensionless load as a function of geometric parameters. It can be seen the results are not bad, and show relatively good correlation. The descrepency between theory and practice is about 20% when the inverbucktube dimensions go towards smaller values of geometry factor and reduces to about 9% when it goes towards larger values of geometry factor.

For the complete understanding of the range in which inverbuckling will occur, a number of tests were carried out, which showed that inverbucktubes had limits within proper collapse took place. Theoretically these were ascertained by analysing results from the computer. It was

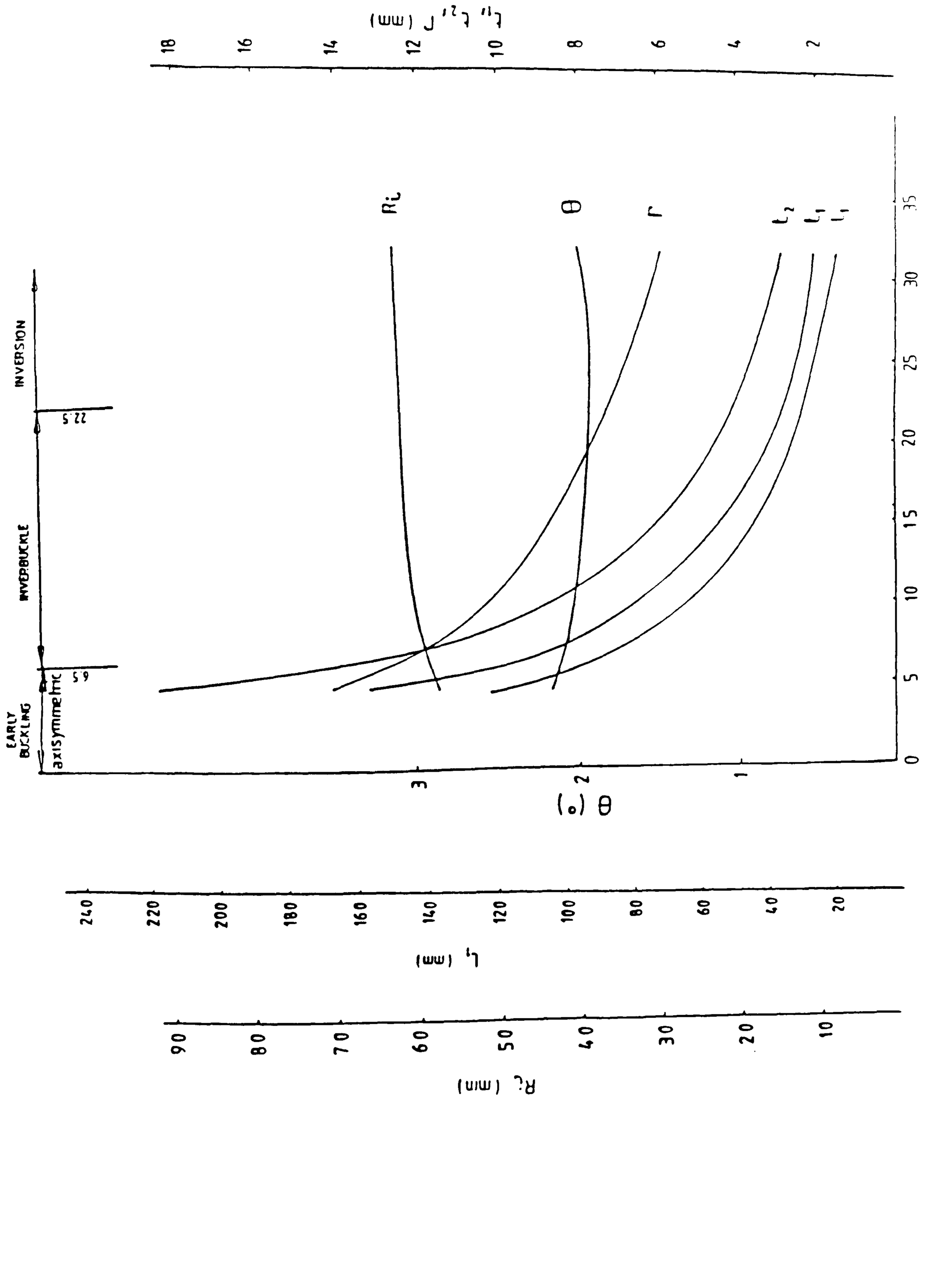

Fig.5.1 Relationship between buckling mode and geometry factor

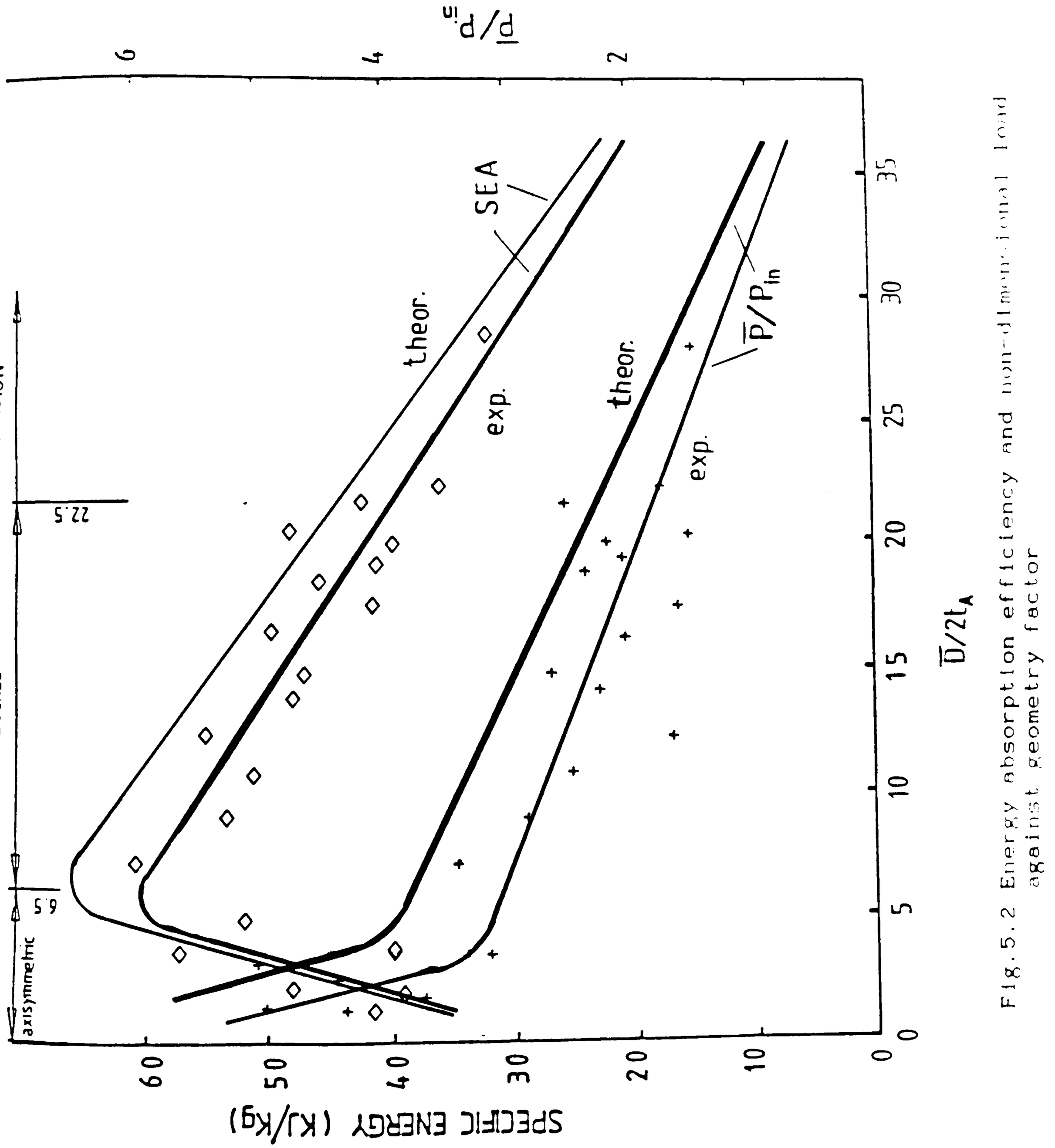

Fig.5.2 Energy absorption efficiency and non-dimensional load against geometry factor

noticed that after $\bar{D}/2t_o \approx 6.5\pm2.5\%$, the mean load was about 3 times higher than experimental mean load and went on increasing as the geometry factor went towards zero mark. On the other hand, it was difficult to locate straight away the limit at high values of geometry factor. To locate this, a great number of load/shortening curves were made using data obtained from the computer. Once this was done , a point was located where transition from inverbuckling to proper inversion was observed. This was at about 22.5±5%. It is better to state that the transition point as such did not exist, but a band where it was occuring was taken as the abrupt point itself.

Normal pressure distribution was measured for a wide range of inverbuckling conditions as stated in chapter III, table 3.1. Figure 5.3 shows typical pressure distribution characteristics determined through experiment (for $\bar{D}/2t_o$ = 13.85) and theory developed. The theoretical curves shown here were computed using eq.4.54. As it was difficult to measure friction coefficient, we made μ in eq.4.54 variable for every condition of geometric parameters.

Results show that the normal stresses computed were in good agreement with the experimental curve at either μ=0.40, μ=0.42 or μ=0.43. It can also be seen that as the friction coefficient increases the pressure peak value tends to become smaller and move towards the 90° mark.

Figure 5.4 gives the relationship between the maximum theoretical normal pressure and geometry factor. It can be seen that the behaviour follows that of the non-dimensional load shown in fig.5.2

In addition, pure theoretical pressure distribution curves are presented in appendix C(figs.C1 to C50) to show

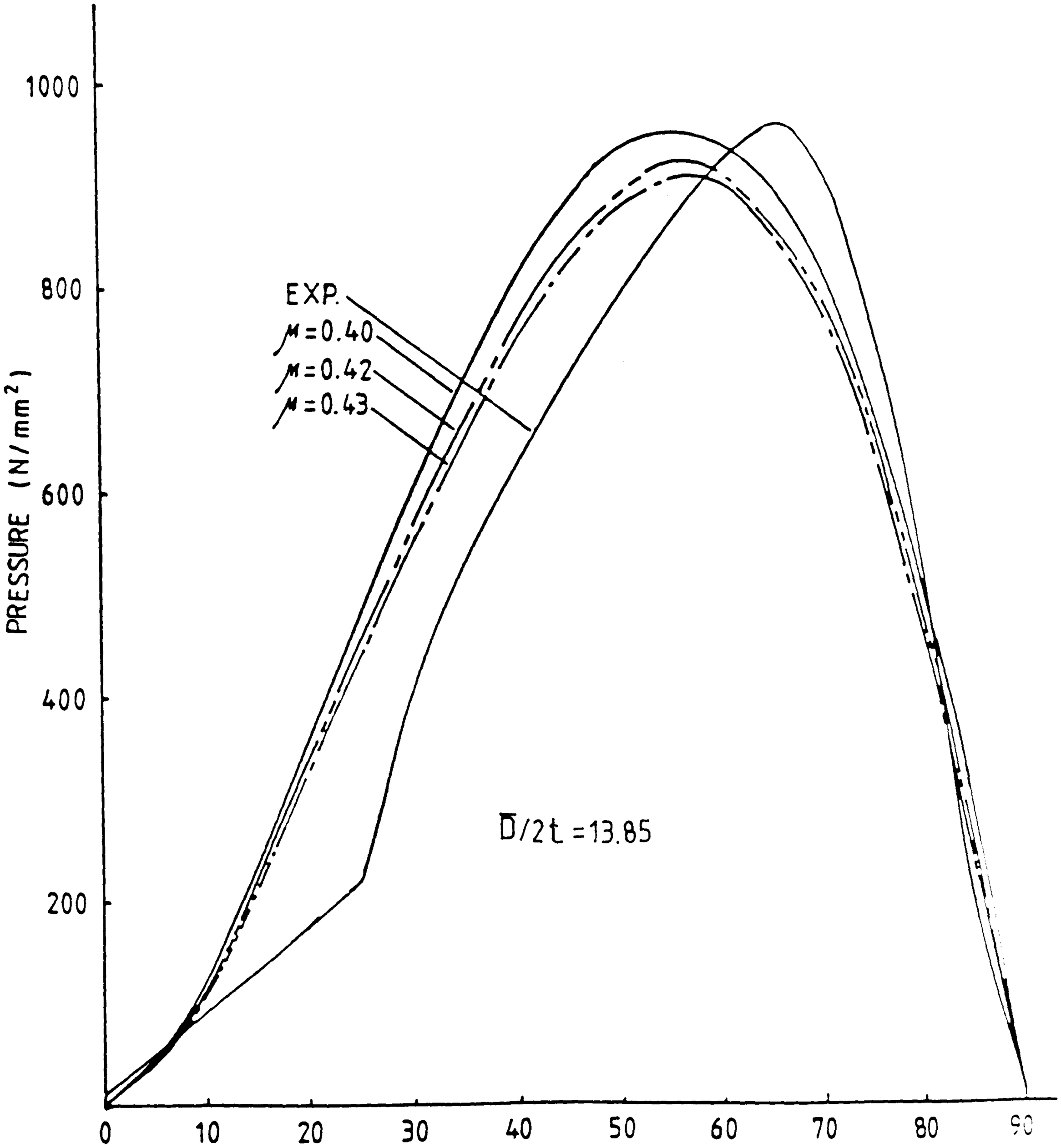

Fig.5.3 Comparison between experimental and theoretical normal pressure curves

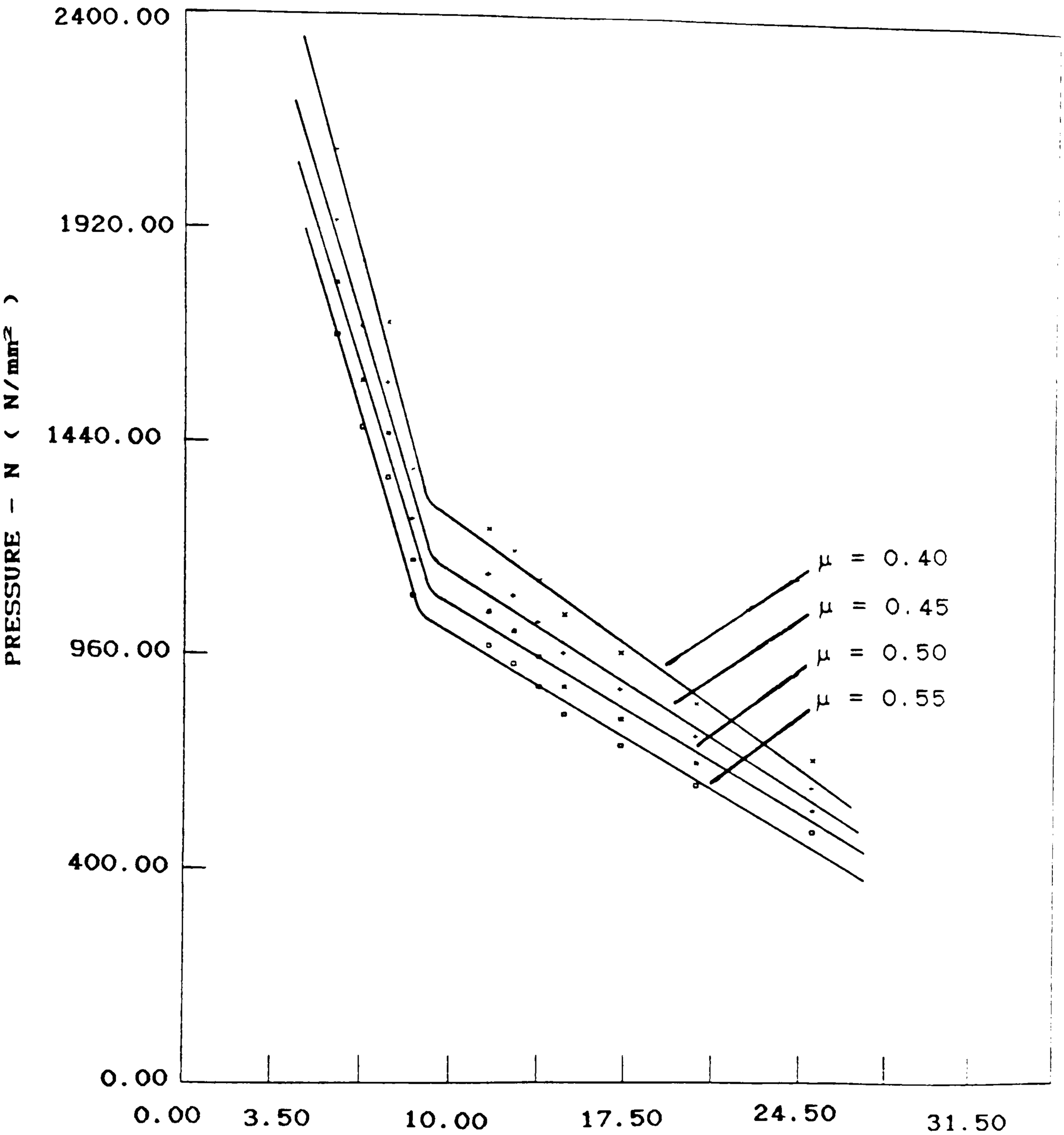

Fig.5.4 Theoretical normal pressure against geometry factor

the effect of various geometrical factors on the shape of the normal pressure distribution in the die fillet radii. Generally speaking, results obtained from experiments and theory showed good covenant.

5.2 CONCLUSION

The responses of inverbuckling thin-walled tubes to quasi-static and impact axial loading have been examined with respect to the pattern and propagation of deformation, mode of collapse, deceleration imposed on the impacting mass and the force transmitted.

Dimensional and physical parameters such as inverbucktube material, geometrical parameters, impact velocity, limits within which inverbuckling is feasible, pressure distribution, energy absorption, peak and mean load, were investigated under numerous conditions. Quasi-static tests were performed and analysed to identify aspects of deformation behaviour which remained unaltered under dynamic loading. The theory which is rather complicated gave good results which correlated with the experimental results.

The following conclusive remarks are made on the basis of the investigations carried out and theory developed on the inverbuckling collapse behaviour:

(i) Quasi-static and dynamic tests produce similar and in some cases, when $\bar{D}/2t_o$ = 9.5 to 15.8, identical modes. Energy absorption is high and better than proper, pure inverted tubes of the same mass.

(ii) The limits within which inverbuckling occurs have been defined. This is a very important parameter especially in design.

(iii) Inertia effects are significant during deformation in impact loadings.

(iv) Impact velocity affects the rise in inverbuckling load.

(v) Inverbuckling tightness is not affected by change in impact speed.

(vi) Pressure distribution has been successfully determined for the first time and the pressure transducer developed yields a high degree of accuracy for normal stress measurements.

(vii) Lubrication does not *"eliminate"* friction forces as thought by many researchers prior to this investigation. It minimises them.

(viii) Using the present method of analysis, it is possible to predict closely the energy absorption, mean load expected, the normal stress distribution along the inverbucktube/die interface. The method is easy to apply and results can be obtained quickly on a computer.

(ix) In general the experiments and the method of analysis have yielded very successful results. Now the inverbucktube can be designed and employed as an energy absorber in practice without any hesitations.

5.3 RECOMMENDATION FOR FUTURE WORK

More work could be carried out in the following areas:

(i) Friction force and friction coefficient measurements could be carried out. Within the present experiments it proved to be difficult, but with more time, the method

explained here could be used effectively to achieve accurate measurements.

(ii) Normal stresses could be measured under dynamic loadings.

(iii) Other practicable methods (e.g. employing strain guages) for pressure determination could be tried. This will be useful to confirm the results obtained here.

(iv) A purely stress flow method (stress analysis) could be used to solve the problem. The computation involved would be considerable, but worthwhile.

BIBLIOGRAPHY

1. Pugsley, A.
   Macaulay, M. — "The large-scale crumpling of thin cylindrical columns", Quart. J. Mechs. and App. Maths., Vol.13, 1960

2. Pugsley, A. — "The crumpling of tubular structures under impact conditions", Proc. Symp. The use of Aluminium in Railway Rolling stock, Inst. Loco. Engrs., The Aluminium Development Association, London, 33-41, 1960

3. Alexander, J.M. — "An approximate analysis of the collapse of thin cylindrical shells under axial loading", Quart. J. Mechs. and App. Maths., Vol. 13, 1960

4. Pugsley, A. — "On the crumpling of thin tubular struts", Quart. J. Mechs. and App. Maths., Vol. 32, 1979

5. McGehee, J.R. — "Frangible tube energy dissipation", U.S. Patent Office, Patented Aug. 4, 1964, Pat.No.3,143,321

6. Spielman, J.F. — "Energy-absorbing means", U.S. Patent Office, Patented Oct. 23 1962, Pat. No. 3,059,966

7. Herrmann, G. — "Dynamic stability of structures", Proceedings of an International Conference held at NorthWestern University, Evanston, Illinois, Oct.18-20, 1965

8. Conrad, E.W. — "Non-reusable kinetic energy absorber", U.S. Patent Office, Patented Jan.5, 1965, Pat. No. 3,164,222

BIBLIOGRAPHY (Cont.)

9. Jackson, M.A. — "Energy absorption device", U.S. Patent Office, Patented Oct.12, 1965, Pat. No. 3,211,260

10. De Runtz, J.A., Jr. Hodge, P.G., Jr. — "Crushing of a tube between rigid plates", J. App. Mechs., Sept. 1963

11. Marquis, D.P. — "Second generation energy-absorbing column with locking feature", SAE paper No.700002, 1970

12. Banshoya, J. — "Development of energy-absorbing steering column assembly for small passenger cars", SAE paper No.670914, 1967

13. Kroell, C.K. — "A simple efficient one short energy absorber", 30th Symposium on Shock, Vibration and Associated Environments, Detroit, Mich., Oct. 10-12, 1961

14. Burns, A.B. Plascyk, J.A. — "The alightment systems investigation", ASD-TR-63-454, June 1963. American Machine and Foundry Co., Stamford, conn.

15. Searle, J.A. Brabin, E.J. — "The invertube", MIRA Bulletin No.2, March/April 1970

16. Brabin, E.J — "Energy Absorbing devices used in crash testing", MIRA Bulletin No.2, 1968

17. Sadeghi, M.M. — "Shock Absorbing Element", Report No.CIC 102, to Stracham and Henshaw, May 1983

18. Hull, D.H. — "Impact response of structural composites", Composite Materials, Jan.1985

BIBLIOGRAPHY (Cont.)

19. Mamalis, A.G.
Manolakos, D.E.
Saigal, S.
Viegelahn, G.
Johnson, W.
"Entensible plastic collapse of thin-wall frusta as energy absorbers", Int. J. Mech. Sci. Vol.28, No.4, pp.219-229, 1986

20. Reddy, T.Y.
Reid, S.R.
"Axial splitting of circular metal tubes", Int. J. Mech. Sci. Vol.28, No.2, pp.111-131, 1986

21. Mahmood, H.F.
Paluszny, A.
"Stability of plate type box columns under crush loading", Proc. ASME winter sessions, computational methods in ground transportation vehicles, Phoenix, Arizona, 1982

22. Vankuren, R.C.
Scott, J.E.
"Energy absorption of high-strength steel tubes under impact crush conditions, SAE paper No.770213

23. Siebel, E.
Lueg, W.
"Untersuchunger Uber die Spannungsverteilung im Walzspalt", Mitteilungen aus dem Kaiser-Wilhem-Institut fün Eissenforschung, Vol.15 No.1, pp.1-14, 1933

24. Фролов, Е.Я.
Голубев, Т.М.
(Frolov, E. Ya.
Golubev, T.M.)
"Напряжение при холодной металло-обработке", Сибирцкий Институт Металла, 1937
(Stresses in cold metal working), Siberian Inst. Met., 1937

25. Smith, C.C.
Scott, F.H.
Sylwestrowicz, W.
"Pressure distribution between stock & rolls in hot and cold flat rolling", J. Iron Steel Inst., Vol.170, April 1952

26. MacGregor, C.W.
Palme, R.B.
"Contact stresses in the rolling of metals-1, J. of App. Mech., Vol.70, 1948

BIBLIOGRAPHY (Cont.)

27. MacGregor, C.W.
Palme, R.B.
"The distribution of contact pressures in the rolling of metals", Trans. ASME, J. of Basic Eng., 1959

28. Cole, I.M.
Sansome, D.H.
"A review of the application of pin load cell pressure measurement techniques to metal deformation processes", 9th International M.T.D.R. Conference held at the University of Manchester, Sept. 1968

29. Soden, P.D.
Al-Hassani, S.T.S.
Johnson, W.
"The crumpling of polyvinylchloride tubes under static and dynamic axial loads", Institute of Physics Conf. Ser. No.21, 1974

30. Jahnle, H.A.
"Feasibility study of plastic automotive structure", D.O.T. HS 801771, Washington, D.C.,1975

31. McGehee, J.R.
"Experimental investigation of parameters and materials for fragmenting-tube energy-absorption process", NASA TN D-3268, Feb.1966

32. Hull, D.
"Progress in science and engineering of composites", ICCM-IV, Tokyo 1982

33. Provensal, J.
Cosatti, B.
"Energy dissipation of composite structures", Proc., 18th inter. FISITA Congress, May 5-8, Hamburg 1980

34. Thornton, P.H.
"Energy absorption in composite structures", J. Comp. Mat., Vol. 13, July 1979

BIBLIOGRAPHY (Cont.)

35. Thornton, P.H.
Edwards, P.J.
"Energy absorption in composite tubes", J. Comp. Mat., Vol. 16, Nov. 1982

36. Abramowicz, W.
Jones, N.
"Dynamic axial crushing of circular tubes", International J. of Impact Engineering, Vol. 2, No.3, 1984

37. Orowan, E.
Scott, F.H.
Smith, C.L.
"A photoelastic dynamometer for rapidly varying forces", J. of Scientific Instruments, Vol. 27 1950

38. Bergen, J.T.
Scott, G.W., Jr.
"Pressure distribution in the caledering of plastic materials", Trans., ASME., J. of App. Mech., 1951

39. Астахов, И.Г.
(Astakhov, I.G.)
"Распределение давления по контактной повехности при прокатке", Инст. Стали, Симпозиум 30, 1951
(Distribution of pressure over the surface of contact in rolling), Inst. Steel, Symp. No.30, 1951

40. Van Rooyen, G.T.
Backofen, W.A.
"Friction in cold rolling", J. of the Iron & Steel Inst., Vol.186, 1957

41. Чекмарев, А.П.
Клименко, П.Л.
(Chekmarev, A.P.
Klimenko, P.L.)
"Экспериментальный метод определения удельной силы трения и коэффициента трения по дуге захвата при прокатке", Ж. Металлургия, 1958
(An experimental method of determining the specific friction force and coefficient of friction in the arc of contact in rolling)

BIBLIOGRAPHY (Cont.)

42. Королев, А.А. (Korolev, A.A.) — "Новые исследования деформации металла при прокатке", МАШГИЗ, Москва 1958 (Recent investigations on the deformation of metals in rolling), MASHGIS, Moscow 1958

43. Matveev, Yu. M. Lavrov, P.P. — "Effect of foward pressure and tension on the process of rolling tubes on a long mandrel" Stalingrad 1964

44. El-Behery, A.M. Lamble, J.H. Johnson, W. — "The measurement of container wall pressure and friction coefficient in axi-symmetric extrusion", Proc. 4th Int. M.T.D.R. Conf., Manchester, Sept. 1963

45. Frisch, J. Thomsen, E.G. — "An experimental study of metal extrusions at various strain rates", Trans. ASME, Vol.76, 1954

46. Johnson, W. — "Impact Strength of Materials", E. Arnold, London 1972

47. Rawlings, B. — "Response of structures to dynamic loads", J. Harding ed., 1974

48. Johnson, W. Mamalis, A.G. — "Crashworthiness of vehicles", Mechanical Eng. Publications Ltd., London 1978 ed.

49. Johnson, W. Reid, S.R. — "Metallic energy dissipating systems", Applied Mechanics Reviews, Vol.31, No.3, 1978

50. Jones, N. Wierzbiski, T. — "Structural aspects of ship collisions", structural crashworthiness, Butterworths Publishers, chap.11, 1983 ed.

BIBLIOGRAPHY (Cont.)

51. Davies, G.A.O. "Structural impact and crash-worthiness", Elsevier Applied Science Publishers, England 1983 ed.

52. Wierzbicki, T. "Optimum design of integrated front panel against crush", report for Ford Motor Co., vehicle component dept., July 1983

53. Abramowicz, W.
Jones, N. "Dynamic axial crushing of square tubes", Int. J. of Impact Eng., Vol.2, No.2, 1984

54. Adams III, A.
Cassle, R.S. "Chrysler Energy Absorbing, anti-theft steering column", SAE paper No.700001, 1970

55. Ezra, A.A.
Fay, R.A. "An assessment of energy absorbing devices for prospective use in aircraft impact situations", Dynamic response of structures, edited G. Hermann & N. Perrone Pergamon Press.

56. Shaw, M.C. "Designs for safety: The mechanical fuse", Mechanical Engineering, April 1972

57. Thornton, P.H.
Mahmood, H.F.
Magee, C.C. "Energy absorption by structural collapse", structural crash-worthiness, edited N. Jones and T. Wierzbicki, Butterworths 1983

58. Reddy, T.Y. "Impact Energy Absorption using laterally compressed metal tubes", Ph.D Thesis, University of Cambridge, 1978

BIBLIOGRAPHY (Cont.)

59. Reid, S.R. — "Laterally compressed metal tubes as impact energy absorbers", Structural Crash-worthiness, Edited N. Jones & Wierzbicki, Butterwords, 1983

60. Esgar, J.B. — "Survey of energy-absorption devices for soft landing of space vehicles", NASA TN D-1308, 1962

61. Guist, L.R.; Marble, D.P. — "Prediction of the Inversion load of a circular tube", NASA Technical note D-3622, 1966

62. Al-Hassani, S.T.S.; Johnson, W.; Lowe, W.T. — "Characteristics of inversion tubes under axial loading", J. Mech. Eng. Sci., Vol.14, No.6, 1972

63. Al-Hassani, S.T.S. — "Tube inversion: A process for obtaining gross expansion in the diameter of thin-walled tubes", Proceedings of the 15th Inter. Machine tool design and research Conf., Sept. 1974

64. Al-Qureshi, H.A.; De Morrais, G.A. — "Analysis of multi-inversion of tube ends", Design Eng. Conf., ASME paper No.77-DE-35, 1977

65. Abramowicz, W.; Sawczuk, A. — "On plastic inversion of cylinders", Res. Mechanica letters 1, Nov.1981

66. Kinkead, A.N. — "Analysis for inversion load and energy absorption of a circular tube", J. Strain analysis, Vol. 18, No.3, 1983

67. Stronge, W.J.; Yu, T.X.; Johnson, W. — "Long stroke energy dissipation in splitting tubes", Int. J. Mech. Sci., Vol.25, No.9-10, 1983

BIBLIOGRAPHY (Cont.)

68. Al-Saheli, F.A.R.
Firbank, T.C.
Lancaster, P.R.
"An experimental determination of the roll pressure distributions in cold rolling", Int. J. Mech. Sci. Vol.15, pp. 693-710, 1973

69. Johnson, W.
"Impact Strength of Materials", Edward Anorld, London, Crane Russak, New York 1972

70. Abramowicz, W.
Jones, N.
"Dynamic progressive buckling of circular and square tubes", Int. J. Impact Eng., Vol.4, No.4, 1986

71. Wierzbicki, T.
Bhat, S.U.
"A moving hinge solution for axisymmetric crushing of tubes", Int. J. Mech. Sci., Vol.28, No.3, 1986

72. Gokyu, I.
Kishi, T.
"Measurement of the die pressure distribution", Japan Inst. Metals Journal, Vol.31, Part I, 1967

APPENDIX A

A.1 TENSILE TEST ANALYSIS

The primary data output of force and extension were converted to engineering or nominal stresses and strains respectively (table A.1). The engineering stress was defined as the magnitude of the current axial force, P, divided by the initial cross-sectional area of the guage length, A_o.

$$\sigma_{nom} = P/A_o \qquad A.1$$

The ultimate tensile strength or ultimate stress was referred to a point of instability when the maximum axial force, P_{max}, was attained. Furthermore, if it is assumed that the current cross-sectional area of the guage length is , A_{ik}, then the ultimate stress, σ_u, will be given by

$$\sigma_u = P_{max}/A_{ik} \qquad A.2$$

The corresponding engineering strain, e, was defined as the difference between extended length, l_i, and initial guage length, l_o, divided by initial guage length.

$$e = (l_i - l_o)/l_o = \Delta l/l_o \qquad A.3$$

The true strain, ε, was calculated from summing the increments over small strain intervals

$$\varepsilon = [(l_1-l_o)/l_o + (l_2-l_1)/l_1 + \ldots + (l_i-l_{i-1})/l_{i-1}] \qquad A.4$$

or by the increment of logarithmic or natural strain, $d\varepsilon$, introduced by Ludwik, which was based on the current guage length and defined as

$$d\varepsilon = dl/l \qquad A.5$$

When the initial guage length, l_o, is extended to a current length, l_i, the total logarithmic, ε, is then defined as

$$\varepsilon = \int_{l_o}^{l_i} d\varepsilon = \ln l_i/l_o \qquad A.6$$

Knowing the relation between engineering strain and true strain as

$$e = (l_i-l_o)/l_o - 1 \qquad A.7$$

which is the same as

$$e + 1 = l_i/l_o \qquad A.8$$

Therefore the true strain is finally

$$\varepsilon = \ln(e+1) \qquad A.9$$

From the experiments, it was difficult to stop the testing machine for cross-sectional area measurements at intervals. Thus, it was assumed that small changes in volume were insignificant and that the material was incompressible. Then the relation could be defined as

$$A_o * l_o = A_m * l_i = \text{const.} \qquad \text{A.10}$$

or

$$A_m = A_o * l_o / l_i = A_o / (e+1) \qquad \text{A.11}$$

Therefore the true stress now becomes

$$\sigma = \sigma_{nom}(e+1) \qquad \text{A.12}$$

Eq. A.12 is the relation of true stress to engineering stress through the enginerring strain. This is found in all literatures of plasticity theory.

Using the derived equations, a plot can be safely made for the relation of true stress/strain curve and these values are in table A.1.

A.2 STRENGTH COEFFICIENT AND STRAIN HARDENING EXPONENT

In order to determine these two constants for a particular material, a log true stress/log true strain is inevitable. For normalized(900-920°C) SKF280, this diagram is shown in fig.2.3. The values calculated (table A.1) were used to determine the diagram. The tangent of the angle obtained is the value 'n' which is defined as

$$n = \tan\psi \qquad \text{A.13}$$

and when the diagram is extended to the point were it intersects the unit strain value , we obtain the value 'A' on logσ. This is defined as

$$A = 10\log^{\sigma} \qquad \text{A.14}$$

TABLE A.1 Tensile test data for SKF280

LOAD (N)	EXTENSION (mm)	ENGINEERING STRESS (N/mm^2) $P/A_o=\sigma_{nom}$	ENGINEERING STRAIN $\Delta l/l_o=e$	TRUE STRESS (N/mm^2) $\sigma=\sigma_{nom}(1+e)$	TRUE STRAIN $\varepsilon=\ln(1+e)$	LOG TRUE STRESS (N/mm^2)	LOG TRUE STRAIN
0.0	0.0	0.0	0.0	0.0	0.0	0.0	0.0
33181.17	0.292	452.68	0.00584	455.32	0.00582	2.658	-2.230
34623.81	1.597	472.36	0.03194	487.45	0.03144	2.687	-1.503
37990.03	2.832	518.28	0.05664	547.64	0.05509	2.738	-1.259
40875.31	3.708	557.64	0.07416	598.99	0.07150	2.777	-1.146
42317.99	4.073	557.33	0.08146	602.73	0.07830	2.780	-1.106
43279.79	5.372	590.45	0.10744	653.89	0.10205	2.815	-0.991
44241.58	6.321	603.57	0.12642	679.87	0.11900	2.832	-0.924
45203.32	7.640	616.69	0.15280	710.92	0.14170	2.852	-0.849
45684.22	8.808	623.25	0.17616	733.04	0.16230	2.865	-0.789
46165.11	9.246	629.81	0.18492	746.27	0.16970	2.873	-0.770
46164.84	10.306	629.81	0.20612	759.63	0.18740	2.881	-0.727
46164.84	11.255	629.81	0.22510	771.58	0.20300	2.887	-0.693
46164.84	12.700	629.81	0.25400	789.78	0.22600	2.898	-0.645
46164.84	14.230	629.81	0.28460	809.05	0.25000	2.908	-0.602
46164.84	15.240	629.81	0.30480	821.78	0.26600	2.915	-0.575
45683.01	16.000	623.23	0.32000	822.66	0.27800	2.915	-0.556

APPENDIX B

GRAPHICAL METHOD DESIGN OF INVERBUCKTUBES AND DIES

Knowing the ratio $\bar{D}/2t_A$ and the length of the middle part of the inverbucktube 'l_2', all other geometric parameters can be determined using the curves presented in figs.B.1 to B.6 of this appendix. But, before these curves are used, it is recommended first of all to find the geometric factor from fig.5.2, provided the predicted load is specified.

For example, if $\bar{P}/P_{lm}=3.43$ then $\bar{D}/2t_A=9.5$. From the $\bar{D}/2t_A$ axis of these curves presented in this appendix draw a perpendicular to cut the chosen $l_2=8mm$ at $t_1=2.91mm$, $t_2=2.07mm$, $l_1=26.4mm$, $\theta=1.8°$, $R_1=26.1mm$ and $r=4.2mm$.

If 'l_2' is not one of the curves shown in the following figures of this appendix, then the curve could be interpolated or extrapolated as for $l_2=11mm$.

After determining l_1, the total inverbucktube length could be found using eq.2.2.

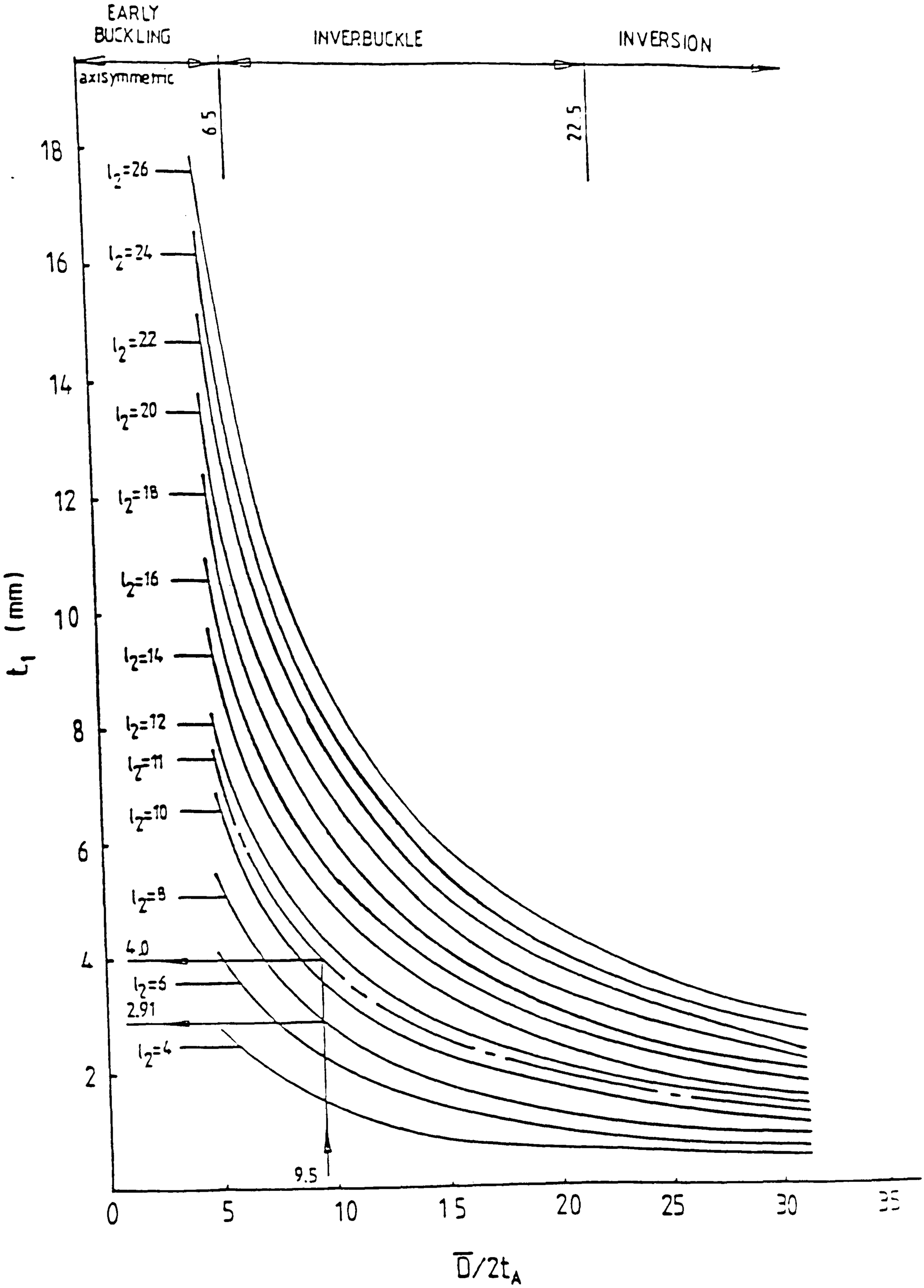

Fig.B.1 Variation of constant middle thickness

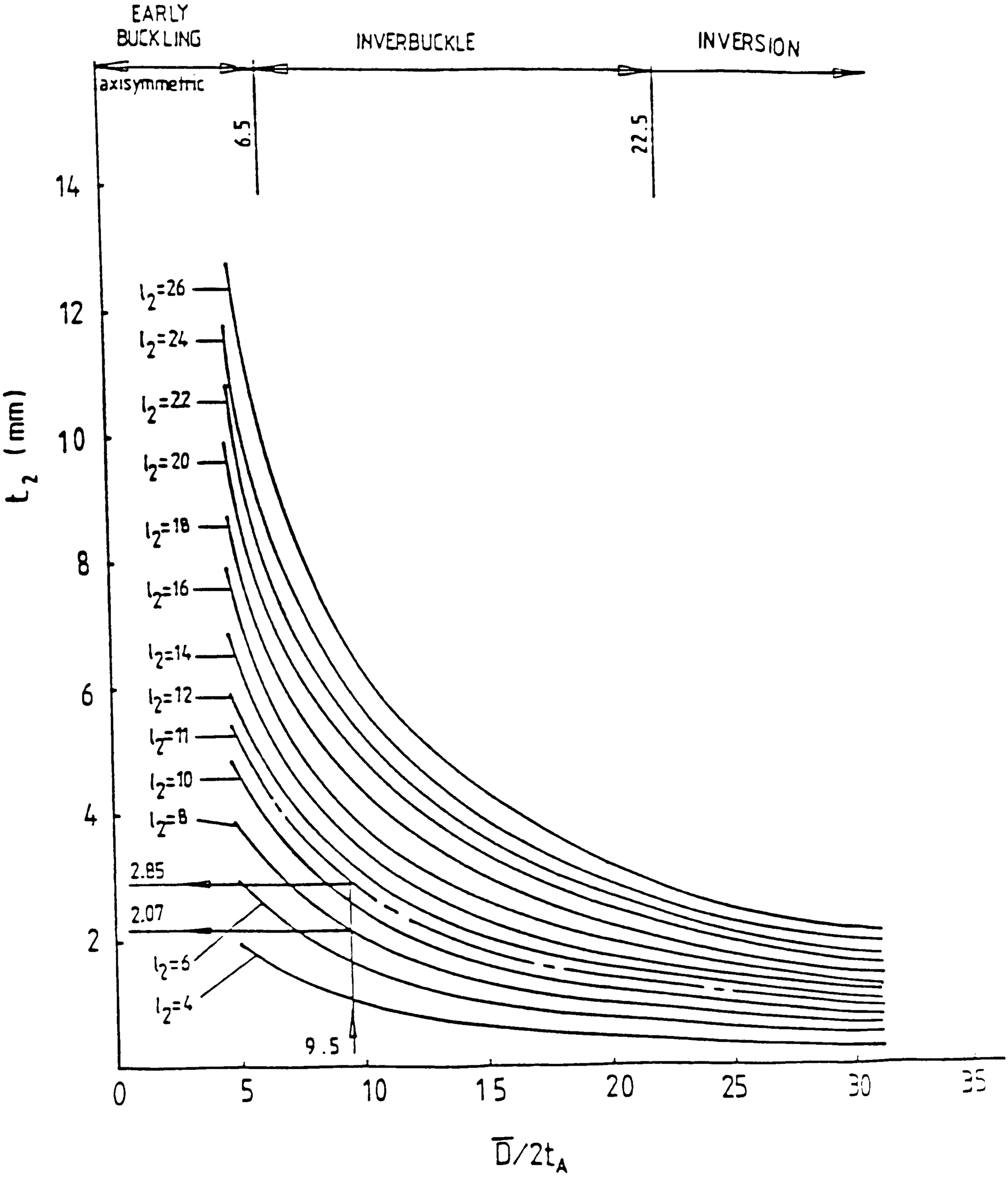

Fig.B.2 Variation of tip end thickness

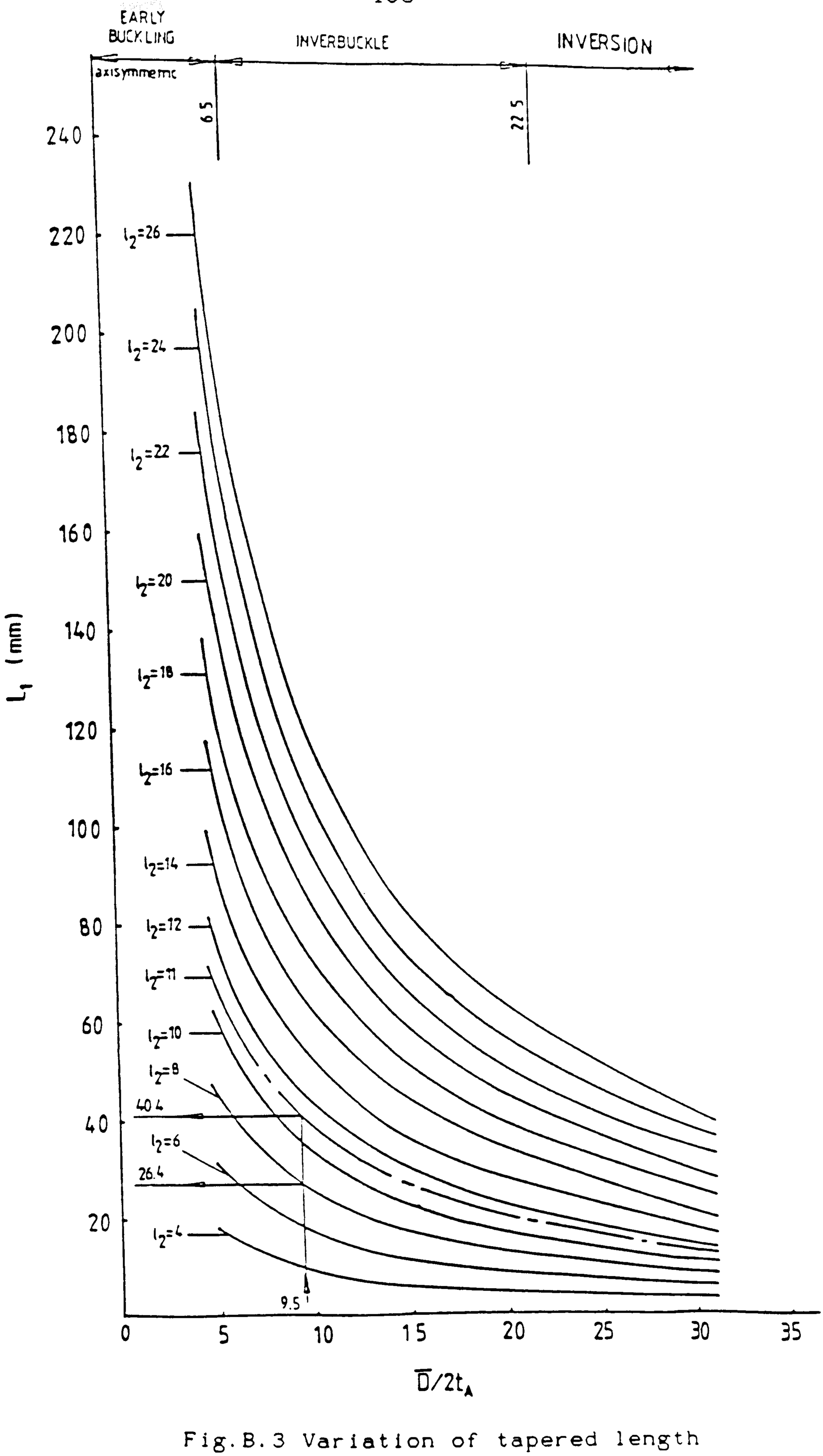

Fig.B.3 Variation of tapered length

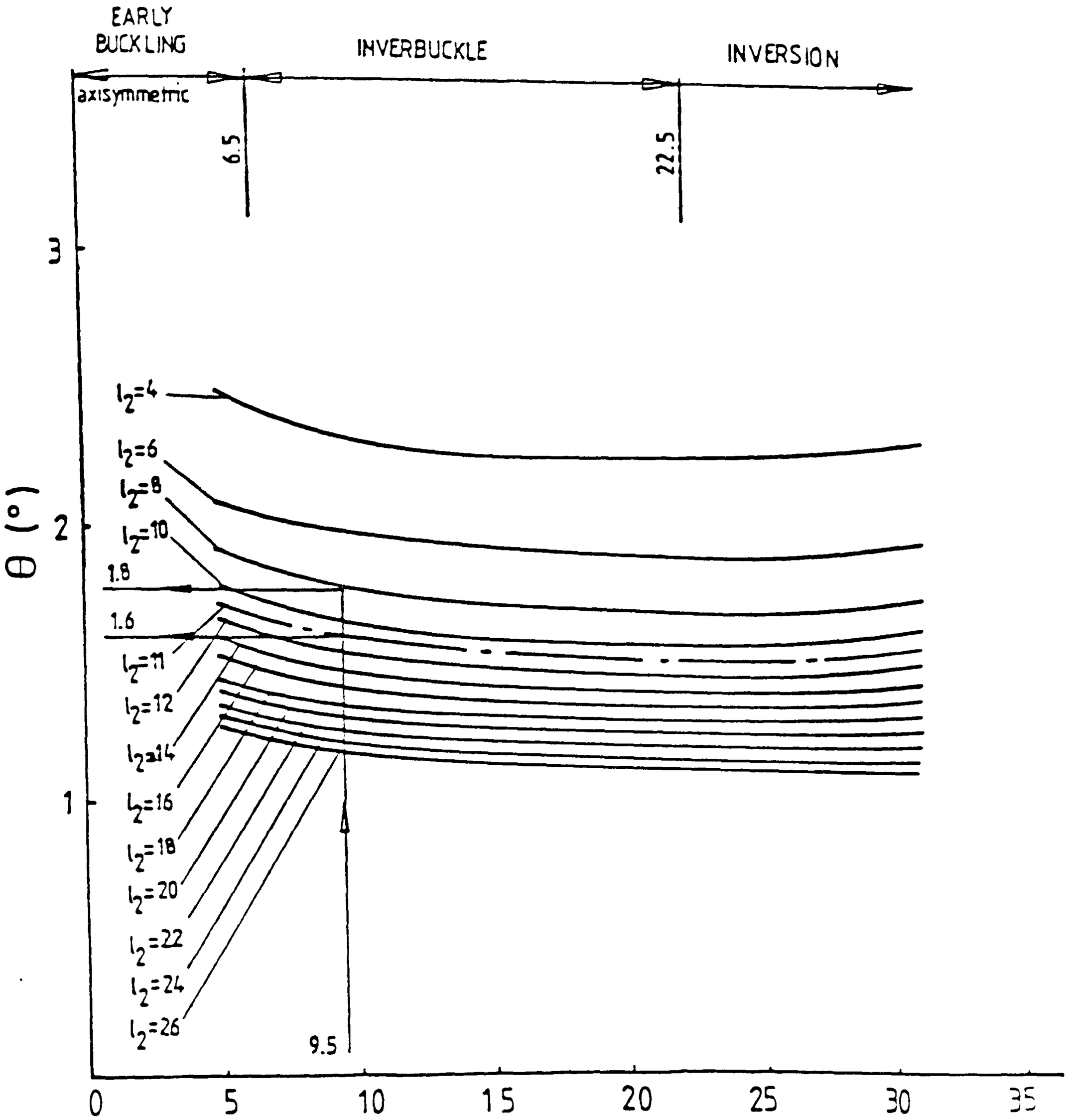

Fig.B.4 Variation of tapered angle

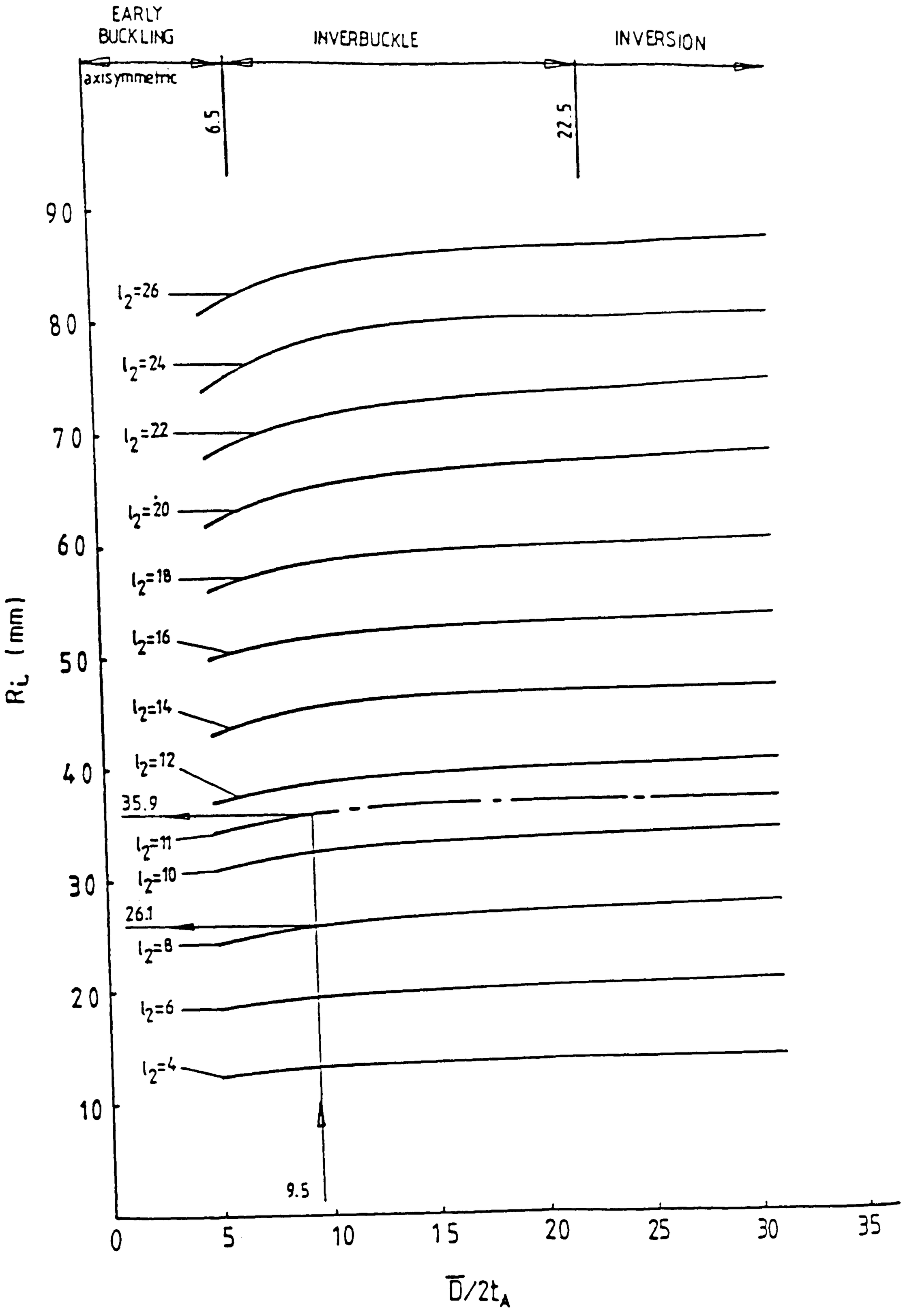

Fig.B.5 Variation of internal inverbucktube radius

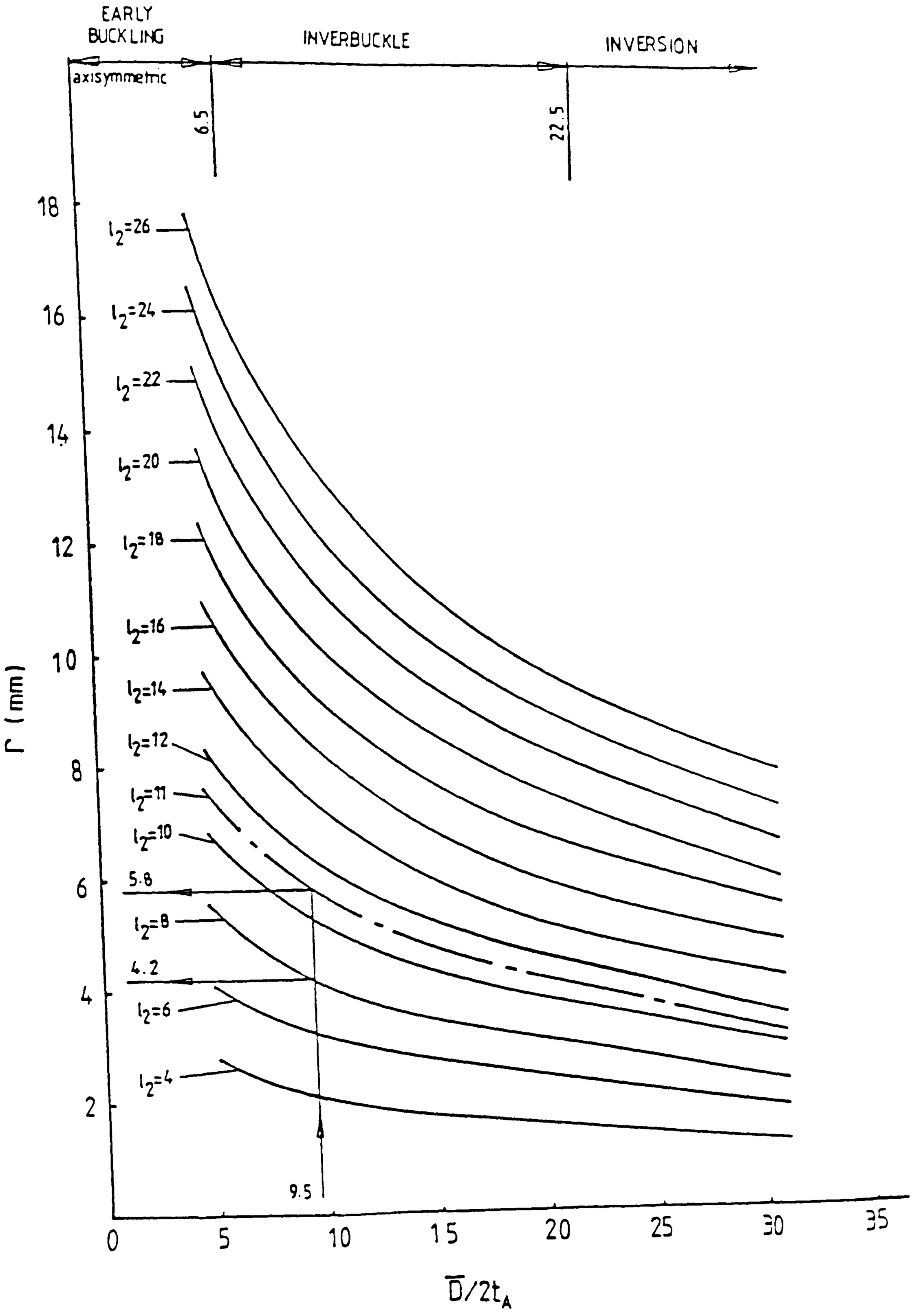

Fig.B.6 Variation of die fillet radius

APPENDIX C

THEORETICAL PRESSURE DISTRIBUTION CURVES

The analysis involving the determination of pressure history in the die fillet radius is described in chapter IV. Using eq.4.54 from the present method of analysis developed, it is possible to predict closely the normal stress distribution of any inverbucktube. It must be stated that the coefficient of friction, μ, in eq.4.54 has to be chosen (first approximation) depending on the inverbucktube and die material. In this present work steel was used in both cases.

Employing a computer, theoretical normal stress curves presented in this appendix were obtained. These are shown in figs.C1 to C50, for μ=0.40, μ=0.45, μ=0.50 and μ=0.55, and for different values of $\bar{D}/2t_{\theta}$.

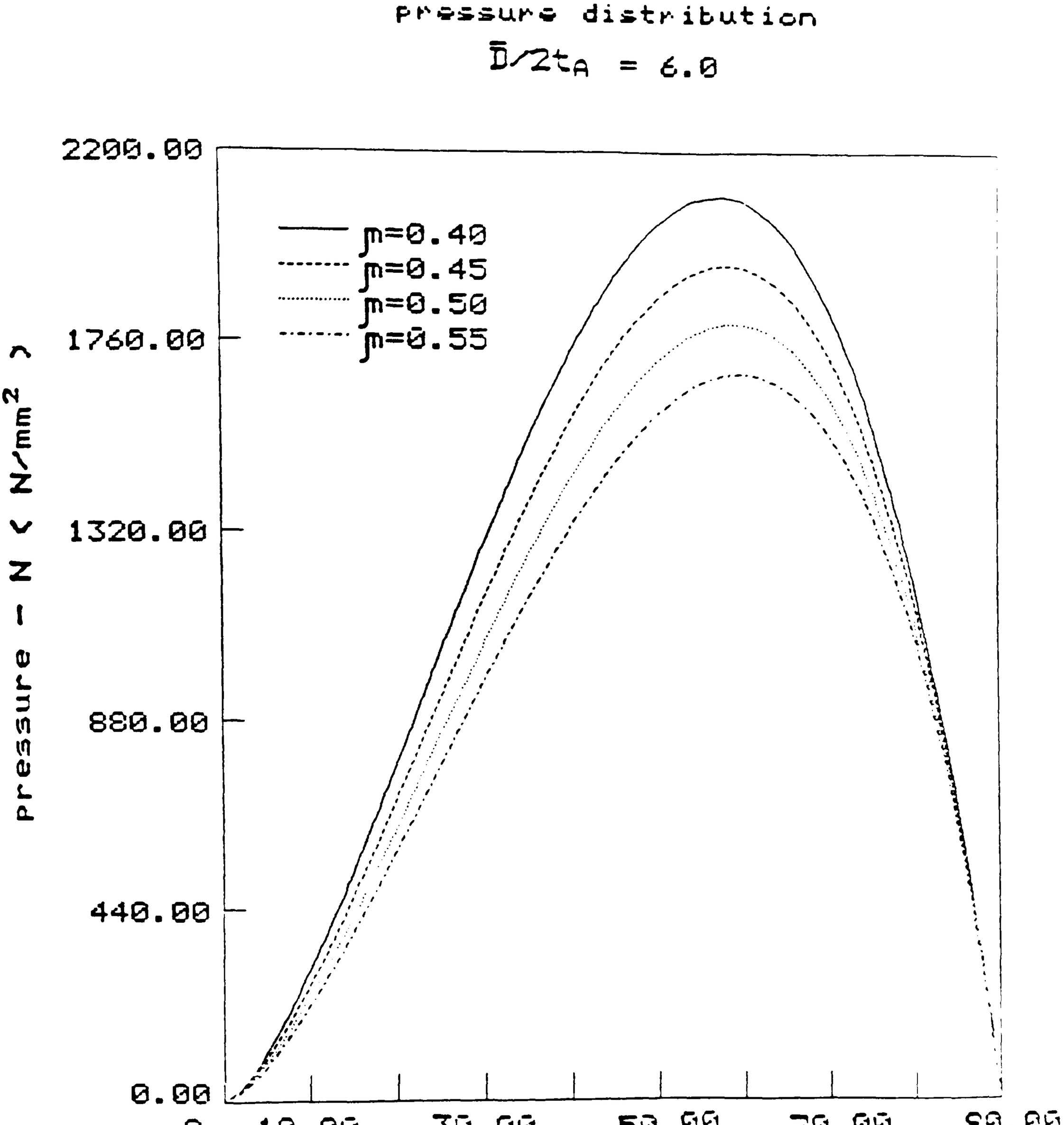

Fig.C1 Theoretical normal pressure curves

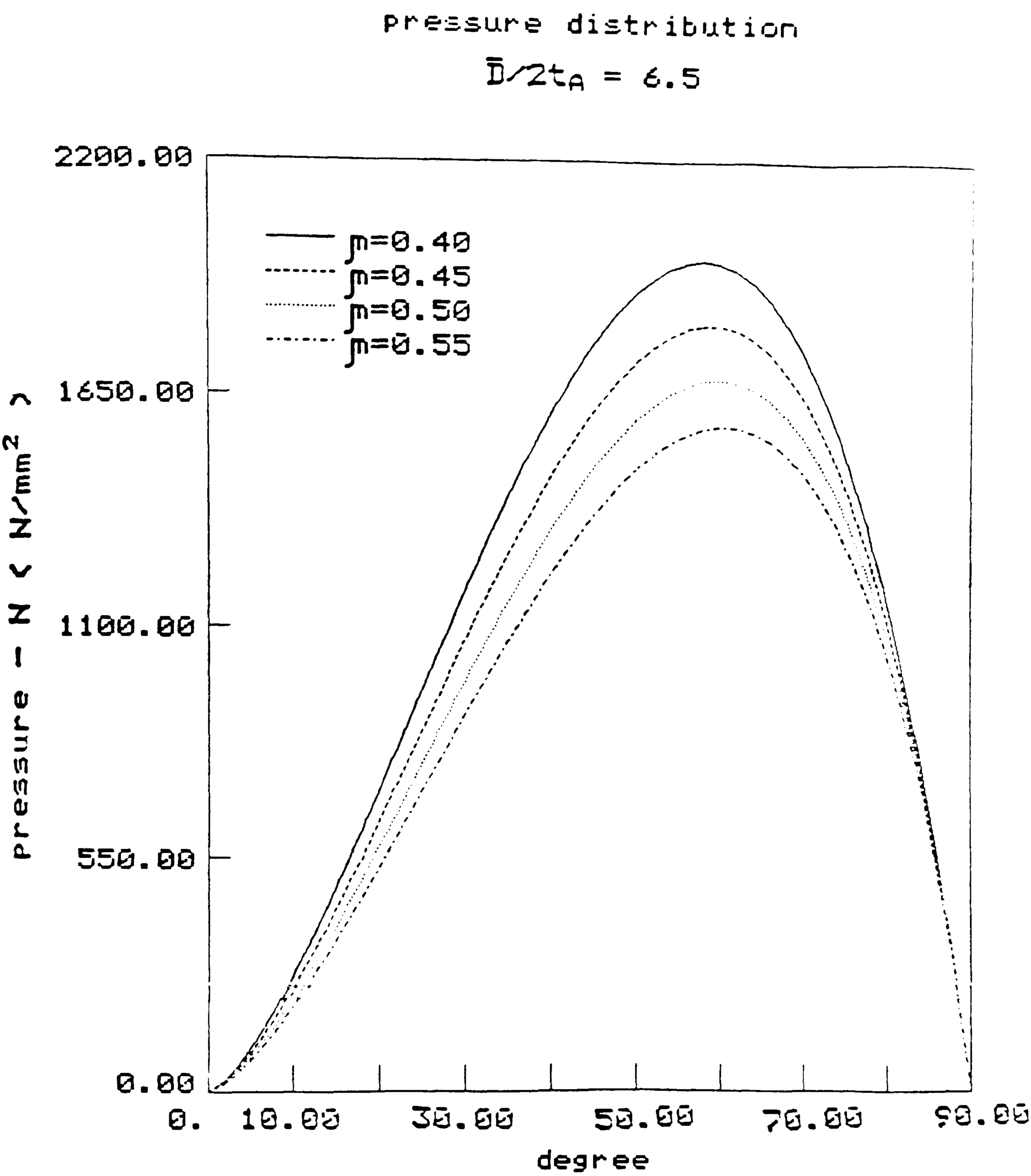

Fig.C2 Theoretical normal pressure curves

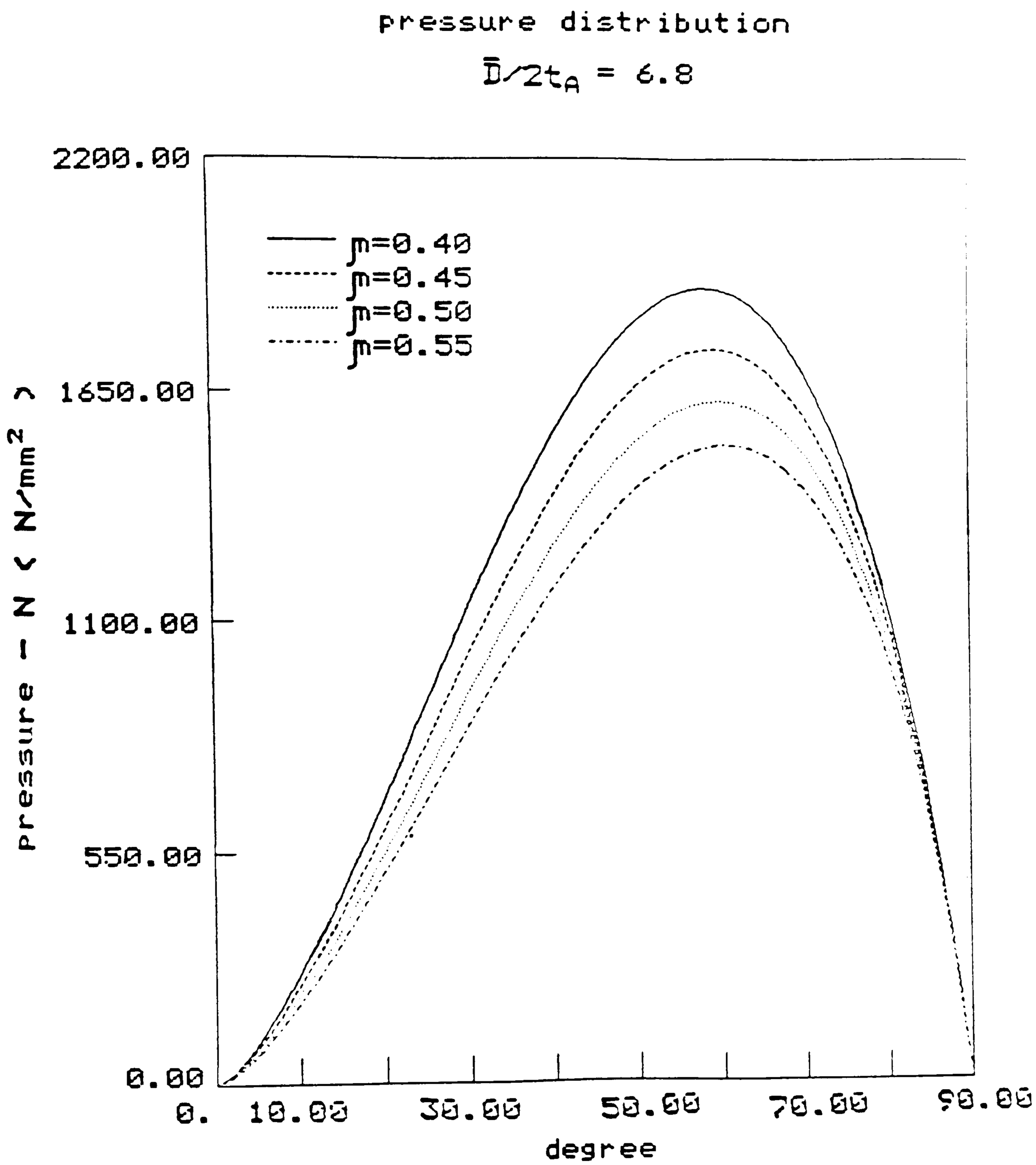

Fig.C3 Theoretical normal pressure curves

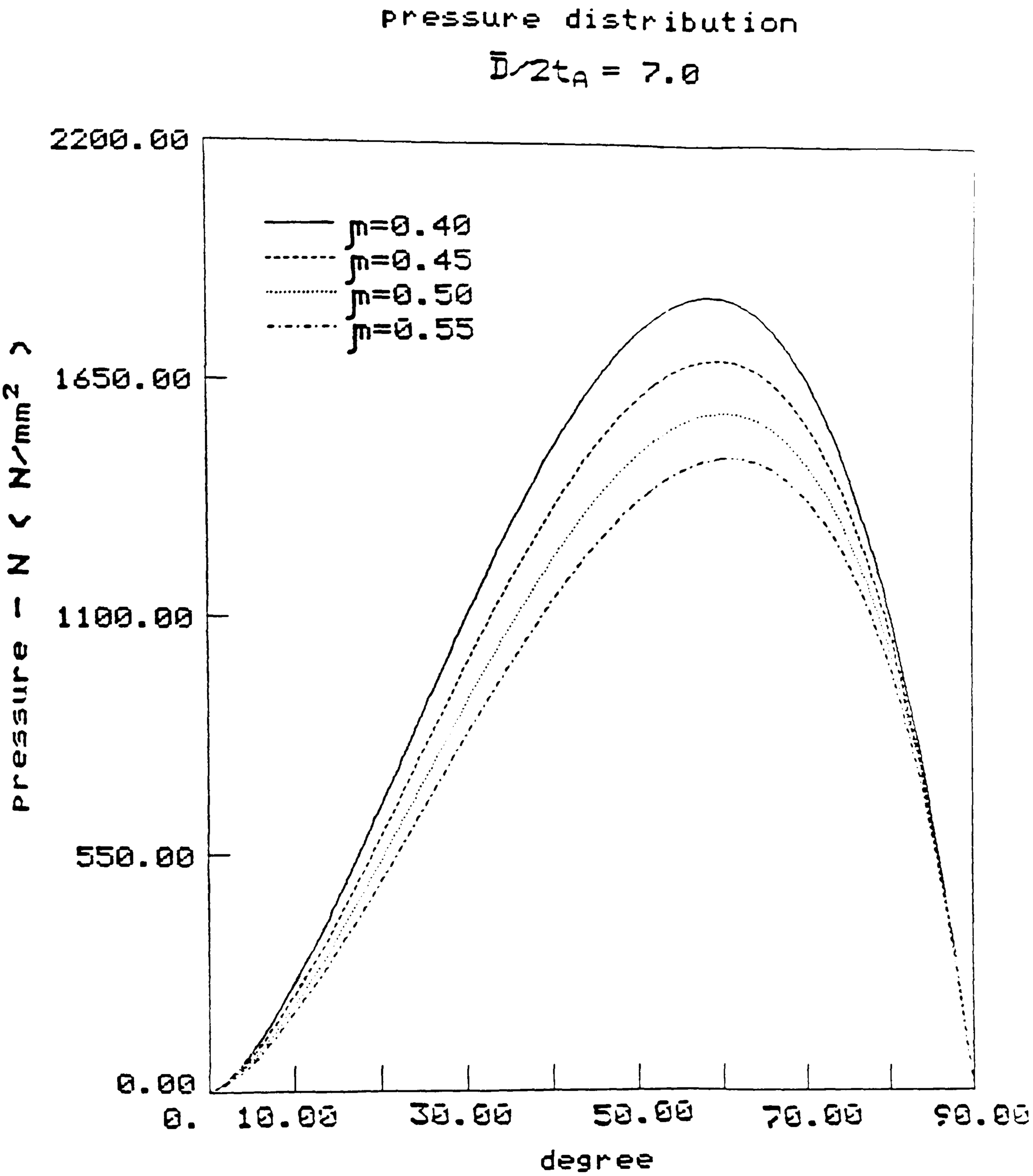

Fig.C4 Theoretical normal pressure curves

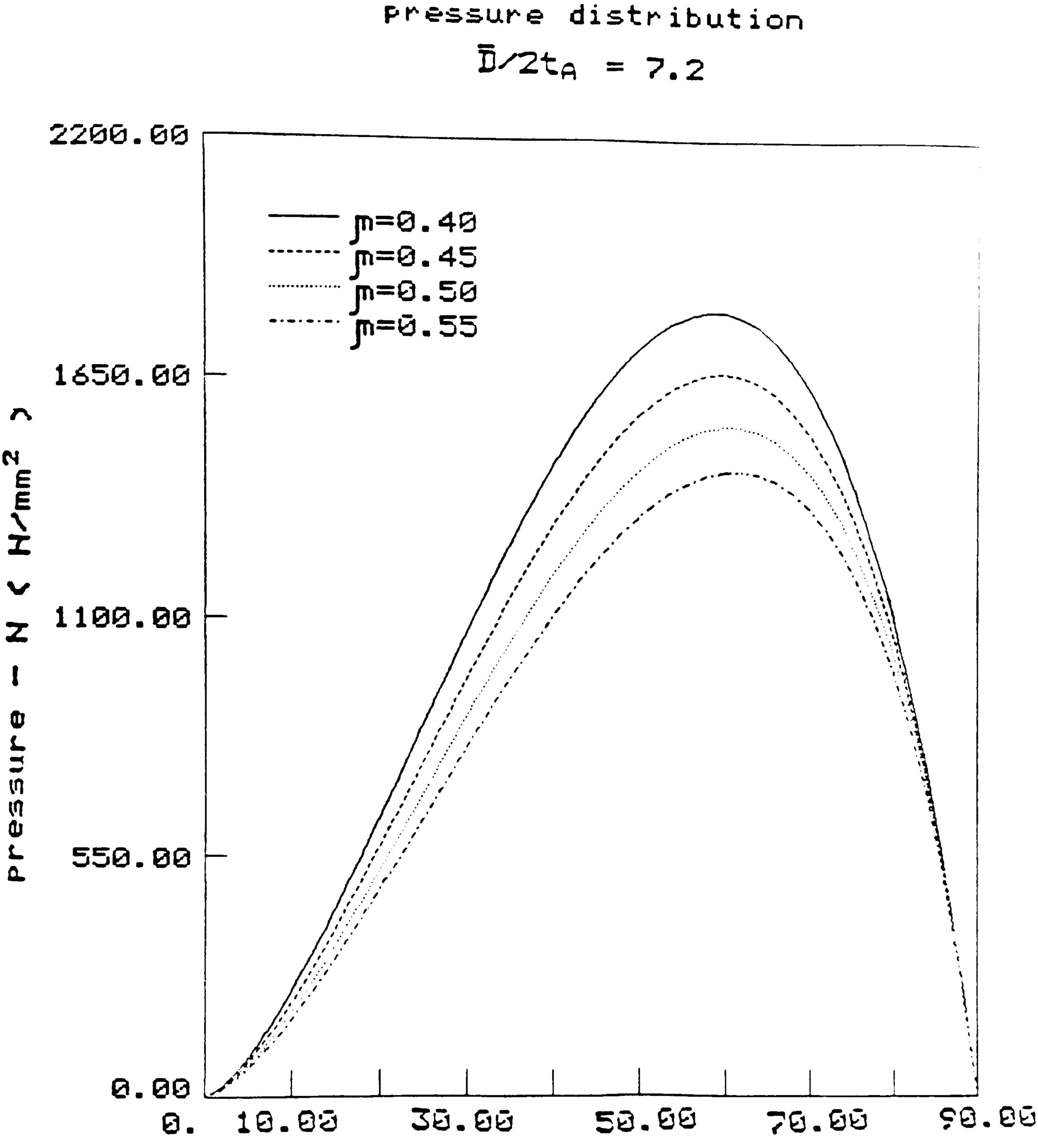

Fig.C5 Theoretical normal pressure curves

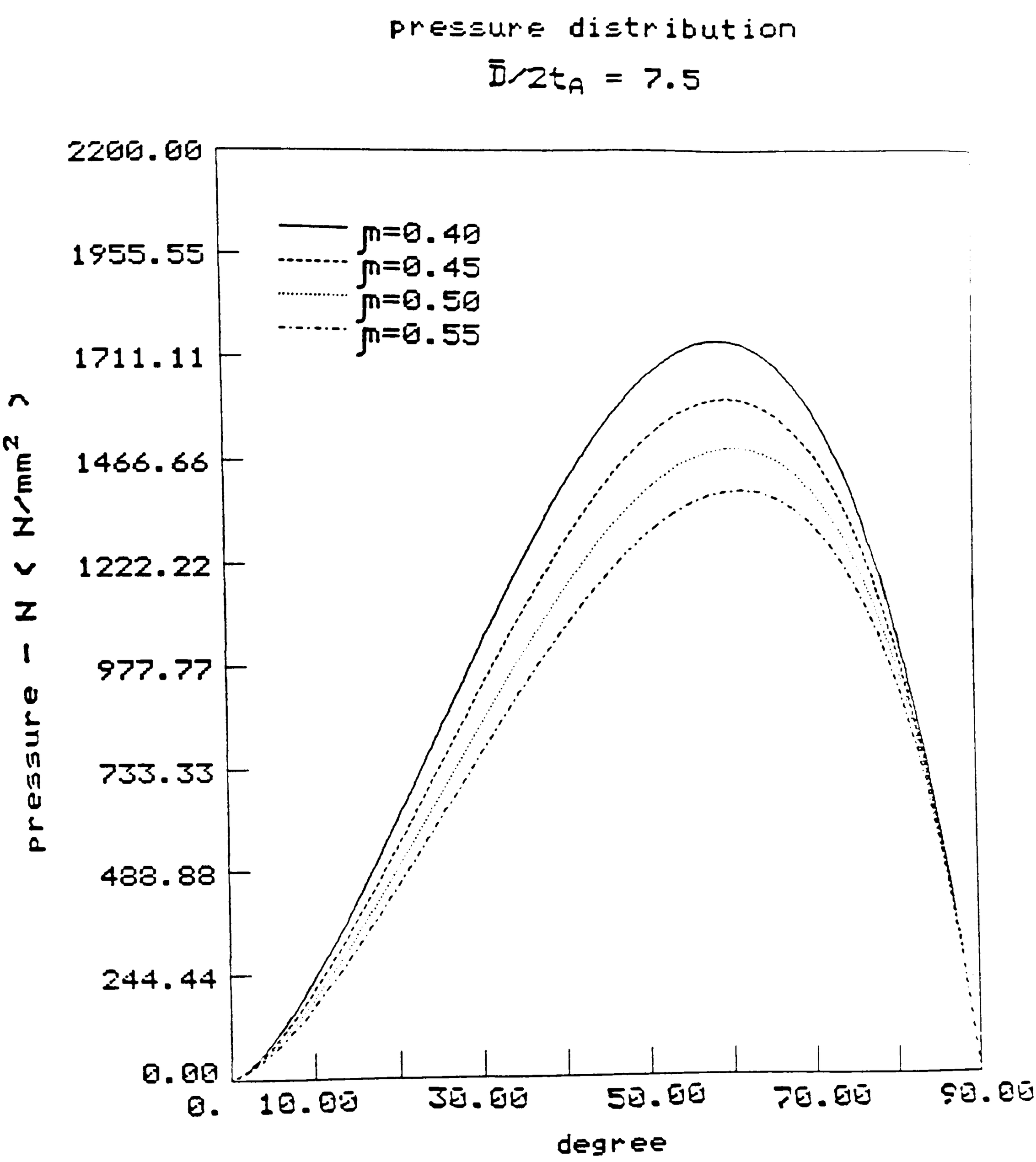

Fig.C6 Theoretical normal pressure curves

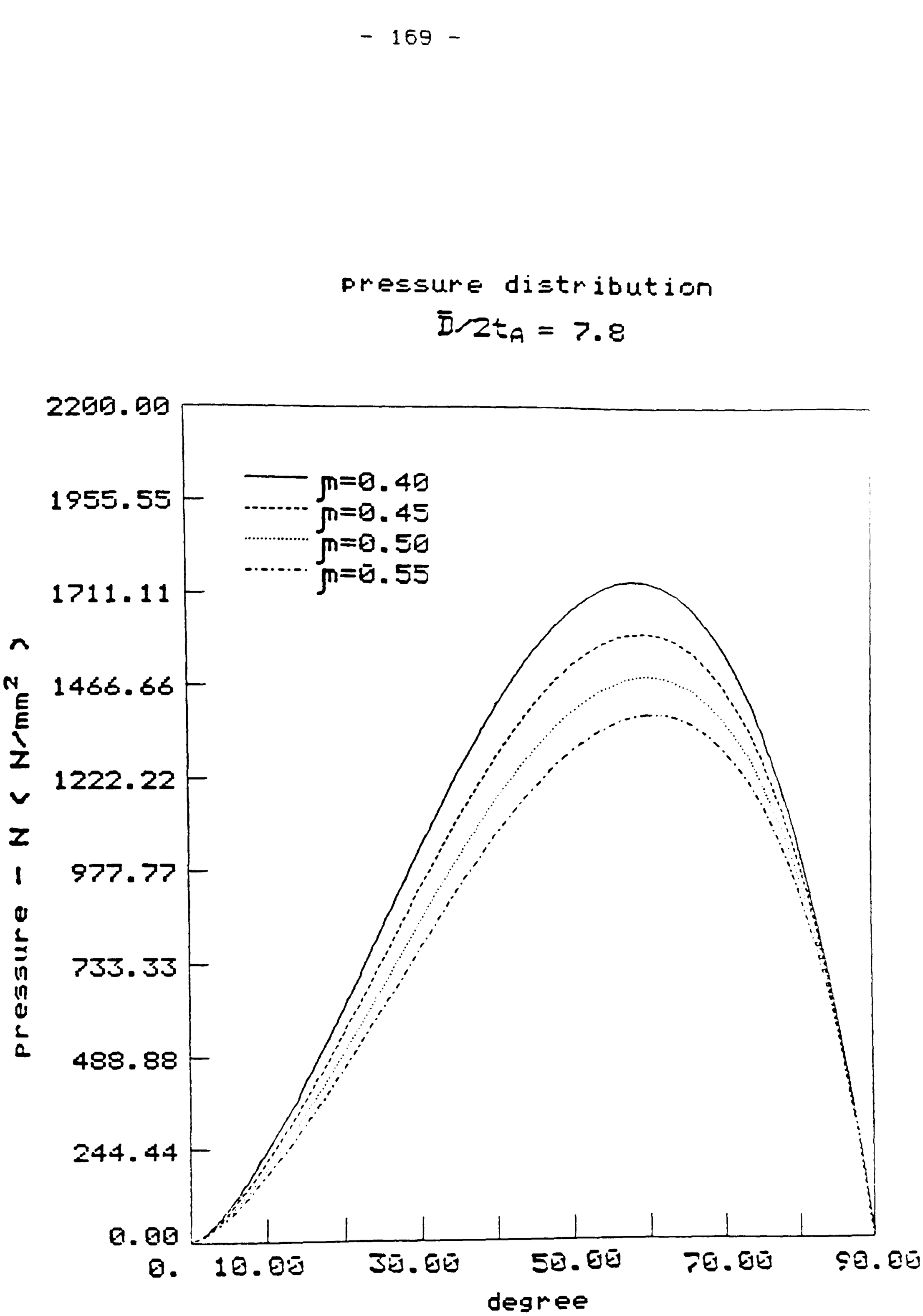

Fig.C7 Theoretical normal pressure curves

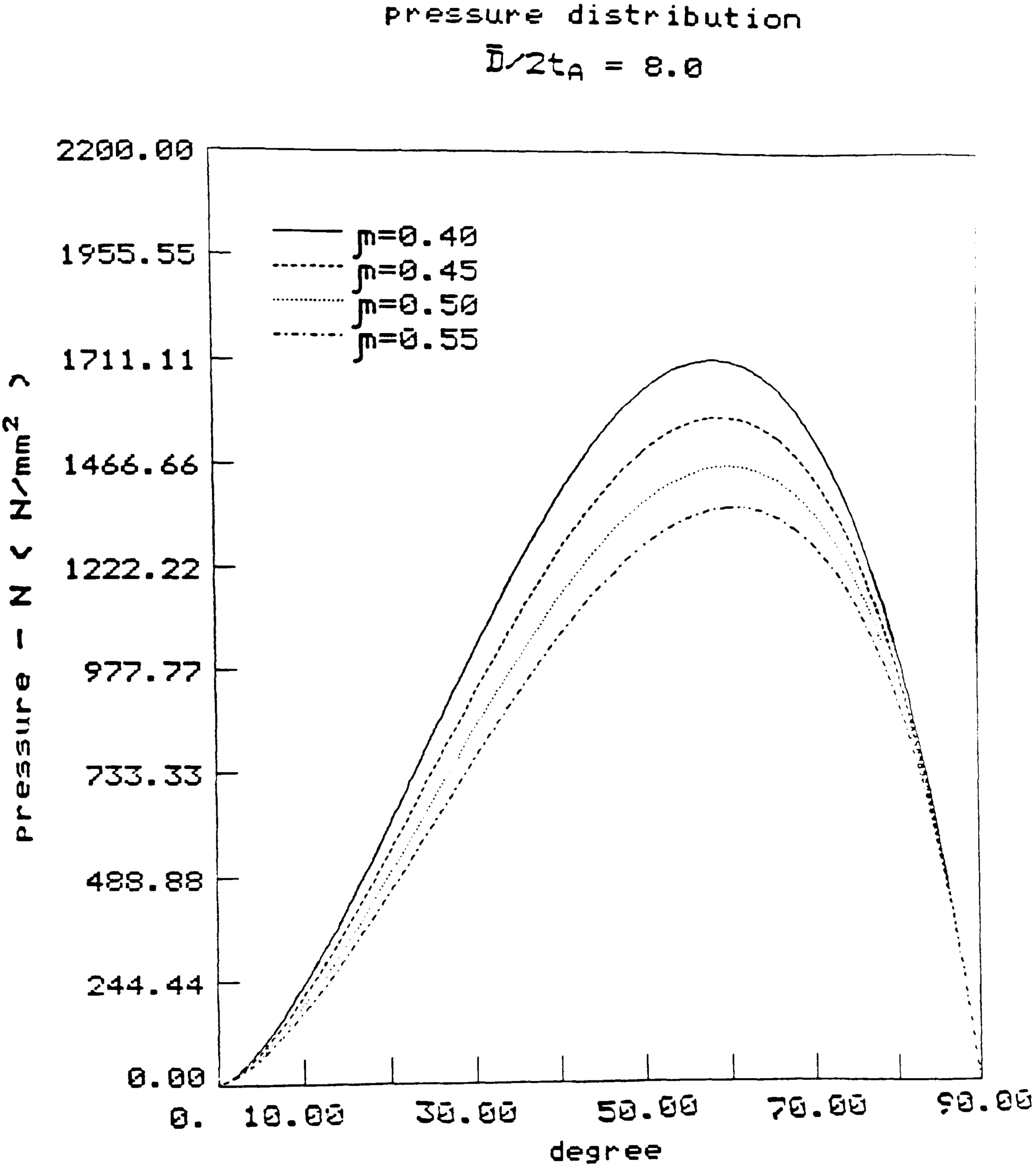

Fig.C8 Theoretical normal pressure curves

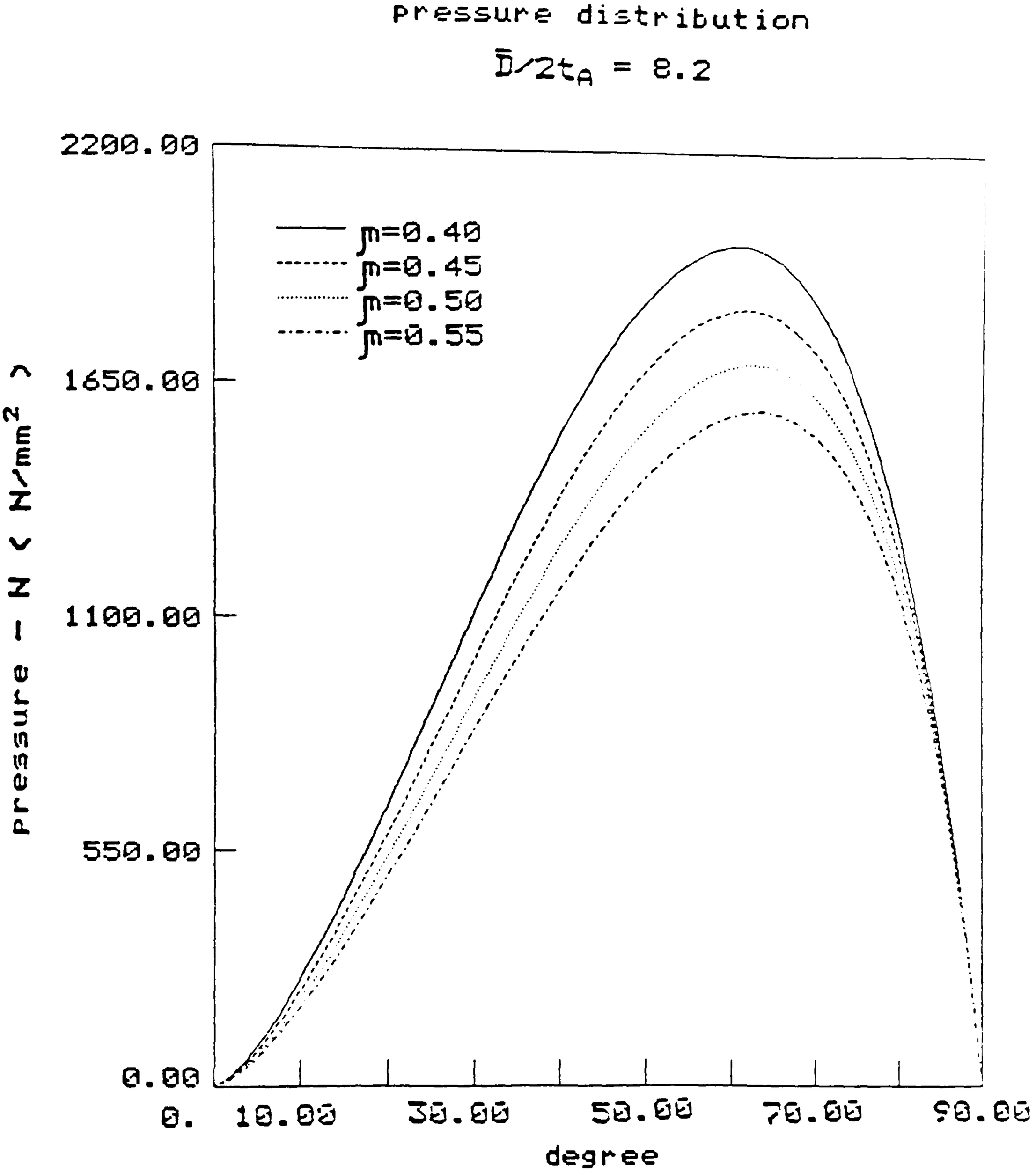

Fig.C9 Theoretical normal pressure curves

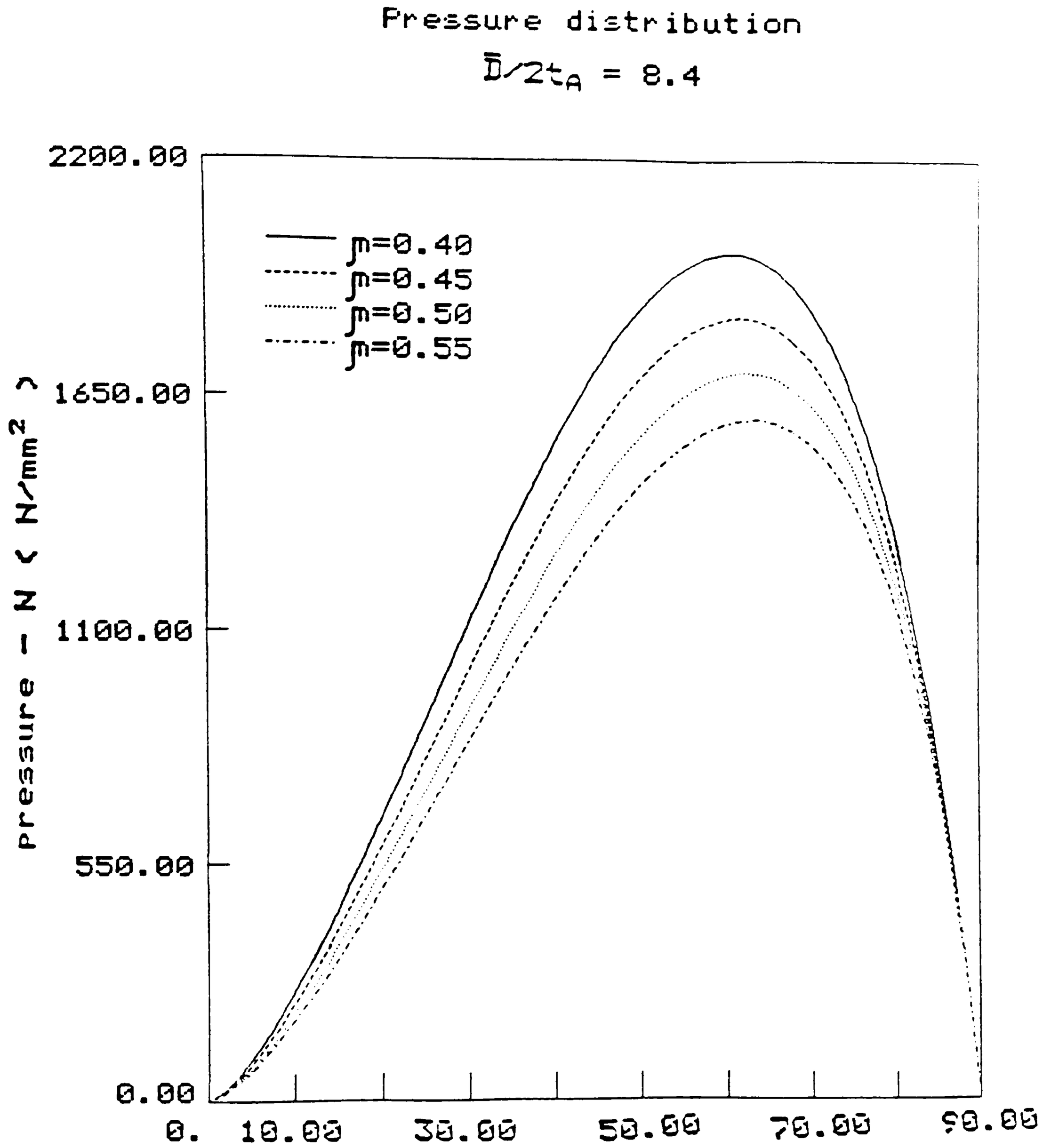

Fig.C10 Theoretical normal pressure curves

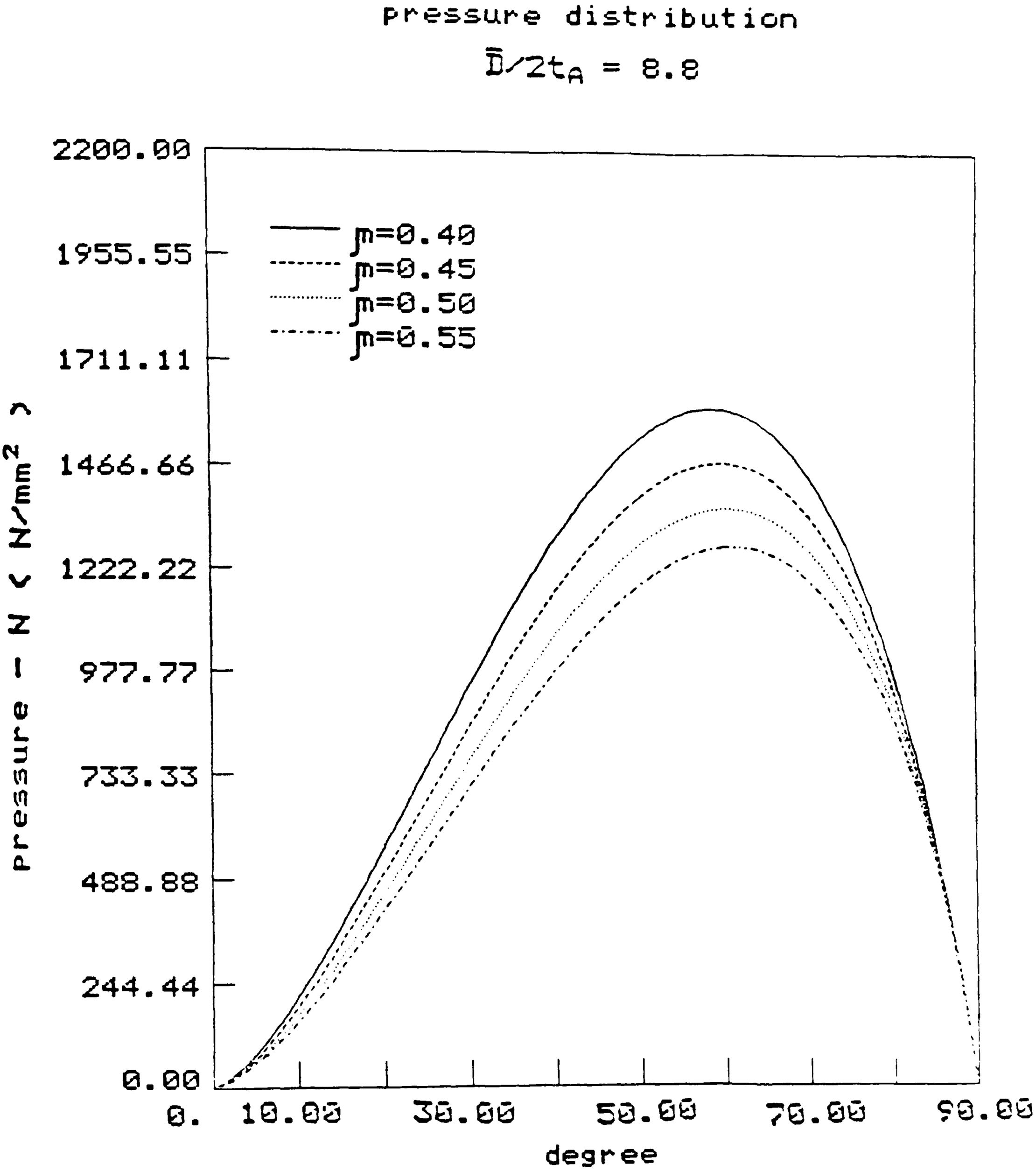

Fig.C11 Theoretical normal pressure curves

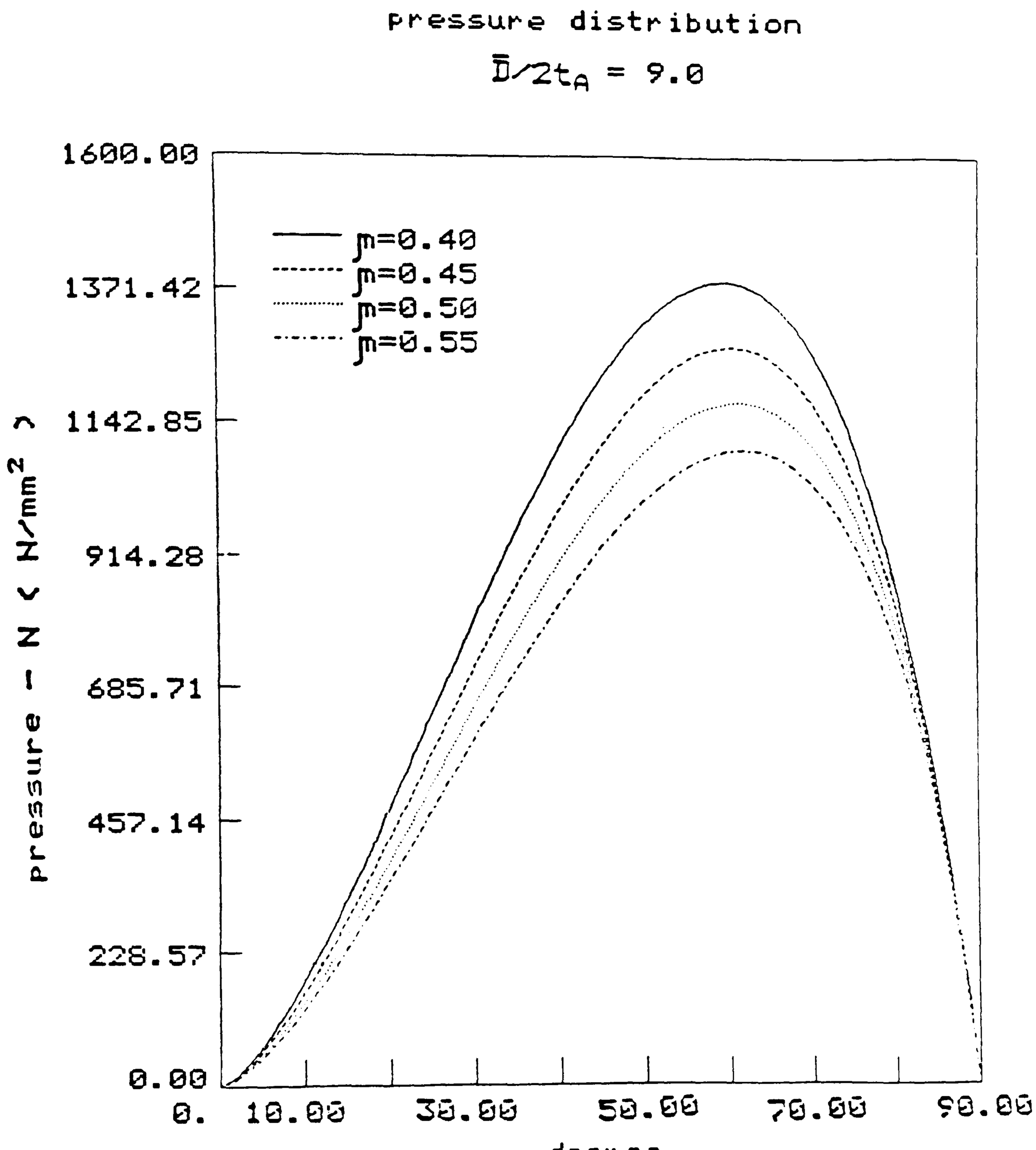

Fig.C12 Theoretical normal pressure curves

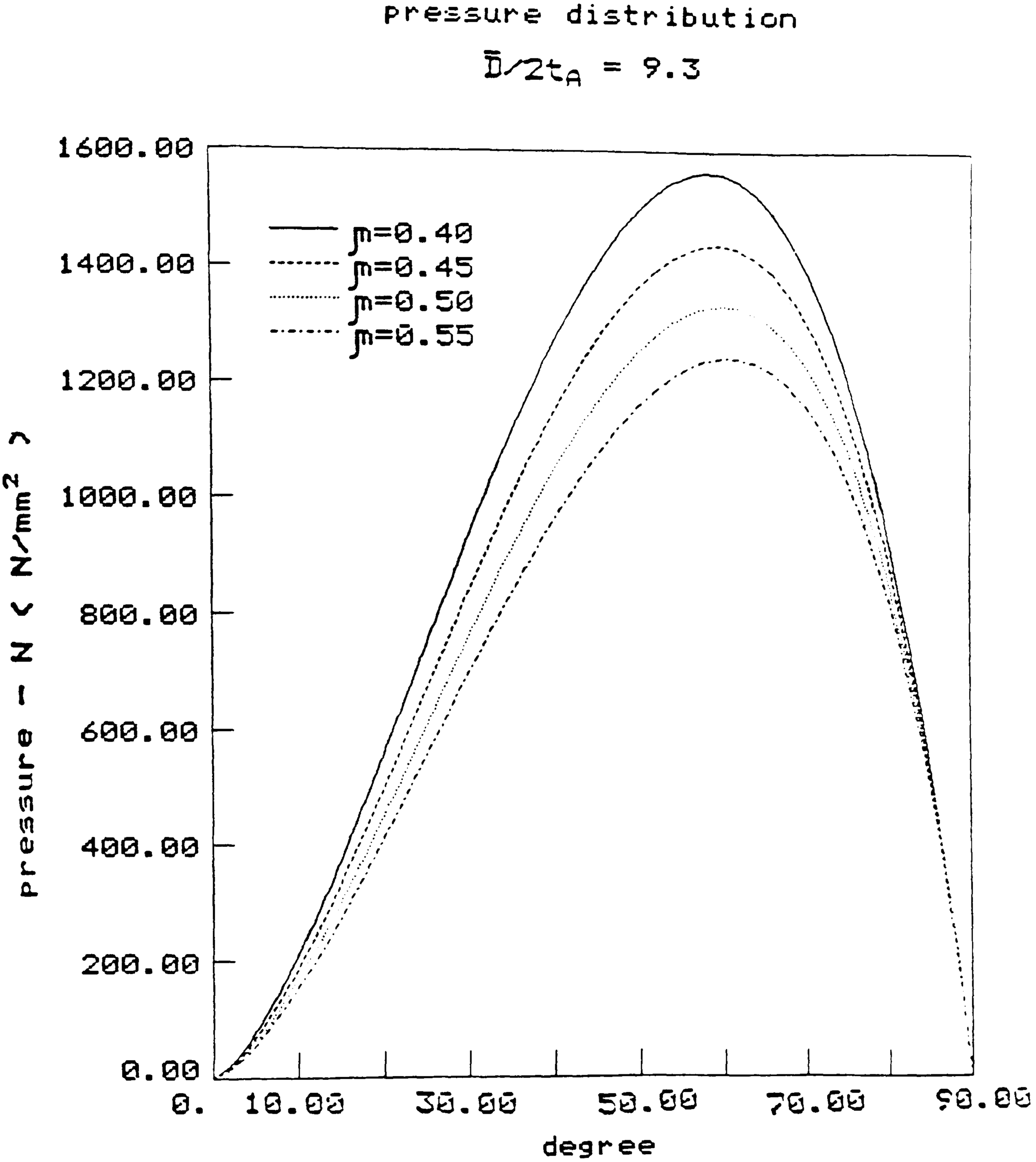

Fig.C13 Theoretical normal pressure curves

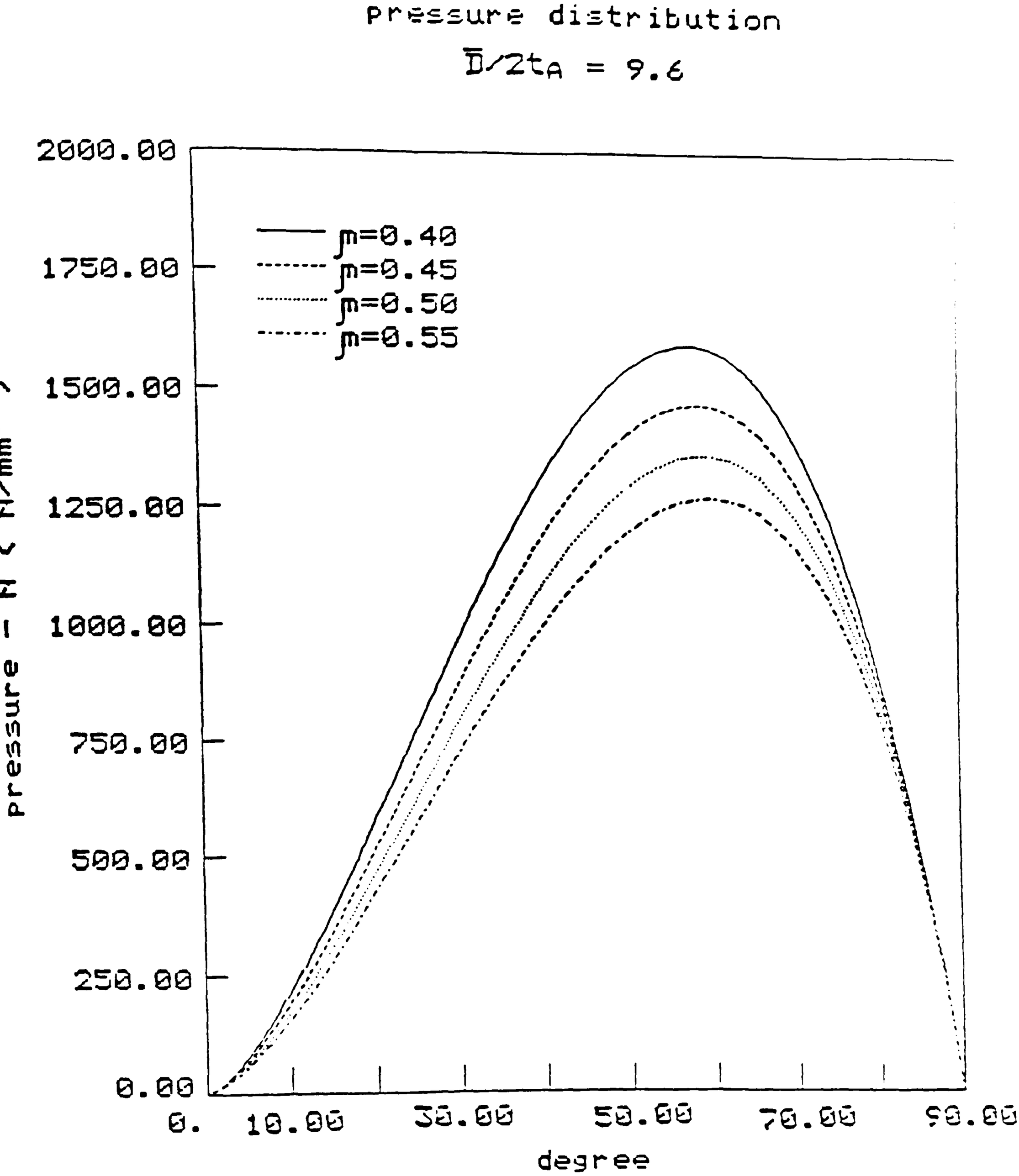

Fig.C14 Theoretical normal pressure curves

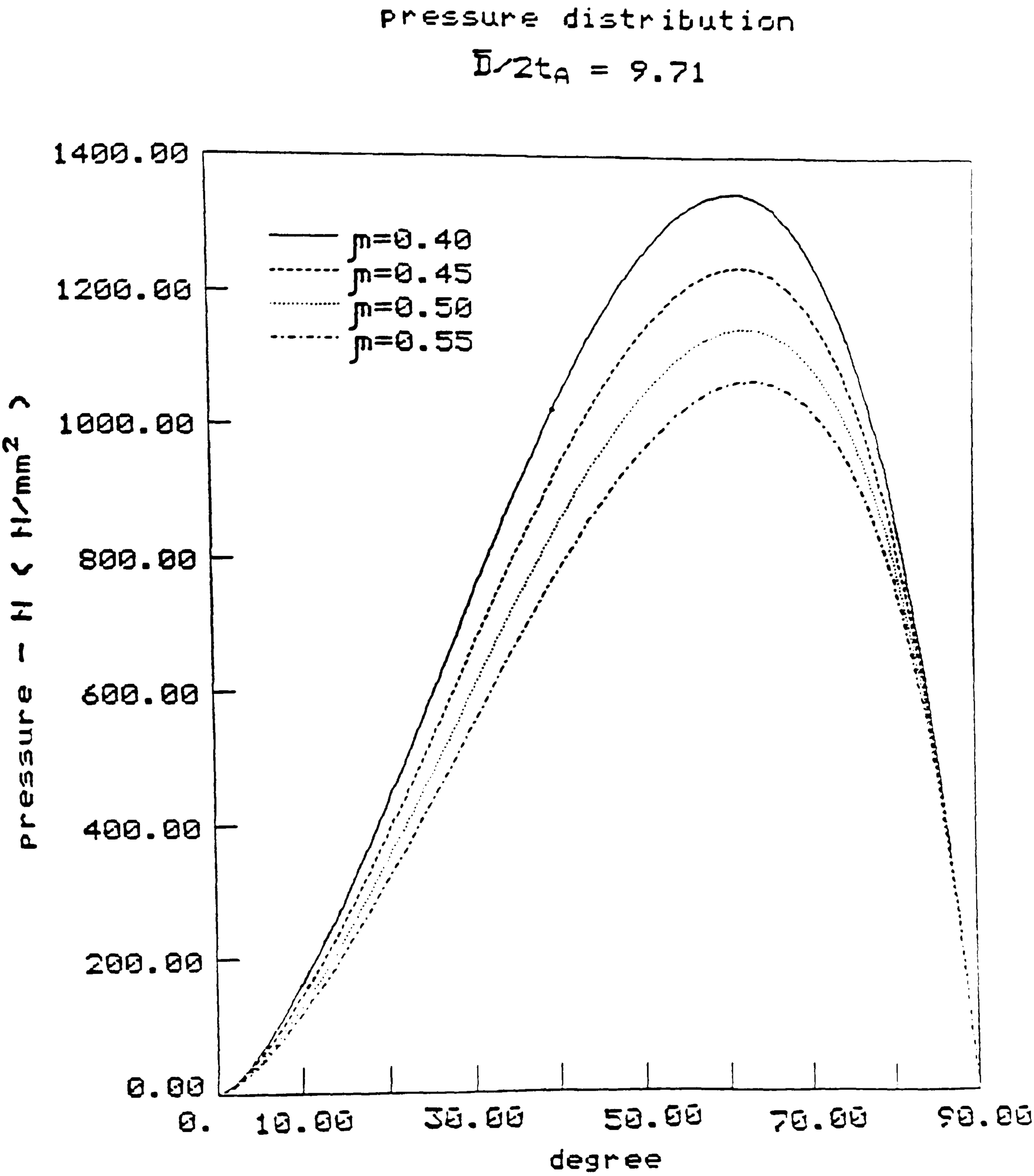

Fig.C15 Theoretical normal pressure curves

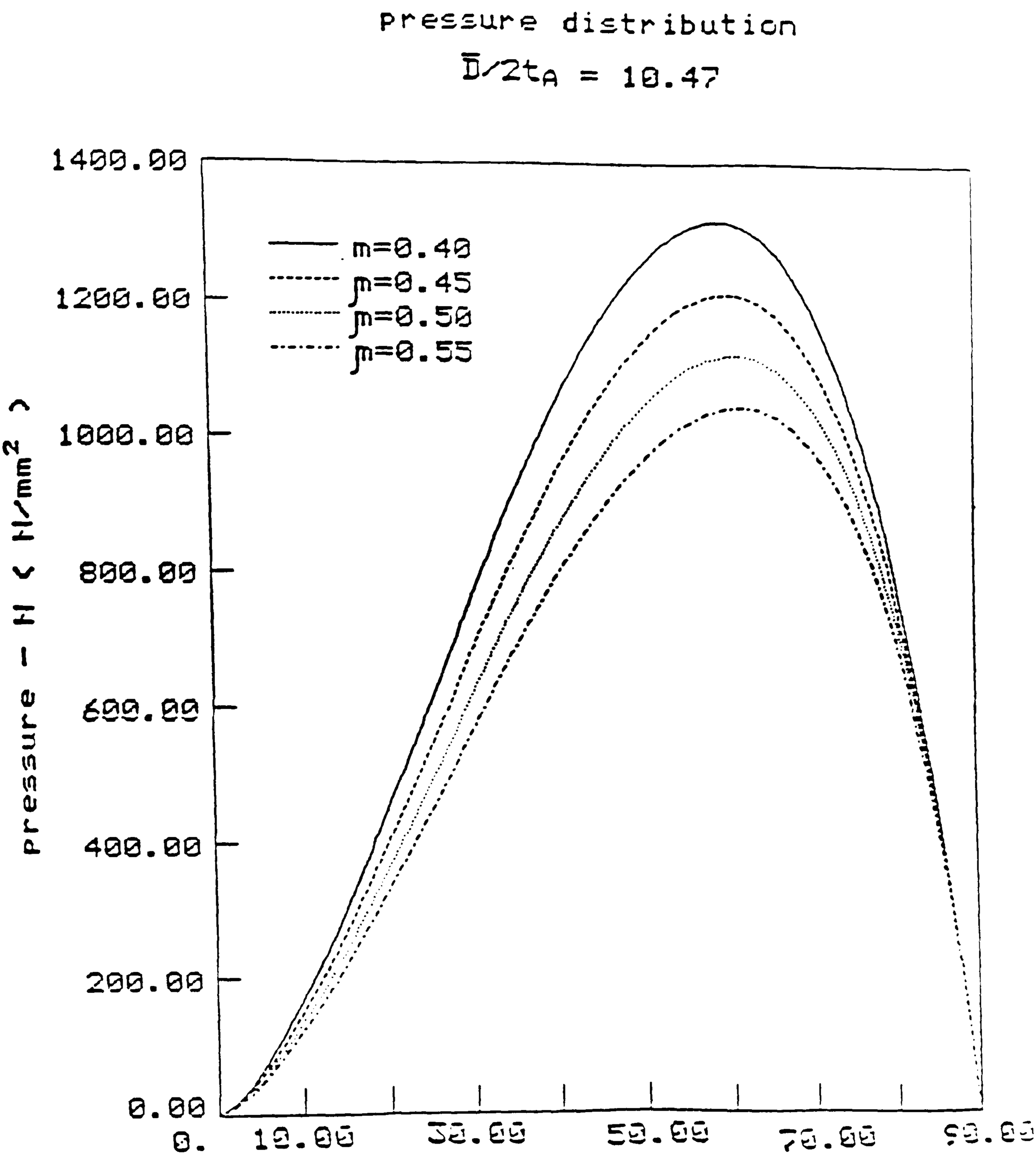

Fig.C16 Theoretical normal pressure curves

pressure distribution

$\bar{D}/2t_A = 10.5$

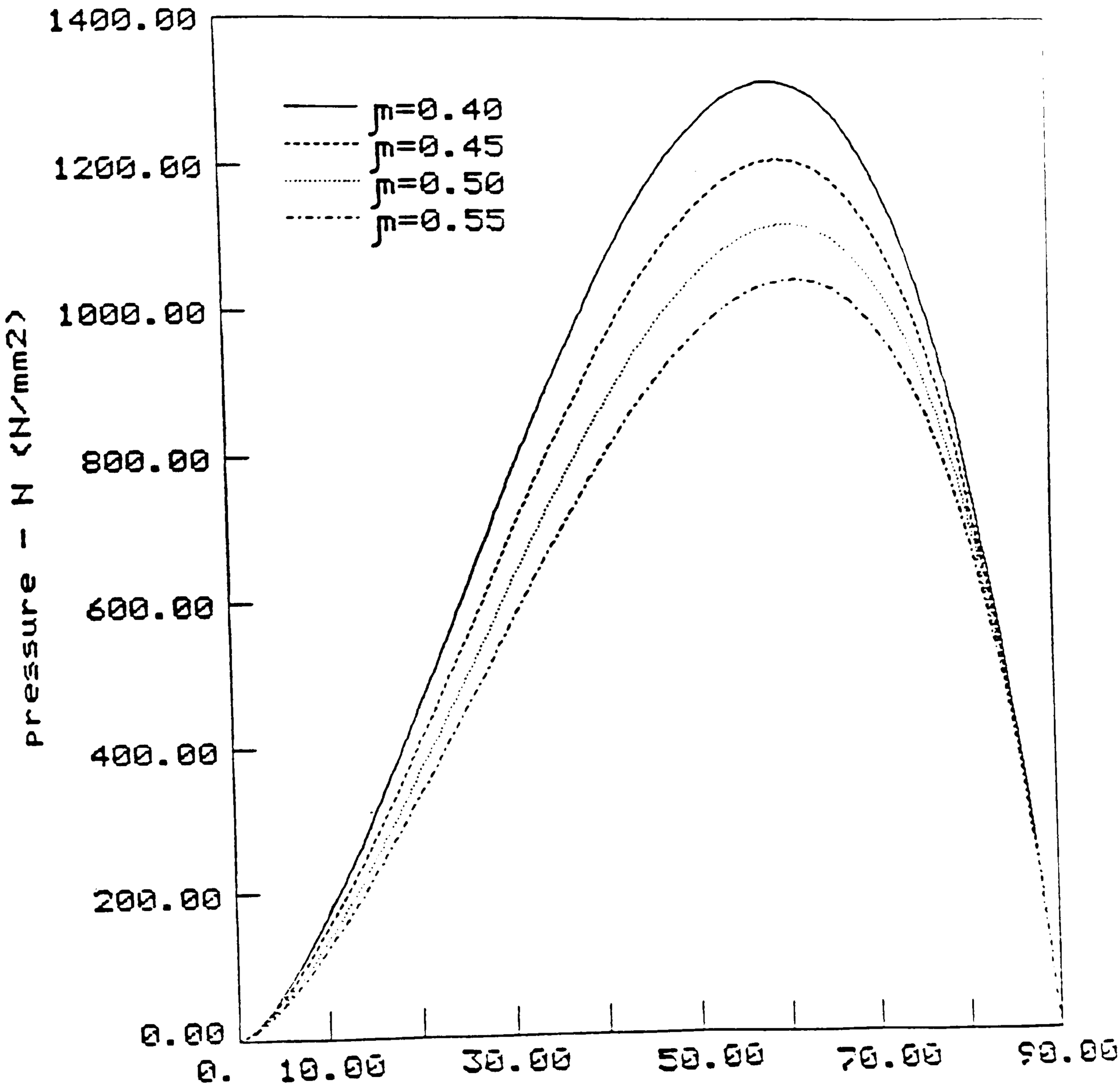

Fig.C17 Theoretical normal pressure curves

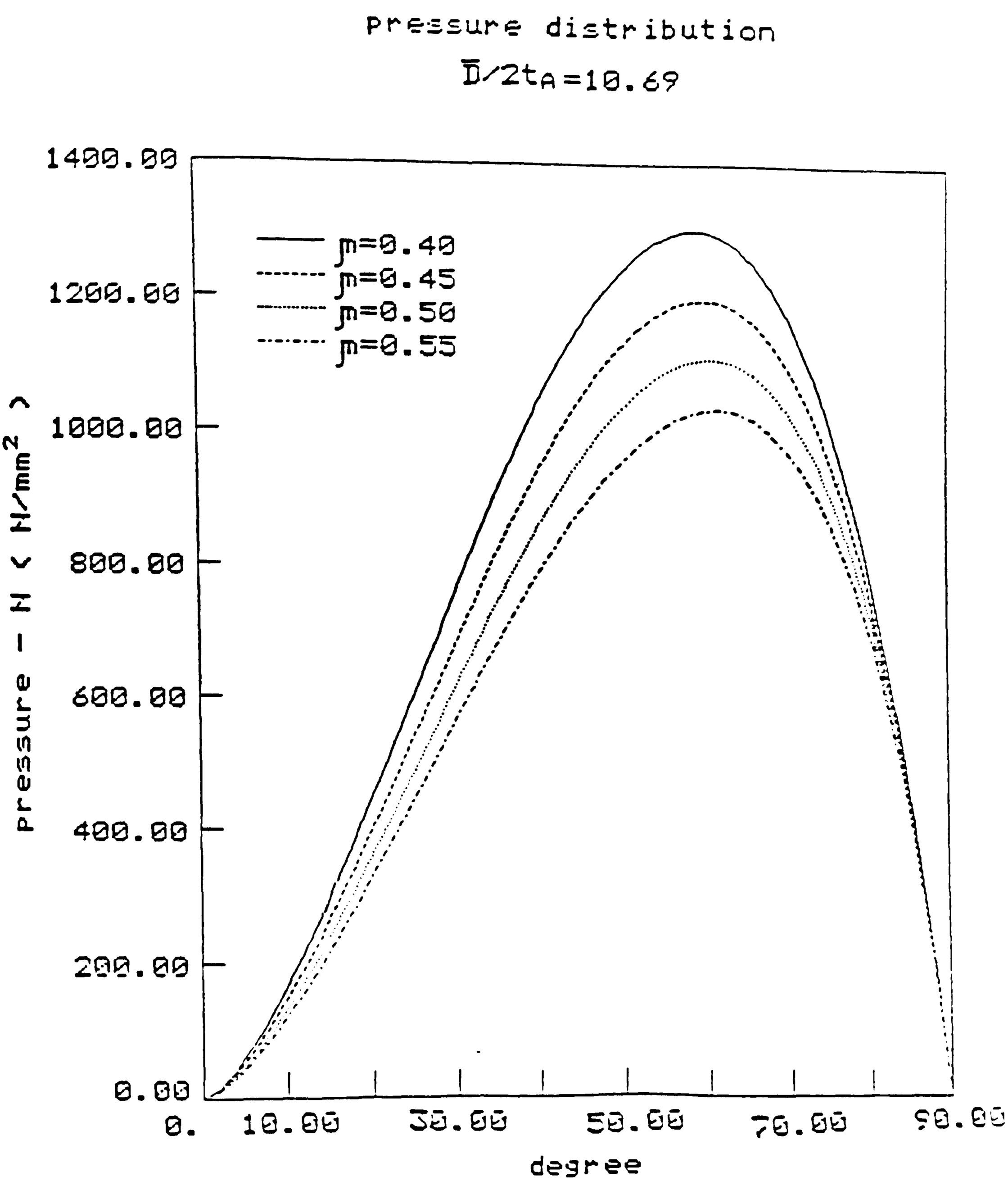

Fig.C18 Theoretical normal pressure curves

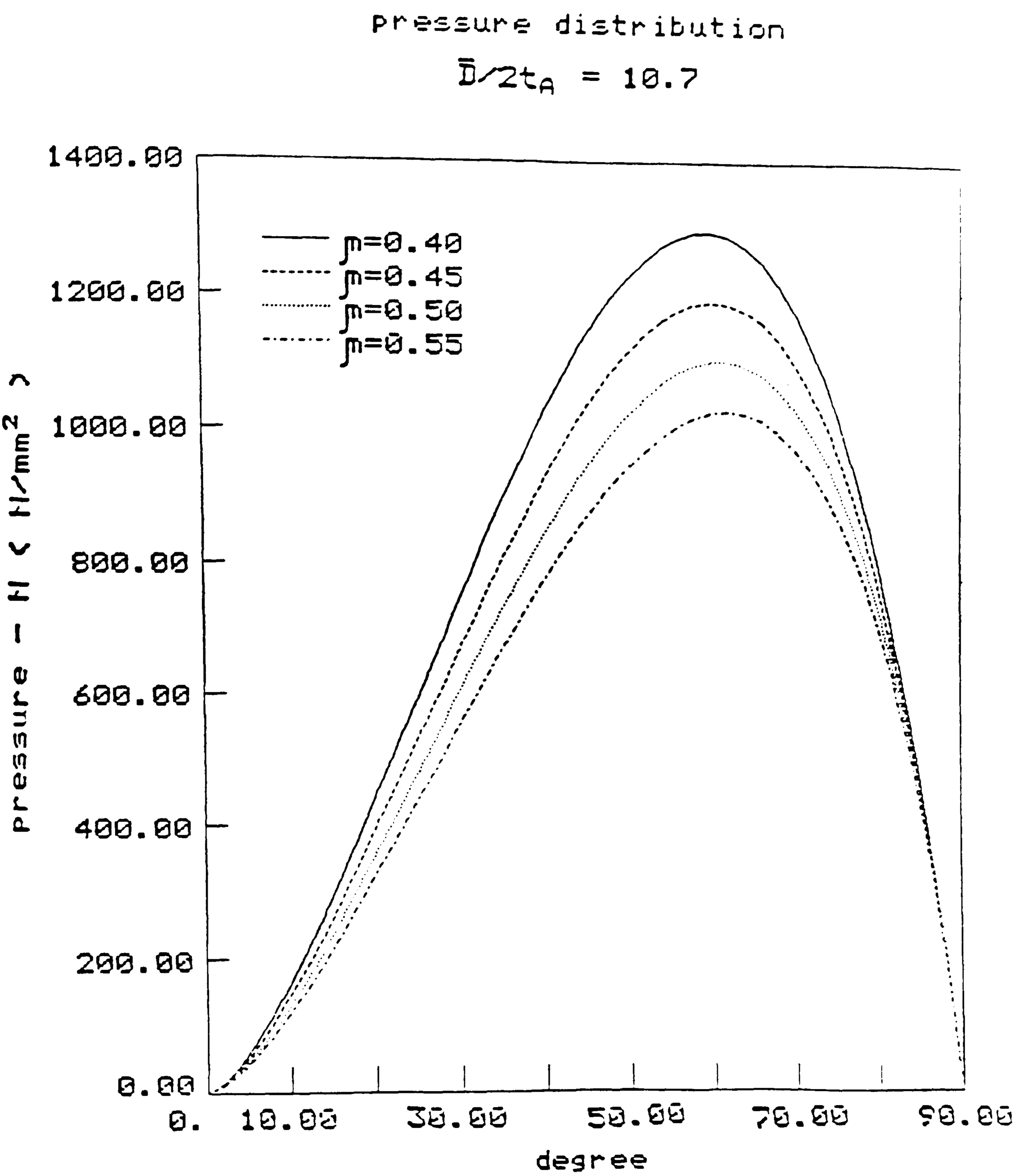

Fig.C19 Theoretical normal pressure curves

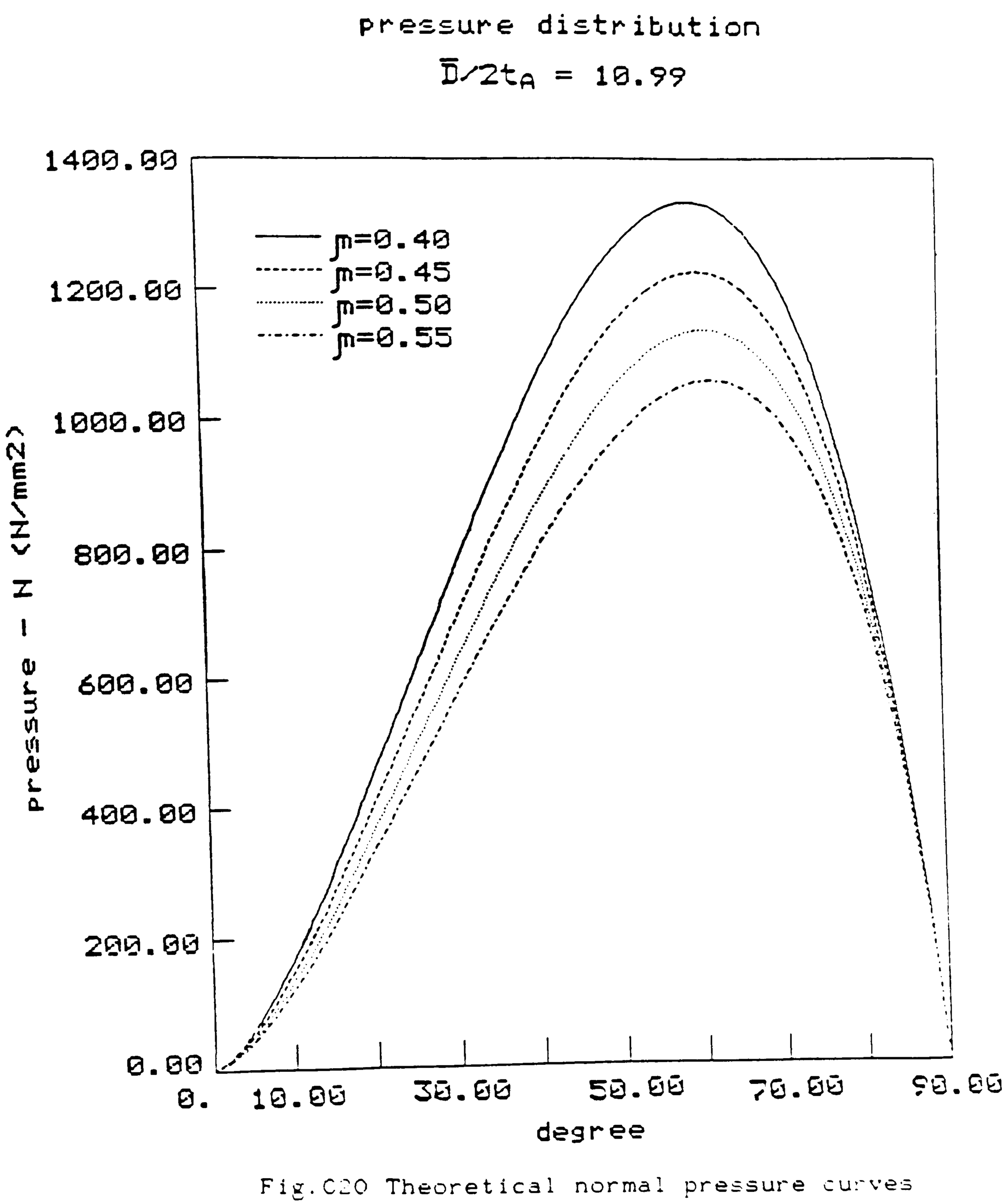

Fig.C20 Theoretical normal pressure curves

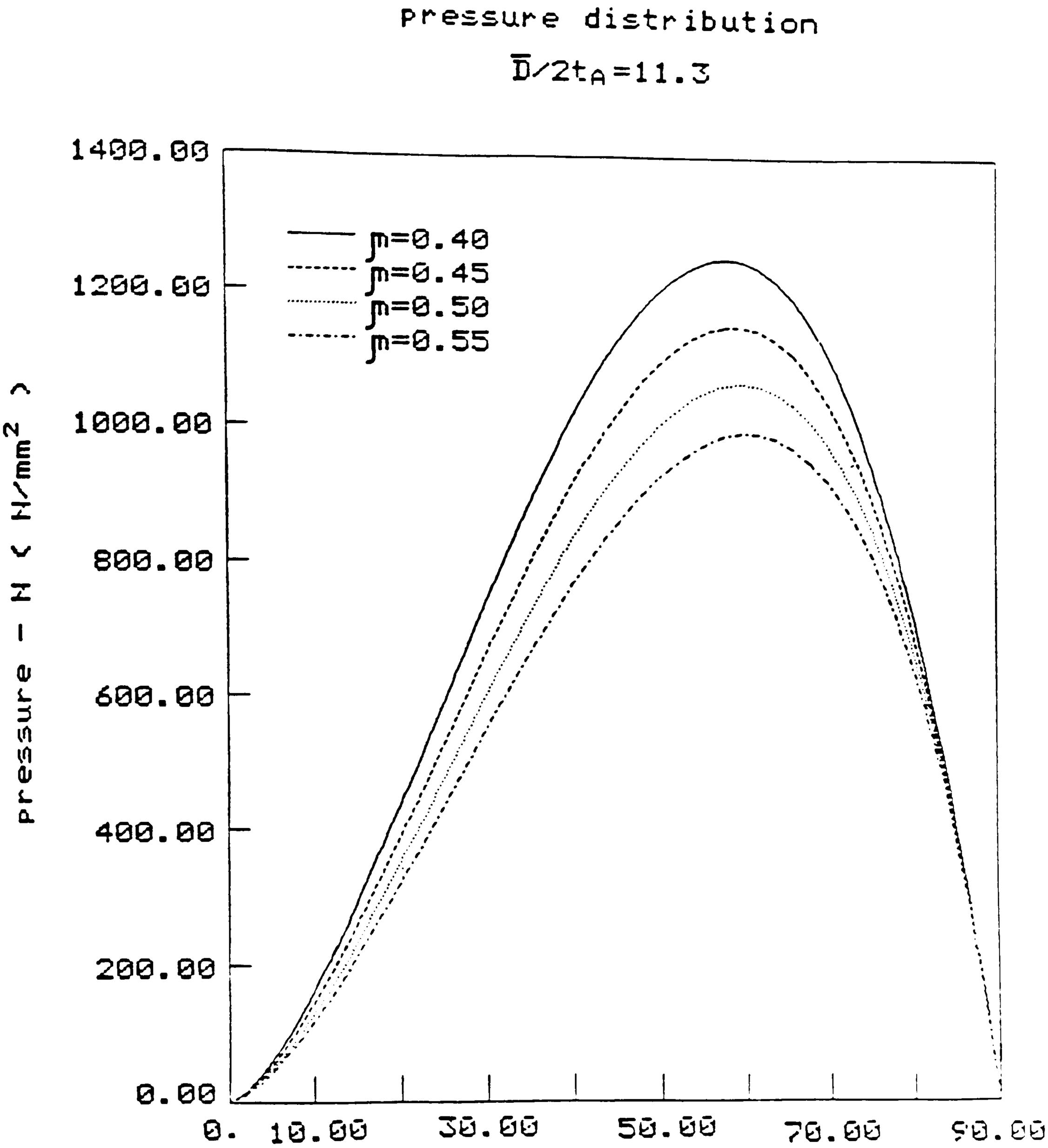

Fig.C21 Theoretical normal pressure curves

pressure distribution

$\bar{D}/2t_A = 11.6$

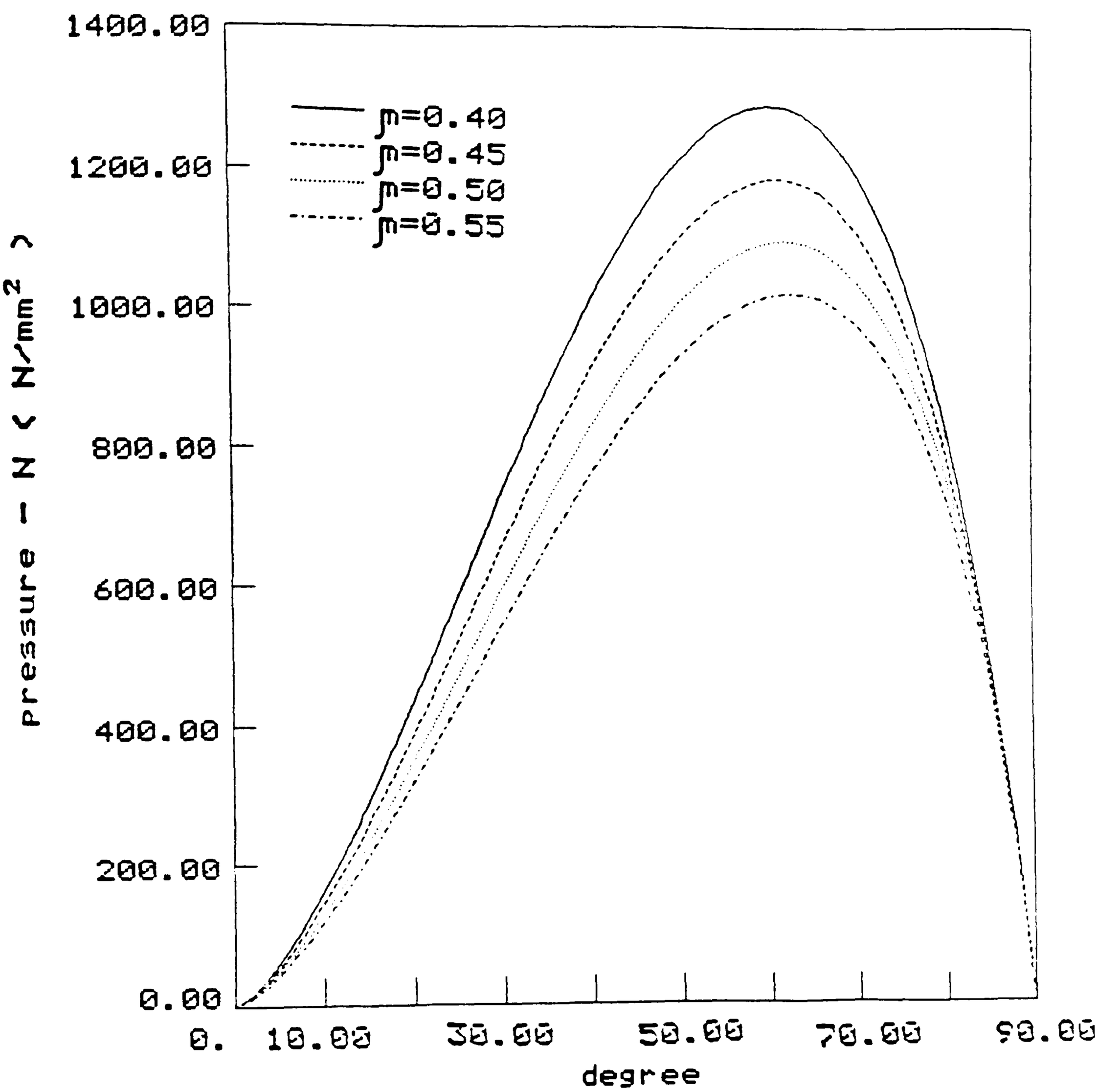

Fig.C22 Theoretical normal pressure curves

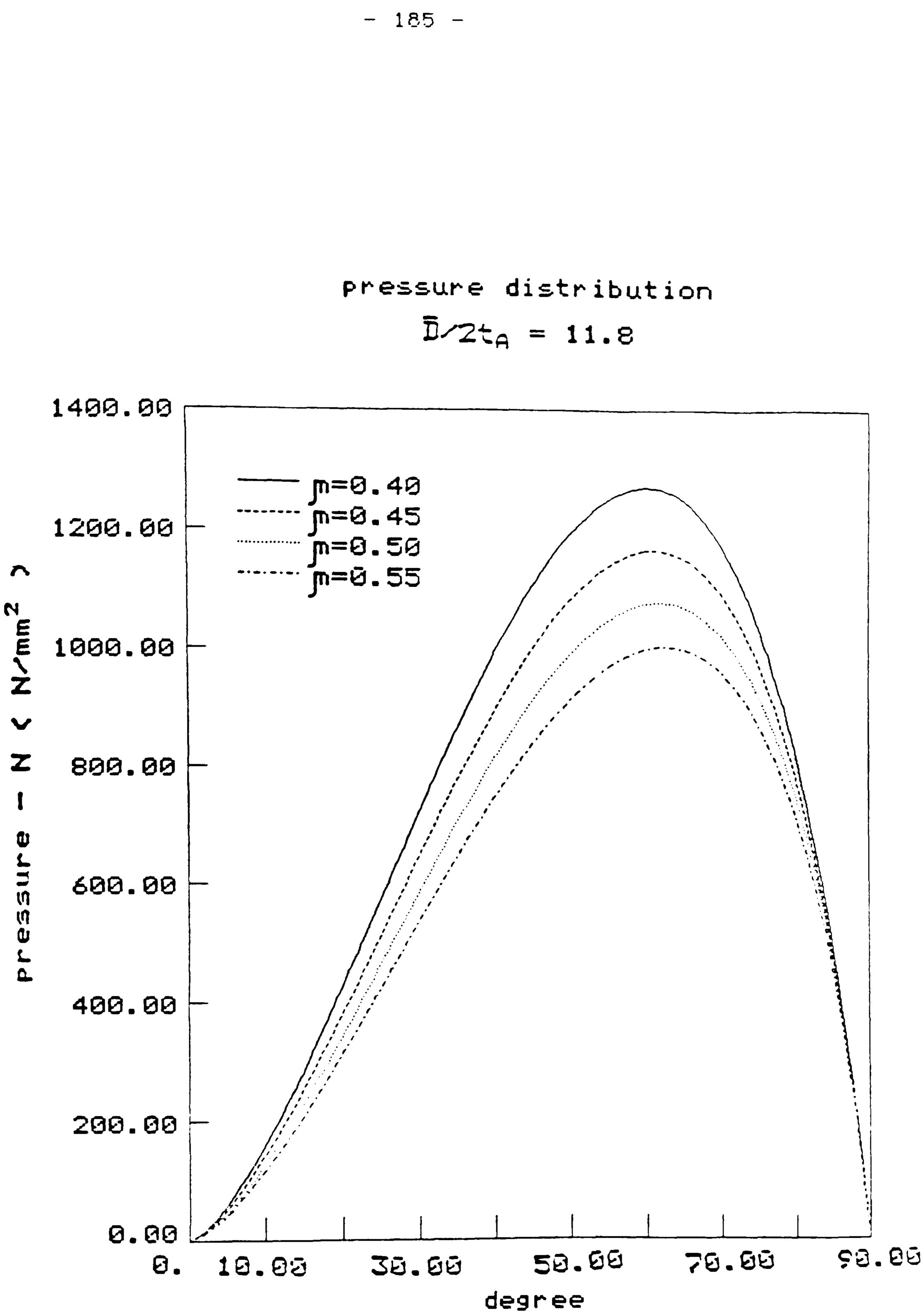

Fig.C23 Theoretical normal pressure curves

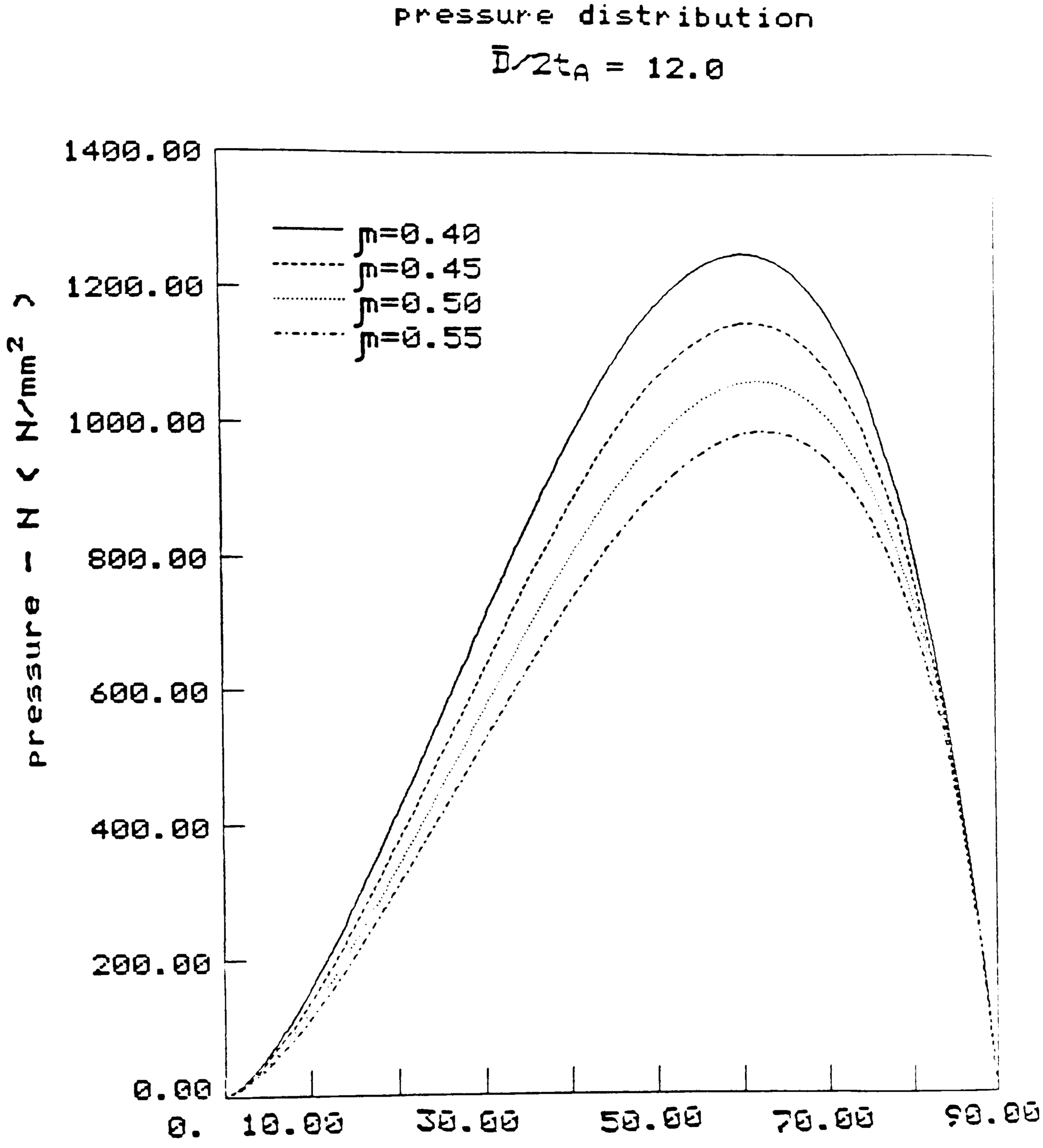

Fig.C24 Theoretical normal pressure curves

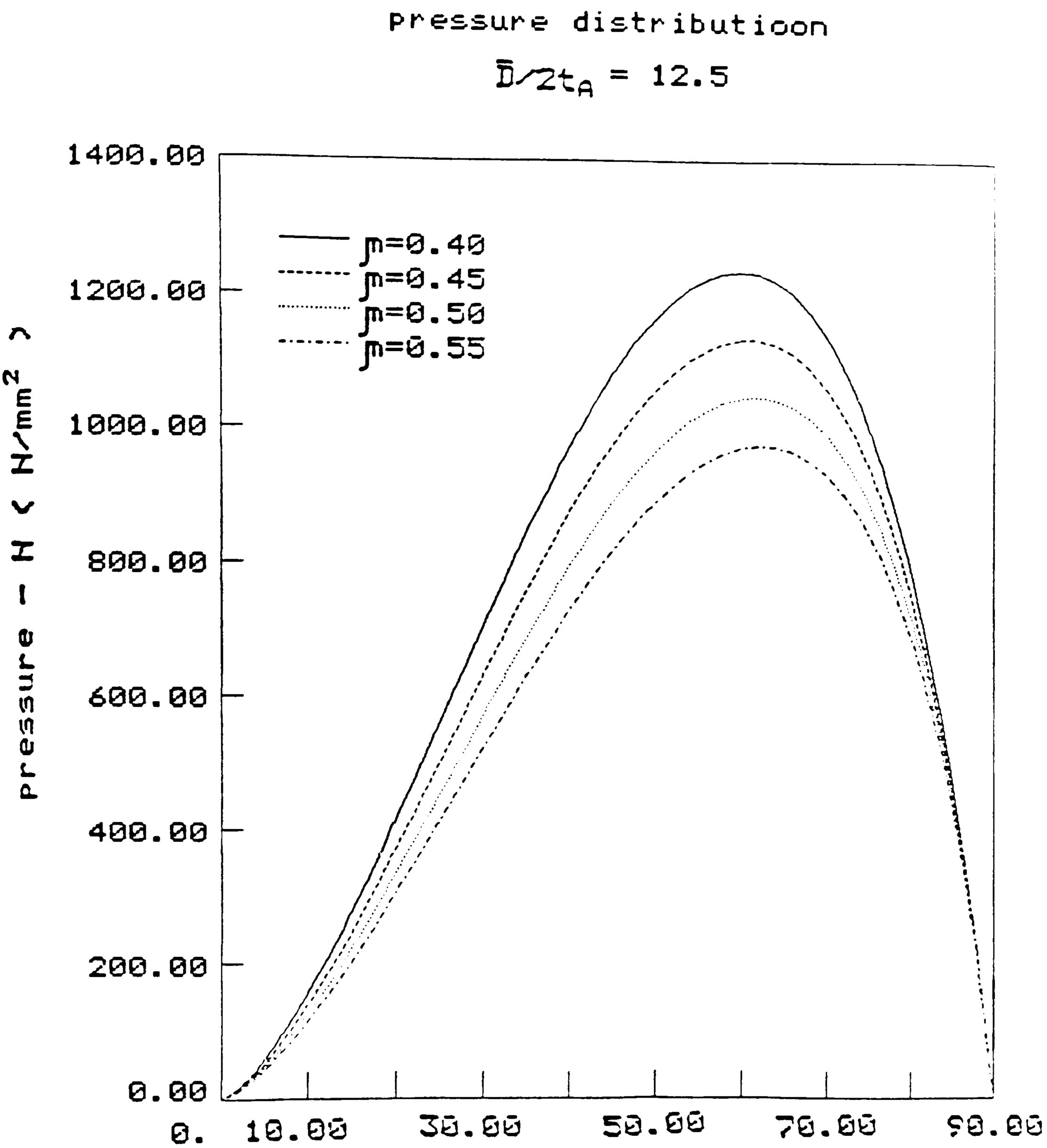

Fig.C25 Theoretical normal pressure curves

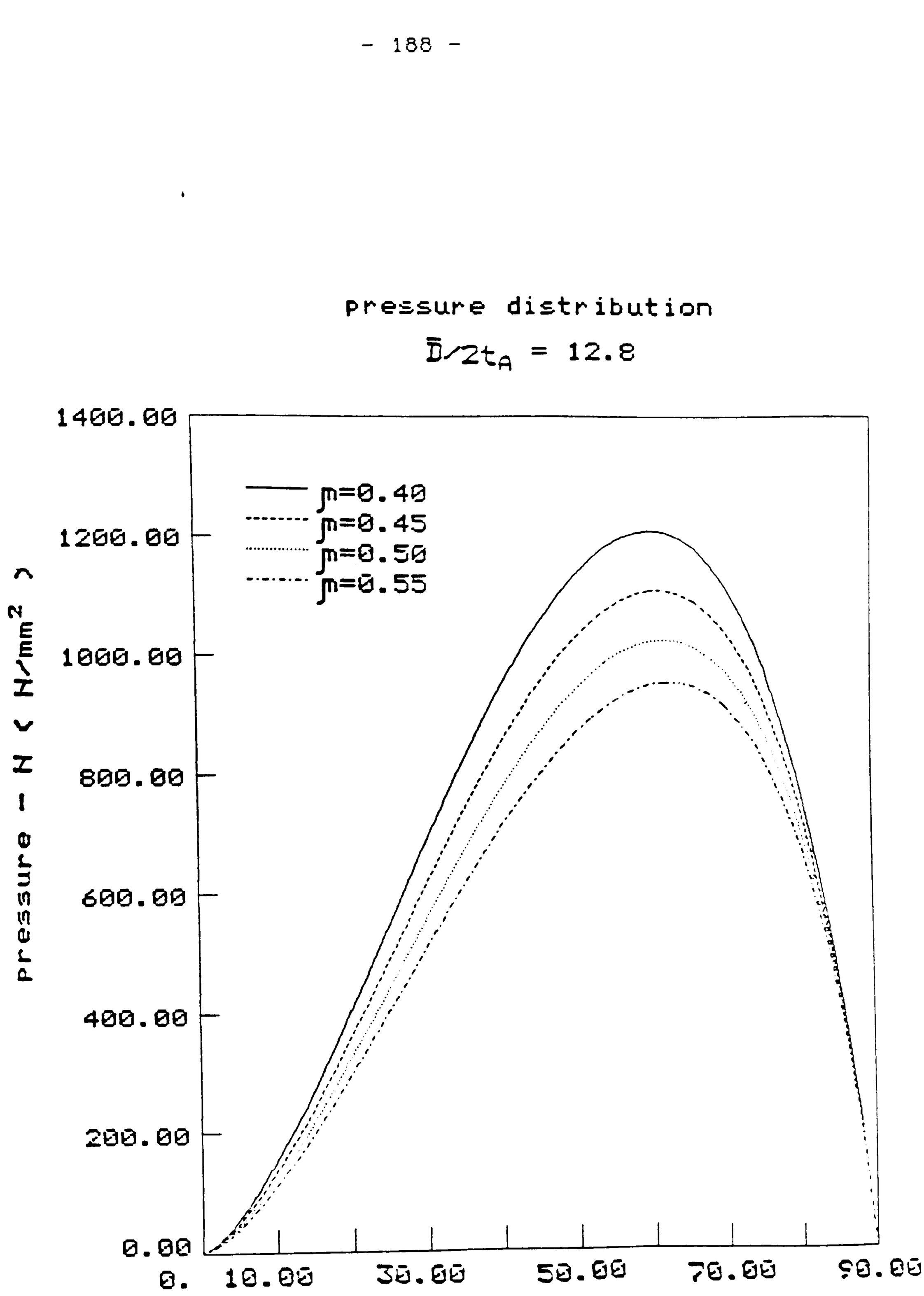

Fig.C26 Theoretical normal pressure curves

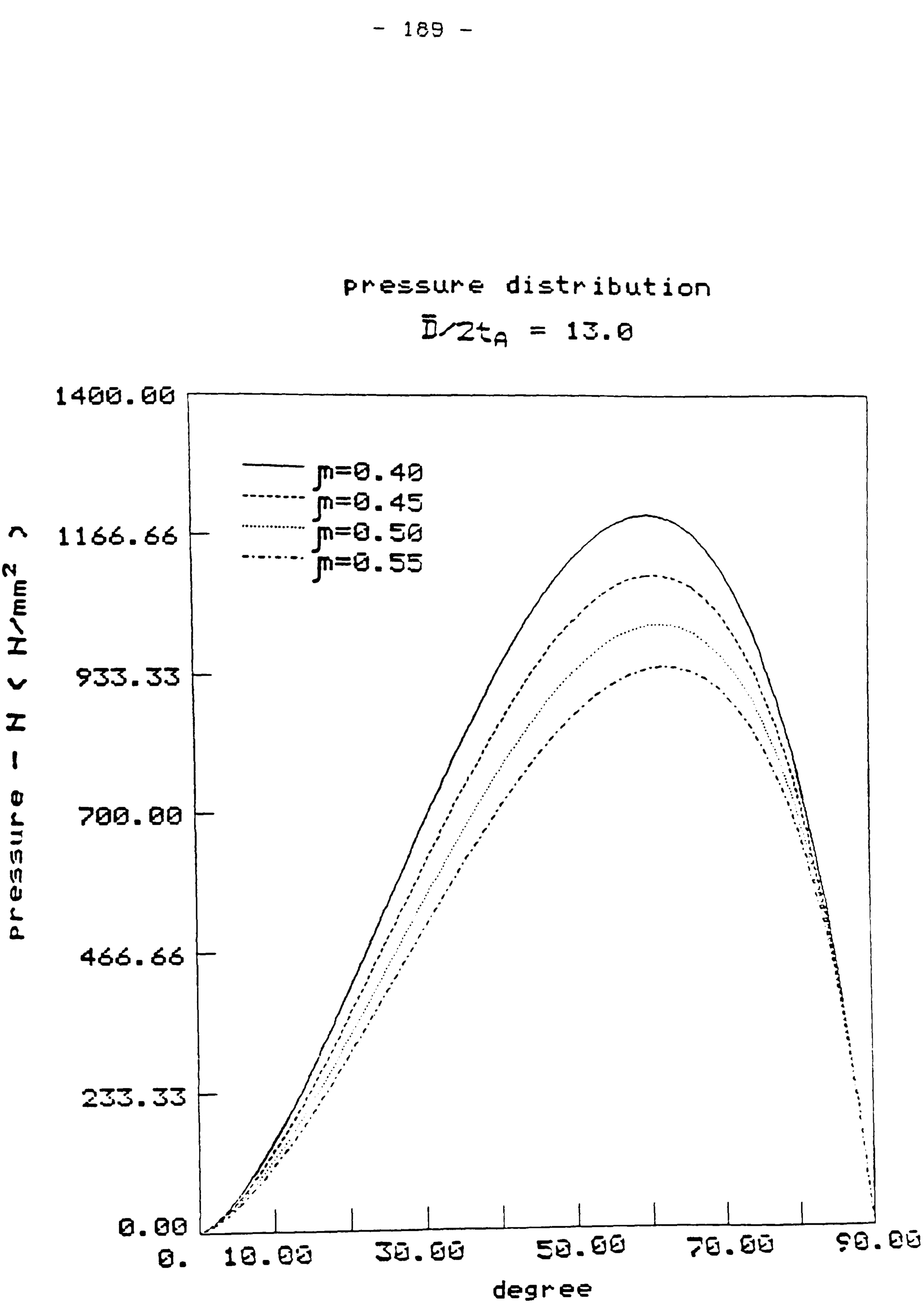

Fig.C27 Theoretical normal pressure curves

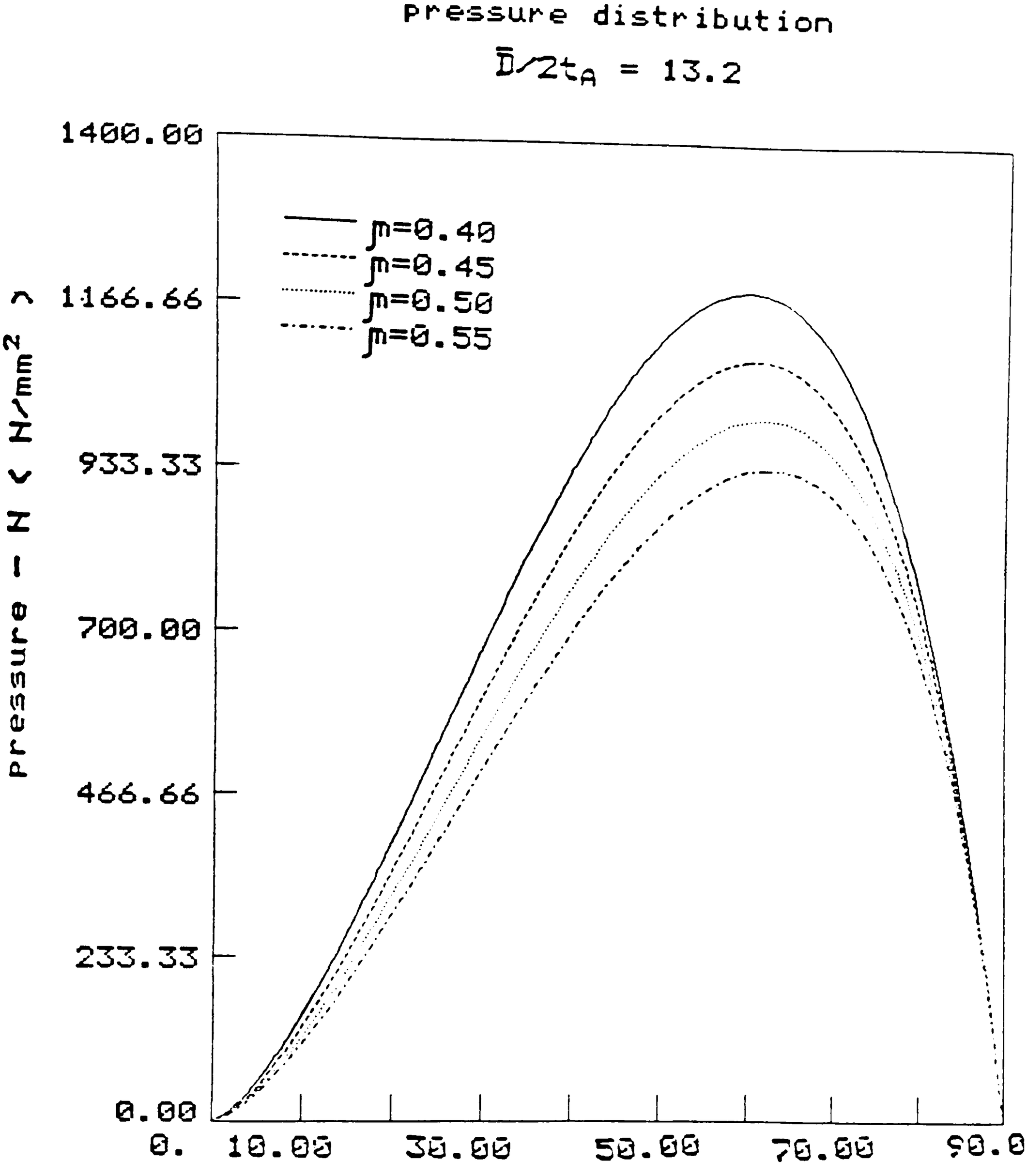

Fig.C28 Theoretical normal pressure curves

Pressure distribution

$\bar{D}/2t_A = 13.53$

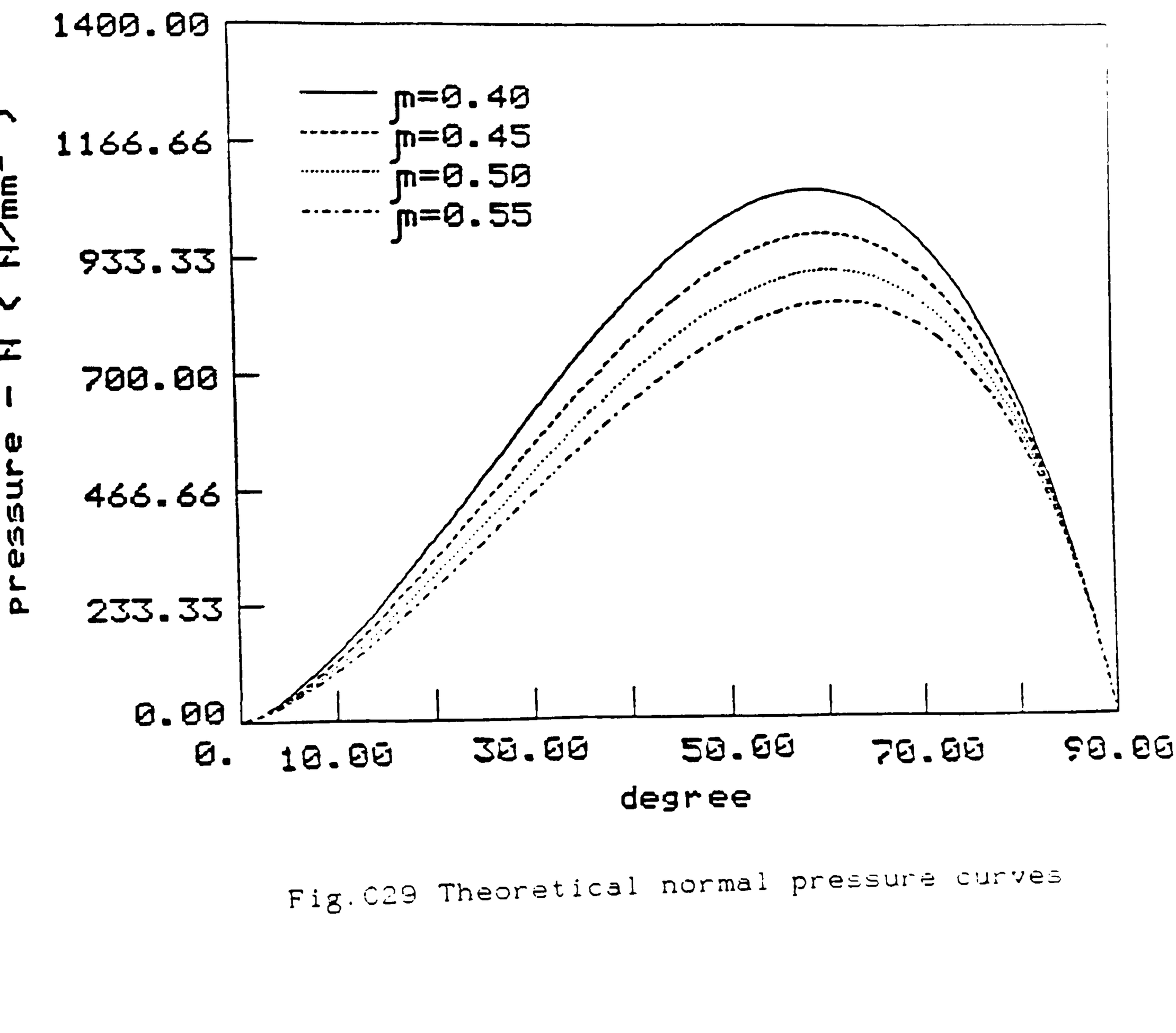

Fig.C29 Theoretical normal pressure curves

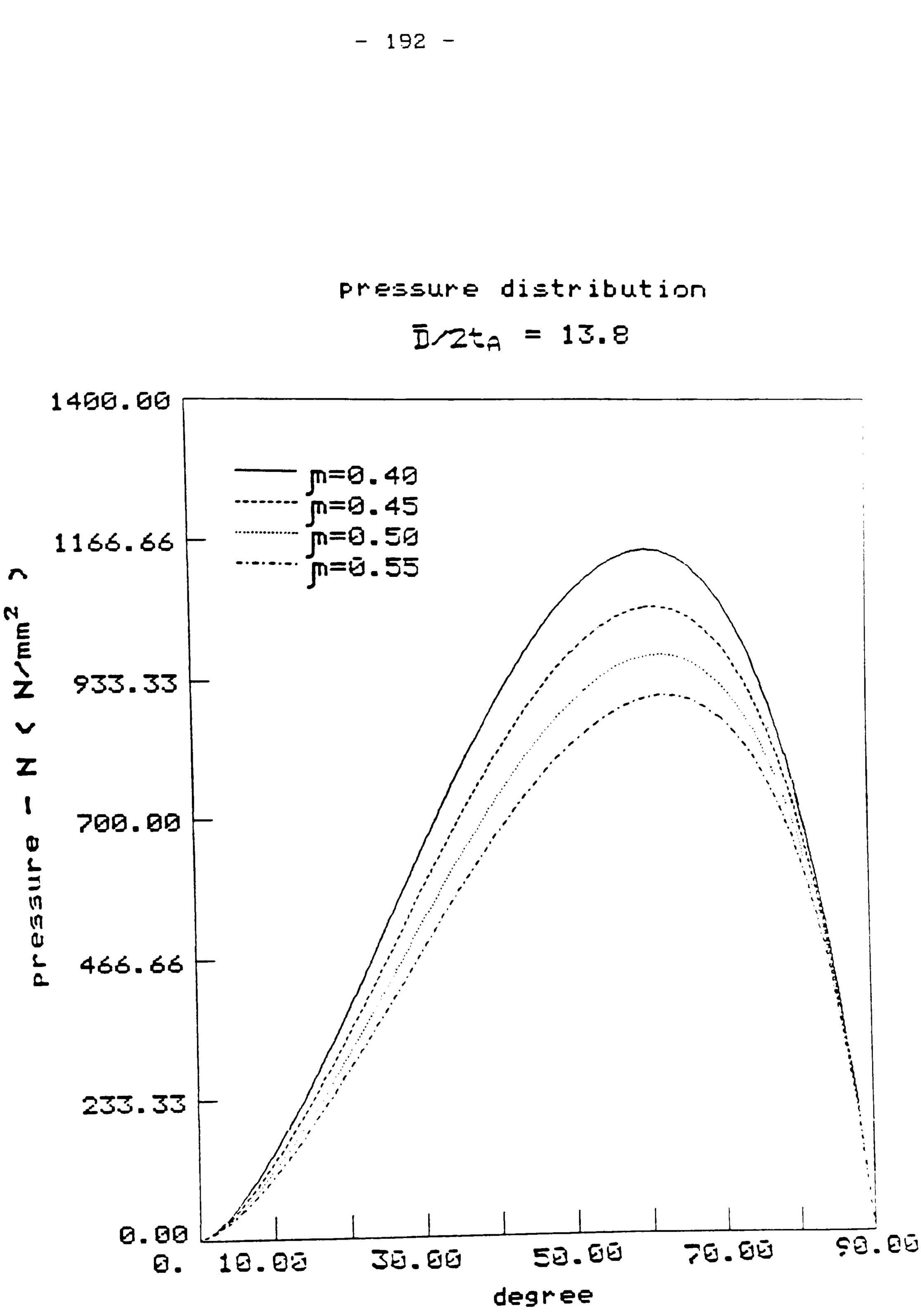

Fig.C30 Theoretical normal pressure curves

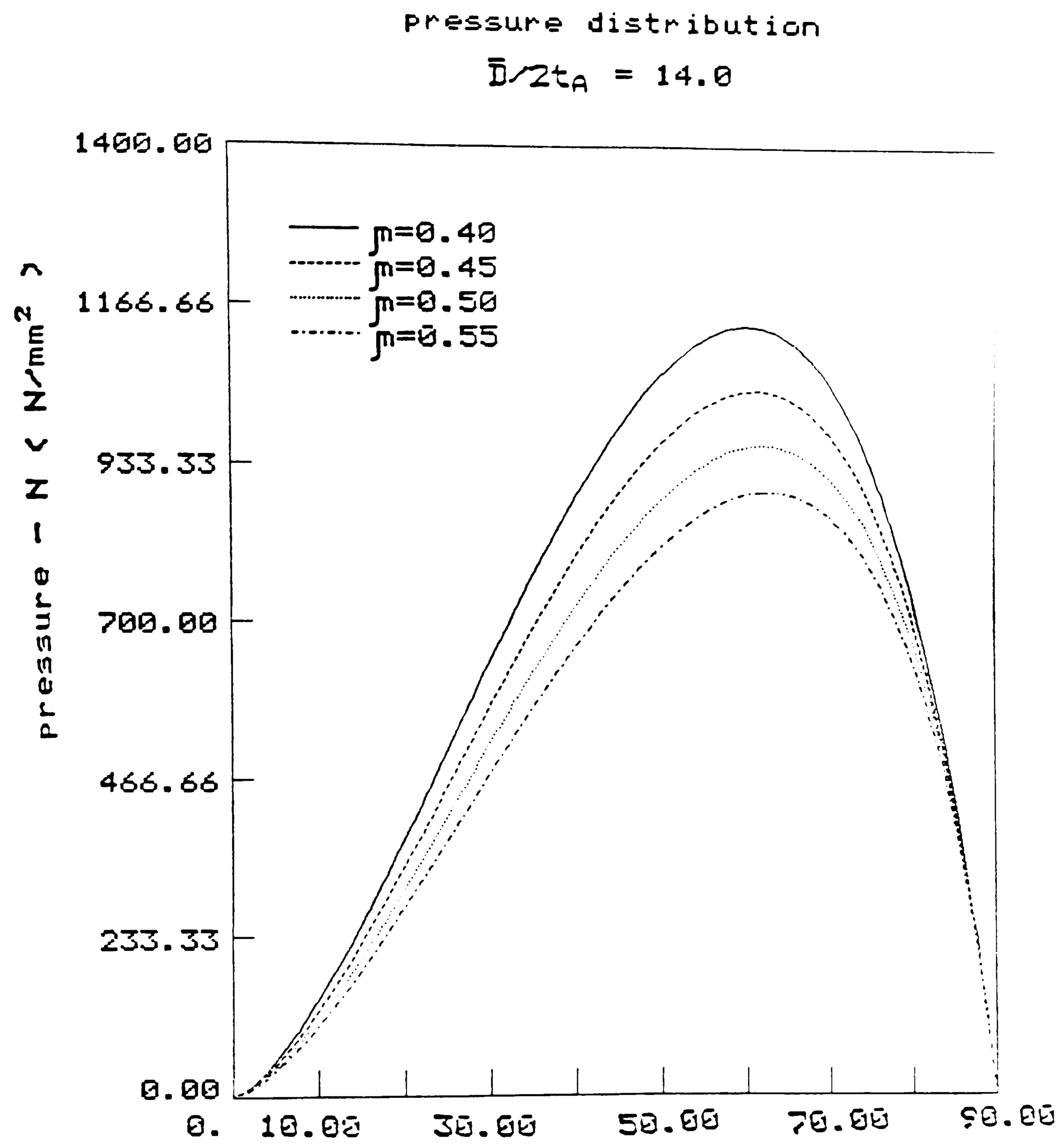

Fig.C31 Theoretical normal pressure curves

pressure distribution

$\bar{D}/2t_A = 14.5$

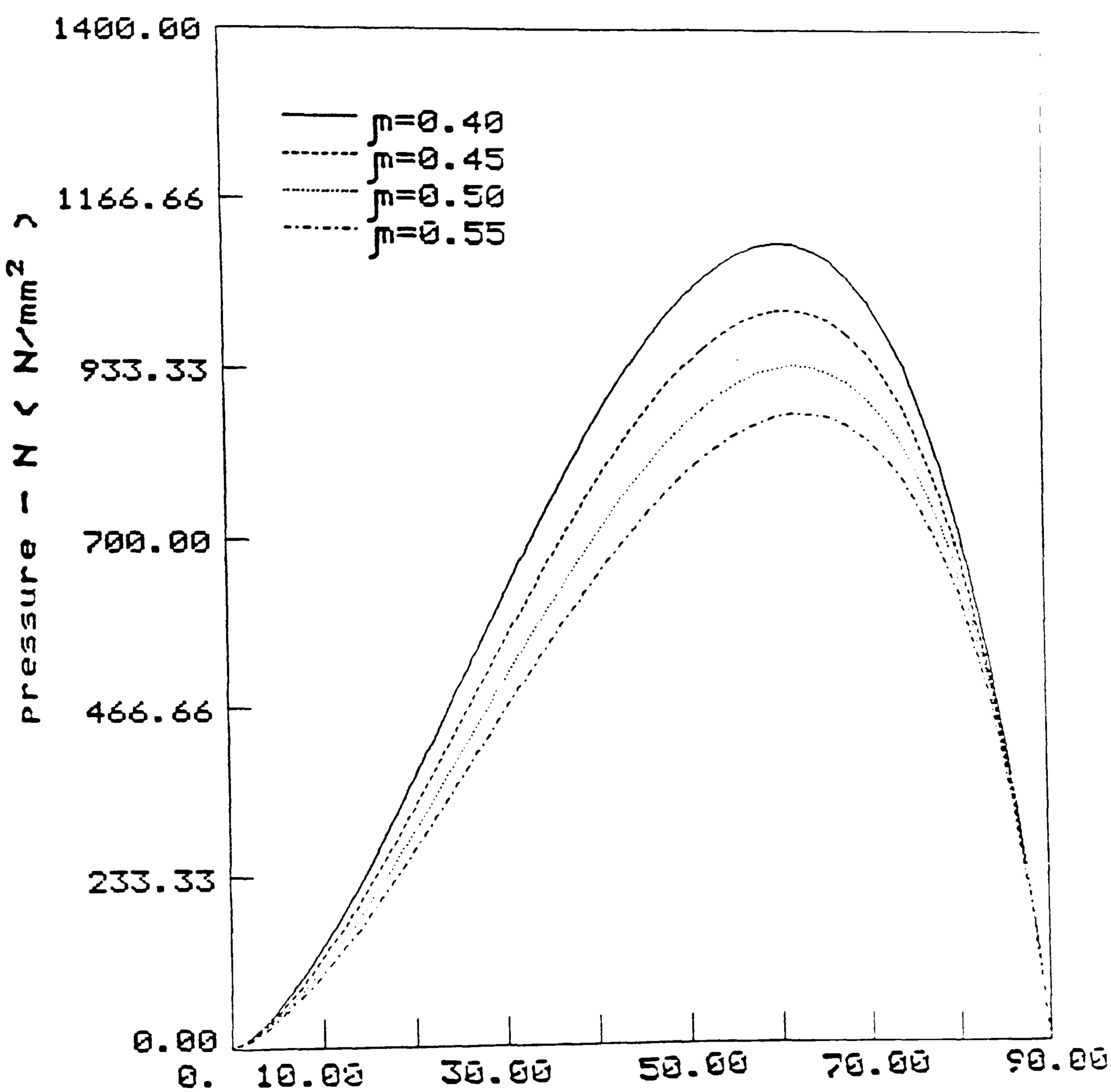

Fig.C32 Theoretical normal pressure curves

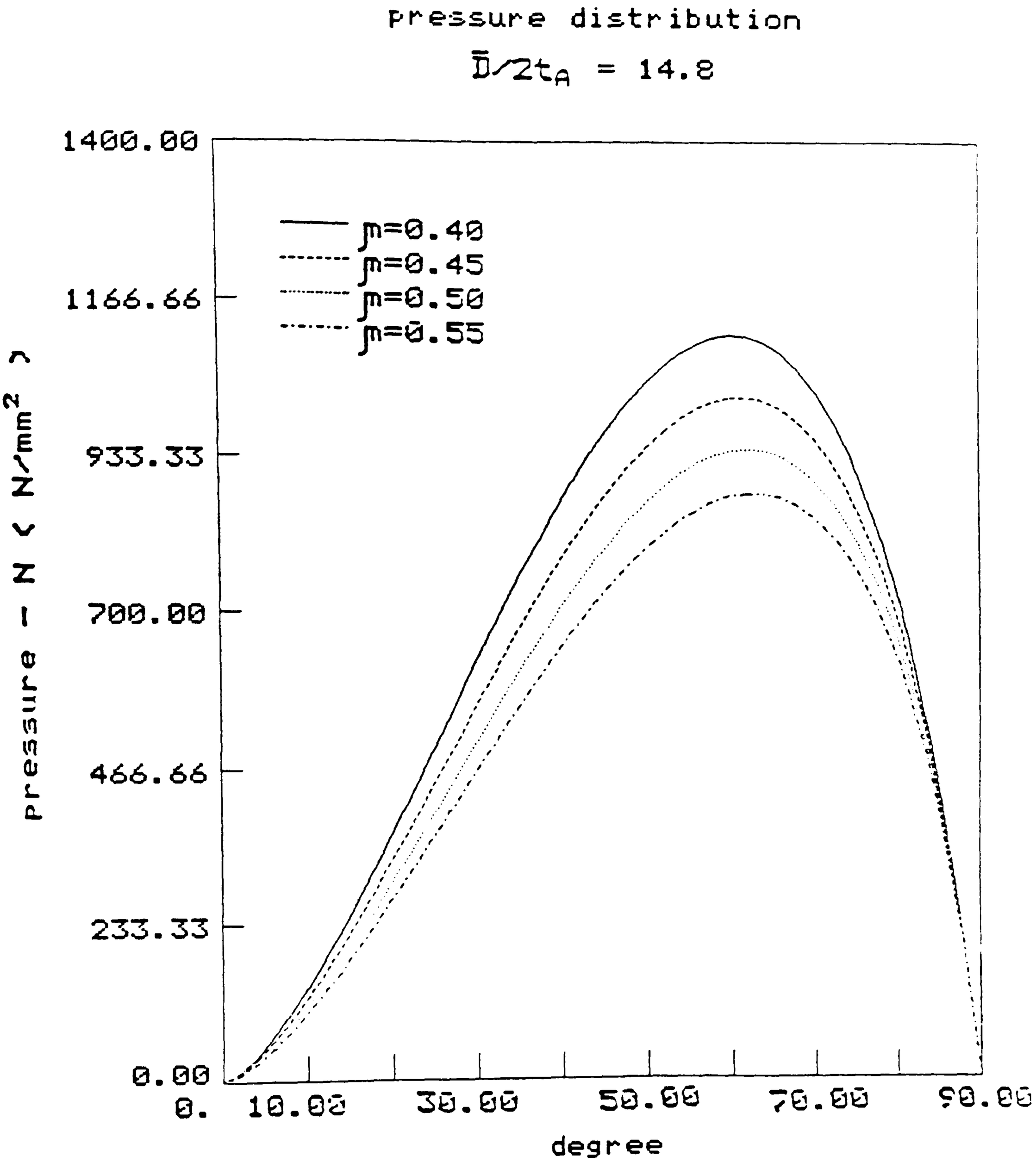

Fig.C33 Theoretical normal pressure curves

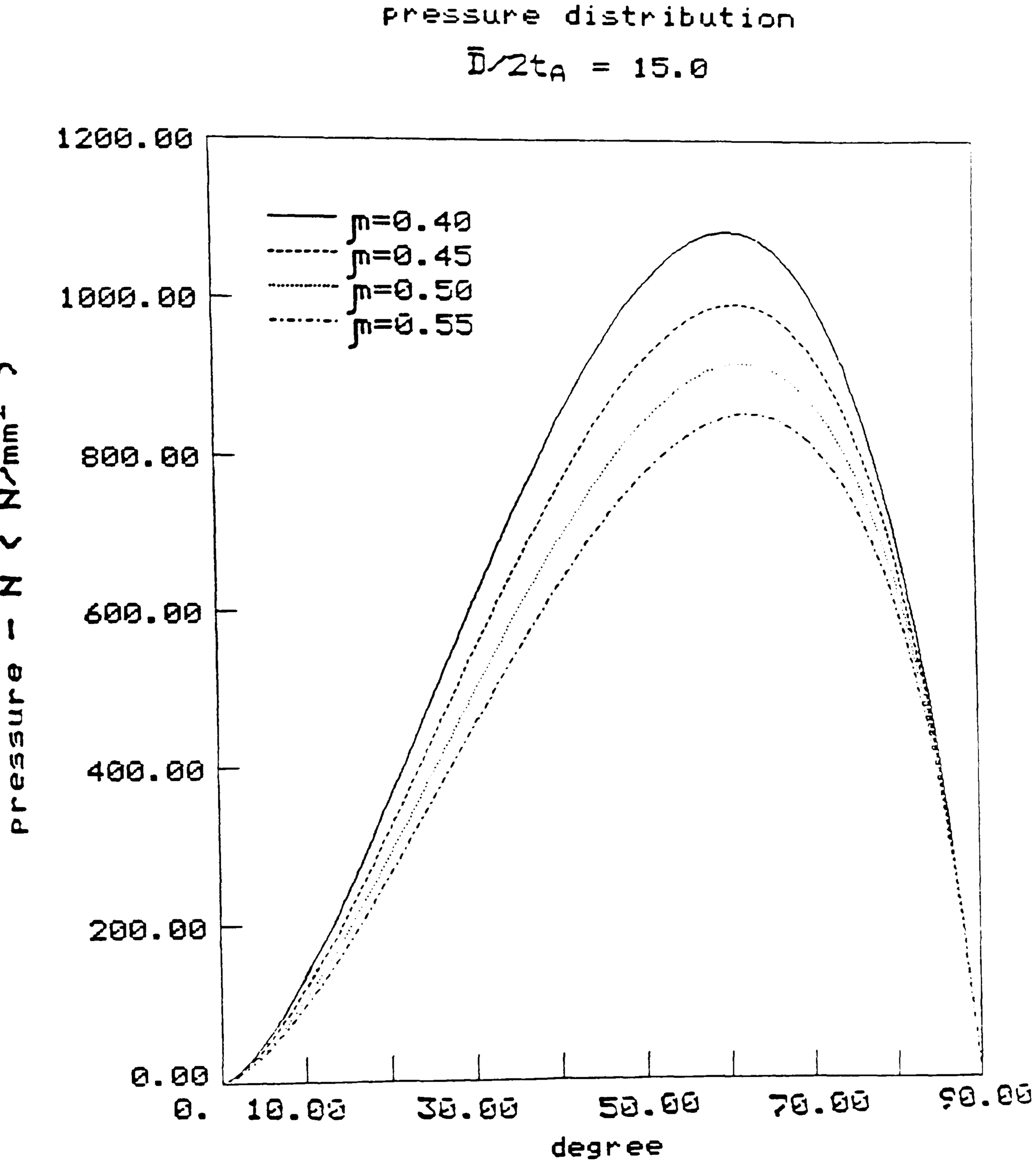

Fig.C34 Theoretical normal pressure curves

pressure distribution

$\bar{D}/2t_A = 15.4$

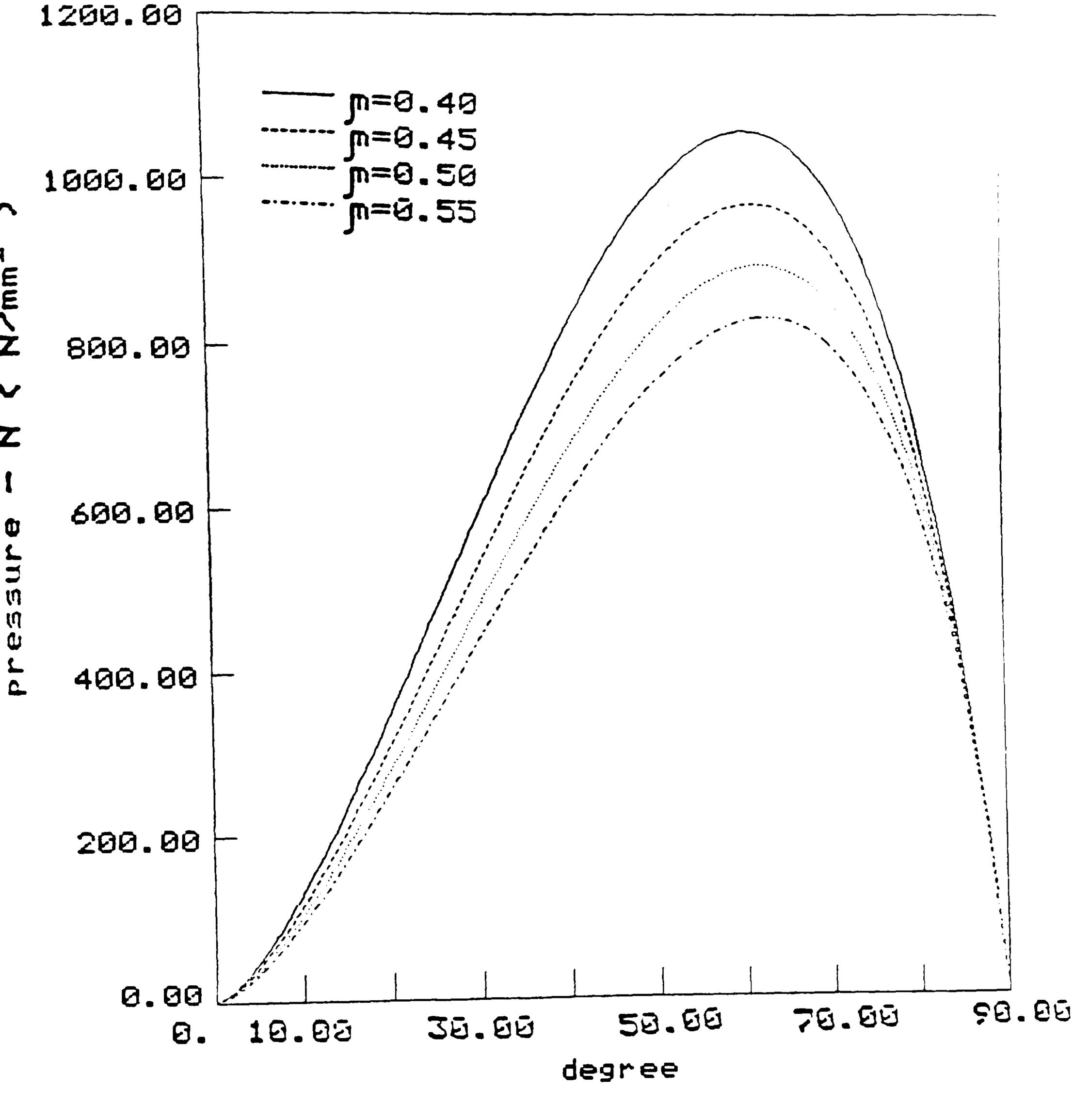

Fig.C35 Theoretical normal pressure curves

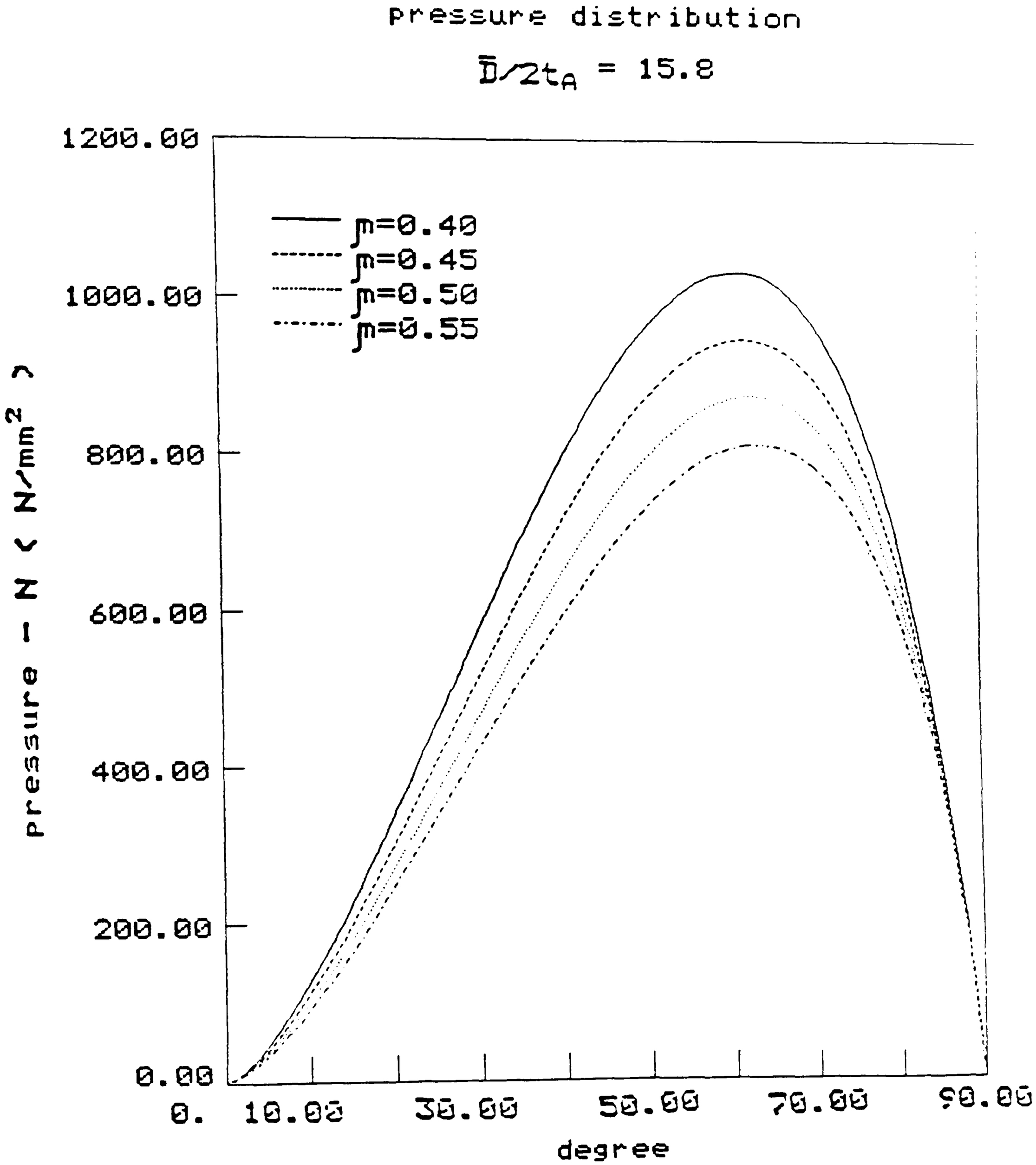

Fig.C36 Theoretical normal pressure curves

pressure distribution

$\bar{D}/2t_A = 16.2$

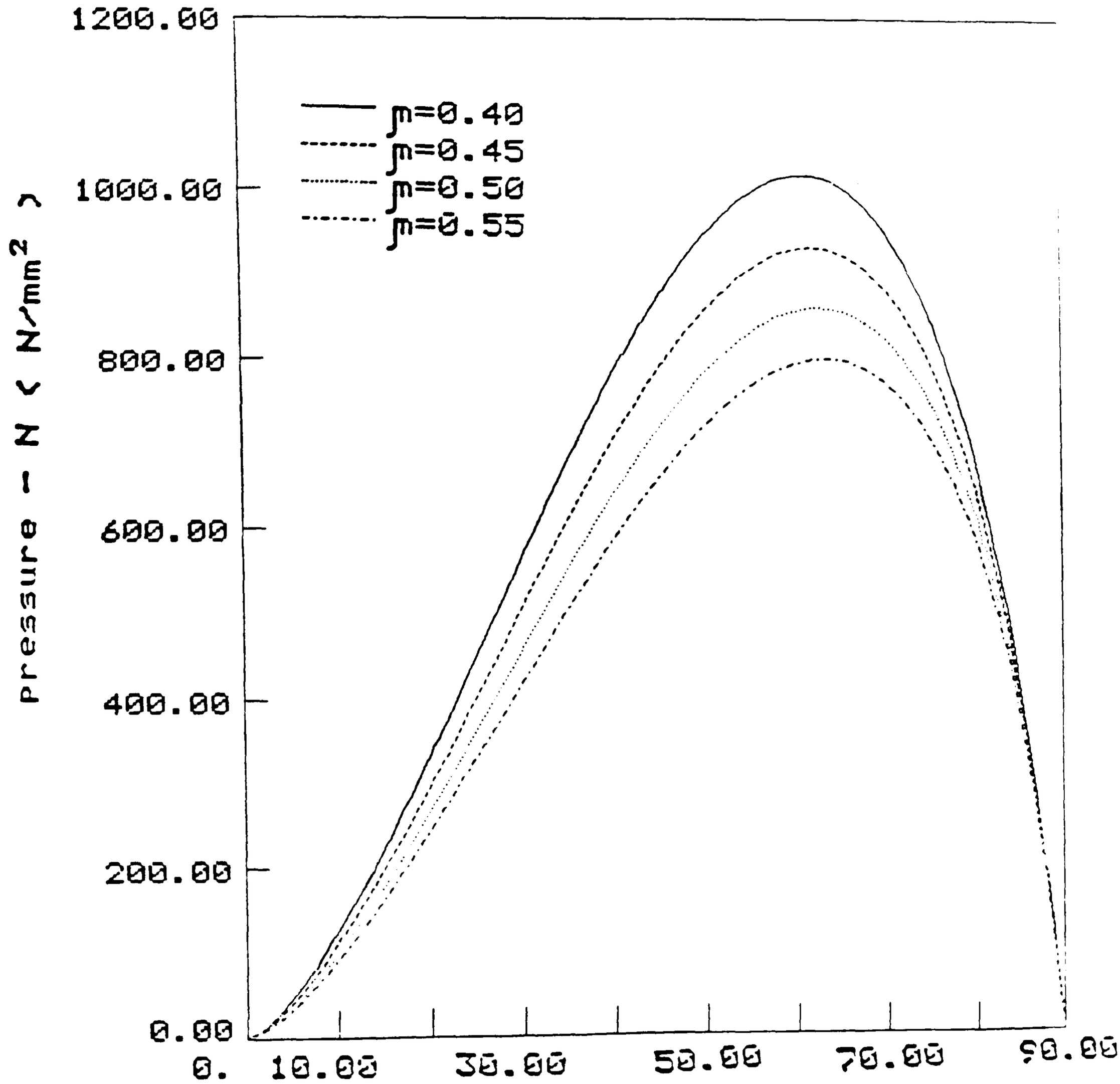

Fig.C37 Theoretical normal pressure curves

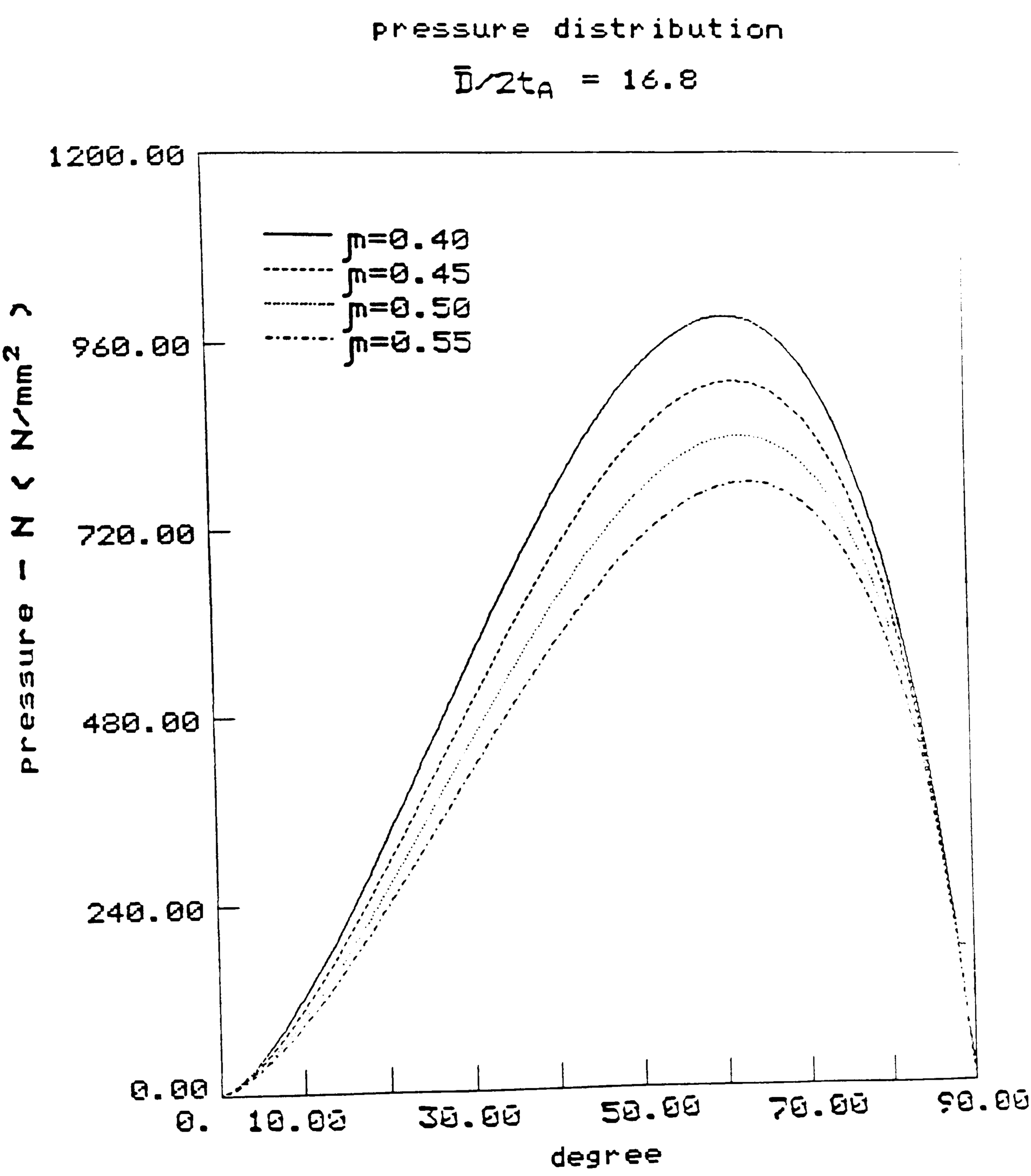

Fig.C38 Theoretical normal pressure curves

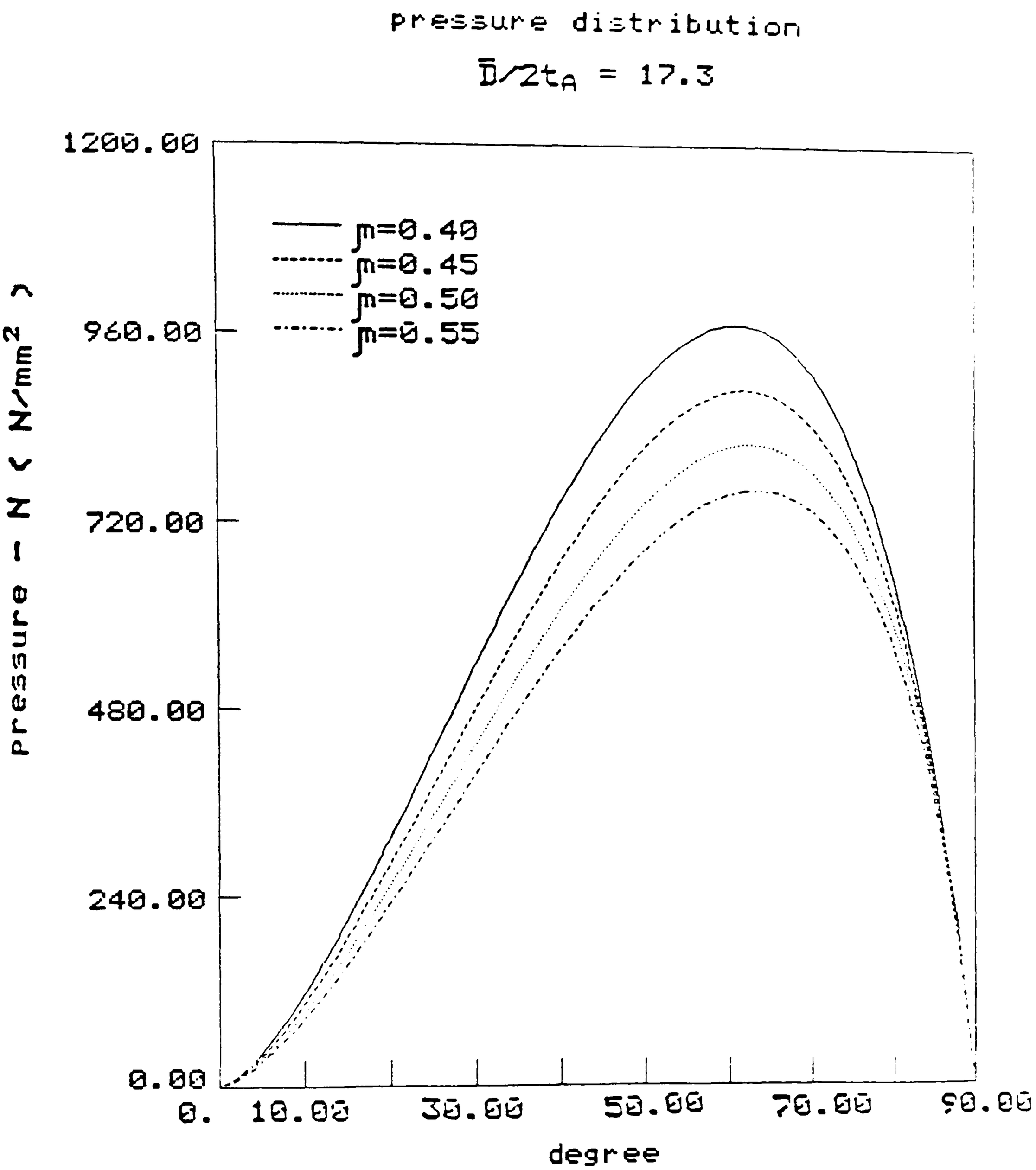

Fig.C39 Theoretical normal pressure curves

pressure distribution

$\bar{D}/2t_A = 17.7$

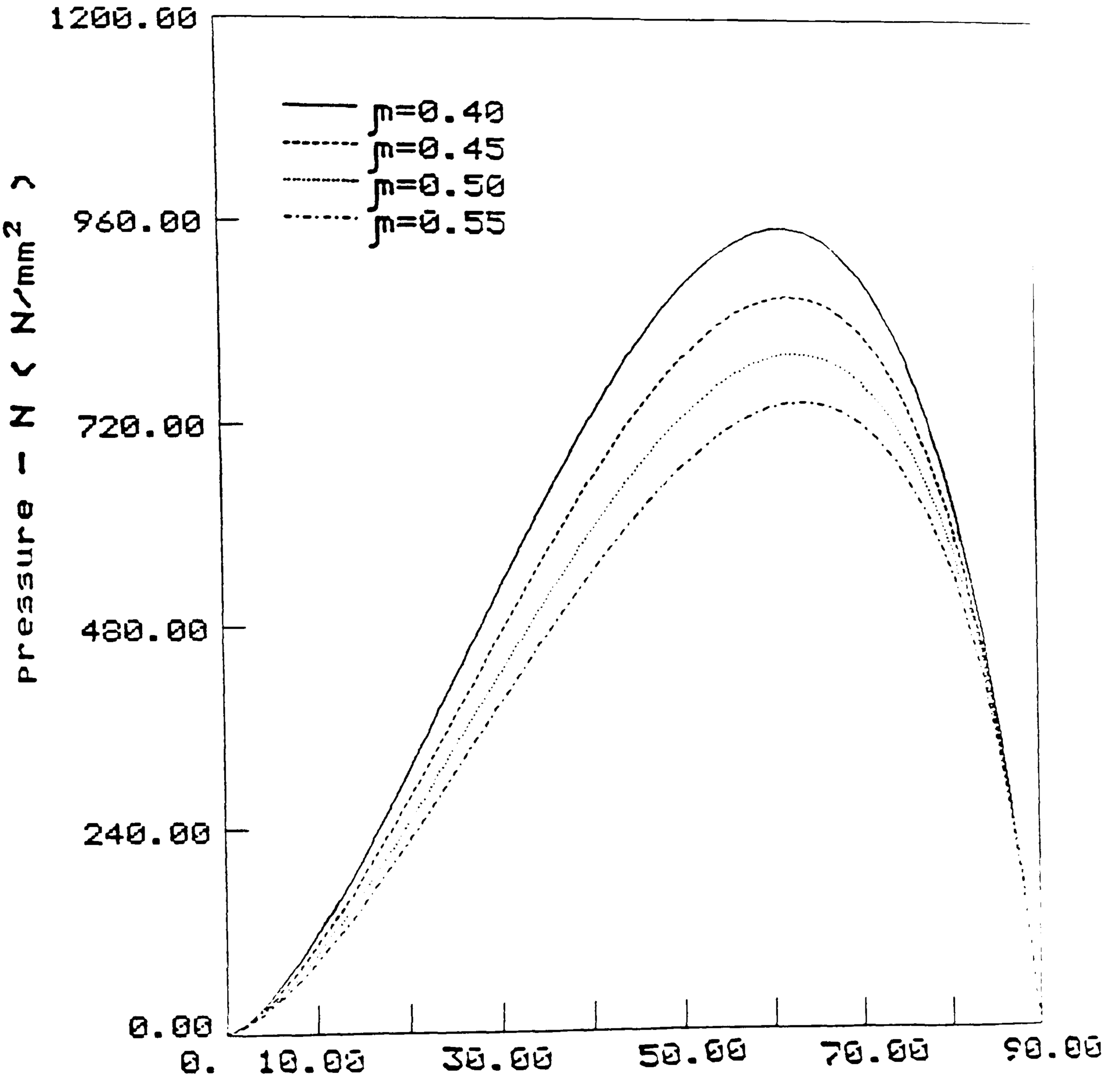

Fig.C40 Theoretical normal pressure curves

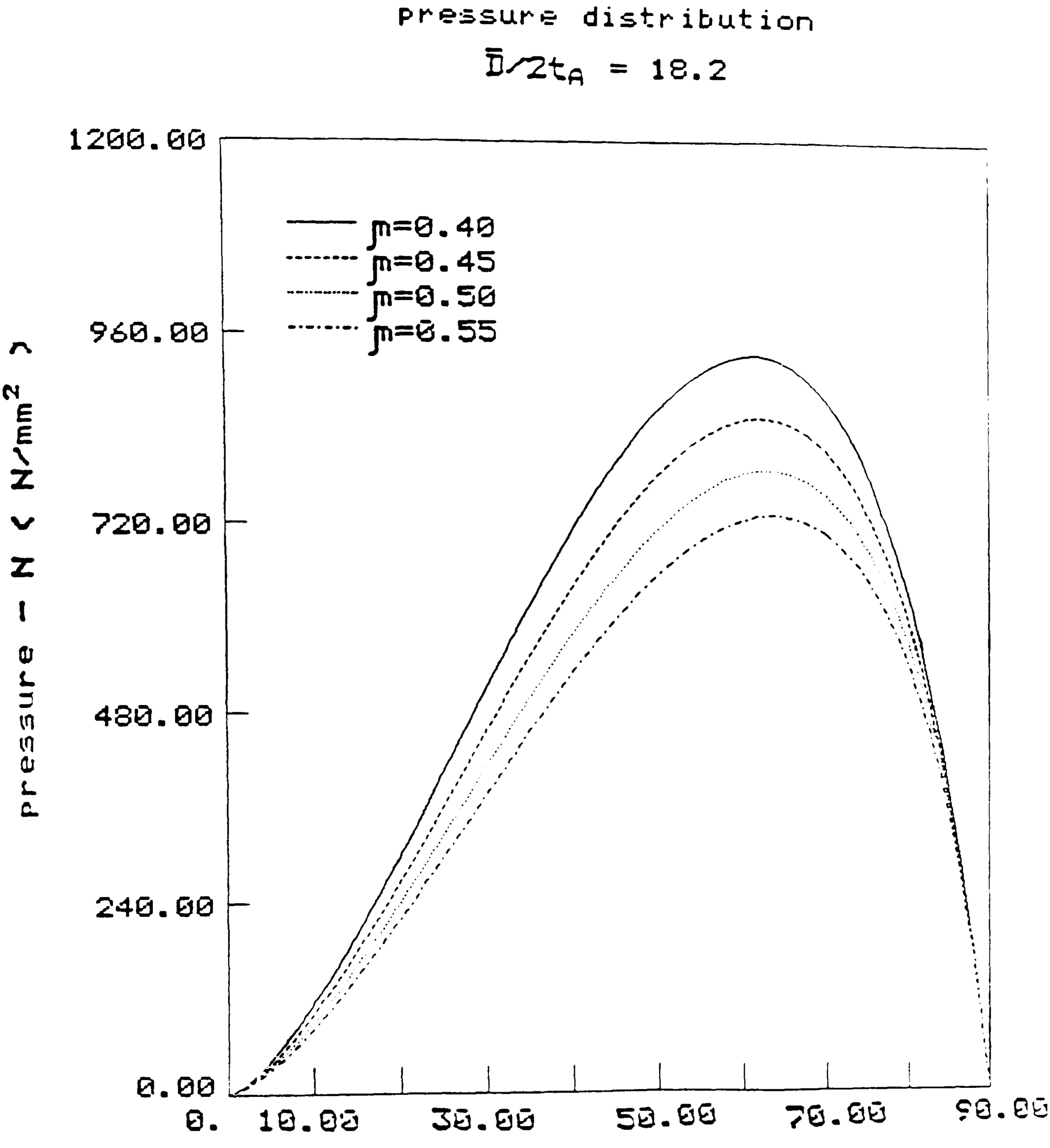

Fig.C41 Theoretical normal pressure curves

Pressure distribution

$\bar{D}/2t_A = 18.6$

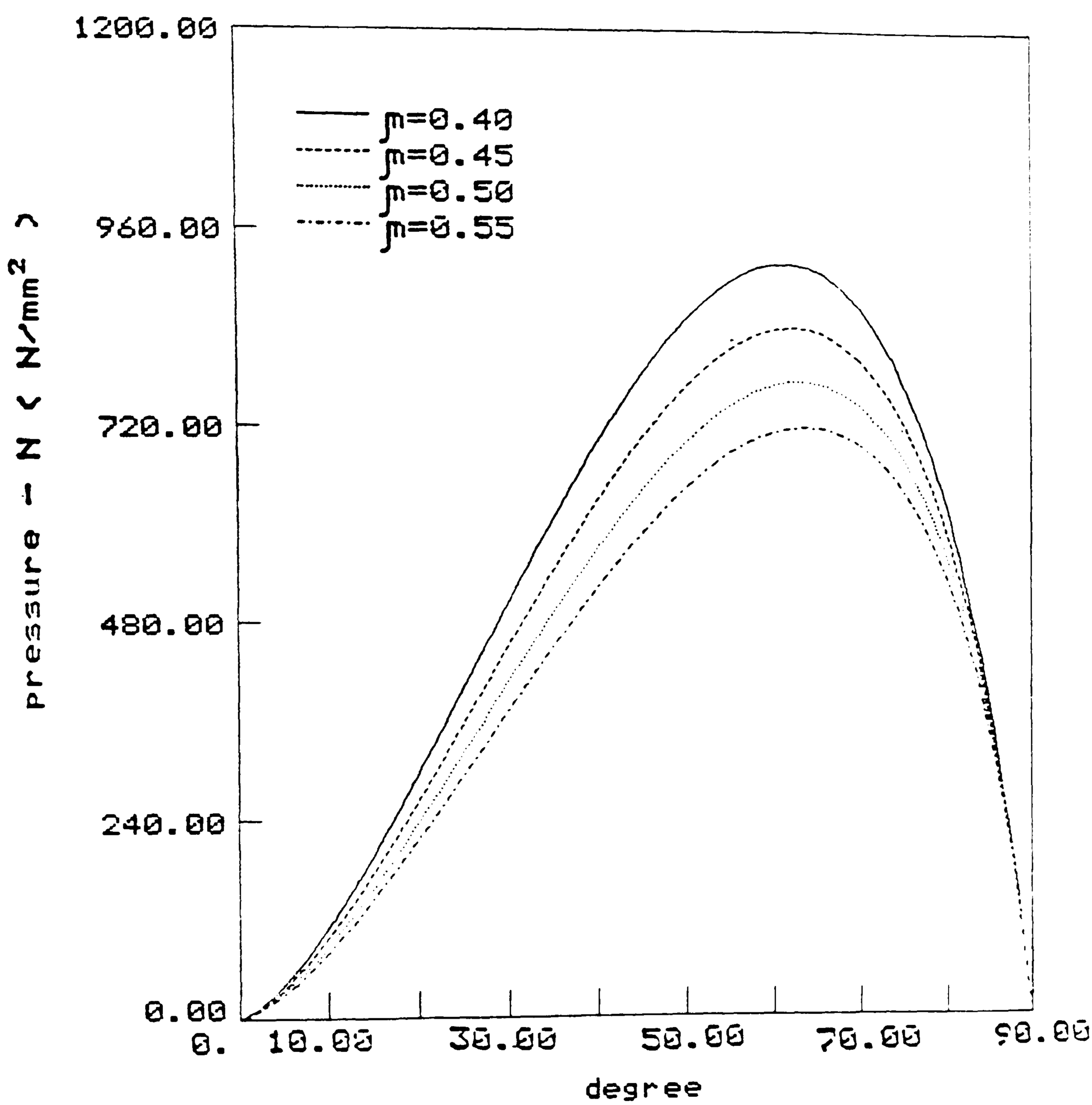

Fig.C42 Theoretical normal pressure curves

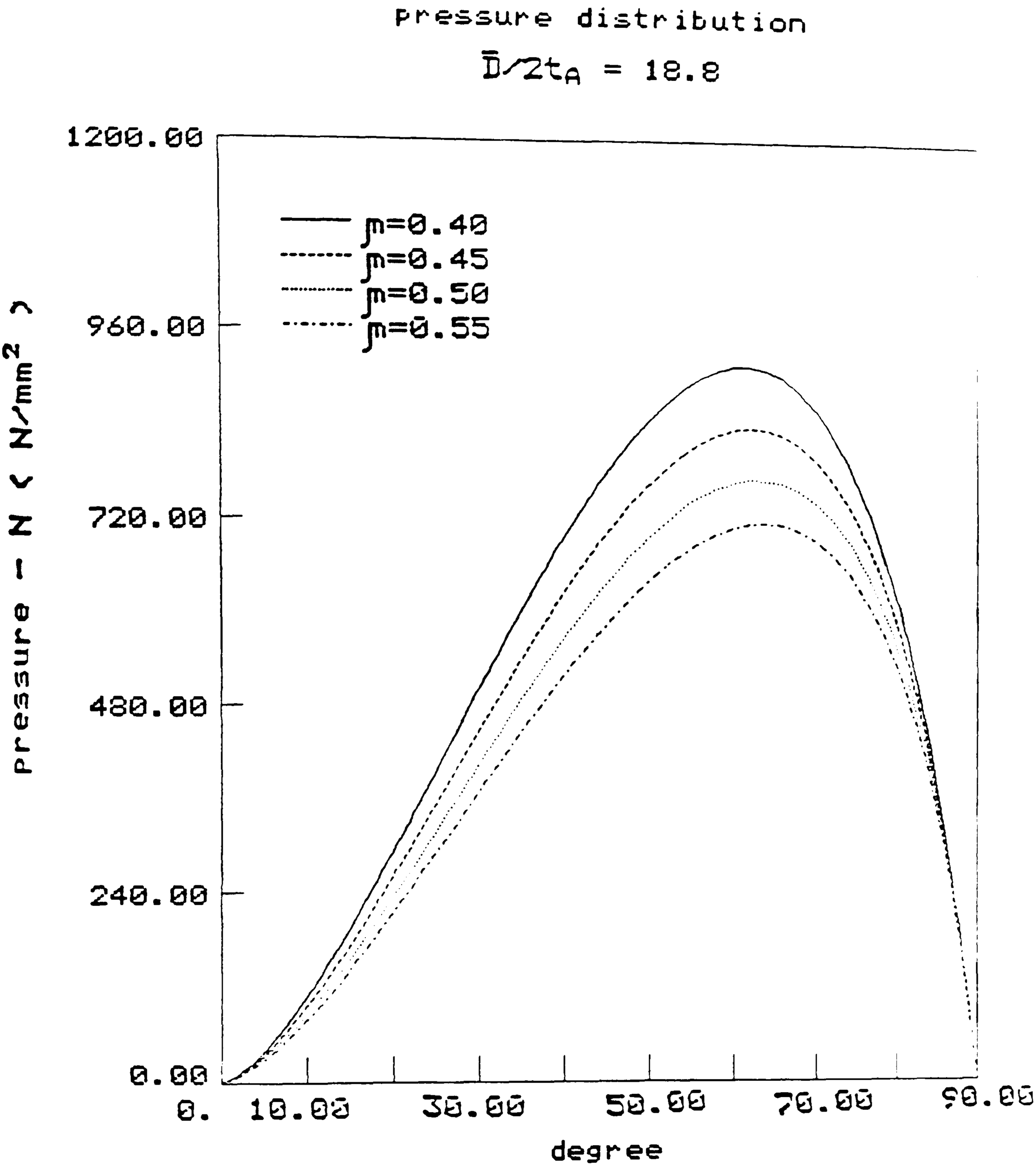

Fig.C43 Theoretical normal pressure curves

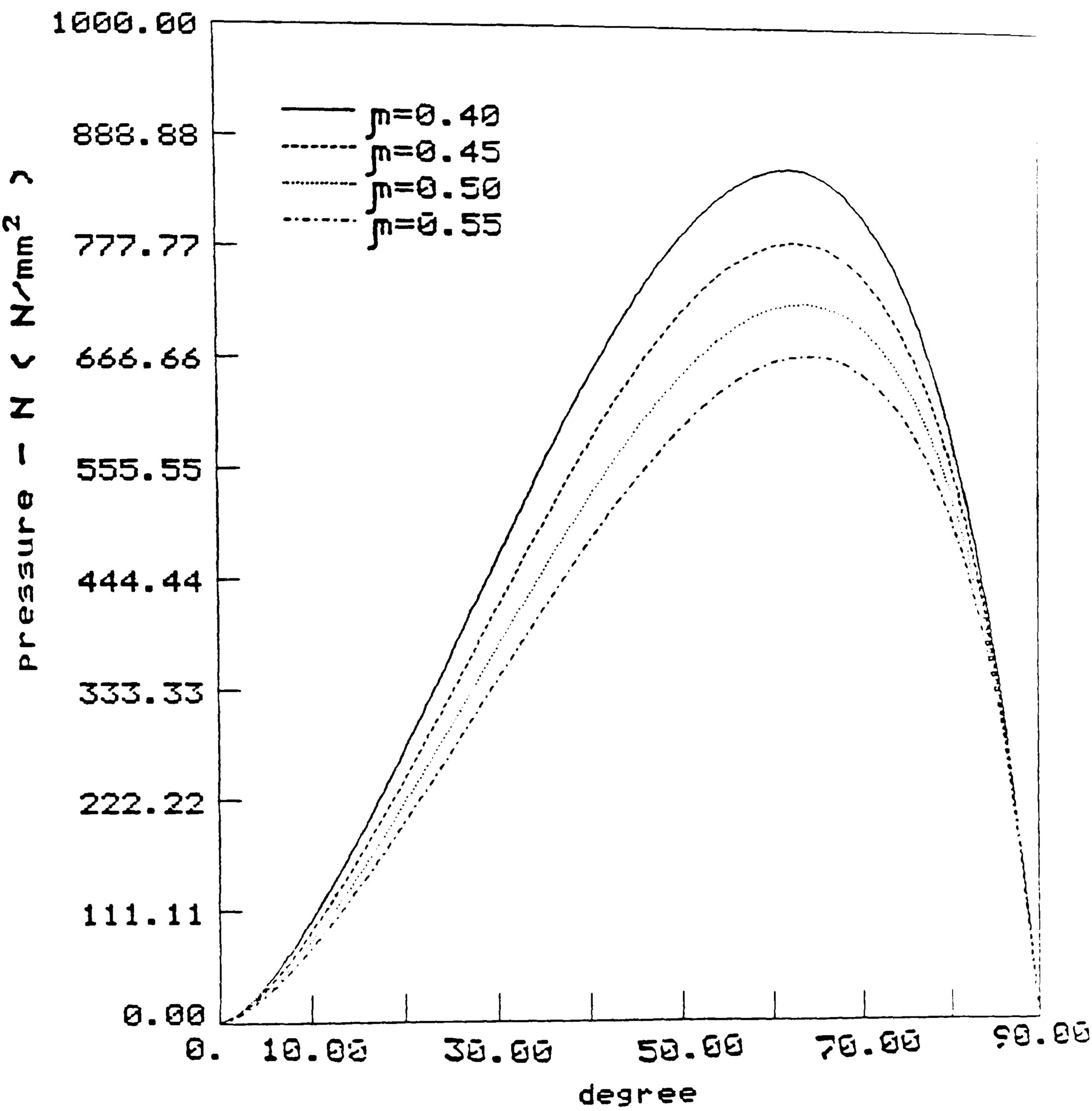

Fig.C44 Theoretical normal pressure curves

pressure distribution

$\bar{D}/2t_A = 20.8$

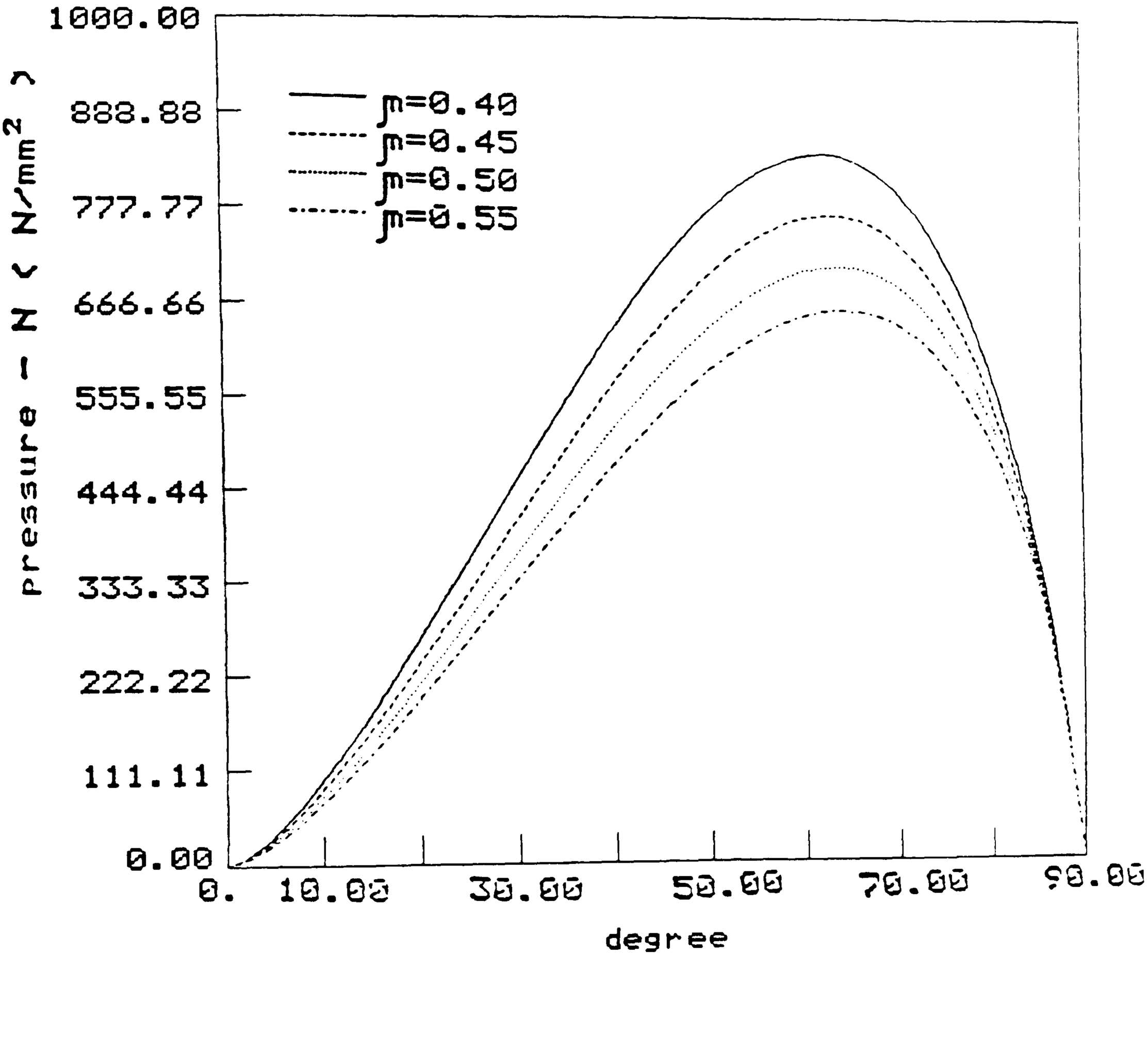

Fig.C45 Theoretical normal pressure curves

Pressure distribution

$\bar{D}/2t_A = 21.4$

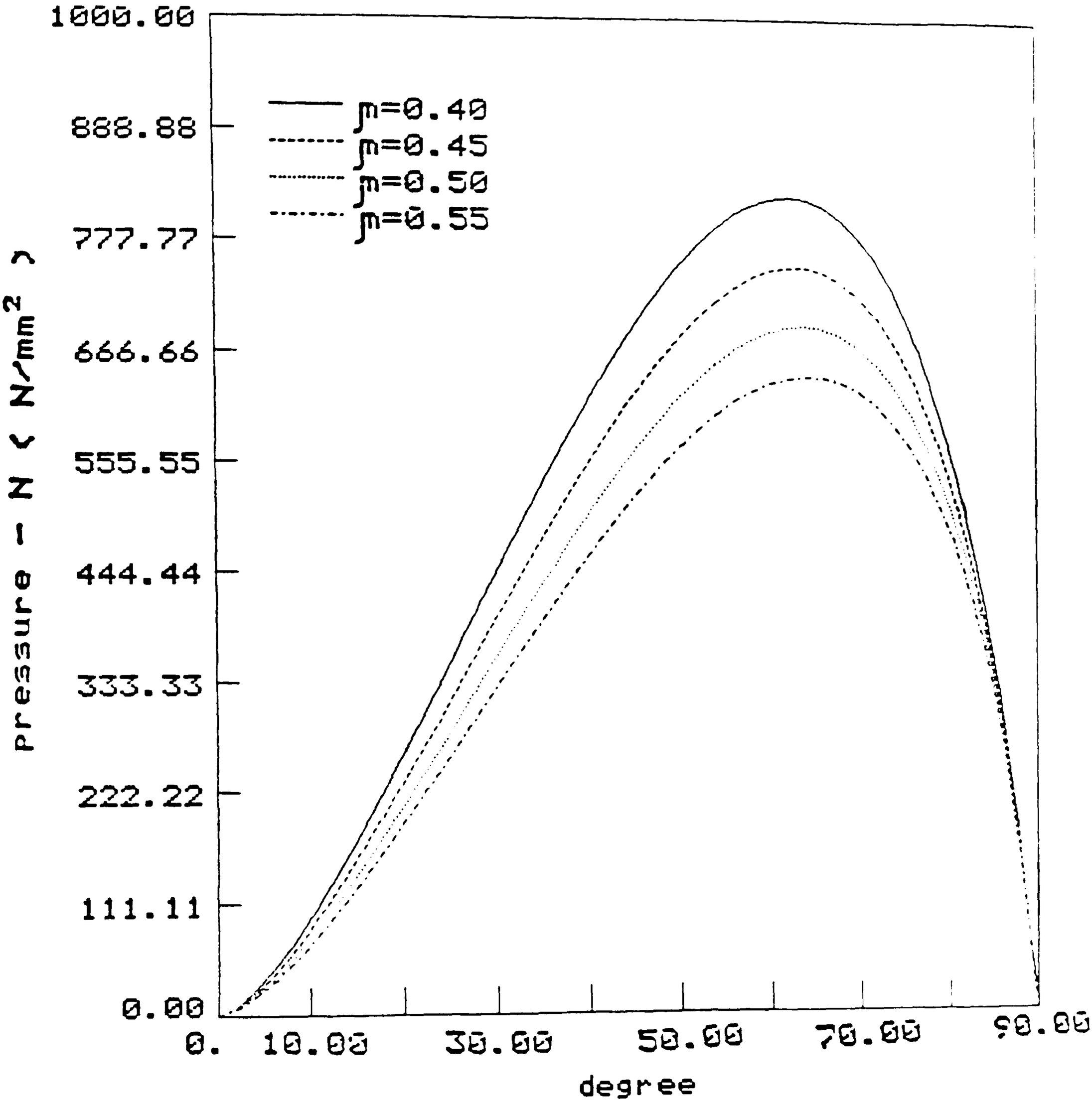

Fig.C46 Theoretical normal pressure curves

pressure distribution

$\bar{D}/2t_A = 22.0$

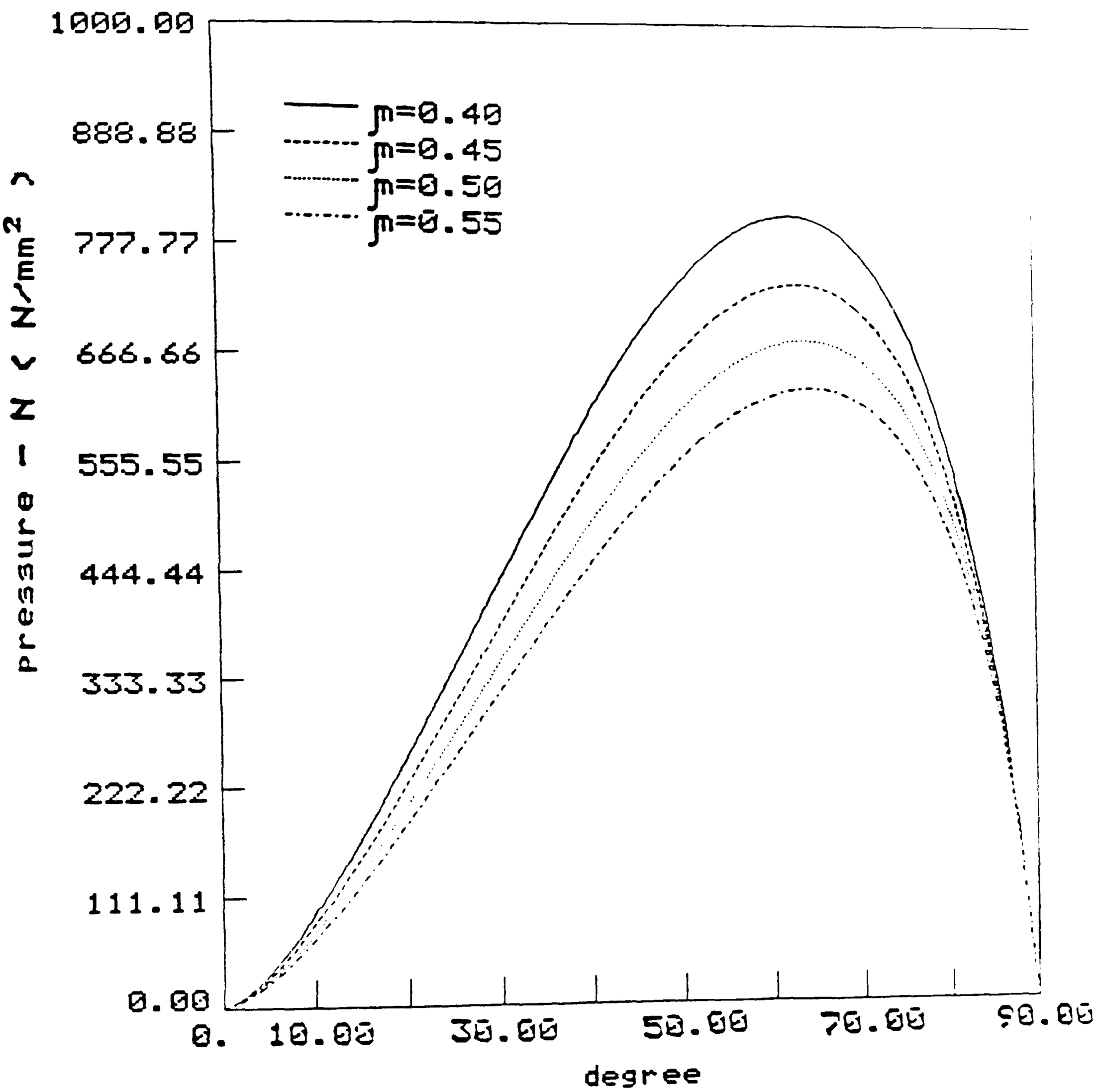

Fig.C47 Theoretical normal pressure curves

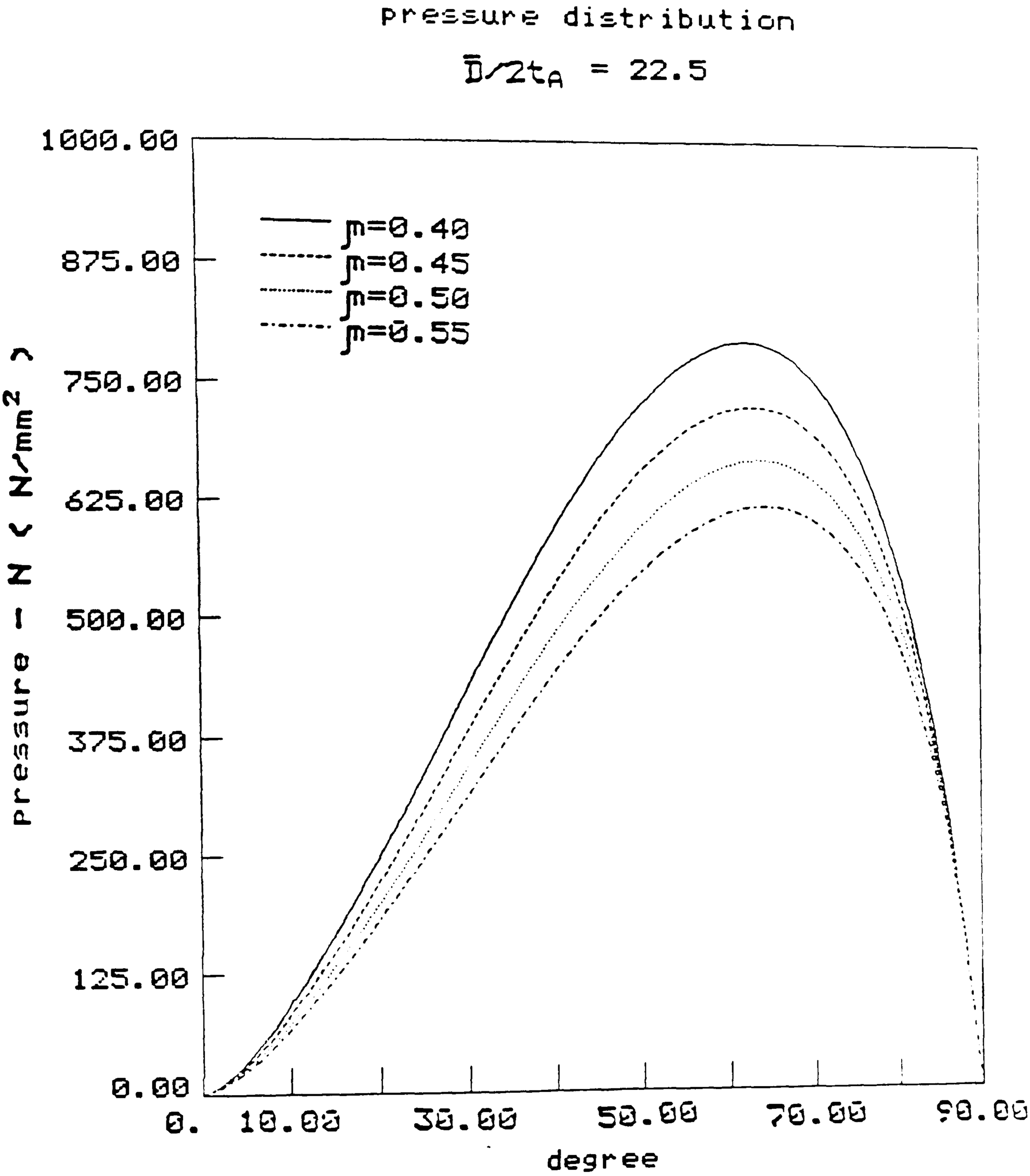

Fig.C48 Theoretical normal pressure curves

Pressure distribution

$\bar{D}/2t_A = 23.4$

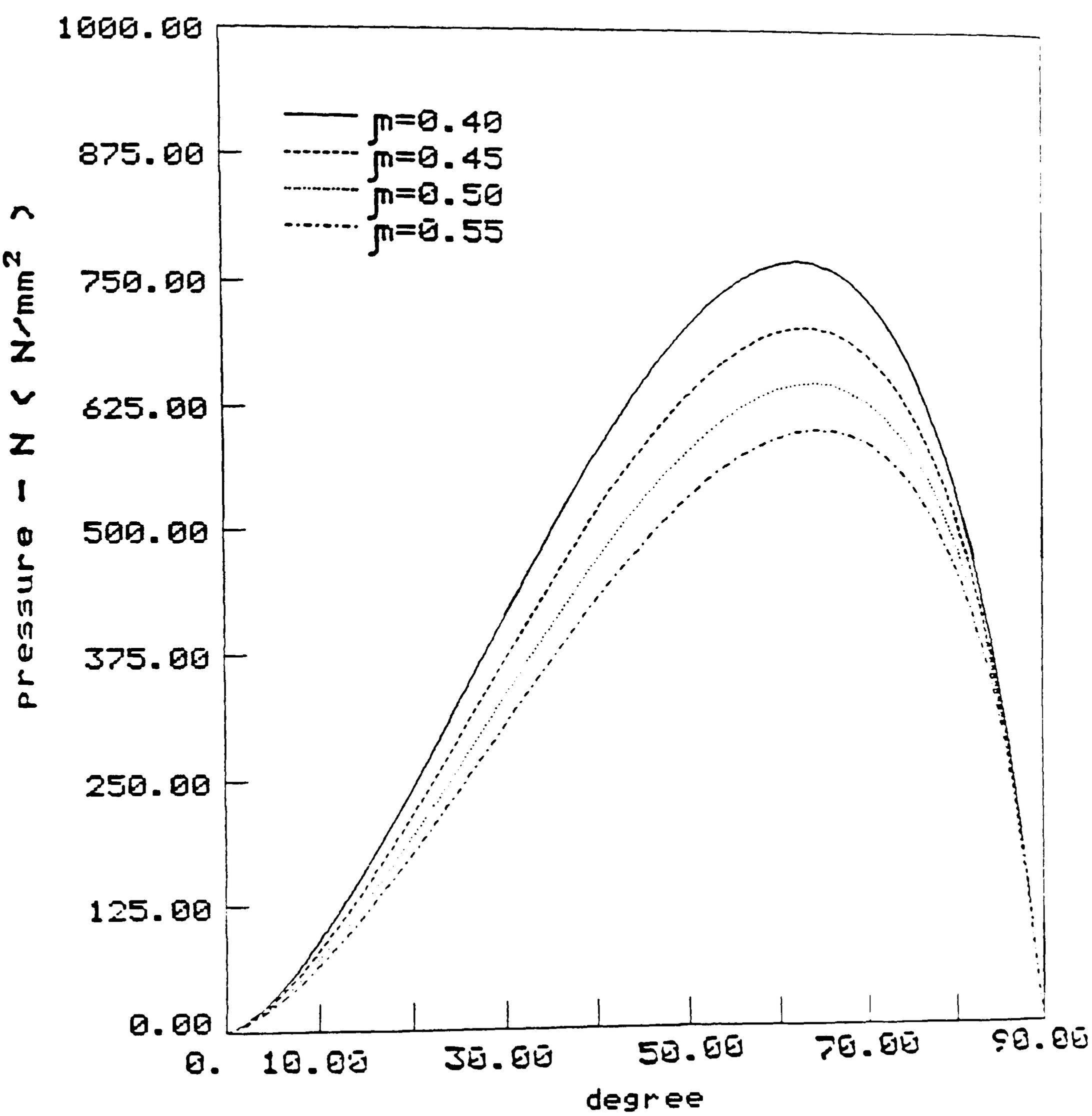

Fig.C49 Theoretical normal pressure curves

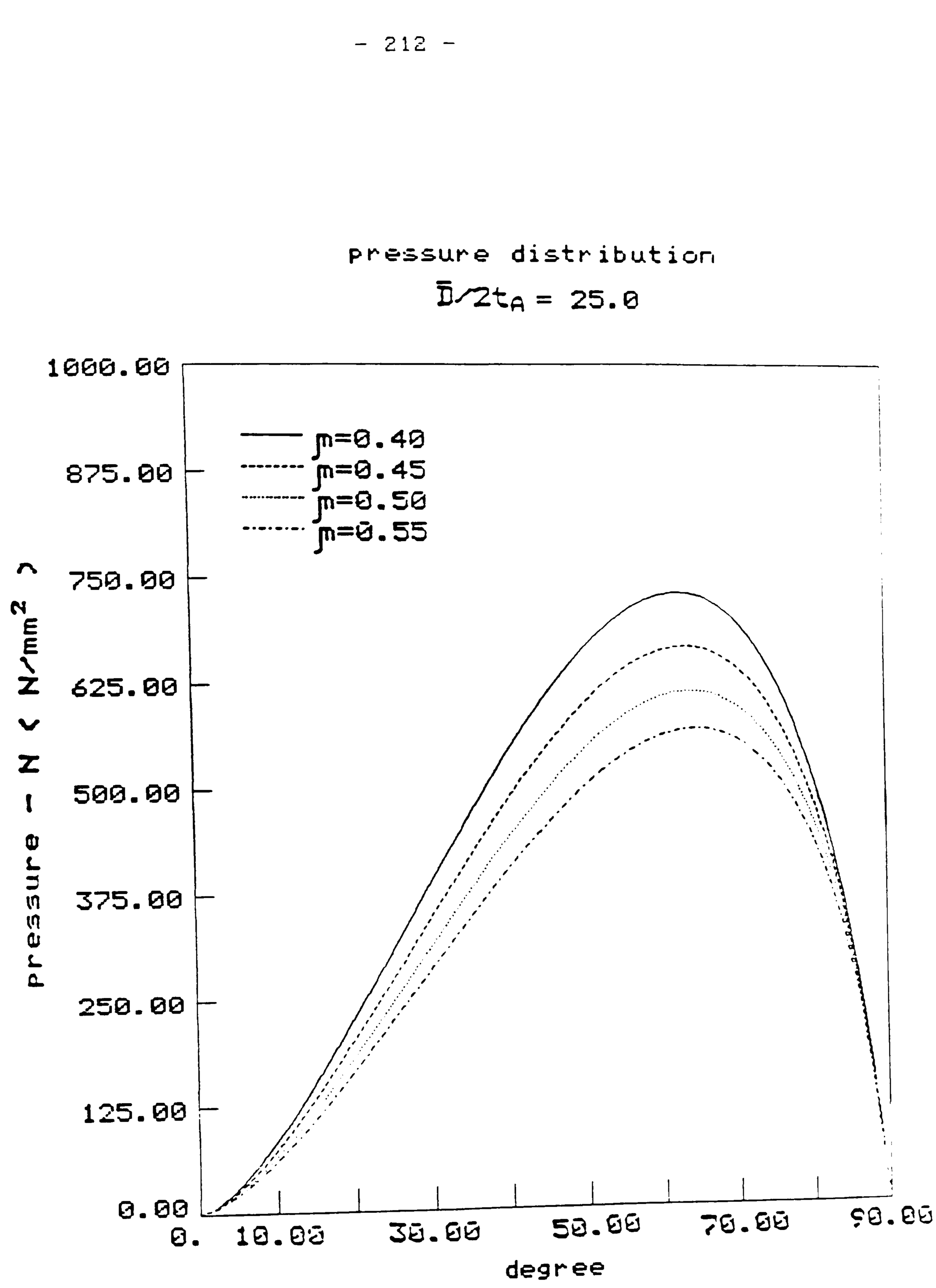

Fig.C50 Theoretical normal pressure curves